Roles of bi and tricellular junctions in the homeostasis of the Drosophila melanogaster notum

Thomas Esmangart de Bournonville

UNIVERSITÉ DE RENNES 1

THESE DE DOCTORAT DE

L'UNIVERSITE DE RENNES 1

ECOLE DOCTORALE N° 605
Biologie Santé
Spécialité : « Biologie Cellulaire, Biologie du Développement »

Par
Thomas ESMANGART de BOURNONVILLE

Rôles des jonctions bi et tricellulaires septées dans l'homéostasie du *notum* de *Drosophila melanogaster*

Thèse présentée et soutenue à Rennes, le 30 Septembre 2021
Unité de recherche : Institut de Génétique et Développement de Rennes – IGDR UMR 6290 CNRS

Rapporteurs avant soutenance :

Pauline SPEDER Junior Group leader, Institut Pasteur, Paris
Franck PICHAUD Professor of cell and developmental biology, University College London, London

Composition du Jury :

Président :

Eric CHEVET DR1 INSERM, INSERM U1242, Université Rennes 1 – CLCC Eugène Marquis, Rennes

Examinateurs :

Bénédicte SANSON Reader in developmental morphogenesis, Wellcome Trust investigator, University of Cambridge, Cambridge
Romain LEVAYER Junior Group leader, Institut Pasteur, Paris
Pauline SPEDER Junior Group leader, Institut Pasteur, Paris
Franck PICHAUD Professor of cell and developmental biology, University College London, London

Directeur de thèse :

Roland Le BORGNE DR1 CNRS, IGDR UMR 6290, Rennes

UNIVERSITÉ DE RENNES 1

THESE DE DOCTORAT DE

L'UNIVERSITE DE RENNES 1

ECOLE DOCTORALE N° 605
Biologie Santé
Spécialité : *Biologie Cellulaire, Biologie du Développement*

par

Thomas Esmangart de Bournonville

Rôles des jonctions bi et tricellulaires septées dans l'homéostasie du *notum* de *Drosophila melanogaster*

Thèse présentée et soutenue à RENNES le 30/09/2021
Unité de recherche UMR6290 IGDR Institut de Génétique et Développement de Rennes, Université de Rennes 1

---

devant le jury composé de:

Pauline SPEDER

Junior group leader. Institut Pasteur Paris / *rapporteuse*

Franck PICHAUD

Professor of cell and developmental biology. University College London / *rapporteur*

Bénédicte SANSON

Reader in developmental morphogenesis, Wellcome Trust investigator. University of Cambridge *examinatrice*

Romain LEVAYER

Junior group leader. Institut Pasteur Paris / *examinateur*

Eric CHEVET

DR1 INSERM. INSERM U1242- Université de Rennes 1- CLCC Eugène Marquis Rennes / *président*

Roland Le BORGNE

DR1 CNRS. IGDR Rennes / *directeur de thèse*

cnrs dépasser les frontières
ÉQUIPE LABELLISÉE PAR LA LIGUE CONTRE LE CANCER
Fondation pour la Recherche Médicale
ANR AGENCE NATIONALE DE LA RECHERCHE

***IN MEDIA VITA*.** — Non ! La vie ne m'a pas déçu ! Je la trouve au contraire d'année en année plus riche, plus désirable et plus mystérieuse, — depuis le jour où m'est venue la grande libératrice, cette pensée que la vie pouvait être une expérience de celui qui cherche la connaissance — et non un devoir, non une fatalité, non une duperie ! — Et la connaissance elle-même : que pour d'autres elle soit autre chose, par exemple un lit de repos, ou bien le chemin qui mène au lit de repos, ou bien encore un divertissement ou une flânerie, pour moi elle est un monde de dangers et de victoires, où les sentiments héroïques eux aussi ont leur place de danses et de jeux. « *La vie est un moyen de la connaissance* » — avec ce principe au cœur on peut non seulement vivre avec bravoure, mais encore *vivre avec joie, rire de joie !* Et comment s'entendrait-on à bien rire et à bien vivre, si l'on ne s'entendait pas d'abord à la guerre et à la victoire ?

Friedrich Wilhelm Nietzsche, *Die fröhliche Wissenschaft*

Abstract

Epithelia are tissues of organisms that provide a role of barrier against chemical and physical aggressions and undergo morphogenesis, repair or regenerate thanks to cell division. Epithelial cells are polarized and linked by bicellular junctions (BCJ) called adherens junction (AJ) at the apical level or septate junction (SJ) below and tricellular junctions (TCJ) where three cells met. Recently, TCJ have emerged as a key regulator of processes regulating cell division, stem cells but also tumourigenesis. Surprisingly, little is known concerning TCJ itself. During my PhD work, I used *Drosophila notum*, a monolayered epithelium, in combination with genetics, imaging and biophysics tools to decipher TCJ homeostasis. Four proteins have been described at TCJ: Sidekick (Sdk), enriched at the AJ level, and Gliotactin (Gli), Anakonda (Aka) and M6 at the SJ level. I first characterized TCJ components *de novo* recruitment at TCJ that assemble during epithelial cytokinesis. Second, I reported that Aka and M6 are the keystone of TCJ assembly. However, while Gli is not required for Aka recruitment at TCJ, Gli activity is needed to stabilize Aka there. I also uncovered that loss of TCJ components results in SJ morphology impairment leading to a major defect of the epithelium. Conversely, the specificity of localization of TCJ components relies on SJ integrity. In parallel, I observed that loss of TCJ integrity leads to E-cadherin as well as acto-myosin cytoskeleton enrichment at both TCJ and BCJ. These phenotypes also appear upon loss of pSJ proteins. Moreover, the AJ and acto-myosin cytoskeleton remodeling comes with ESCRT components HRS and Shrub defects along with Crumbs enrichment at the apical part of the cell. Moreover, I observed that the establishment of the new daughter/daughter cell interface is impaired upon TCJ loss of function. Hence, my PhD work sheds light on the links between TCJ, pSJs and AJs in the tissue and how defects at a specific junctional level, results in a global impairment of cell homeostasis.

Résumé

Les épithélia sont des tissus de l'organisme, jouant un rôle de barrière contre l'extérieur et impliqués dans le développement, la morphogénèse et la réparation tissulaire grâce à la division cellulaire. Ils sont composés de différentes cellules polarisées qui forment des jonctions bicellulaires (BCJ) dites adhérentes (AJ) ou septées (SJ) ainsi que des jonctions tricellulaires (TCJ) au contact de trois cellules. De récentes études démontrent que les TCJs sont impliquées dans de nombreux processus intervenant dans la division cellulaire, la régulation de cellules souches ou encore la tumorigénèse. Curieusement, les TCJs demeurent méconnues. J'utilise le *notum* de Drosophile, un épithélium monocouche, en combinaison avec des outils génétiques, d'imagerie et de biophysique pour étudier l'homéostasie des TCJs. Quatre protéines transmembranaires sont reportées enrichies aux TCJs : Sidekick (Sdk) dans le plan des AJs ; Gliotactine (Gli), Anakonda (Aka) et M6 dans le plan des SJs. J'ai caractérisé leur dynamique d'assemblage dans la division et démontré que M6 et Aka étaient les pièces maîtresses des TCJs en recrutant Gli. Cette dernière, bien que non nécessaire à la présence d'Aka à la TCJ, la stabilise. J'ai ensuite observé que la perte d'intégrité de la TCJ conduit à des déformations des SJs entraînant un défaut majeur de l'intégrité de l'épithélium. A l'inverse, la spécificité de localisation des protéines de la TCJ est régulée par l'intégrité des SJs. En parallèle, j'ai également remarqué que la perte d'intégrité de la TCJ entraîne un enrichissement d'E-Cadhérine et d'acto-myosine tout comme la perte de protéines des pSJs. De plus, j'ai pu observer que ces défauts étaient accompagnés d'agrégats des protéines ESCRT HRS et Shrub ainsi qu'un enrichissement de Crumbs au niveau apical de la cellule. De plus, enlever la protéine Aka conduit à un défaut d'établissement de la nouvelle jonction cellulaire lors de la division. Ce travail de thèse a donc permis de comprendre le lien qui existe entre la TCJ, les pSJs et AJs au sein du *notum* et comment des défauts dans un certain plan jonctionnel conduisent à des problèmes généralisés dans la cellule.

Table of contents

List of Abbreviations

Actn: α-Actinin **AJ:** Adherens Junction **Aka:** Anakonda **aPKC:** atypical Protein Kinase C **ARP2/3:** actin-related protein 2/3 **aSF**: apical stress fibres

bAJ: Bicellular Adherens Junction **Baz:** Bazooka **BBB:** Blood brain barrier

BCJ: Bicellular Junction **Bou:** Boudin **BSJ:** Bicellular Septate Junction

Cno: Canoe **CNS:** Central nervous system **Cold:** Coiled **Cont:** Contactin

Cora: Coracle **Crb:** Crumbs **Crim:** Crimpled **Crok:** Crooked **Csk:** C-terminal Src kinase **DC:** Dorsal closure **Dlg:** Discs-large **DE-Cad**: DE-Cadherin

DS: Dorsal vessel **EB:** enteroblasts **EC:** enterocytes **EE:** enteroendocrine cells

EGF: epidermal growth factor **EMC:** enteroendocrine mother cells

ESCRT: Endosomal sorting complexes required for transport **Ex:** Expanded

FA: Focal Adhesion **Fas:** Fasciclin **FERM:** 4.1/Ezrin/Radixin/Moesin

FRAP: fluorescent recovery analysis after photobleaching **GEF:** Rho-Guanine nucleotide exchange factors **Gli:** Gliotactin **GUK:** Guanlytate Kinase

HI: Head involution **ISC:** intestinal stem cells **JNK:** Jun N-terminal kinase

Jub: Ajuba **Kune:** Kune-Kune **Lac:** Lachesin LAP**:** Leukaemia-associated-protein

Lgl: Lethal Giant Larvae **LRR:** Leucine-Rich Repeated **Ly6:** Leucocyte Antigen 6

MAGUK: Membrane-Associated Guanylate Kinase Homologs

Mcr: Macroglobulin complement-related **Mega:** Megatrachea

MVBs: Multivesicular Bodies **NMY-II:** Non-muscle Myosin II **Nrg:** Neuroglian

Nrv2: Nervana 2 **Nrx-IV:** Neurexin-IV **OELP:** outer epithelial layer of the proventriculus **Pasi:** Pasiflora **PATJ:** Protein Associated with Tight Junction

Par: Partitioning Defective **PDZ:** PSD-95, Dlg, ZO-1 **PLP:** myelin proteolipid protein

pSJ: Pleated Septate Junction **Pyd:** Polychaetoid **RLC:** regulatory light chains

ROCK: Rho-associated, coiled coil-containing kinase **Rok:** Rho-kinase

Scrib: Scribble **Sdk:** Sidekick **Sdt:** Stardust **Serp:** Serpentine

SG: Salivary glands **Sinu:** Sinuous **SJ:** Septate Junction **sSJ:** Smooth Septate Junction **Ssk:** Snakeskin **tAJ:** Tricellular Adherens Junction

TCJ: Tricellular Junction **TEM:** Transmission electron microscopy

TJ: Tight Junction **Tsf2:** Transferrin 2 **tSJ:** Tricellular Septate Junction

Udt: Undicht **Vari:** Varicose **Verm:** Vermiform **Vinc:** Vinculin **Wrm:** Würmchen

WT: Wild-type **Wun:** Wunens **Yrt:** Yurt

List of figures

Introduction:

Introduction

General introduction

Metazoans originate from ancestral unicellular organisms, at many times during evolution (Niklas 2014), and display very different shapes and features. This complexity requires that organisms build new tissues associated with different specialised functions. Among these tissues which emerged during evolution, epithelium had appeared as one of the most important factors for animals' survival. Originally, epithelia were described in the group of bilaterians and characterised by key features, such as apico-basal polarity of the cell, basement membrane and cellular junctions' presence (Miller, Clarke et al. 2013).

This particular organisation allows many activities in the cell like polarised transport, filtering role or mechanical resistance just to name of few. Despite heterogeneity among metazoans epithelia, conserved features are observed like the cellular polarity and the crucial adhesive junctions (Abedin and King 2010). Moreover, epithelia are involved in a wide range of processes all along the individuals' life. For example, during development, flat epithelial tissues start to deform and are remodelled to acquire 3D shapes thanks to cell divisions, movements and shape changes. Beginning at early developmental stages like the gastrulation and neural tube formation, epithelia then continue to mature and give rise to organs such as kidneys, heart, lungs, intestine and many others.

Because epithelia face the outside and cover internal parts of organisms, they act as fences to protect organisms against external chemical or physical injuries. Thereby, epithelial cells show high degree of coherence and protection as well as flexibility in order to resist and repair upon damages. Epithelial cells are also a target of numerous pathogens such as bacteria, the latter sometimes focusing on cellular junctions. An example of this process is highlighted in the case of *Shigella,* which specifically targets the adherens junction protein E-Cadherin to spread across the cells (Sansonetti, Mounier et al. 1994).

Despite protecting organisms, epithelial cells can also be responsible of diseases, with defects during embryo development or being the origin of solid tumours. Indeed, more than 85% of solid tumours take place inside an epithelium. The dysregulation of cell divisions, loss of cell polarity or cell identity are well known causes of the tumourigenesis process (Koch and Radtke 2010). These cancerous cells are even

more dangerous upon epithelial-mesenchymal transition. During this process, they remodel their junctions, lose their identity and leave the original tissue in order to establish themselves at distant places in the organism (Nieto, Huang et al. 2016, Dongre and Weinberg 2019). This is why understanding the fundamental mechanisms underlying cellular junction homeostasis, remains of a capital importance to shape future discoveries.

At the time being, many approaches and technics exist to address the problems of diseases' aetiology, ranging from classical model organisms, to organoids, *in vitro* and *in silico* studies, and their number as well as diversity are still growing.

Still, one capital model organism remains popular among biologists, namely the fruit fly *Drosophila melanogaster*. This organism possesses around 60% of homology with human genes (Wangler, Yamamoto et al. 2015), most of them being required in regulating cell division or cellular junctions. Moreover, the first gene discovered to be involved in tumourigenesis, Notch, had been identified in the *Drosophila* (Poulson 1937). Then, many outstanding scientists had made great discoveries using the *Drosophila*, from the discovery of homeotic genes (Lewis 1978), to the identification of developmental key players (Nüsslein-Volhard and Wieschaus 1980) or the Toll signalling pathway and its role in the innate immunity (Lemaitre, Nicolas et al. 1996). Moreover, the cutting-edge technics of genetics (Chow and Reiter 2017), biophysics and live-imaging in wild-type (WT) conditions (Wu, Kumar et al. 2019), make the *Drosophila* a model of choice to decipher complex cellular processes.

This is why in our team, we are using the *notum* of the *Drosophila melanogaster*, a monolayered epithelium, to study how cells remodel their junctions during the division, maintain their homeostasis during interphase and how defects in these processes lead to problems in cell viability and/or identity.

Chapter I: Epithelial cell polarity

a. Generalities

Epithelial cells are the basic units of the most abundant tissue in metazoans, namely the epithelium. They face the outside and protect organisms against injuries, for example pathogens invasion, mechanical damage or chemical products. Epithelial cells also provide key functions such as nutrient uptake, air exchange as well as functioning as a filtering barrier. To play this continuous protective role, epithelial cells need to be closely packed, thereby establishing different junctional complexes such as the mechanical barrier provider Adherens Junction (AJ) and the filtering Septate Junction (SJ). Moreover, a striking feature of the epithelial cells is their polarity, a specific organisation of different proteins that set the identity of cellular and membranous domains along an apico-basal axis. Polarity proteins are pivotal actors in many processes such as the establishment and positioning of junctions, cell shape regulation to the fate specification of daughter cells upon asymmetrical divisions. In invertebrates, and more specifically in the *Drosophila*, three main complexes have been described: the Partitioning Defective (Par) complex, the Crumbs (Crb) complex and the Scribble (Scrib) complex **(Figure 1).** This chapter introduces the principal components and roles of these polarity modules in cell polarity.

I focus on the Crumbs protein since it is part of my work as demonstrated in the results section.

b. The Par complex

Initially discovered for their role during the zygotic asymmetrical division of *C. elegans* (Kemphues, Priess et al. 1988), the PAR proteins were shown to be spread throughout the animal kingdom with orthologous in humans and *Drosophila*. In the latter, the first identified PAR orthologous was the multi-PSD-95, Dlg, ZO-1 (PDZ) domains protein named Bazooka (Baz; orthologous of PAR-3 in C elegans and Par3 in mammals). Together with the atypical Protein Kinase C (aPKC), Par-6 and the small GTPase Cdc42, it forms the Par polarity complex in the *Drosophila melanogaster* (Nance and Zallen 2011, Tepass 2012).

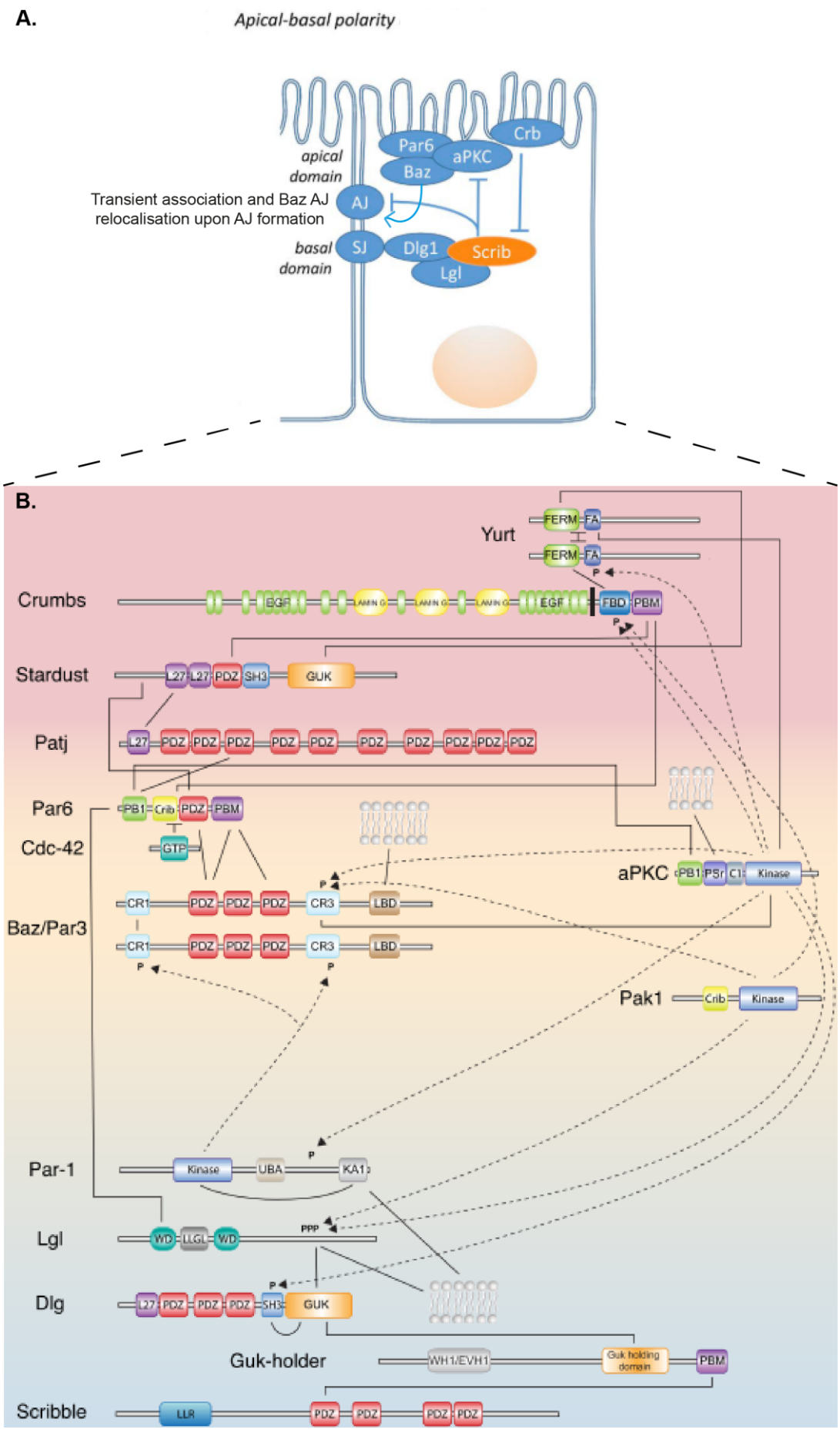
A.
Apical-basal polarity
apical domain
Par6
aPKC
Crb
Baz
Transient association and Baz AJ relocalisation upon AJ formation
AJ
basal domain
SJ
Dlg1
Scrib
Lgl
B.
Yurt
FERM
FA
Crumbs
EGF
LAMIN G
FBD
PBM
Stardust
L27
PDZ
SH3
GUK
Patj
Par6
PB1
Crib
PBM
Cdc-42
GTP
aPKC
PSr
C1
Kinase
Baz/Par3
CR1
CR3
LBD
Pak1
Par-1
UBA
KA1
Lgl
WD
LLGL
PPP
Dlg
Guk-holder
WH1/EVH1
Guk holding domain
Scribble
LLR

Figure 1. Polarity complex proteins distribution and interplay in Drosophila epithelial cell. A. Scheme representing the three different polarity complexes in a Drosophila epithelial cell: The **Par** complex and the **Crb** complex localizing apically and the **Scrib** complex localizing basolaterally. Mutual exclusion between the different complexes allows cell polarity establishment. **B.** Overall view of polarity proteins interplay. Solid lines show physical interactions. Dashed lines reveal phosphorylation events. Abbreviations: FERM, 4.1-Ezrin-Radixin-Moesin; FA, FERM-adjacent (FA) domain; EGF, epidermal growth factor domain; L27, Lin-2 and Lin-7 domain; SH3, SRC homology 3 domain; GUK, guanylate kinase-like; FBD, FERM binding domain; PBM, PDZ domain-binding motif; PB1, Phox and Bem1 domain; Crib, Cdc42-interactive and Rac-interactive binding motif; CR1, CR3, conserved region 1 and 3; LBD, lipid binding domain; KA1, kinase associated domain; WD, WD40 repeat; LLGL, lethal giant larvae specific domain; WH1/EVH1, Enabled/VASP homology 1; LLR, leucine rich repeat domain; PSr, pseudosubstrate region of aPKC Adapted from (Bonello and Peifer 2019) and (Riga, Castiglioni et al. 2020).

Baz is a scaffold protein that interacts with many proteins including the *Drosophila* β-catenin Armadillo, Echinoid (the equivalent of the mammal Nectin), itself and Par6, Cdc42 and aPKC. The Baz polarity module is found just above the AJs spanning the all cell area perimeter and it is required for AJ assembly during embryogenesis (McGill, McKinley et al. 2009). Upon the formation of the Baz-aPKC/Par-6/Cdc42 complex, aPKC phosphorylates Baz on the Serine 980 which leads to its exclusion from the complex whereas aPKC/Par-6/Cdc42 binds the sub-apical polarity complex Crumbs/Stardust. This leads to the demarcation of the AJ and the apical membrane in the developing photoreceptor cells (Walther and Pichaud 2010) or the AJ and basolateral part of the egg chambers follicular epithelial cells (Morais-de-Sa, Mirouse et al. 2010), thus ensuring epithelial cell polarity.

c. The Crb complex

i. Crumbs complex description

Crumbs (Crb) is a transmembrane protein that regulates apical epithelial polarity (Tepass and Knust 1990, Tepass, Theres et al. 1990). It is localized just above the AJ as demonstrated by the TEM approach (Tepass 1996). Crb possesses a large extracellular domain composed of 29 epidermal growth factor (EGF)-like repeats with four laminin A globular domain-like repeats and a small cytoplasmic portion of 37 amino acids containing a 4.1/Ezrin/Radixin/Moesin (FERM)-domain binding motif and a C-terminal-PDZ-domain binding motif ERLI.

Crb interacts with many proteins, some of which are part of the core components of the *Drosophila* Crb complex. Firstly, Stardust (Sdt) is a cytosolic Membrane-

Associated Guanylate Kinase Homologs (MAGUK) protein that binds Crb via its PDZ domain (Bachmann, Schneider et al. 2001, Hong, Stronach et al. 2001). Secondly, the group of core components also includes PATJ (Protein Associated with Tight Junction; formerly known as Disc Lost) which is a multiple PDZ domains cytosolic protein that interacts with Crb via its binding to Sdt using its Lin-2/Lin-7 (L27) domain (Roh, Makarova et al. 2002). The last component is a small protein called Lin7 with a C-terminal PDZ domain (Bachmann, Timmer et al. 2004) and it also binds Sdt via the Lin27 domain (Bulgakova, Kempkens et al. 2008).

ii. Crumbs functions and regulations

As previously stated, the Crumbs complex was discovered for its role in establishing and maintaining the apical polarity of epithelial cells. Indeed, during the embryonic development of the Drosophila, upon formation of AJs via Baz, Crb is recruited by the former and is needed to maintain Baz at its apical position (Bilder, Schober et al. 2003, Tanentzapf and Tepass 2003). Mutants lacking either Crb or Sdt will fail to establish proper AJs or maintain cell polarity, which leads to major epidermis defects (Tepass, Theres et al. 1990, Grawe, Wodarz et al. 1996, Tepass 1996). More particularly, loss of Crb leads to disruption of the apical membrane character (Wodarz, Grawe et al. 1993). Conversely, its overexpression increases the apical size associated with the reduced baso-lateral domain in epidermal cells of embryos (Wodarz, Hinz et al. 1995) as well as photoreceptor cells (Pellikka, Tanentzapf et al. 2002, Richard, Muschalik et al. 2009, Muschalik and Knust 2011). However, the protein Crb is not always required to establish polarity, as shown in the Malpighian tubules (Campbell, Knust et al. 2009), the imaginal discs (Pellikka, Tanentzapf et al. 2002) or the epidermis of embryos (Tanentzapf and Tepass 2003). Crb is also involved in the regulation of the PAR complex since it interacts with Par-6 via its PDZ domain in the pupal photoreceptor (Nam and Choi 2003, Walther and Pichaud 2010), recruiting the PAR complex to specify the Zonula Adherens (similar to AJ) site from the rest of the cell. Therefore, Crb one of the major regulators of eye morphogenesis in *Drosophila*.

Most of those effects are mediated by the small intracellular part of Crb, as highlighted by the fact that the intracellular part of Crb could rescue the polarity phenotype of *crb* mutant in the embryo or because overexpression of the Crb intracellular part phenocopies the apical domain expansion. More particularly concerning the cytosolic

portion, it interacts with aPKC (Sotillos, Diaz-Meco et al. 2004), Moesin/βH-spectrin (Medina, Williams et al. 2002), Expanded (Ling, Zheng et al. 2010) and Yurt (Laprise, Beronja et al. 2006), regulating both the cytoskeleton organisation and epithelial cell morphogenesis in embryos. Crb also binds to the extracellular part of the Notch receptor, regulating its interaction with its ligand Delta (Ohata, Aoki et al. 2011).

Moreover, during the salivary gland placode formation in the Drosophila embryo, Crb anisotropic localisation has been reported to mediate the formation of the non-muscle Myosin II (NMY-II) cable surrounding the placode via the modulation of the time residency of Rho-kinase (Rok) , an activator of NMY-II, at the plasma membrane (Roper 2012). This mechanism appears to rely on the recruitment of the kinase Pak1 which phosphorylates Rok and reduces its presence at the membrane (Sidor, Stevens et al. 2020). Pak1 is previously recruited by the Crb/Par-6/Cdc42 complex **(Figure 2).**

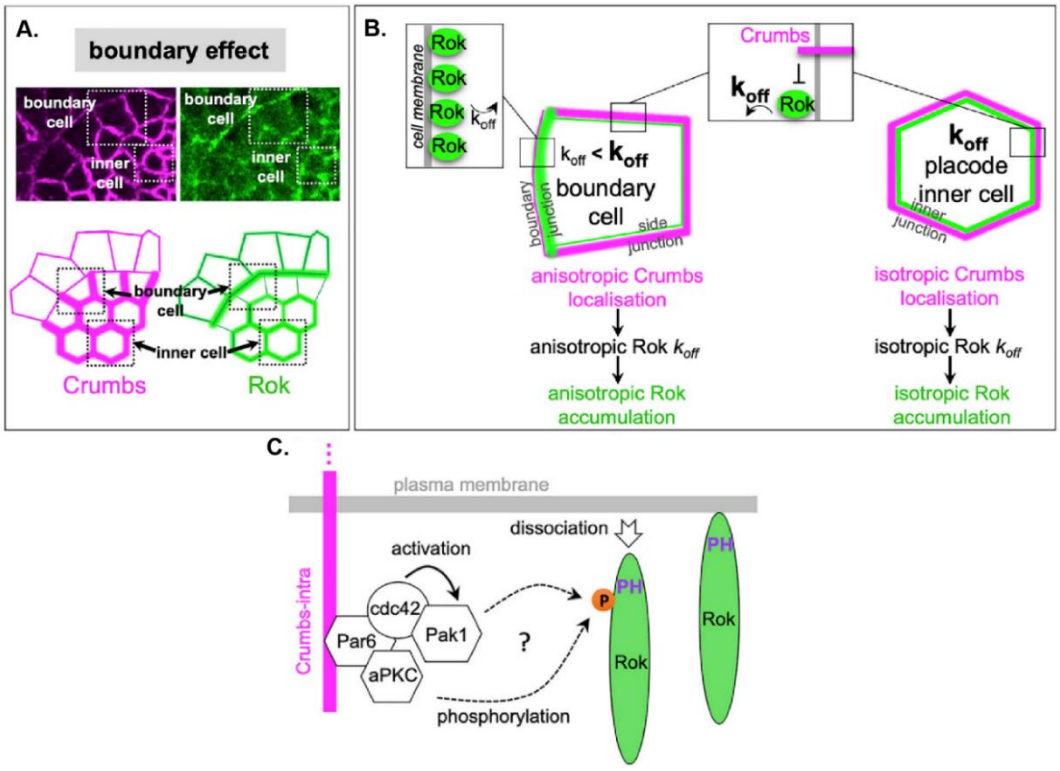

Figure 2. Crumbs regulation of Rok presence in the placode epithelial cells of Drosophila. **A.** Representation of the boundary effect. mNG-Rok has an isotropic distribution at the centre of the placode due to Crb isotropic distribution. On the contrary, at the boundary where Crb is present in an isotropic manner, the negative regulatory effect applied by Crb on Rok leads to mNG-Rok enrichment at the boundary and lower mNG-Rok signal where Crb is enriched. **B.** Model explaining how differences in the local level of Crb modulating Rok presence time at the membrane conducts to Rok isotropic distribution where Crb is isotropic and planar polarisation of Rok where Crb's distribution is anisotropic. **C.** Scheme representing the intracellular part of Crb that is linked to two kinases, Pak1 and aPKC, known to phosphorylate Rok and regulate its presence at the membrane. Adapted from (Sidor, Stevens et al. 2020)

Moreover, it has recently emerged that the extracellular domain of Crb also has an important role. Specifically, the Crb extracellular part mediates homophilic interactions, favouring the recruitment of other Crb proteins at the membrane, hence producing more Crb/aPKC complexes where aPKC phosphorylates Crb. This process was first shown in (Sotillos, Diaz-Meco et al. 2004), and prevents it from being internalized for recycling in the follicular cells of the egg chamber (Fletcher, Lucas et al. 2012). Furthermore, overexpressing a form of Crb devoid of its intracellular part shows normal localisation at the apical part, suggesting that the extracellular part is sufficient to establish homophilic interaction. However, expressing only the transmembrane with the intracellular part of the protein leads to substantial endocytosis of Crb, which suggests that the extracellular part is required for Crb localisation and stabilisation at the apical domain via *cis* interaction (Letizia, Ricardo et al. 2013).

One can regulate Crb through its phosphorylation as demonstrated, but it can also be regulated via trafficking pathways. In the imaginal disc epithelium, Crb is known to be internalized at the membrane via the syntaxin protein Avalanche and the Rab5 protein (Lu and Bilder 2005). Another study of (Roeth, Sawyer et al. 2009) shows that in embryo epidermis Rab11, a marker for recycling endosomes, is also required for Crb localisation at the apical level. The Exocyst complex, a multisubunit protein complex

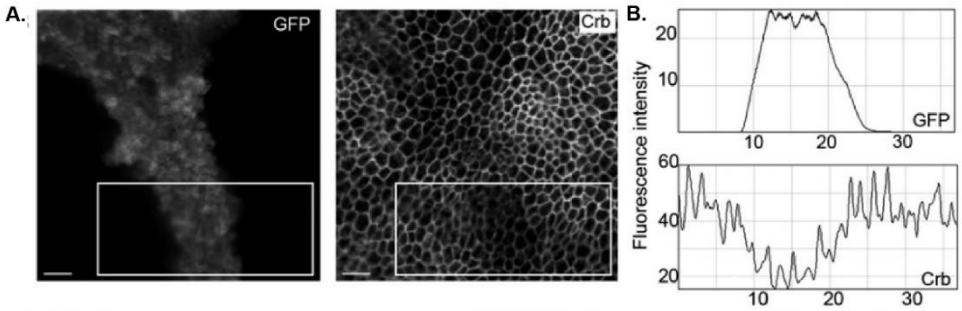

Figure 3. Crumbs relies on Retromer complex for proper apical localisation in imaginal wing discs. A. Third-instar wing discs stained with Crb antibody and displaying clonal cells lacking Vps35, identified via GFP marking. **B.** Profile plot extracted from the boxed region in A., which shows the depletion of Crb signal in the region of the wing disc devoid of Vps35. Adapted from (Pocha, Wassmer et al. 2011)

that plays a role in tethering vesicles to the plasma membrane, also regulates Crb. Loss of Exo84, a component of the Exocyst complex, leads to loss of Crb at the apical surface, in both embryo epidermis (Blankenship, Fuller et al. 2007) and renal tubules (Campbell, Knust et al. 2009). The protein Cdc42 also ensures Crb endocytosis via the Par complex (Harris and Tepass 2008) and Cdc42 by stabilizing Par6 at the apical

membrane in photoreceptor cells, ensures Crb stability via Par6-aPKC binding (Nunes de Almeida, Walther et al. 2019).

Moreover, Crb relies on the retromer complex activity, a complex involved in the transport of proteins from endosomes/multivesicular bodies to the trans-Golgi network. In two different studies using the wing discs, follicle cells and embryos, Crb has been shown to interact with the retromer protein Vps35 and cells mutant for retromer core complex display the lowest signal at their apical part (Pocha, Wassmer et al. 2011, Zhou, Wu et al. 2011) **(Figure 3).** Cells mutant for retromer show similar phenotypes to the *crb* mutant, such as disruption of epithelial polarity, which confirms the importance of retromer action on Crb maintenance.

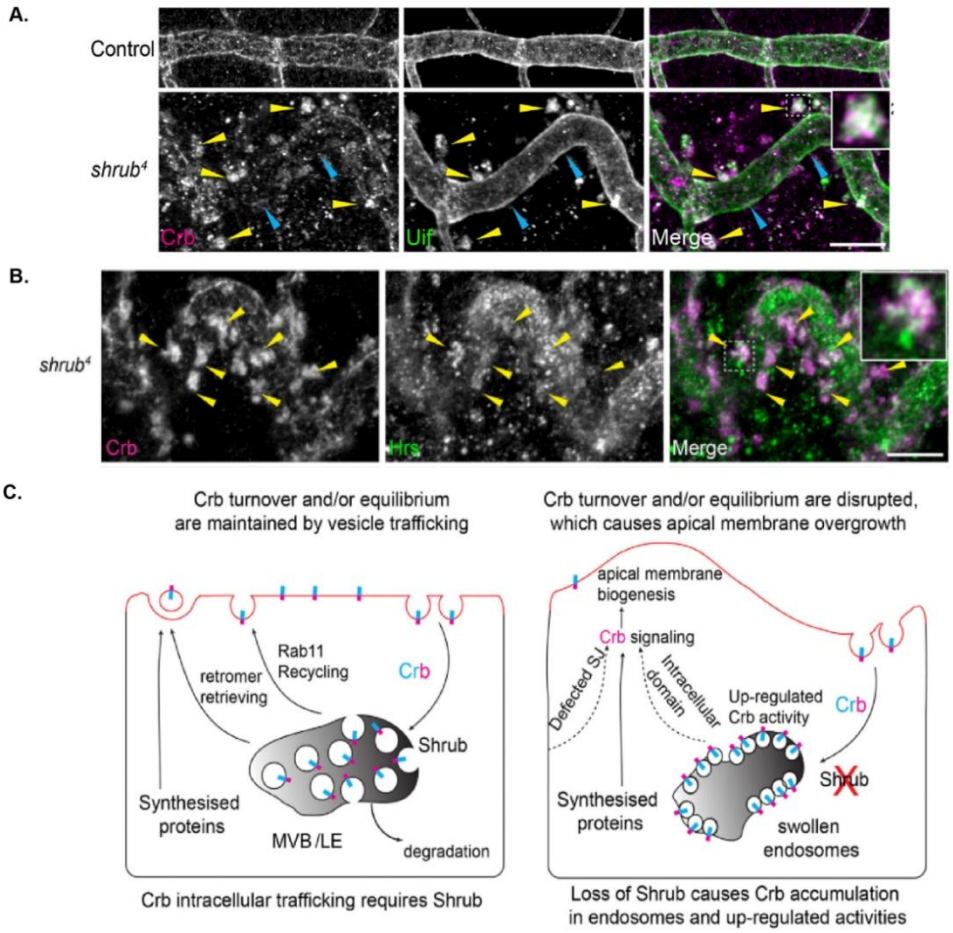

Figure 4. Shrub regulating Crumbs localisation and activity, controls trachea length and morphology during Drosophila embryo development. A. WT and shrb mutant embryos trachea stained for Crb and Uninflatable (Uif). Loss of Shrb leads to over elongated and sinuous trachea compared to WT situation. Crb is accumulated into cytoplasm (yellow arrows) and is quasi absent from local apical region (blue arrows). **B.** Shrb embryos mutant tracheal cells display Crb accumulation in the cytoplasm, more precisely in multivesicular bodies colocalizing with ESCRT-0 protein HRS. **C.** Scheme of how Shrb, by regulating Crb activity and presence via intracellular trafficking, controls trachea epithelial apical membrane size and therefore, trachea length and morphology. Adapted from (Dong, Hannezo et al. 2014)

Another recent study identified a new partner of Crb named Apnoia, a transmembrane protein that interacts physically with Crb (Skouloudaki, Papadopoulos et al. 2019). The knockout of Apnoia leads to over elongated *Drosophila* embryos trachea associated with Crb being trapped in enlarged Vps35 vesicles, a phenotype reminiscent of the one observed with the loss of the Endosomal sorting complexes required for transport (ESCRT) III component Shrub/Vps32, where Crb accumulates in endosomes of tracheal mutant cells (Dong, Hannezo et al. 2014). Indeed, loss of Shrub leads to Crb accumulation into early endosomes/ multivesicular bodies associated with the tracheal defects. As stated by the authors, this atypical Crb localisation induces apical cell domain overgrowth **(Figure 4).** Notably, similar phenotypes in the trachea are observed in several mutants for SJ components, raising the possibility of analogies in the underlying causal as presented in the following chapters.

Another component involved in Crb regulation is the SJ protein Yurt, which is discussed further in the pSJ section. Studies show that Yurt regulates the determination of the apico-basal domain, notably through Crb regulation. Indeed, during embryonic development, Yurt antagonizes Crb at the basolateral part and restricts it at the apical level. Once present at the apical level, Crb activity is then regulated by Yurt which prevents apical domain overgrowth (Laprise, Beronja et al. 2006, Laprise, Lau et al. 2009, Gamblin, Hardy et al. 2014). To bind Crb, Yurt has to oligomerize, which is prevented by the phosphorylation of Yurt by aPKC, adding another layer of complexity to Crb regulation (Gamblin, Parent-Prevost et al. 2018).

d. <u>The Scrib complex</u>

The last polarity complex is the Scrib complex, formed by three proteins namely Scrib, Discs-Large (Dlg) and Lethal Giant Larvae (Lgl). Scrib is a scaffold protein containing 16 Leucine-Rich Repeats domains (LRR) at the N-terminal part followed by two Leukaemia-associated-protein (LAP) domains and four PDZ domains, which are involved in its proper localisation at the baso-lateral part of the cell (Bonello and Peifer 2019). The next chapters describe Dlg and Lgl since they are part of the SJ. Scrib binds its partner Lgl via the LRR domain (Kallay, McNickle et al. 2006) and is in association with Dlg via the binding of the protein, GUK-holder (Mathew, Gramates et al. 2002). GUK-holder also shows direct binding to the Scrib PDZ-domain (Caria, Magtoto et al. 2018). The Scrib module acts as an antagonist of Par and Crb

complexes. Scrib represses Baz activity to promote basolateral identity and on the other hand, Crb inhibits Scrib activity (Bilder, Schober et al. 2003, Tanentzapf and Tepass 2003). Therefore, this tight interplay regulates the polarity of mature epithelial cells. Moreover, loss of Scrib disrupts SJ organisation in wing discs epithelial cells as well as in the hindgut (Zeitler, Hsu et al. 2004).

e. Conclusion

This chapter described how epithelial cell polarity is established and how it is preserved among mature epithelia. We were able to observe that not only are polarity proteins involved in polarity processes but they are also involved in many different activities as highlighted by the example of Crb.

Chapter II: Adherens junctions and cellular cytoskeleton

a. Generalities

As previously described, epithelial cells display different junctions. Among them, the Adherens Junction (AJ) is characterized by its role in the mechanical barrier of the tissue. These peculiar junctions, responsible for cell-cell adhesion and localized apically, consist of transmembrane proteins such as the *Drosophila* gene called shotgun and referred here as DE-Cadherin (DE-Cad). This protein mediates *trans* and *cis* homophilic interactions via its extracellular domains and is connected to the adjacent cytoskeleton by its intracellular part via the Catenin proteins family.

Briefly, during a process called cellularisation, when the first embryonic epithelium is formed, clusters of D-Ecad and Catenin appear at the tip of apical cellular protrusions enriched in actin (Harris, Sawyer et al. 2009). Those clusters then move to a lower position and grow as spot AJs with the help of the scaffold protein Baz which localizes at the membrane closed to centrosomes at this stage (Harris and Peifer 2005). After cellularisation, gastrulation occurs and the spot AJs move toward a more apical localisation in the cell, where they are enriched and form a belt like structure associated with actin. This event requires both the activity of aPKC to detach spot AJs from Baz and the activity of Crb to establish the link with the underlying actin complex (Harris, Sawyer et al. 2009, Tepass 2012). Additional factors come into play during AJ

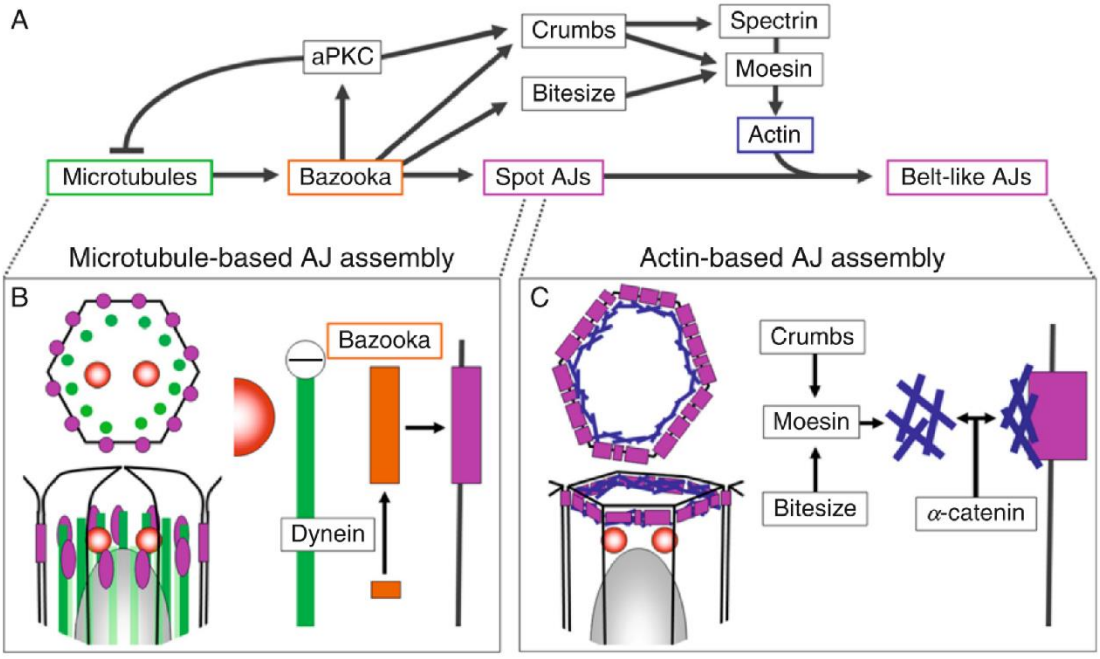

Figure 5. Adherens junction establishment in the Drosophila epithelial cells. A. Pathway showing the different proteins involved in regulating the Adherens Junction establishment. **B.** Microtubules and associated protein Dynein localize spots AJs (violet ellipses) close to centrosomes (red circles) and microtubules minus end via interaction with Bazooka. **C.** Adherens junction maturation into belt like structure (violet rectangles) occurs as a result of their links with actin cytoskeleton (blue lines) and the help of the Crumbs complex and Bitesize. As maturation happens, Adherens junctions start connecting to the adjacent actin cytoskeleton via α-catenin. Adapted from (Harris, Sawyer et al. 2009)

establishment such as the actin cytoskeleton organizers and linkers Bitesize, Spectrins (e.g. the β-heavy Spectrin named Karst in the *Drosophila*) and Moesin **(Figure 5).** Once established, AJs remain dynamic and require different actors of endocytosis/intracellular trafficking to cope with the different morphological events that occur during the individual's life.

b. DE-Cadherin complex and its partners

i. DE-cadherin complex

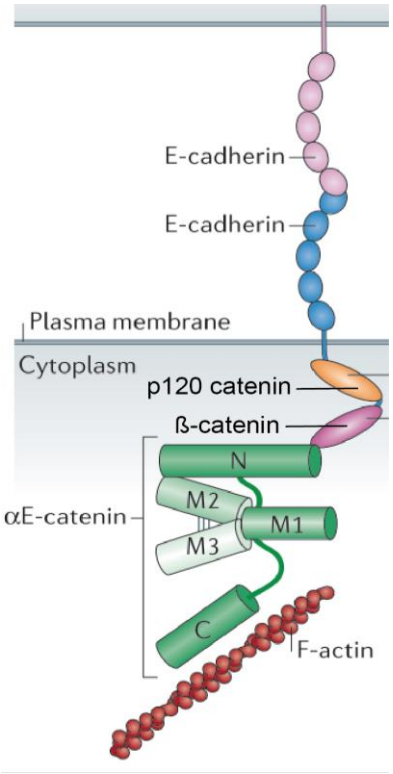

DE-cad, the main component of AJs, is a transmembrane protein composed of seven Extracellular Cadherin domains (five in the mammals), which mediate *cis* and *trans* homophilic interactions via Ca^{2+} binding mechanism, one Laminin G domain and an intracellular part attached to Catenin proteins (Meng and Takeichi 2009, Shapiro and Weis 2009). More specifically, DE-Cad binds via its C-terminal intra cytoplasmic part to the proteins p120-catenin and Armadillo (the Drosophila β-catenin) which in turn associate with the actin-binding protein α-catenin, forming the so-called core complex E-cadherin/ β-catenin/ α-catenin **(Figure 6).**

Figure 6. E-Cadherin complex. Model of the E-cadherin displaying its EC domains whose mediate binding in trans to another E-cad molecule. E-cadherin binds via its intracellular part the p120-catenin and β-catenin which in turn binds α-catenin linked to F-actin. Adapted from (Takeichi 2014)

AJs appear in a form of DE-Cad clusters with different sizes and mobility along the plasma membrane and are regulated by the juxtaposed F-actin/NMY-II network that exerts mechanical forces (Lecuit and Yap 2015). α-catenin operates conformational

changes on forces produced by the acto-myosin cytoskeleton, which initiates a reinforced DE-Cad binding state (Yonemura, Wada et al. 2010). α-catenin is not the only link to the adjacent cytoskeleton since in mature epithelia, Vinculin (Vinc), a key mechano-effector of the cell, participates in actin-binding via NMY-II activity (le Duc, Shi et al. 2010) **(Figure 7).** Indeed, the "open" conformation of the α-catenin triggers by increased tension is stabilized by Vinc which strengthens the AJ, associated with slower turnover of NMY-II at AJ level (Charras and Yap 2018).

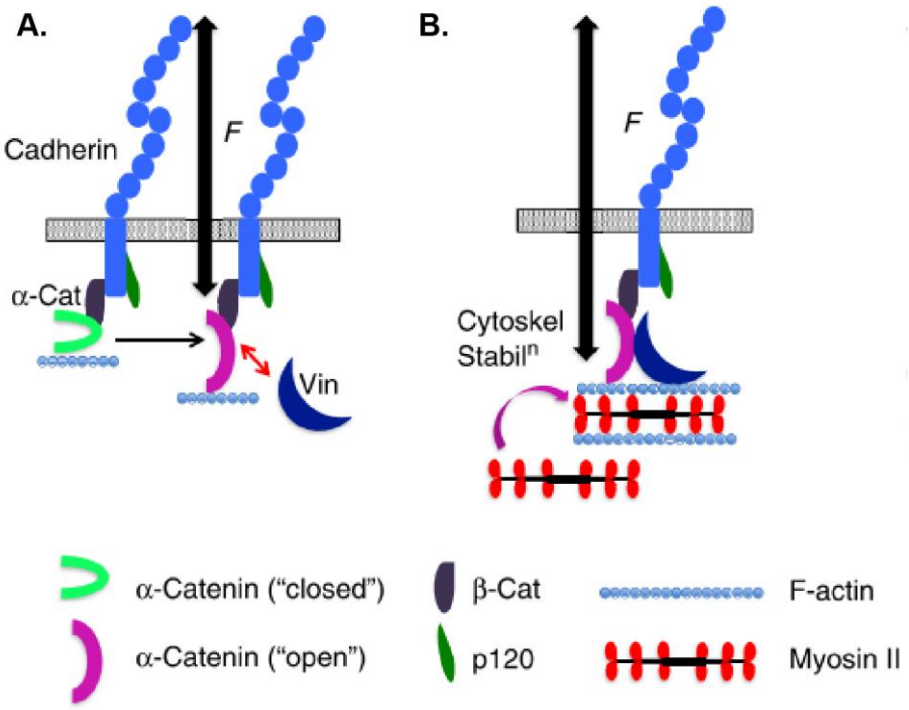

Figure 7. Tension sensible adaptation of Adherens junctions. A. E-cad/α-cat complex senses tension, which leads to α-cat opened conformation and recruitment of Vinculin. **B.** Continuous applied tension, transmitted to acto-myosin cytoskeleton, changes proteins dynamics such as the NMY-II turnover as illustrated here. Adapted from (Charras and Yap 2018)

Moreover, external forces applied to AJs show an active remodelling and changing of their composition in a tension-dependent manner (Hoffman and Yap 2015, Lecuit and Yap 2015), demonstrating that AJs are key platforms to integrate and transmit information in response to different mechanical inputs. All of these forces act during processes such as cell-cell contact rearrangements or cell geometry regulation and those mechanisms require additional partners which are described in the next part **(Figure 8).**

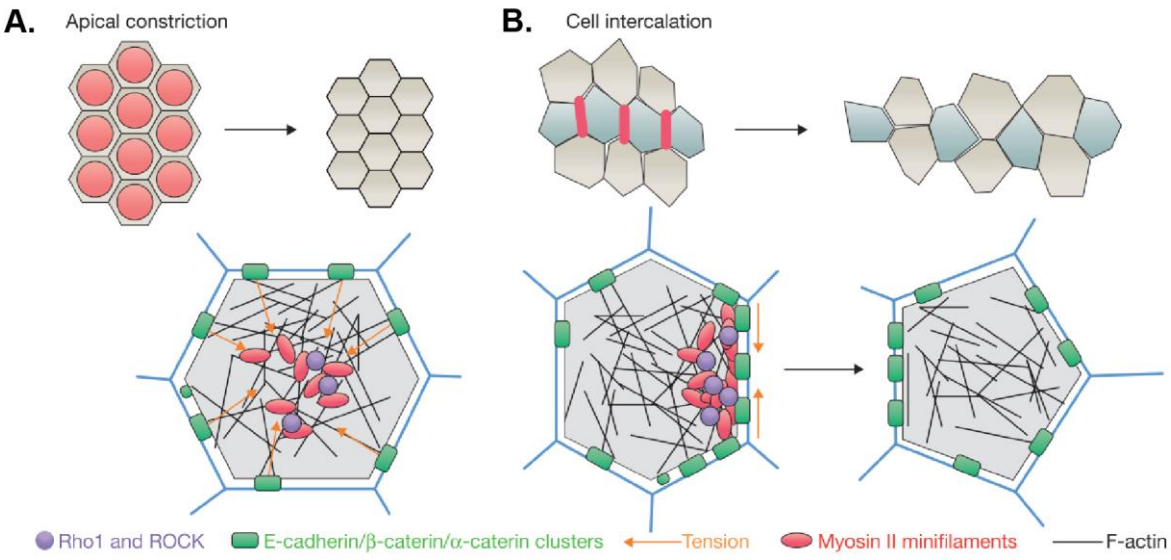

Figure 8. Apical constriction and cell intercalation. A. Pulsatile acto-myosin contraction forces, controlled by Rho1 and ROCK kinases activity, leads to apical domain size shrinkage, because of their connections with the adjacent E-Cad/α-cat complex. **B.** During cell intercalation, anisotropic contraction of AJ junction, mediated by acto-myosin activity, conducts to cell vertical junction (red line) shrinkage. This process requires forces to be transmitted to E-cad/α-cat clusters. Cell intercalation allows neighbours exchange and is involved during tissue elongation. Adapted from (Lecuit and Yap 2015)

ii. Partners of DE-Cad complex

Canoe (Cno; Afadin in mammals) is a PDZ domain, actin-binding scaffold protein required during epithelial morphogenesis (Mandai, Nakanishi et al. 1997, Sawyer, Harris et al. 2009). Cno binds to Echinoid (Wei, Escudero et al. 2005), α-catenin (Pokutta, Drees et al. 2002) but also Polychaetoid (Pyd; which is the mammalian orthologous of the tight junction protein ZO-1)(Takahashi, Matsuo et al. 1998) and the Ras subfamily GTPase Rap1 (Boettner, Harjes et al. 2003). The following study (Choi, Harris et al. 2013) states that in *Drosophila* embryos, Cno is already targeted to the specific egg plasma membrane. Moreover, Rap1, which localizes Cno with the help of F-actin (Sawyer, Harris et al. 2009) **(Figure 9),** together with Cno mediate Baz apical

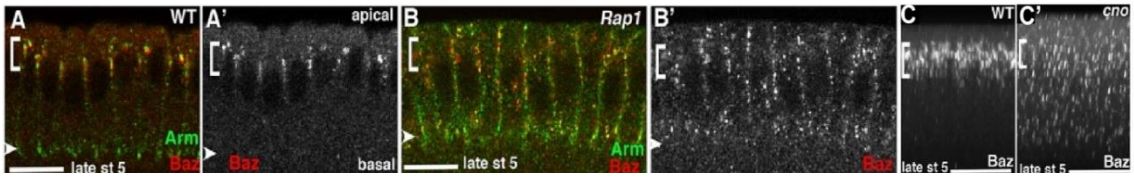

Figure 9. Rap1 and Canoe are required to localize Baz during Adherens junction's establishment. A-A'. Stage 5 embryos stained for Armadillo (Arm; β-catenin; green) and Baz (red; white in A', B' and C') in WT conditions. Baz is restricted at the apical part (white brackets) on the contrary of Rap1 embryos in **B, B'**, where Baz is spreading at the lateral membrane. Similar results are observed upon loss of Cno in **C, C'**. Adapted from (Choi, Harris et al. 2013)

restriction, making them key players in the apico-basal polarity formation (Choi, Harris et al. 2013, Bonello, Perez-Vale et al. 2018). Similar results appear in the pupal photoreceptors, where Cno, with the assistance of the kinase Mushroom bodies tiny, restrains Baz at the AJ level, leading to a proper Zonula Adherens establishment (Walther, Burki et al. 2018). Furthermore, in *cno* mutant, AJs maintenance is impaired since apical acto-myosin network constriction during mesoderm invagination is uncoupled from cell apical constriction, which demonstrates the importance of Cno to mediate AJ links to the acto-myosin network (Sawyer, Harris et al. 2009). Further works reveal the importance of Cno in maintaining epithelial tissue integrity via the junctional-cytoskeletal linkage during morphogenetic events such as the germband extension or dorsal closure (Sawyer, Choi et al. 2011, Choi, Harris et al. 2013, Manning, Perez-Vale et al. 2019).

Interestingly, Cno is shown to be enriched at Tricellular contacts during cellularisation, both at AJ level and 2 µm below AJ level with a pool of F-actin. Then during gastrulation when AJs are established, Cno still localizes at AJ level and is enriched at Tricellular contacts, colocalizing with an enriched subset of F-actin at the vertex (Sawyer, Harris et al. 2009) **(Figure 10).**

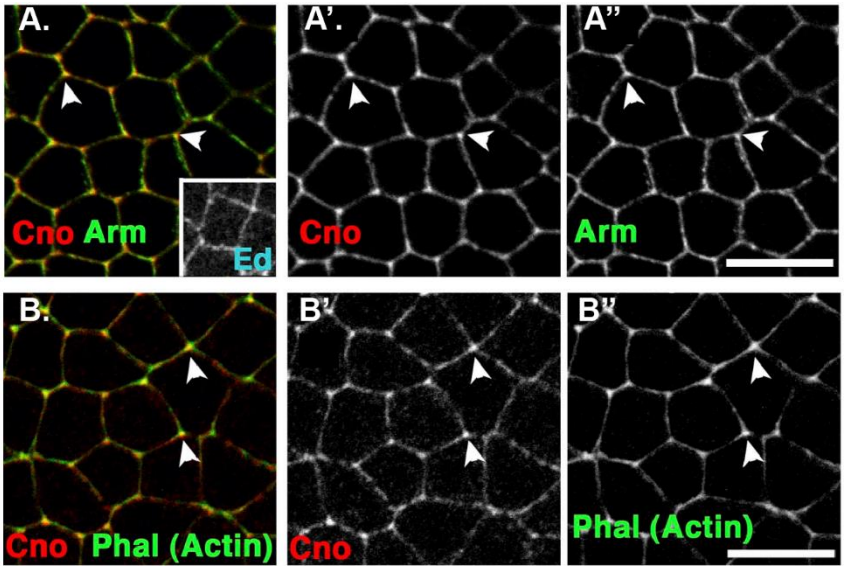

Figure 10. Canoe is enriched at TCJ with actin during Adherens junction establishment. A-A''. Cno (red; white in A') is enriched at TCJ (white arrows) at AJ level marked by Arm (β-cat; green; white in A'') at mid-gastrulation. Small close up shows Echinoid (Ed), partner of Cno. **B-B''.** A sub pool of actin (marked by Phalloidin; green; white in B'') is enriched at TCJ and colocalizes with Cno during gastrulation. Adapted from (Sawyer, Harris et al. 2009)

This vertex specific enrichment at the end of cellularisation relies on Rap1 activity regulated by the specific Rho-Guanine nucleotide exchange factors (GEF) known as Rap1GEF Dzy (Bonello, Perez-Vale et al. 2018). Moreover, it was recently discovered that Cno binds the specialised Tricellular Adherens Junction protein Sidekick, which is discussed further in the Tricellular Junctions chapter of the manuscript. This link mediates the special enrichment of Cno at the vertex, which, in turn, allows a specialised actin organisation network at three cells contact, a key feature in regulating cell-cell contact rearrangements (Letizia, He et al. 2019).

Similar to Vinc and Cno, α-Actinin (Actn) is an F-actin binding scaffold protein from the superfamily of the Spectrin, organizing the cytoskeleton by playing a cross-linker role both in muscle (Clark, McElhinny et al. 2002) and non-muscle cell types (Otey and Carpen 2004). It also binds to AJs via α-catenin or binds to AJs partner proteins such as Vinc (Otey and Carpen 2004). In non-muscle cell types, Actn is known to localize at many places in the cell such as lamellipodia, cell-cell and cell-matrix contacts as well as the stress fibres, which are anchored at focal adhesions where cells connect with the Extracellular Matrix via Integrins, both of which are found *in vitro* cultured cells and *in vivo*. Moreover, in the case of stress fibres, it has been shown in (Lopez-Gay, Nunley et al. 2020) that in the *Drosophila notum*, apical stress fibres form and disappear at/or close to Tricellular contacts at the AJ level. They facilitate cell and tissue elongation and regulate cell proliferation by clustering proteins at their tip, such as Ajuba, members of the key Hippo/YAP-pathway.

This pathway involves many different proteins, more than 40 reported to date, including the core component kinases Hippo (Homologous of human MST1 and MST2), Salvador (Human SAV1), Mob as tumour suppressor (Human MOBKL1), the FERM-domain protein Expanded and its partner Kibra and Merlin, Warts (Human LATS1 and LATS2) and the transcriptional coactivator protein Yorkie (Human YAP and TAZ). The Hippo/YAP pathway relies on many inputs from different parts of the cells with different actors, such as the planar cell polarity proteins Fat and Dachsous, but also apico-basal polarity proteins such as Crb, L(2)gl, Scrib and Par-1 (Fulford, Tapon et al. 2018, Misra and Irvine 2018, Manning, Kroeger et al. 2020). The Hippo kinase phosphorylates and activates the protein Warts, which then recruits Yorkie and phosphorylates it. Once phosphorylated, Yorkie is prevented from binding its DNA targets, such as the

transcriptional factor Scalloped, by being kept in the cytoplasm. However, if Hippo is deactivated, Yorkie becomes functional and induces the transcription of genes involved in cell proliferation and inhibition of apoptosis (Huang, Wu et al. 2005) **(Figure 11).**

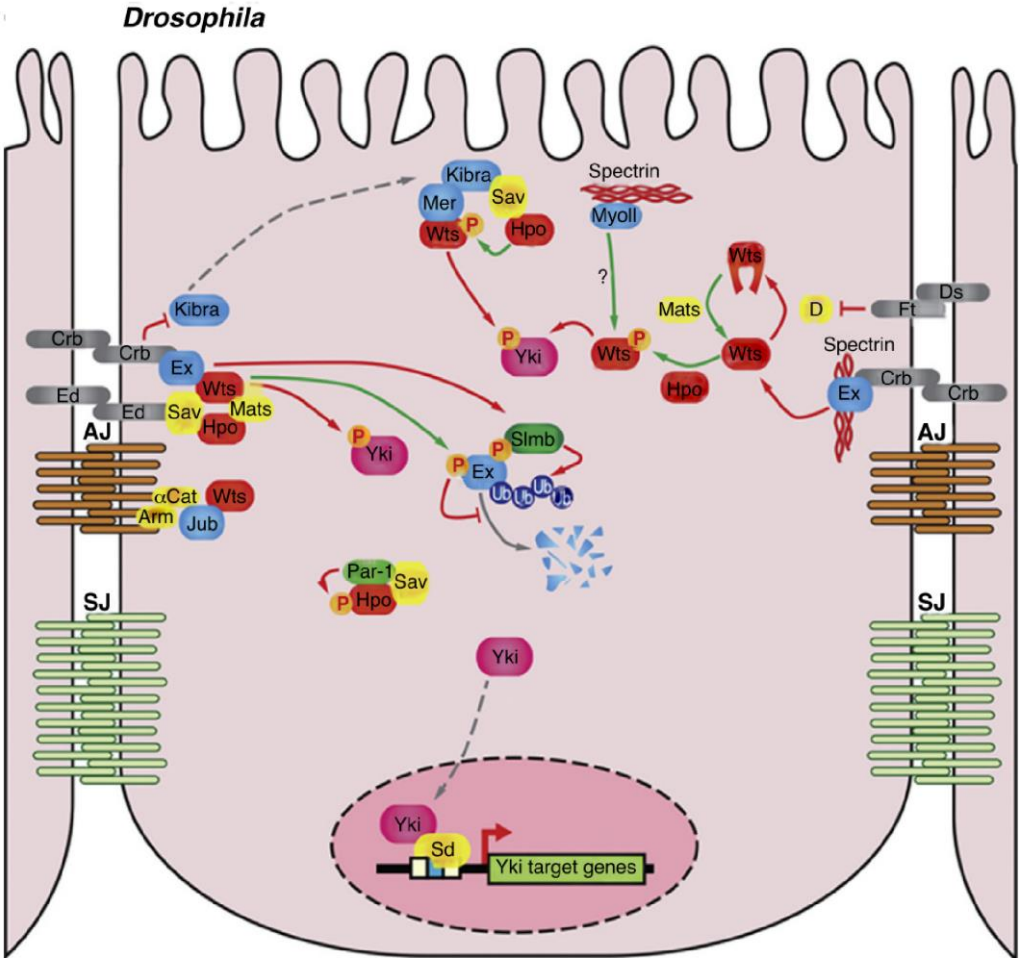

Figure 11. Overall view of the Hippo/YAP pathway regulators. AJ and SJ represent adherens and septate junctions respectively. Adapted from (Fulford, Tapon et al. 2018)

A key player in this pathway is the Warts binding partner Ajuba LIM protein (Jub), as mentioned. This is a force-sensitive protein that localizes at AJs. When mechanical tension mediated by the NMY-II increases, Jub is recruited to AJs via α-catenin and retains Warts at this site, preventing it from phosphorylating Yorkie, which promotes Hippo/YAP pathway activation and, therefore, cell proliferation (Rauskolb, Sun et al. 2014, Alegot, Markosian et al. 2019). Jub is also involved in AJs remodelling during morphogenesis in *Drosophila* embryos, being required at AJs when adhesion is low or when the contractility of NMY-II increases (Razzell, Bustillo et al. 2018)

c. The Acto-Myosin complex

i. Actin cytoskeleton

The Actin cytoskeleton could be regarded as the ensemble of actin filaments with their associate partners. It is the main actor of the cell mechanical apparatus that is associated with pulling or pushing forces, cell migration and, control of cell shape, ensuring organelles and intracellular traffic, as well as mechanical properties of the cell surface and cell adhesion (Svitkina 2018). .

Actin is a highly conserved protein, ranging from bacteria to metazoans, which can polymerize into filaments, forming one of the three major cytoskeleton components. Actin monomers (referred to as G-actin) can bind ATP or ADP and associate spontaneously with other G-actin, initiating as a trimer and then forming a mini filament with slow pointed-end growth and rapid barbed-end growth. This form of Actin is known as filamentous Actin or F-actin. On the other hand, depolymerisation of F-actin could occur once ATP hydrolysis occurred in the actin microfilament, leading to a less stable microfilament and therefore the release of G-actin binding ADP (Pollard 2016). G-actin could be bound by a protein named Profilin, which regulates F-actin polymerisation/depolymerisation. Moreover, F-actin could be severed by proteins such as Gelsolin proteins family or Cofilin (named Twinstar in *Drosophila*).

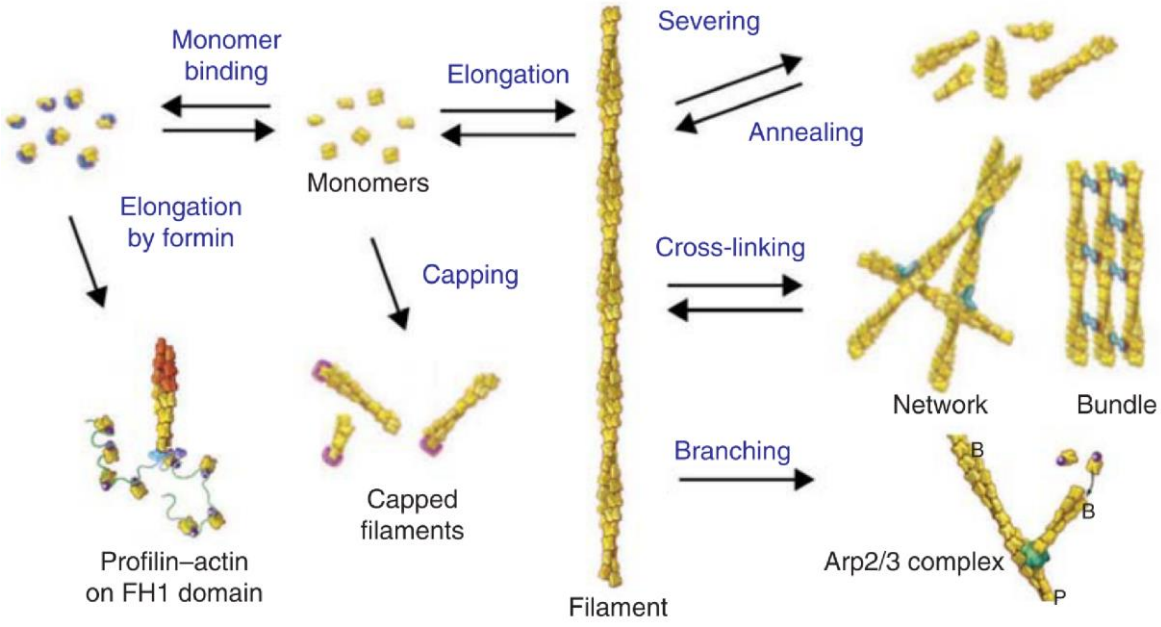

Figure 12. Scheme showing different actin organisation and families of actin-binding proteins such as polymerases formins, capping, severing, cross-linking proteins and branching protein ARP2/3 complex. Adapted from (Pollard 2016)

In addition to its ability to polymerize spontaneously, different proteins participate in F-actin nucleation, such as the seven-protein actin-related protein 2/3 (ARP2/3) complex. This complex initiates the polymerisation of a new F-actin “daughter” branch that was linked to a previous F-actin “mother” microfilament and it binds the daughter filament at the pointed-end (Pollard 2016) **(Figure 12)**.

Furthermore, F-actin can be organized into different states because of the action of actin bundlers such as Fascin and Plastin, as well as cross-linkers such as Filamin or the previously described Actn. Those differential networks of organized F-actin can take the form of dendritic network, which mediates by the ARP2/3 complex and, creates pushing forces at the plasma membrane level **(Figure 13).**

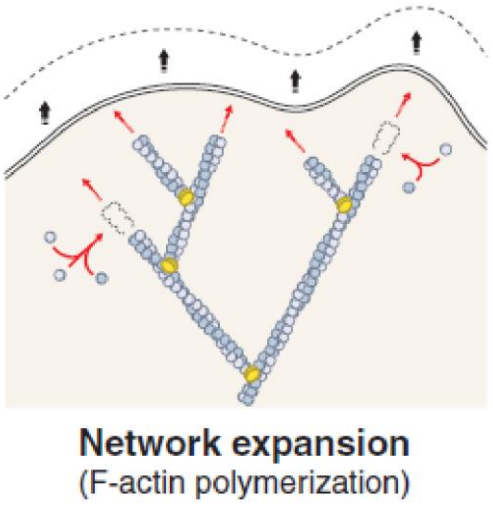

Figure 13. Scheme representing the pushing forces exert on the plasma membrane by actin polymerisation in a branched actin network. Adapted from (Clarke and Martin 2021)

It could also exist as linear actin bundles as a result of Formins action, making uniform or non-uniform polarity bundles as well as isotropic networks made of crosslinked F-actin filaments with both the action of Formins and ARP2/3 (Skau and Waterman 2015). The latter is found at the cell cortex which binds plasma membrane via Ezrin/Radixin/Moesin (ERM) proteins, shaping the cell and allowing it to deform, adapt and propagate mechanical

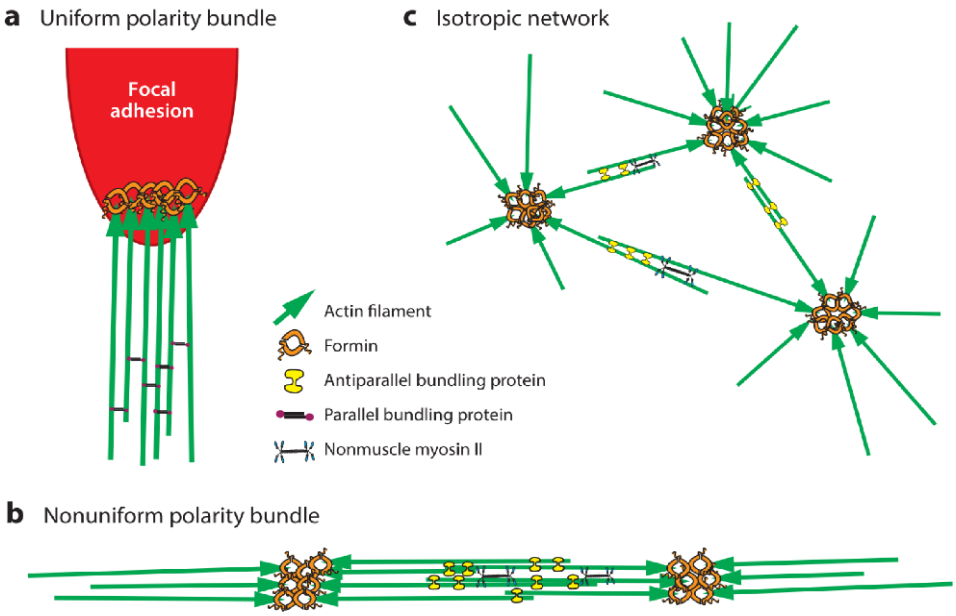

Figure 14. Scheme representing different actin network organisations. A. Linear, polar oriented and parallel actin fibres, as a result of Formin, are connected to focal adhesion. Specific crosslinkers for similar oriented actin fibres are depicted. **B.** Formins back-to-back arrangement allows antiparallel and non-uniform polarity bundles formation. NMY-II and crosslinkers are connected to actin fibres. **C.** Specific back-to-back localisations of Formins generate an isotropic network of actin, which is connected to NMY-II and specific actin crosslinkers. Adapted from (Skau and Waterman 2015)

forces to its neighbours **(Figure 14).** More precisely, key players of this cortex tension are the molecular motors Non-Muscle Myosin II, which pull on F-actin.

ii. Non-muscle Myosin II and its regulators

NMY-II is a heterooligomer composed of two heavy chains (called Zipper in the *Drosophila*), two regulatory light chains involve in regulating NMY-II action (RLC; named Spaghetti Squash in the *Drosophila*) and two essential light chains. NMY-II molecules are organized in the following manner: one globular head domain binding ATP and Actin is linked to the neck region formed by the essential light chain which with RLC is connected to the long α-helical coiled-coil rod domain made by the heavy chain. NMY-II molecules exist as a dimer since the heavy chain interacts with another one, leading to the creation of the hexa-peptide molecule already mentioned. When not

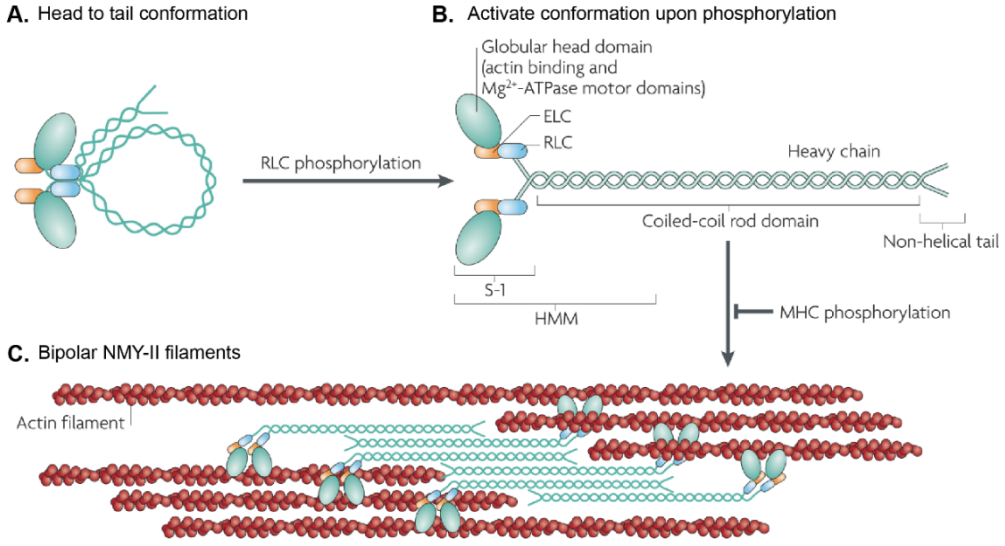

Figure 15. Subunit and domain structure of non-muscle myosin II. A. In the absence of regulatory light chains (RLC; blue ellipses) phosphorylation, NMY-II forms a compact molecule through a head to tail interaction. It could not bind another NMY-II monomer. When RLC is phosphorylated, the compact structure unfolds and binds another NMY-II monomer through its coiled-coil rod domain as depicted in **B.** Essential light chains (ELC; orange ellipses)) with RLC bind the Heavy chains (green ellipses). **C.** NMY-II proteins form bipolar filaments that bind actin via the Head domain. The ATP-ase activity of the Head domain allows it to change its conformation, therefore exerting forces on actin fibres that move in an antiparallel way. Adapted from (Vicente-Manzanares, Ma et al. 2009)

activate, this NMY-II dimer exists in a head-to-tail conformation, preventing it from interacting with other NMY-II dimers.

Upon phosphorylation of the RLC, NMY-II operates a change in its configuration and can bind Actin via its head and form bipolar filaments. Using the ATP-ase activity of the head, NMY-II will achieve conformational switches that enable to move Actin micro-filaments in an anti-parallel way (Vicente-Manzanares, Ma et al. 2009) **(Figure 15).**

The key event to regulate NMY-II is, as demonstrated, phosphorylation of RLC. Many different kinases are known to participate in this mechanism, and among them are the Rho-associated, coiled coil-containing kinase (ROCK; also known as Rok in *Drosophila*). Rok acts also on NMY-II activation by inhibiting myosin light chain phosphatase, an inhibitor of NMY-II activation. The Rok kinase is previously activated by Rho1 kinase (RhoA in mammals), a member of the Rho GTPase family, which in turn requires activation via GTP binding mediated by GEF proteins (Riento and Ridley 2003). Interestingly, NMY-II can act in a feedback way by controlling Rho GTPase signalling, for example by concentrating Rho and Rok locally or preventing inactivation of RhoA at the AJ level, therefore regulating many processes such as cell adhesion and morphogenesis (Wu and Priya 2019).

d. <u>The AJs and acto-myosin cytoskeleton relationships</u>

NMY-II and F-actin exist as a complex and are referred to as the acto-myosin cytoskeleton, for ease of use, in the rest of the manuscript. This acto-myosin cytoskeleton as mentioned just before is implied in many mechanisms and more particularly playing a role of contractile apparatus. The acto-myosin can be seen as

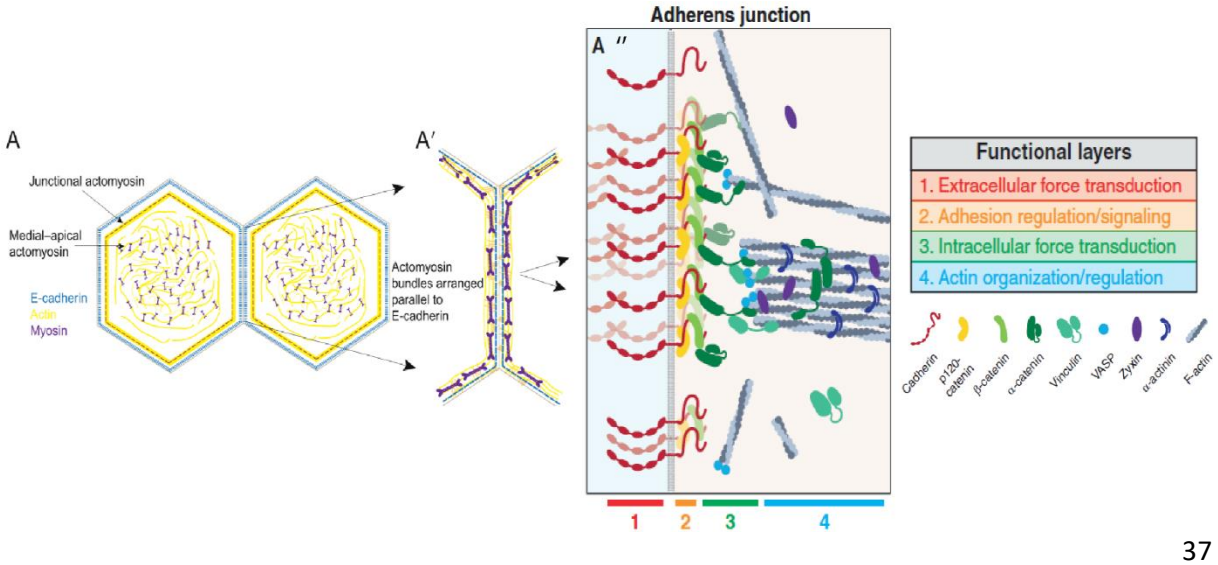

Figure 16. Acto-myosin network organisation and links to Adherens junctions. A. Scheme of the medial apical network and the junctional acto-myosin in Drosophila epithelial cells. **A'.** Junctional acto-myosin displays parallel-arranged bundles and is connected to the AJs. **A''.** Close up showing the connection of E-Cad/α-catenin complex to the acto-myosin network and their partner proteins. Adapted from (Priya and Yap 2015) and (Clarke and Martin 2021)

two major forms in *Drosophila* epithelial cells: a network called the medial-apical network and the junctional acto-myosin. The junctional acto-myosin is organized as bundles parallel to DE-Cad whereas the medial-apical network resembles an isotropic network. The coupling of the contractile activity exerted by the medial-apical network to the junctional network and AJs allows mechanical forces to be transmitted across cells and even tissues. AJs function as platforms for F-actin assembly since ARP2/3 is present here (Priya and Yap 2015) **(Figure 16).**

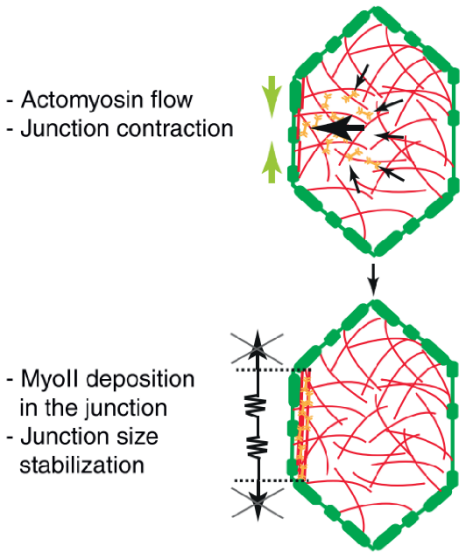

Figure 17. Scheme representing dorso-ventral junction shrinkage mechanism during germband extension. Green represents E-Cad spot, red the F-actin, orange the NMY-II, black arrows the acto-myosin flow, green arrows the junctional contraction and black springs the increased tension at the junction. Adapted from (Levayer and Lecuit 2012)

AJs rely also on acto-myosin cytoskeleton and their effectors for their integrity, since NMY-II contraction via anchoring to DE-Cad spot, activates NMY-II flow associated with AJ contraction. Then, the AJ length is stabilized by the recruitment of NMY-II **(Figure 17).** This mechanism associated with DE-Cad endocytosis, also regulated by NMY-II and a Formin protein named Diaphanous, allows cell/cell intercalation during *Drosophila* germband extension (Levayer and Lecuit 2012).

Those interplays between AJs and acto-myosin skeleton are important since they are not only involved in germband extension but also in dorsal closure and mesoderm invagination via apical cell constriction (Martin, Kaschube et al. 2009, Guillot and Lecuit 2013, Heisenberg and Bellaiche 2013, Munjal and Lecuit 2014).

The plasma membrane is connected to the so-called acto-myosin cortex which is composed of a thin layer of actin associated with numerous actin-binding proteins, just beneath the cell surface. By contraction that is mediated notably via NMY-II activation,

the actomyosin cortex plays a role in many processes, such as cell morphology regulation and cytokinesis, which is described in the last chapter of this introduction (Chugh and Paluch 2018).

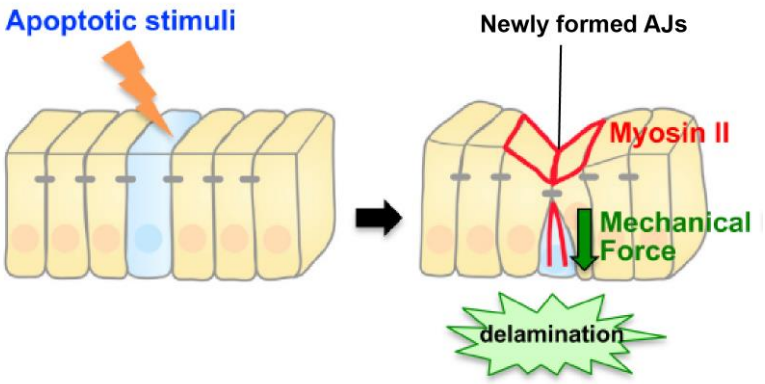

Figure 18. Apoptosis and Drosophila leg folding. The cell that enters apoptosis (light blue), shrinks apico-basally due to NMY-II apico-basal cables that exert pulling forces on the apical domain. Neighbour cells are still connected through AJs and display enrichment of NMY-II at the AJ level. The apoptotic cell that extrudes, shapes the future folding of the tissue due to apical constriction operated by adjacent cell via NMY-II enrichment. Adapted from (Ohsawa, Vaughen et al. 2018)

Another key moment in epithelial life is the control of their cell number, especially using cell delamination/extrusion. For example, as the cell is committed to apoptosis, the apical size is reduced via acto-myosin medial network contraction, without losing their AJs to their neighbouring cells. The dying cell exerts forces and deforms the surrounding epithelium because of its NMY-II contraction activity, both at AJ level and via NMY-II apico-basal cables in *Drosophila* epithelia for example. Expressing a dominant negative form of NMY-II specifically into apoptotic cells prevents the deformation of surrounding cell, confirming the role of NMY-II in shrinkage and deformation mechanisms. Thereafter, AJs between the dying cell and its surrounding are progressively removed whereas newly AJs are formed between non-apoptotic cells at the same time that apoptotic cells are expelled basally. Expelling the dying cell also requires neighbouring cells to engage in acto-myosin contraction (Monier and Suzanne 2015) **(Figure 18).**

Cell eliminations could occur because of cell crowding (Marinari, Mehonic et al. 2012, Levayer, Dupont et al. 2016, Valon and Levayer 2019), mechanical stresses or cell competition (Vincent, Fletcher et al. 2013, Matamoro-Vidal and Levayer 2019). An ideal example of the interplay between AJs and acto-myosin cytoskeleton during cell competition is shown in (Levayer, Hauert et al. 2015). Here the authors reveal, in both *Drosophila notum* and wing discs, that fast-growing oncogenic mutant *myc* cells when confronted with slow-growing WT cells, outcompete them and invade WT tissue.

During this process, a differential tension at AJ level between WT and mutant cells, due to lower F-actin presence at AJ, induces cell mixing via cell/cell intercalation. The tension, which correlates with the amount of F-actin at the junction, is greater between winner cells than between winner and loser cells. Therefore, WT looser cells are surrounded by *myc* winner cells and die because of the apoptosis initiated by cell contact death that takes place upon cell competition (de la Cova, Abril et al. 2004) **(Figure 19).**

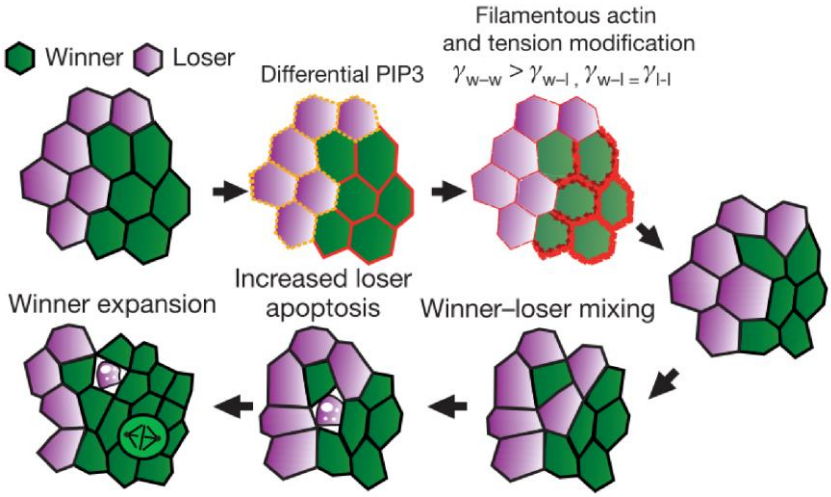

Figure 19. Cell mixing during cell competition upon junctional cell-cell exchange. Winner cells (myc) display higher amount of Phosphatidylinositol (3,4,5)-trisphosphate (PIP3) compared to Loser cells (WT), leading therefore to higher amount of F-actin at Winner-Winner cell boundaries and lower amount at Loser-Loser or Loser-Winer cell boundaries. This phenotype of F-actin is responsible for the difference in junctional tension between Winner-Loser boundaries and Winner-Winner boundaries. Overexpression of the Formin Diaphanous in Loser cells prevents loss of clonal compaction, showing the importance of F-actin in this process. Hence, low tensed clone of Loser cells is less compacted than clone of Winner cells and Winner cells start to invade the tissue via cell-cell mixing. γ: interfacial tension; w: Winner; l: Loser; thick red lines: increased interfacial tension; red lines: F-actin. Adapted from (Levayer, Hauert et al. 2015).

e. Conclusion

In this part, we observed how AJs via their multiple interplays with acto-myosin cytoskeleton and their partners, act as the key regulators of tissue mechanical barrier integrity. They are needed to ensure cell-cell adhesion but also integrate many differential inputs and transduce them as mechano-responses. AJs regulate both morphogenesis at the cellular and tissular level as well as signalling pathway such as Hippo/YAP growth pathway. The following parts of the manuscript demonstrates how AJs and connected acto-myosin cytoskeleton are possibly linked to both Septate Junctions and Tricellular Junctions components.

Chapter III: Septate Junctions

a. Generalities, ultrastructure and Embryonic development

i. Generalities

Septate Junctions (SJ) in Arthropods are similar to their vertebrate counterparts, Paranodal Junctions (Einheber, Zanazzi et al. 1997, Bhat, Rios et al. 2001), which are localized at the Ranvier nodes, an area characterized by the myelin thinning and which links axon and the glial cell (Faivre-Sarrailh 2020). These junctions establish the paracellular permeability barrier, filtering ions, water and solutes, as revealed first by (Lord and DiBona 1976) using transmission electronic microscopy (TEM) and the freshwater planarian, *Dugesia tigrina* and then by (Lamb, Ward et al. 1998), using injected fluorescent rhodamine-labelled dextran (10 kDa) in *Drosophila* embryos hemocoel. Some of their components, namely Discs large (Dlg), are also involved in epithelial cell polarity establishment (Abbott and Natzle 1992, Woods, Wu et al. 1997). Moreover, many studies suggest additional roles, which are discussed in the following sections.

Historically described for the first time as “septate desmosomes” in the *Hydrae* (Wood 1959, Filshie and Flower 1977), an animal belonging to the *Cnidarian* order, SJs are evolutionarily conserved and are found, for example, in the order of sea anemone (Green and FLower 1980). In the arthropods, they were firstly studied in the midgut of Lepidopteran Caterpillars (Flower and Filshie 1975).

ii. Ultrastructure

SJs were analysed by TEM in combination with freeze-fracture replicas or using lanthanum infiltration, which revealed many types of shapes (Jonusaite, Donini et al. 2016). Of those, two main shapes have been described in the *Drosophila melanogaster*: the pleated Septate Junctions (pSJ) and the smooth Septate Junctions (sSJ) (Tepass and Hartenstein 1994, Furuse and Tsukita 2006, Izumi and Furuse 2014). SJs form a belt like structure around the apicolateral area in the epithelial cells. The septa connect the parallel membranes of adjacent cells, forming discontinuous

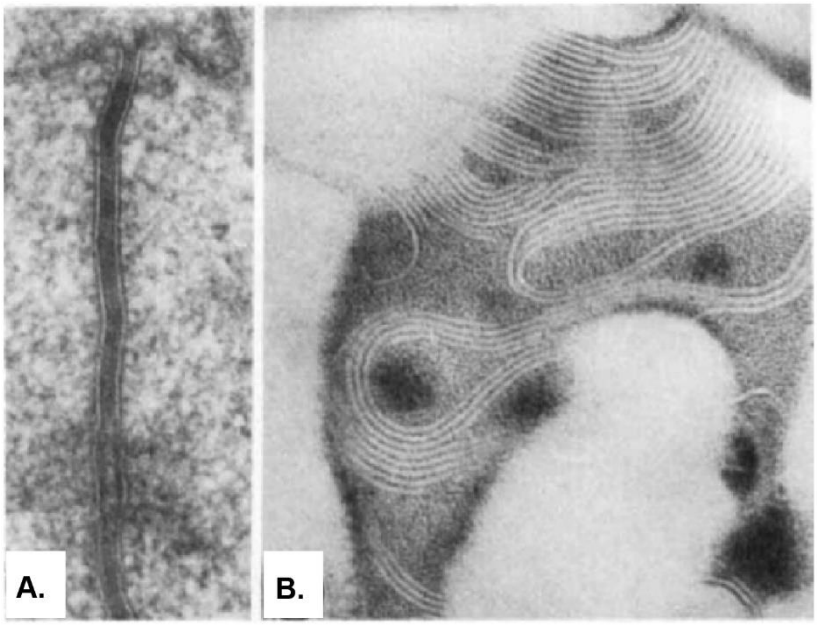

Figure 20. TEM images of the midgut Smooth Septate Junctions. A. Transversal section of American Cockroach midgut reveals the space filled by electron dense material and no septa could be observed. However, using Lanthanum impregnation, septa appear in a negative contrast, resembling parallel sided ribbons, as showed by the tangential section in **B.** The upper part of the cell displays parallel septa and a deeper part of the cell shows more curved and irregular septa. Adapted from (Noirot-Timothée and Noirot 1980)

ladder-like structures that span the intermembrane space, which is estimated to be approximately 15 nm (Noirot-Timothée and Noirot 1980, Green and Bergquist 1982).

Septa size is estimated at around 2-11 nm and they are spaced by 20-22 nm (Noirot-Timothée and Noirot 1980). Using TEM and lanthanum, septa in pSJs appear as undulated rows while sSJs show regularly spaced and parallel lines **(Figures 20-21).**

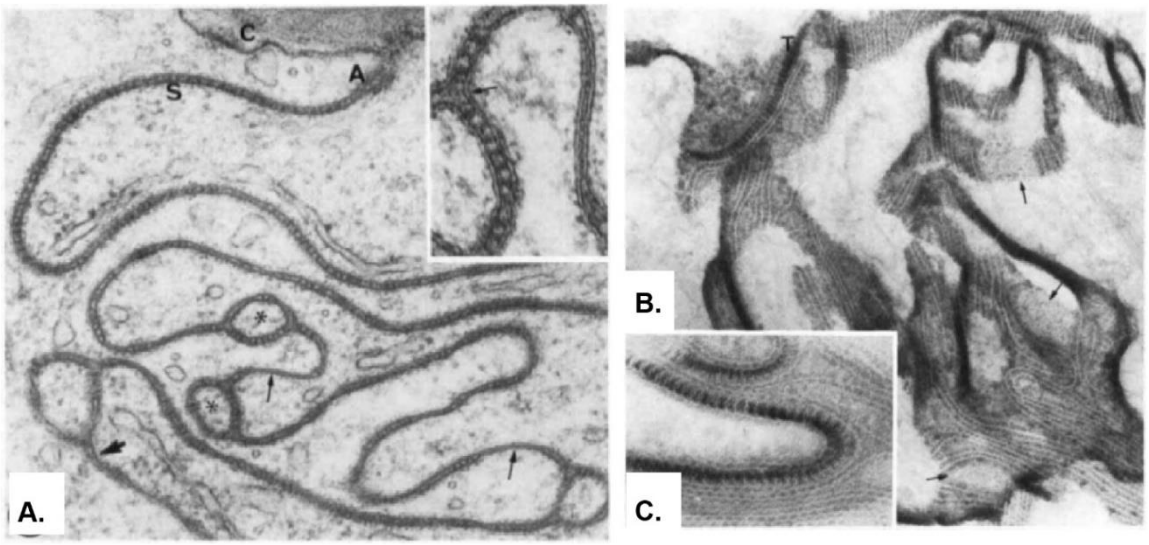

Figure 21. TEM images of the hindgut Pleated Septate Junctions. **A.** Transversal section of the termite (Kalotermes flavicollis) hindgut, revealing Adherens Junction (AJ) below the cuticle (C) and pSJ (S). Unlike sSJ, pSJ display pleated septa. Finger-like processes of a third cell are highlighted by asterisks and small arrows show the intercalated gap. The large arrow shows the basal part of the cell devoid of junctional complex. A close-up highlights a tricellular junction. **B.** Tangential section (and close up **C.**) of firebrat (Thermobiu dornesticu) hindgut stained with Lanthanum. We could observe the characteristics negatively contrasted pleated septa, sometimes parallel or more curved. T shows a tricellular junction. Adapted from (Noirot-Timothée and Noirot 1980)

Moreover, they originate from different embryonic tissues. The pSJ is an ectodermally derived epithelial junction component whereas sSJ develop from the endoderm. Therefore, pSJs form SJ in the salivary glands, the trachea, the epidermis, the gut (foregut and hindgut), imaginal discs, the nervous system (forming Blood Nerve or Blood-Brain Barrier) (Tepass and Hartenstein 1994), the adult gonads (Mahowald 1972) and the *notum*. They are also formed in the capsule that lamellocytes create to surround parasitic wasp eggs (Russo, Dupas et al. 1996). On the contrary, the endodermally derived sSJs are found in the midgut and the gastric *caeca.* Notably, even though Malpighian tubules (fulfilling the role of kidneys in the *Drosophila*) and the outer epithelial layer of the proventriculus (OELP) are ectodermally derived, sSJs are present in those tissues (Tepass and Hartenstein 1994).

Another difference is their respective position regarding the AJ position. The pSJs are found basal to AJs when sSJs are above spotted AJs.

iii. Embryonic development

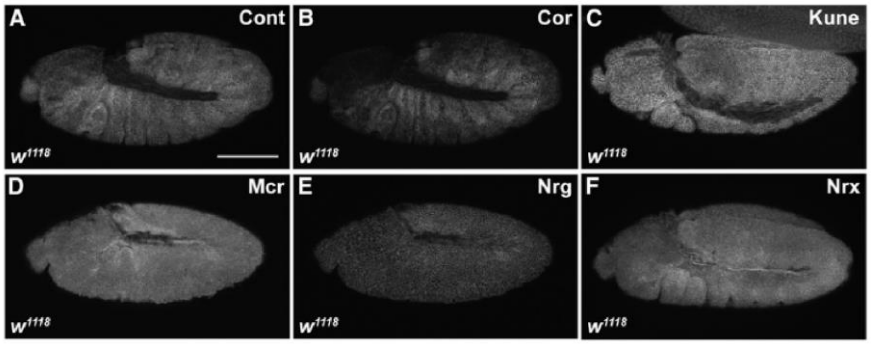

Figure 22. Stage 10 WT (w^{1118}) Drosophila embryos stained with pSJ proteins antibody. Adapted from (Hall and Ward 2016)

pSJs components start to be expressed as soon as stage 10 of embryogenesis (Hall and Ward 2016) **(Figure 22).** Thereafter, they continue to be strongly expressed and start to appear at the lateral membrane around stage 11/12 (8 hours after the beginning of embryonic development). The pSJ proteins are found both in early or recycling

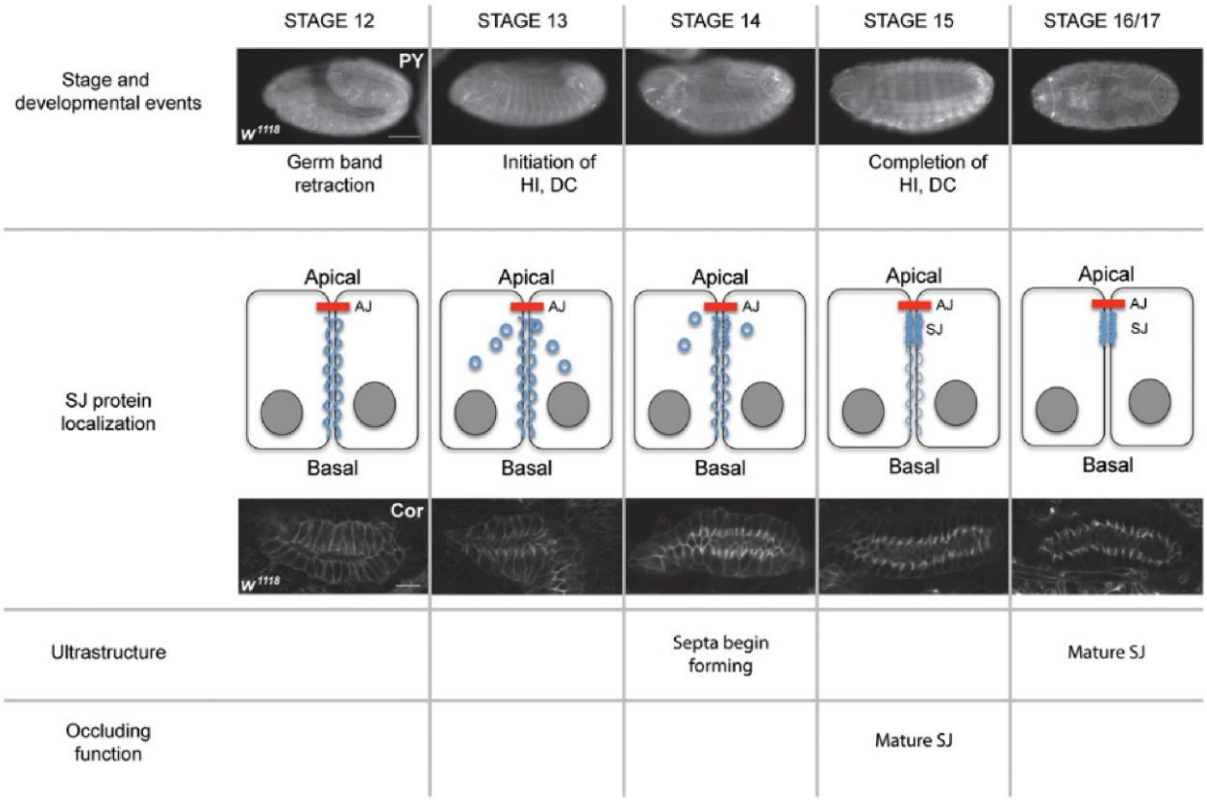

Figure 23. Septate Junctions establishment during Drosophila embryogenesis. First row: Stage 12-14: the anterior is to the left and the dorsal part is up. Stage 15-17: facing is up. PY: FITC-labelled antiphosphotyrosine antibodies; HI: Head Involution; DC: Dorsal Closure; AJ: Adherens Junction; SJ: Septate Junction. Adapted from (Hall and Ward 2016)

endosomal compartments as well at the membrane around stage 13 (Tiklova, Senti et al. 2010). Starting at stage 14, when polarity is established and AJs are formed (Harris and Peifer 2004), pSJ components are increasingly enriched at the apicolateral part of the cells. At stage 16 (14 hours after the beginning of embryonic development), they localize at their defined position although some of them are still spread at the lateral membrane. TEM analysis showed mature pSJ at stage 17, even though dispersed electron-dense intercellular septa were detectable around stage 14 (Tepass and Hartenstein 1994), coinciding with fluorescent microscopy analysis (Hall and Ward 2016). Examining their physiological roles, paracellular permeability is established as soon as stage 15, like demonstrated using the 10kDa fluorescent rhodamine-labelled dextran assay (Paul, Ternet et al. 2003) **(Figure 23).** pSJ is a very stable complex as highlighted by (Oshima and Fehon 2011). The authors used fluorescent recovery analysis after photobleaching (FRAP) experiments to demonstrate that at stage 12, the immobile fraction of pSJ proteins is around 0.2 using ATP-α-GFP as a reference, and this immobile fraction starts to increase during development, beginning at stage 13 and

reaches 0.6 at the end of stage 13. Moreover, they show that the loss of any of the so-called core-components proteins, such as Nervana-2, Coracle or Neuroglian, for example, leads to a diminished immobile-fraction, dropping from 0.6 to 0.2 or no immobile fraction at all, arguing that pSJ stability depends on the presence of all the pSJ compounds **(Figure 24).** Much less is known about sSJ. In the *Drosophila* embryos, at early stage 17 in the OELP, sSJs were assembled and then at late stage 17 in the midgut (Tepass and Hartenstein 1994). In a recent work by (Furuse and Izumi 2017), the authors were able to stain Mesh, one of the sSJ components, earlier at stage 16 in the OELP at the apicolateral membrane region, suggesting an earlier sSJ assembly than previously thought.

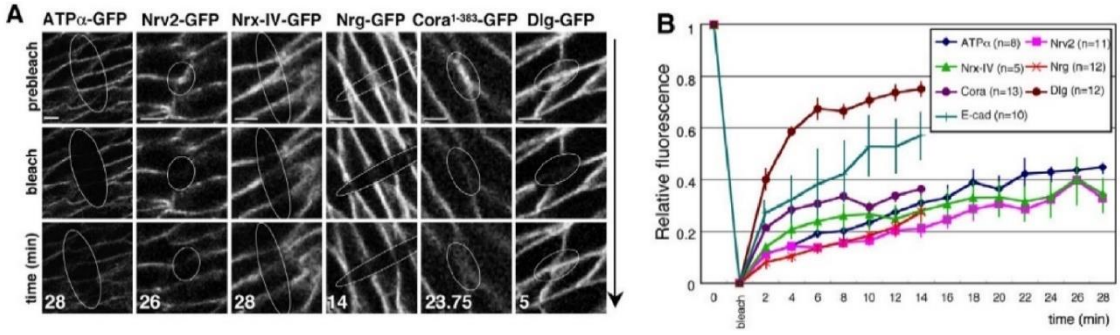

Figure 24. Pleated Septate Junctions exhibits highly stable proteins complex. A. FRAP analysis performed on pSJ proteins core components. Time is in minutes and T=0 corresponds to the bleaching event. This reveals the higher immobile fraction of pSJ core-components in B. (mean around 0.6 at T=25 min) compared to non-core-component Dlg (immobile fraction of 0.2 at T=14 minutes) or AJ component such as E-Cad (immobile fraction of 0.4 at T= 14 minutes). Adapted from (Oshima and Fehon 2011)

b. Composition and organisation

i. Pleated Septate junction

Currently, more than 25 proteins are related to pSJ formation and/or maintenance. Most of them are transmembrane proteins but there are also cytoplasmic and GPI-anchored proteins **(Figure 25)**. Many rely on the other proteins to establish a highly stable complex. Usually, the loss of one of these components leads to the destabilisation of the entire complex, which makes it difficult to understanding specific roles (Oshima and Fehon 2011).

- **Polarity and tumour suppressors proteins**

One of the first described proteins in *Drosophila* known to localize at pSJ was the cytoplasmic MAGUK protein **Discs large (Dlg)**, which takes its name's origin in the work of (Stewart, Murphy et al. 1972).

Name		Vertebrate homolog	Barrier related phenotypes upon *lof*	SJ morphology upon *lof*	Reference
ATPα		Na^+/K^+ ATPase α-subunit	salivary glands - leaky	no septa	Genova et al., 2003
Bark beetle/ Anaconda	Bark/ Aka		trachea - leaky	small patches of septa	Hildebrandt et al., 2015
Gliotactin	Gli	Neuroligin3		no septa	Auld et al., 1995
Kune-kune	Kune	Claudin	salivary glands, trachea, CNS - leaky		Nelson et al., 2010
Macroglobulin complement-related	Mcr	α2M	trachea, hindgut - leaky	no septa	Hall et al., 2014, Bätz et al., 2014
Megatrachea/ Pickel	Mega/ Pck	Claudin	salivary glands, trachea - leaky		Behr et al., 2003
Nervana 2	Nrv2	Na^+/K^+ ATPase β-subunit	salivary glands, CNS - leaky	no septa	Genova et al., 2003
Neurexin IV	NrxIV	Caspr	CNS - leaky	no septa	Baumgartner et al., 1996
Neuroglian	Nrg	Neurofascin 155	salivary glands, CNS - leaky	reduced number of septa	Genova et al., 2003
Pasiflora1	Pasi1		trachea, CNS - leaky		Deligiannaki et al., 2015
Pasiflora2	Pasi2		trachea, CNS - leaky		Deligiannaki et al., 2015
Sinuous	Sinu	Claudin	salivary glands, trachea - leaky	reduced number of septa	Wu et al., 2004
Wunen	Wun	Plpp1	trachea, CNS - leaky	normal septa	Ile et al., 2012
Boudin	Bou		trachea - leaky		Hijazi et al., 2009
Coiled	Cold	Lypd8	trachea, CNS - leaky	no septa	Nilton et al., 2010
Contactin	Cont	Contactin	salivary glands, trachea - leaky	reduced number of septa	Faivre-Sarrailh et al., 2004
Crimpled	Crim		trachea - leaky		Nilton et al., 2010
Crooked	Crok		salivary glands, trachea - leaky	reduced number of septa	Nilton et al., 2010
Lachesin	Lac	Negr1	trachea - leaky		Llimargas et al., 2004
Melanotransferrin	MTF	MTF	trachea - leaky	reduced number of septa	Tiklova et al., 2010
Undicht	Udt		trachea, CNS - leaky	no septa	
Coracle	Cora	4.1B	trachea - leaky		Ward IV et al., 2001, Fehon et al., 1994
Discs large	Dlg	Cask		reduced number of septa	Woods et al., 1996
Varicose	Vari	Pals2	trachea - leaky		Wu et al., 2007

Figure 25. Pleated Septate Junctions known components. Green: transmembrane proteins. **Blue**: GPI-anchored proteins. **Yellow**: cytoplasmic proteins. Tricellular junctions' proteins are also mentioned such as Anakonda/Bark Beetle and Gliotactin. Adapted from (Petri, Syed et al. 2019)

Dlg belongs to a subfamily of MAGUK proteins with the vertebrate tight junction proteins ZO-1 (Willott, Balda et al. 1993), ZO-2 (Duclos, Boschert et al. 1993, Jesaistis and Goodenough 1994), PSD-95/SAP90 (Cho, Hunt et al. 1992, Kistner, Wenzel et al. 1993) and hDlg/p97 (Lue, Marfatia et al. 1994, Müller, Kistner et al. 1995). Dlg is composed of three PDZ domains, one Src Homology Region 3 (SH3) and one region highly similar to the yeast Guanlytate Kinase (GUK) (Woods, Hough et al. 1996). Recessive lethal mutations of Dlg lead to imaginal discs overgrowth, which places it in the tumour-suppressor gene category (Woods and Bryant 1991). Moreover, (Abbott and Natzle 1992) report abnormal epithelial cell organisation called rosettes, which result from the loss of close contact and cell polarity following the loss of Dlg. This loss of cell polarity is confirmed by (Woods, Hough et al. 1996, Woods, Wu et al. 1997), where the authors observed the rearrangement of actin and tubulins cytoskeleton components and the delocalisation of known key proteins involved in polarity, such as Expanded (Ex) and Coracle (Cora; another pSJ protein), and the loss of other pSJ transmembrane proteins Fasciclin III (Fas III) and Neuroglian (Nrg). Mutant cells for Dlg also show disorganized septa when examined by TEM (Woods, Hough et al. 1996). Notably, Dlg is also shown in sSJ (Izumi, Yanagihashi et al. 2012, Izumi, Motoishi et al. 2016).

Scribble (Scrib) is a cytoplasmic scaffolding protein, which, similar to Dlg, is involved in polarity establishment and maintenance and which also has a tumour-suppressor role both in embryos (Bilder and Perrimon 2000) and follicle cells of ovaries (Bilder, Li et al. 2000). It is a LAP protein that contains four PDZ domains in addition to 16 LRR domains. A recent work of (Khoury and Bilder 2020) demonstrated that Scrib apicolateral position required a cortically stabilizing mechanism provided by Dlg. Similar *dlg* mutants, embryo *scrib* mutants do not have pSJ formed.

The last member of this group is the cytoplasmic **Lethal (2) giant larvae (Lgl or L(2)gl)**, which was first observed in the brain and imaginal discs (Klambt and Schmidt 1986). It colocalizes and forms the polarity and growth complex with Dlg and Scrib (Bilder, Li et al. 2000). Lgl, similar to many other scaffold proteins has multiple WD-40 repeats (Jacob, Opper et al. 1987, Strand, Raska et al. 1994) and its loss displays the same defects as *dlg* and *scrib* mutants.

- **The Paranodal equivalents**

To date, four proteins found in pSJ have their homologous in the paranodals junctions in vertebrates. As mentioned before, pSJ are equally found in ectodermally derived tissues (except for Malpighian tubules and OELP), from embryonic tissues to imaginal discs and the blood brain barrier (BBB).

One of them is **Neurexin-IV (Nrx-IV)**, a transmembrane protein of the Contactin-Associated Protein (Caspr) family. It is homologous of the human Caspr/Paranodin. Nrx-IV has a large extracellular domain composed of a discoidin domain (DS), five laminin G domains and EGF repeats (Baumgartner, Littleton et al. 1996). The short intracellular part is very similar to that of the glycophorin C protein, known to bind protein 4.1 in red blood cells. When examining with TEM, *nrx-IV* mutant individuals display paralysis due to blood brain barrier defects, a delocalisation of Cora and the absence of septa (Baumgartner, Littleton et al. 1996).

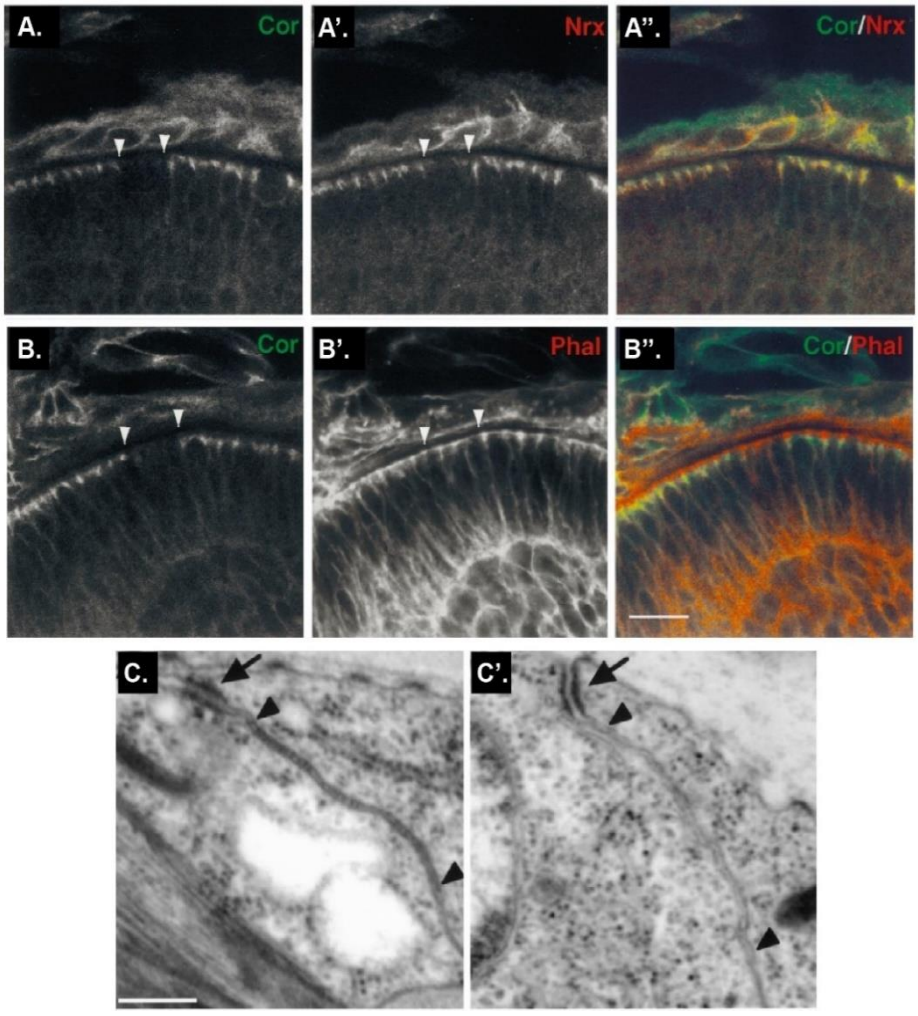

Figure 26. Loss of Coracle leads to Pleated Septate Junctions defects. A-A''. cora mutant cells in Drosophila imaginal wing discs (white in A and green in A'') displays loss of Nrx-IV (white in A' and red in A'') as indicated by white arrows head. **B-B''**. Cora is not colocalizing specifically with F-actin (stained with Phalloidin, white in B' and red in B'') enriched apical portion but just below. Loss of Cora does not induce loss of F-actin as indicated by white arrows head. **C.** TEM analysis of epidermis of stage 17 WT Drosophila embryos. pSJ are present as indicated by black arrows head. Arrow show AJ. **C'**. Embryos mutant for Cora display a lack of individual septae as shown by black arrows head. Arrow indicates that AJs are still present and well localized in cora mutant. Adapted from (Lamb, Ward et al. 1998)

As previously described, another really important pSJ protein is **Coracle (Cora)**. This cytoplasmic protein contains the FERM domain and is a *Drosophila* homologous of the human band 4.1B, which binds Caspr at the paranodes (Denisenko-Nehrbass, Oguievetskaia et al. 2003). Cora was identified for its requirement in dorsal closure during *Drosophila* embryogenesis (Fehon, Dawson et al. 1994) and shows apicolateral localisation in embryonic and imaginal tissues. Moreover, double staining with Rhodamine Phalloidin and Cora antibody does not reveal clear colocalisation between the two even though the resolution is not optimal. Then, (Lamb, Ward et al. 1998), using different mutations and mosaic clonal analysis, demonstrate that loss of Cora leads to septa disorganisation and/or disappearance in embryonic and imaginal discs as well as Nrx-IV removal **(Figure 26).** Those results show the importance of Cora in establishing a paracellular permeability barrier. In addition, Cora binds the intra-cellular part of Nrx-IV to establish a complex (Ward IV, Lamb et al. 1998).

Subsequently, **Neuroglian (Nrg)** has come into play. Its human homologous is Neurofascin-155 and similar to Nrg, belongs to the L1-type family. This is a transmembrane protein with a large extracellular part containing six Ig C2-type

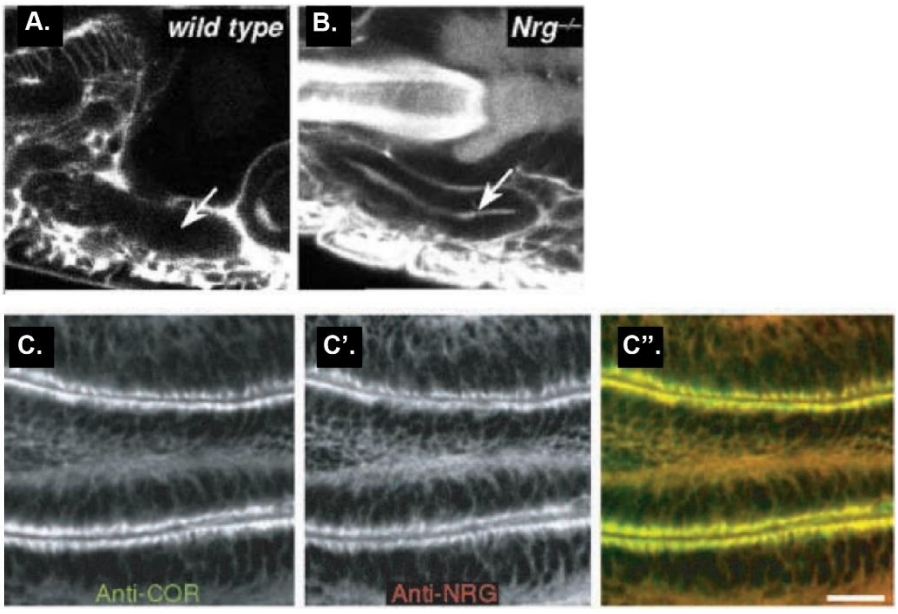

Figure 27. Loss of Neuroglian leads to permeability barrier defects. A. Confocal images of salivary glands of Drosophila embryos injected with a fluorescently labelled dextran. The arrow shows the lumen, devoid of dextran staining here in WT conditions but positive for dextran staining in Nrg mutant in **B.,** showing the impairment of the permeability barrier in the salivary glands. **C-C''.** Confocal images of Drosophila embryos stained with antibodies against Cora (white in C and green in C'') and Nrg (white in C' and red in C''), showing colocalisation between the two. Adapted from (Genova and Fehon 2003)

domains followed by five Fibronectin type III domains (Bieber, Snow et al. 1989). Two isoforms of Nrg come from two different mRNAs, both of which have the same extracellular part but have differences in their intracellular section. The long isoform is known as Nrg^{180} (180 kDa) and is restricted to the surface of neurons in the central nervous system (CNS) and peripheral nervous system (PNS) and at the glial cells level in the PNS. The short isoform is called Nrg^{167} (167 kDa) and is expressed in a wide range of tissues such as the imaginal discs (Hortsch, Bieber et al. 1990). Using fluorescently labelled Dextran, loss of Nrg shows leakage defects in salivary glands and also septa disappearance under TEM analysis. Furthermore, co-immunoprecipitation experiments reveal that Nrg forms a complex with Nrx-IV and Cora. Nrg also demonstrates colocalisation with Cora (Genova and Fehon 2003) **(Figure 27).** Importantly, previous studies showed interactions between the cytoplasmic domain of Nrg and Ankyrin, both in rat and *Drosophila* (Davis and Bennett 1994, Dubreuil, MacVicar et al. 1996). Ankyrin is a membrane-cytoskeletal protein, which suggests the possible anchoring of the Nrg/Nrx-IV/Cora to the cell membrane cortex.

The last protein of this group is **Contactin (Cont)** and its human homologous is also named Contactin. It is a Glycosyl phosphatidyl inositol (GPI) anchored protein with a Lectin domain, six Ig domains and four Fibronectin type III domains. Cont colocalizes with Nrx-IV and Nrg, and the loss of Cont leads to leakage defects in embryo salivary glands and trachea. Unlike previously described proteins, loss of Cont does not lead to septa disappearance but rather an altered organisation (Faivre-Sarrailh, Banerjee et al. 2004). Moreover, co-immunoprecipitated experiments demonstrate that Cont forms a tripartite complex with both Nrx-IV and the Nrg^{167} isoforms expressed in epithelial cells (Faivre-Sarrailh, Banerjee et al. 2004).

- **The Na^+/K^+- ATPase pumps**

We observed the similarity between the components of both the vertebrate paranodal junctions and the pSJs in the *Drosophila*. By screening a collection of P element insertion mutations, previously identified as conducting paracellular barrier defects, (Genova and Fehon 2003) discovered two new proteins involved in pSJ establishment: the α and β subunits of the Na^+/K^+-ATPase.

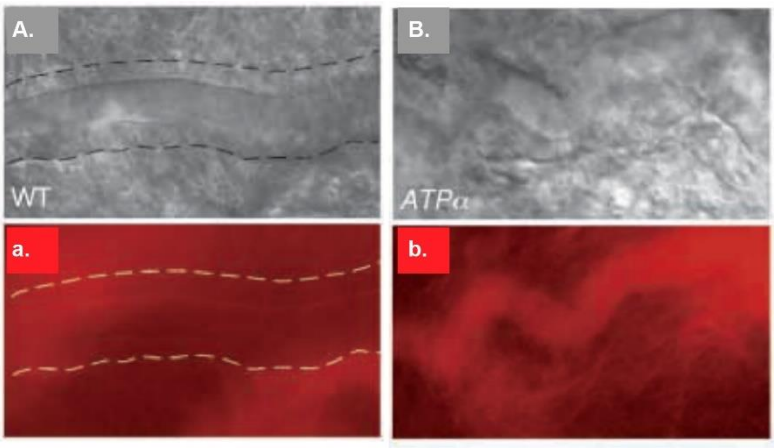

Figure 28. Loss of ATP-α shows Drosophila embryos tracheal defects. A. DIC image of WT embryo trachea injected with fluorescently labelled dextran. a. No dextran is observed in the trachea lumen. B. ATP-α embryo displays undulated trachea and leakage defects revealed by dextran in trachea lumen in b. Adapted from (Paul, Ternet et al. 2003)

The catalytic α subunit is called **ATP-α** and it is an integral membrane cation antiporter protein, first described in (Lebovitz, Takeyasu et al. 1989), which show basolateral localisation in epithelial cells (Dubreuil, Maddux et al. 1997, Dubreuil, Wang et al. 2000). ATP-α is a multi-transmembrane domains protein, composed of 10 transmembrane segments with five extracellular parts and six intracellular parts (including the N and C-terminal parts) (Kaplan 2002). During their study, (Genova and Fehon 2003) highlight that unlike previously stated, ATP-α is restricted to the pSJ level using antibody and GFP-tagged ATP-α in both embryonic and imaginal tissues. Loss of ATP-α is associated with septa disruption in epidermal cells and tracheal permeability defects **(Figure 28).** Removal of Cora or Nrx-IV or Nervana-2 (β subunit of the Na^+/K^+-ATPase pump) impairs ATP-α level and localisation at pSJ (Genova and Fehon 2003, Paul, Ternet et al. 2003). As previously demonstrated by biochemical approaches, ATP-α is also included in the complex formed by Cora/Nrx-IV and Nrg. Interestingly, the ATPase activity is not required to ensure pSJ functions and establishment.

Next, the chaperon β subunit is called **Nervana 2 (Nrv2)** and it is a single transmembrane domain glycoprotein, with two isoforms called Nrv2.1 and Nrv2.2. While two other genes called Nervana 1 and Nervana 3 encode the β subunit, they are

not implied in pSJ formation (Paul, Palladino et al. 2007). Nrv2 was historically described by (Sun and Salvaterra 1995) and demonstrated its ability to form a complex with ATP-α. Similar to its catalytic partner ATP-α, Nrv2 localizes at pSJ level and forms a complex with Cora/Nrx-IV/Nrg and ATP-α. It is also required for maintaining the paracellular permeability barrier in the trachea and salivary glands. Its loss leads to septa disorganisation/disappearance as well as reduced and mislocalized signals of ATP-α, Nrg, Nrx-IV and Cora in epidermal cells (Genova and Fehon 2003).

- **The Fasciclin proteins: cell-cell adhesion molecules**

The glycoprotein **Fasciclin II (FasII)** was revealed for the first time in the grasshopper embryo axons (Bastiani, Harrelson et al. 1987). The same team shows its presence in *Drosophila* and its requirement for neuronal recognition mechanism during embryogenesis (Grenningloh, Rehm et al. 1991). It appears that this protein is the vertebrate neural cell adhesion molecule (N-CAM) pendant and therefore, belonging to the cell adhesion molecule (CAM) family. FasII is a transmembrane protein composed of a large extracellular domain that contains five Ig domains and two fibronectin type III domains. FasII also exists in a GPI-anchored manner via two isoforms (Neuert, Deing et al. 2020). In addition to its important roles during neurogenesis, FasII is also observed at pSJ level, being localized at the same level as ATP-α and Nrx-IV (Hemphala, Uv et al. 2003). Upon closer examination, only the GPI-anchored isoforms are found in non-neuronal cells (Neuert, Deing et al. 2020). Further, FasII binds to PDZ intracellular domain of Dlg at the mature neuromuscular junction, forming a complex (Thomas, Kim et al. 1997, Zito, Fetter et al. 1997). However, its role

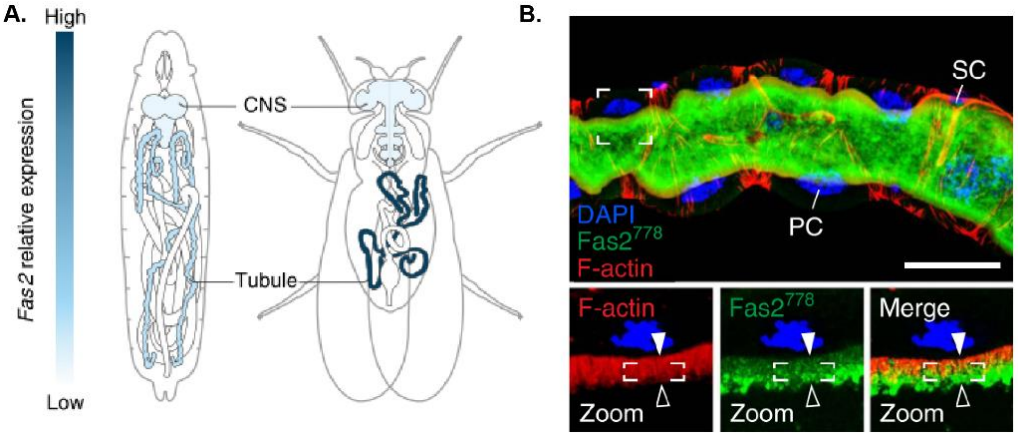

Figure 29. Smooth Septate Junctions of Drosophila Malpighian tubules possess Pleated Septate Junctions protein FasII. A. Overview of the Drosophila anatomy, both at larval and adult stage, associated with the FasII pattern of expression **B.** Super-resolution microscopy (airyscan) images of Malpighian tubules brush border of Drosophila expressing FasII-GFP, stained with GFP antibody (green), DAPI (blue) and Phalloidin (F-actin; red). Zoom shows that FasII is enriched at the tip of the brush border (empty arrow). Filled arrow shows the base of the brush border. Adapted from (Halberg, Rainey et al. 2016)

in the pSJ context is not clear since no particular studies have been done, except some that highlight its role during trachea morphogenesis (Wu and Beitel 2004). Notably, FasII is also present at sSJ level and is required to participate in the brush border maintenance of the Malpighian tubules epithelial cells (Halberg, Rainey et al. 2016) **(Figure 29).**

Like for FasII, **Fasciclin III (FasIII)** was discovered in a subset of neurons in the *Drosophila* central nervous system (Patel, Snow et al. 1987), whoch demonstrated its role as a CAM protein (Snow, Bieber et al. 1989). FasIII is a transmembrane protein composed of three Ig domains and it shows colocalisation with Nrx-IV in the salivary glands (Baumgartner, Littleton et al. 1996). As in the FasII case, much less is known

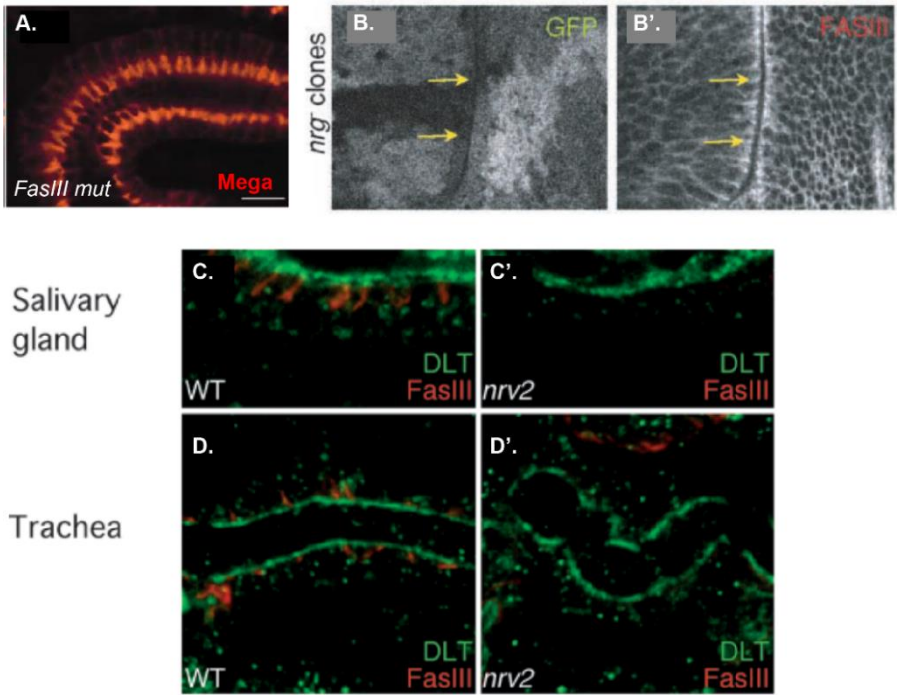

Figure 30. Drosophila embryos mutant for Fasciclin III do not show classical Pleated Septate Junctions mutant defects. A. Epidermis of stage 16 FasIII embryos show no defects in pSJ protein Mega localisation (red). **B-B'.** Loss of Nrg (highlighted by the loss of GFP expression, white in B) display no loss of FasIII signal (white in B') in Drosophila imaginal wing discs. **C-C'.** Salivary glands of embryos stained for PATJ (DLT, green) and FasIII (red) display loss of FasIII signal in nrv2 mutant C'. Similar results are observed in trachea embryos in **D-D'.** Adapted from (Behr, Riedel et al. 2003), (Genova and Fehon 2003) and (Paul, Ternet et al. 2003)

about its pSJ context role, although a study by (Behr, Riedel et al. 2003) shows that Mega Trachea (a pSJ protein) is not delocalized upon loss of FasIII in *Drosophila* embryos. Intriguingly and in contrast to most pSJ proteins, FasIII is not affected by the loss of Nrg in the wing discs, suggesting differences between organs and proteins affected (Genova and Fehon 2003). Nonetheless, *nrv2* mutant cells display FasIII reduced and mislocalized signal in the embryonic salivary glands and trachea (Paul, Ternet et al. 2003) **(Figure 30).** Similar to FasII, FasIII is present in sSJ (Izumi, Yanagihashi et al. 2012, Yanagihashi, Usui et al. 2012).

- **The Claudin like proteins**

The tight junctions of vertebrates are composed of more than 20 different proteins called Claudins, four-pass transmembrane proteins which play pivotal roles in the paracellular permeability barrier (Zihni, Mills et al. 2016, Otani and Furuse 2020). Similar to the paranodal proteins, *Drosophila* has proteins analogous to the Claudins family, seven of which have been predicted (Wu, Schulte et al. 2004) and three among them characterized.

The first is **Megatrachea (Mega** ; also named Pickel**)**, a four-pass transmembrane domains with many similarities to claudin-10 and 18, displaying a potential PDZ domain in the C-terminal intracellular domain, a large and a small extracellular loop and an intracellular loop (Behr, Riedel et al. 2003). It colocalizes with Nrx-IV in embryos and relies on the presence of Nrx-IV and Cora to be at pSJ level. Its loss leads to leakage in the trachea and lack of septa like revealed by TEM analysis (Behr, Riedel et al. 2003). A proteomic study executed by (Jaspers, Nolde et al. 2012) reveals that Mega interacts with 10 known pSJ proteins **(Figure 31).**

CG number	published SJ components
1084	Contactin
1634	Neuroglian
3665	Fasciclin 2
5670	Na+, K+ ATPase alpha-subunit
5803	Fasciclin 3
6827	Neurexin IV
8663	Nervana 3
10620	Melanotransferrin
12369	Lachesin
14779	Megatrachea

Figure 31. Known Pleated Septate Junctions components interacting with Mega. Adapted from (Jaspers, Nolde et al. 2012)

The second is named **Sinuous (Sinu)** and possesses the typical organisation of Claudin proteins. It also colocalizes with Cora and Nrx-IV in embryos. Loss of Sinu

leads to leakage in the trachea as well as delocalisation of Cora, ATP-α and FasIII. Sinu depends on Cora, Nrx-IV, Mega and Nrv-2 for its localisation at pSJ. Unlike Nrx-IV, Cora, Nrv-2, Dlg and Mega whose loss led to septa disappearance, loss of Sinu showed a reduced number of septa with cell domains devoid of septa, which suggests an organizing role at pSJ rather than an establishing one (Wu, Schulte et al. 2004).

The last is **Kune-kune (Kune)** and it is also organized as a Claudin. It is needed for the permeability barrier and colocalizes with Cora. It is required for Cora, Dlg, Sinu, ATP-α and Mega localisation in embryos. Kune is absent or delocalized upon loss of Sinu, Mega, Cora or ATP-α (Nelson, Furuse et al. 2010).

- **The GPI-anchored proteins**

We previously observed that Cont and some FasII isoforms were GPI-anchored proteins. However, they are not the only ones, and many other pSJ components share this property.

One of these components is **Lachesin (Lac)**, a homophilic cell adhesion molecule involved in the trachea morphogenesis of the *Drosophila* (Llimargas, Strigini et al. 2004) and the formation of the BBB (Strigini, Cantera et al. 2006). It belongs to the Ig superfamily with three Ig repeats and is anchored to the membrane by a GPI anchor. Lac colocalizes in embryos with Cora and Nrx-IV (Llimargas, Strigini et al. 2004) and with Nrg in the CNS (Strigini, Cantera et al. 2006). Its removal leads to leakage in the trachea and Cora and Dlg impaired distribution. However, loss of Cora or Nrx-IV drive Lac displacement at the basolateral membrane (Llimargas, Strigini et al. 2004).

Another component is **Undicht (Udt)**, recently discovered by a screening of genes upregulated during epithelial cell wound repair (Petri, Syed et al. 2019). It is suggested to be part of the pSJ complex as revealed by the proteomic study of (Jaspers, Nolde et al. 2012), albeit not characterized at the time. It colocalizes with Nrx-IV in embryos and is required to ensure the ideal localisation of Nrx-IV, Cora and Dlg as well as prevents leakage from the trachea and establishes septa as revealed by TEM analysis (Petri, Syed et al. 2019). Interestingly, forms of Udt lacking the GPI anchor can rescue the mutant phenotype and to integrate into pSJ, even when the protein is expressed at a distant region of the mutant area, suggesting a cell non-autonomous function of this “secreted” form **(Figure 32).** Moreover, the authors show that ADAM10-like

proteases named Kuzbanian and Kuzbanian-like cleave Udt at three amino acids away from the membrane, demonstrating the physiological relevance of secreted Udt. This work highlights the importance of proteases to ensure pSJ establishment and/or maintenance.

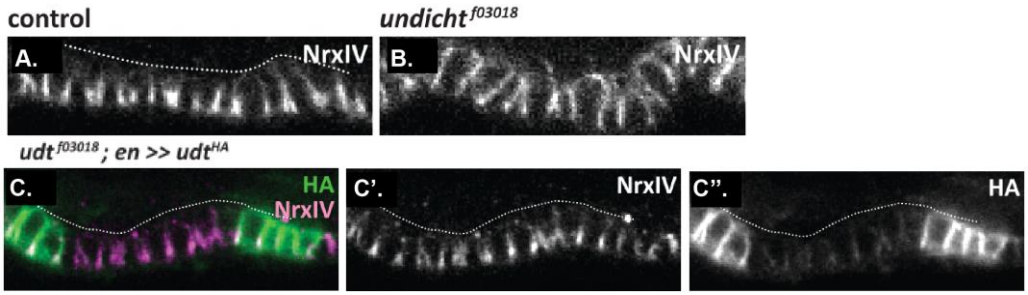

Figure 32. Undicht is a Pleated Septate Junction protein which is cleaved and can incorporate in distal areas. A-B. Stage 17 of Drosophila embryo epidermis stained for Nrx-IV. Loss of Udt leads to Nrx-IV spreading at baso-lateral membrane in B. **C-C''**. A version of a secreted HA-tagged version of Udt (green in C and white in C'') is expressed in an engrailed dependent pattern in an Udt mutant. This secreted Udt can incorporate into distal pSJ as shown in C'' where a reduced signal of HA is detected in the non-engrailed area. Note that Nrx-IV (green in C, white in C') is well localized, meaning that secreted form of Udt is enough to ensure pSJ components correct localisation. Adapted from (Petri, Syed et al. 2019)

Transferrin 2 (Tsf2; also known as Melanotransferrin**)** is a GPI-anchored and an iron-binding protein. It is made of two iron binding sites (similar to the mouse Melanotransferrin) and a GPI anchor (Tiklova, Senti et al. 2010). In the *Drosophila* embryos, it colocalizes with Nrx-IV and Dlg and its loss conducts to the classical pSJ mutant phenotypes: permeability tracheal defects, pSJ principal components delocalisation, septa disappearance. It also relies on Cora and/or ATP-α for its presence at pSJ level. Co-immunoprecipitation experiments also demonstrate that Tsf2 is in a complex with Nrx-IV, Nrg and Cont (Tiklova, Senti et al. 2010). Moreover,

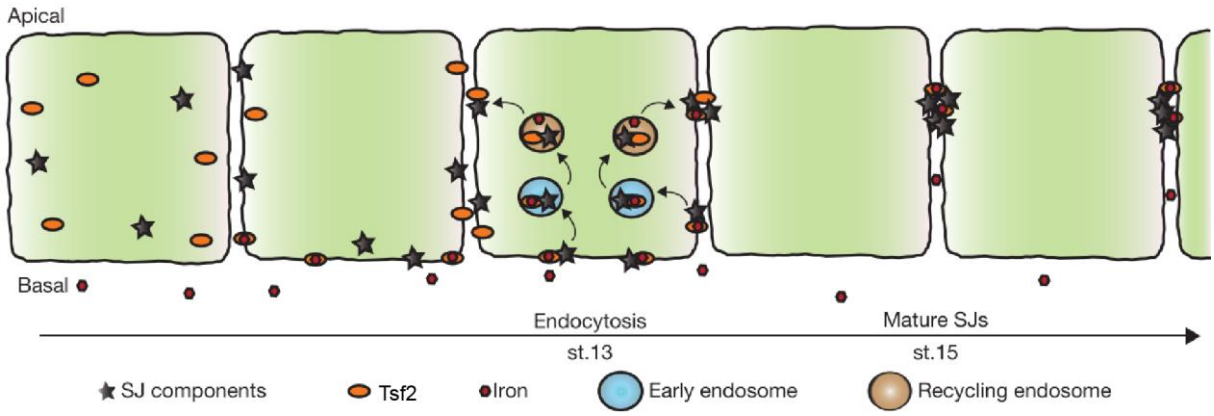

Figure 33. Pleated Septate Junctions assembly relies on endocytosis and Transferrin 2 iron binding. Adapted from (Tiklova, Senti et al. 2010)

the authors suggest that the binding of Tsf2 with iron is needed for proper Tsf2 activity at pSJ and like Udt, cleaved Tsf2 is enough to ensure pSJ integrity. It can incorporate in distant regions into pSJ. Interestingly, intracellular traffic mechanisms involved in pSJ establishment and maintenance are depicted in (Tiklova, Senti et al. 2010). Before pSJ establishment at embryonic stage 14, Tsf2 is found colocalizing with both Cont and Nrx-IV in intracellular punctae. While still at stage 13, Tsf2 shows colocalisation with Rab5 (early endosomal marker) and Rab11(recycling endosomal marker), which is also the case for Cora and Sinu. These colocalisations vanish in later embryonic stages **(Figure 33).** The authors conclude that Tsf2 binding iron is necessary to bind pSJ proteins and to induce recycling from the basolateral membrane at stage 13 to the final pSJ position across embryonic development.

Among the GPI-anchored proteins, a subgroup is defined: The Leucocyte Antigen 6 (Ly6) superfamily proteins, a domain shared by many proteins, such as the vertebrate CD-59, a complement inhibitor (Davies, Simmons et al. 1989). They are respectively called **Coiled (Cold), Crooked (Crok), Crimpled (Crim)** and **Boudin (Bou)**. They are composed of the typical Ly6 region which is a three-finger domain with an inner core stabilised by disulphide bridges (Low, Preston et al. 1976). They localize in the cytoplasm of epithelial cells (in punctate forms and colocalizing with KDEL endoplasmic reticulum marker) as well as at the membrane. Unlike previous pSJ components, their localisation is not restricted to the classical pSJ area. Only Bou shows Nrg overlapping signal even though its signal spreads more basally than Nrg (Tempesta, Hijazi et al. 2017) **(Figure 34).**

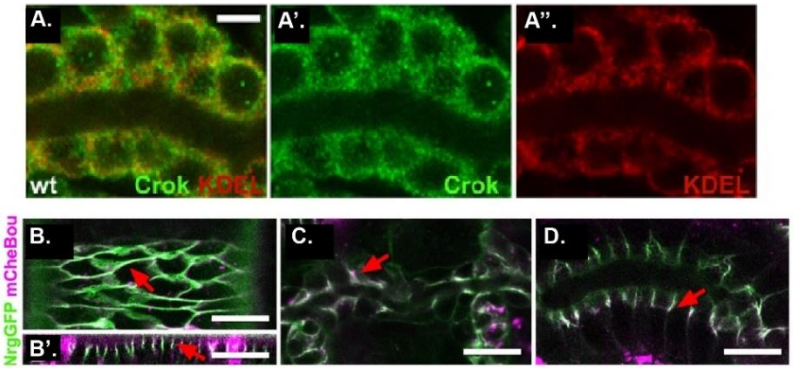

Figure 34. Ly6 Pleated Septate Junction Proteins Crooked and Boudin localisation. A-A''. Drosophila embryo tracheal cells stained for Crok (green) display cytoplasmic signals of Crok associated with a colocalisation with the endoplasmic reticulum marker KDEL (red). **B-D.** Stage 16 Drosophila embryos expressing mCherry tagged Boudin (mCheBou; magenta) and GFP tagged Nrg (NrgGFP; green), demonstrate colocalisation between the two in the epidermis (B), the tracheal (C) and Salivary glands (D). Adapted from (Nilton, Oshima et al. 2010) and (Tempesta, Hijazi et al. 2017)

However, mutants for Cold, Crok, Bou and RNAi for Crim reveal defects in paracellular tracheal barrier integrity, loss or disorganisation of septa as well the impaired localisation of pSJ components (Hijazi, Masson et al. 2009, Nilton, Oshima et al. 2010, Hijazi, Haenlin et al. 2011, Syed, Krudewig et al. 2011, Tempesta, Hijazi et al. 2017). Interestingly, *crok* and *cold* mutant cells display cytoplasmic puncta positive for Dextran and Nrx-IV, suggesting that both Crok and Cold play a role in pSJ trafficking (Nilton, Oshima et al. 2010) **(Figure 35).**

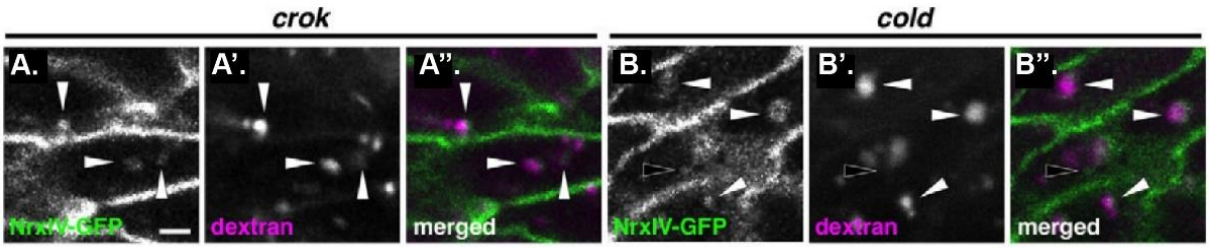

Figure 35. Loss of Ly6 proteins Crooked or Coiled leads to defects of Neurexin-IV intracellular trafficking. **A-A''.** Stage 14-15 Drosophila embryo epidermal cells expressing Nrx-IV tagged GFP (NrxIV-GFP, green) and mutant for Crok show vesicular structures positive for Dextran (magenta) colocalizing with NrxIV-GFP. Similar results are observed for cold mutant embryos in **B-B''**. Adapted from (Nilton, Oshima et al. 2010)

Notably, Bou is demonstrated to act in a cell non-autonomous way (Hijazi, Masson et al. 2009), which is contrariwise to Cold (Hijazi, Haenlin et al. 2011). Specifically, in the case of Bou, this protein travels extracellularly during the embryonic stage. It also relies on Nrg and Kune to be localized at pSJ, showing again the interdependence between pSJ actors (Tempesta, Hijazi et al. 2017).

- **The unclassified ones**

Since establishing groups is complex, I was not able to categorize the next proteins into categories, so they will be presented as such.

Yurt (Yrt) is similar to Cora, a cytoplasmic FERM protein with a PDZ binding domain in the C-terminal part that plays a role in cell polarity. Yrt colocalizes with Na^+/K^+-ATPase in embryos and when depleted of it, embryos display paracellular permeability defects but without strong effects on septa presence and organisation (Laprise, Lau et al. 2009). In this study, immunoprecipitation experiments also reveal that the FERM domain could interact with Nrg and the loss of Nrg diminishes the level of Yrt at pSJ. Moreover, genetic analysis reveals that Yurt acts in a redundant pathway with Cora to ensure cell polarity whereas Cora operates in another pathway with Nrx-IV and Na^+/K^+-ATPase (Laprise, Lau et al. 2009) **(Figure 36).**

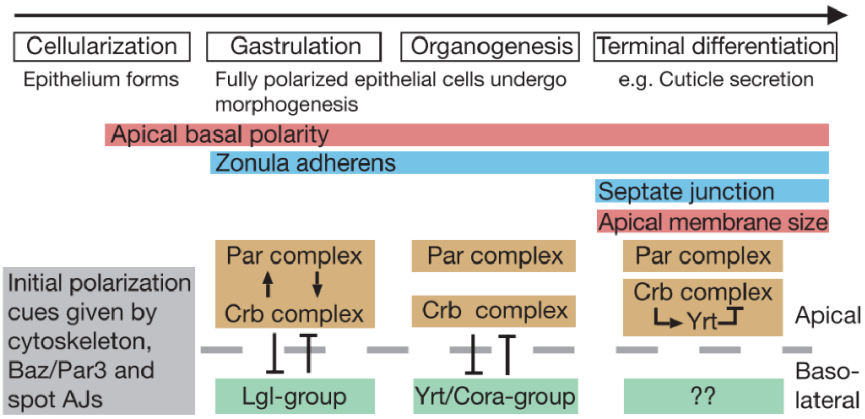

Figure 36. Overview of Drosophila junctions' synthesis, polarity acquisition and interaction between Yurt/Cora with the Crumbs polarity complex during organogenesis. Adapted from (Laprise, Lau et al. 2009)

A second component is **Macroglobulin complement-related (Mcr)**. It is part of the thioester protein family that is involved in innate immune response, with for example the human α-2 macroglobulin that binds to the pathogen surface. Mcr diverges from the thioester protein family with a mutated thioester motif and a transmembrane domain although it is involved in S2 cells phagocytosis of *Candida albicans* (Stroschein-Stevenson, Foley et al. 2006). Mcr colocalizes with many pSJ proteins including Cora, FasIII and Nrg (Batz, Forster et al. 2014, Hall, Bone et al. 2014). Mcr mutant embryos display habitual pSJ mutant defects, including the absent septa. Moreover, loss of pSJ leads to Mcr delocalisation and the almost disappearance in the case of Nrg mutant, which suggests a potential interaction between those two actors (Batz, Forster et al. 2014).

We then examine the tetraspan membrane proteins called **Pasiflora 1 and 2 (Pasi1 and Pasi2)**. They are four transmembrane segments proteins with a large and a small extracellular loop and an N and C-terminal cytosolic part. Despite sharing the same protein topology as Claudins, they exhibit no sequence similarity with them. They localize to the pSJ showing colocalisation with Cora at the membrane and rely on Kune, Nrg, Cold and Crok to be present at pSJ. Conversely, loss of Pasi1 or 2 disrupts pSJ organisation as demonstrated by Cora, Nrg, FasIII and ATP-α marking in the trachea and hindgut as well as trachea leaking (Deligiannaki, Casper et al. 2015).

Varicose (Vari) is similar to Dlg, a cytosolic MAGUK scaffolding protein. As a MAGUK protein, it contains a PDZ, a HOOK, a SH3 and also a L27 (link to scaffolding proteins) domains as well as an inactive guanylate kinase domain. Vari belongs to the subgroup of MAGUK proteins which contains the vertebrate scaffolding PALS2 for example (Wu, Yu et al. 2007, Bachmann, Draga et al. 2008, Moyer and Jacobs 2008). Vari localizes at pSJ, displays salivary glands and trachea leakage defects when absent as well as septa disappearance and biochemical experiments reveal that it binds the Nrx-IV intracellular part via its PDZ domain (Wu, Yu et al. 2007, Bachmann, Draga et al. 2008).

Wunen 1 and **Wunen 2**, referred as the **Wunens (Wun)**, are transmembrane proteins of the lipid phosphate phosphatases family. The lipid phosphate phosphatases family proteins are involved in the regulation of phosphorylated sphingolipids and glycerolipids. Wun has six transmembrane domains with the enzyme active site predicted to be extracellular. Wun is localized apically and apico-laterally at pSJ level, colocalizing with FasIII whereas Wun2 is found on the entire cell membrane (Ile, Tripathy et al. 2012) **(Figure 37).**

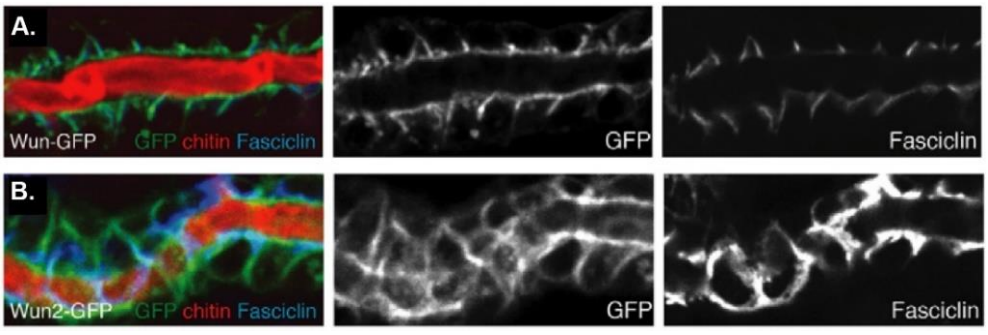

Figure 37. Localisation of Wunen isoforms in Drosophila embryo tracheal cells. A-B. Embryo tracheal cells expressing Wun-GFP (green) and stained for chitin (red) and FasIII (blue) show colocalisation between Wun and FasIII as well as Wun being restricted at pSJ level. On the contrary, Wun-2 GFP (green) spreads along the entire cell membrane in B. Adapted from (Ile, Tripathy et al. 2012)

Intriguingly, the loss of Wun and Wun2 at the same time leads to leakage defects and spreading of Nrx-IV, Cora and FasIII at the lateral part of cell in the tracheal cells at stage 16. However, septa are still present in double *wun* mutants and in the salivary glands, Nrx-IV and Cora are well restricted and only 50% of mutant embryos display FasIII delocalisation. Notably, the catalytic activity of Wun is required to ensure the trachea integrity since inactive H326K Wun2 expression cannot rescue *wun* mutant phenotypes.

The most recently discovered pSJ protein is **Würmchen (Wrm)**, a gene that encodes Würmchen 1 and Würmchen 2, two small transmembrane proteins. Wrm1, the larger one, localizes at pSJ level, colocalizing with Mega, whereas Wrm2 localizes at the most apical part of tracheal cells (Konigsmann, Parfentev et al. 2020) **(Figure 38).** Moreover, loss of Wrm1 but not of Wrm2 display classical pSJ mutant defects, including lack of septa.

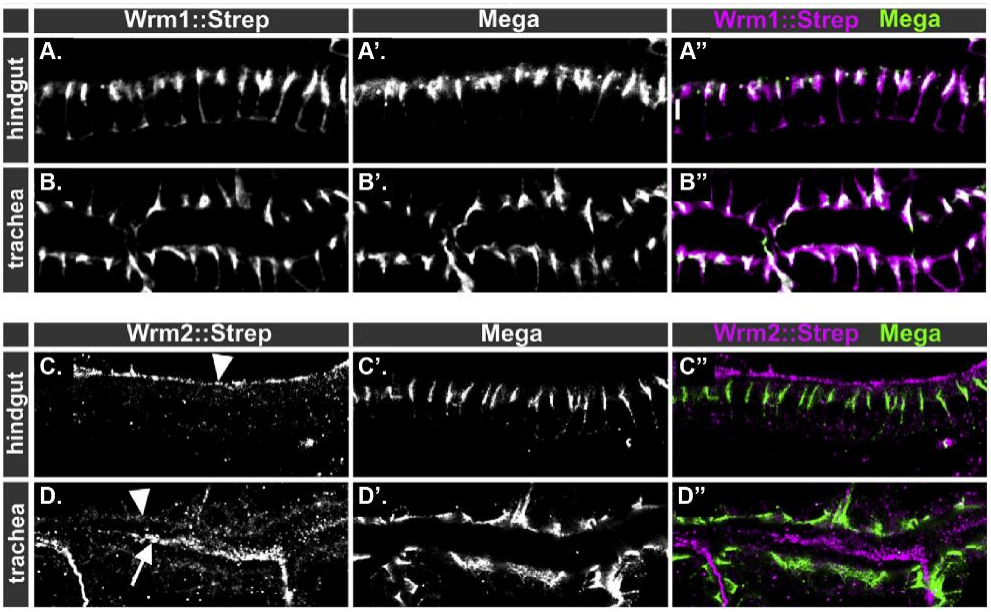

Figure 38. Localisation of Würmchen isoforms in Drosophila embryos. A-B''. Embryos expressing Wrm1::Strep and stained for Strep (white in A and B, magenta in A'' and B'') and Mega (white in A' and B', green in A'' and B'') demonstrate Wrm1 colocalisation with Mega and restriction of the signal to presumptive pSJ complex, in both hindgut and trachea. **C-D''**. Embryos expressing Wrm2::Strep and stained for Strep (white in C and D, magenta in C'' and D'') and Mega (white in C' and D', green in C'' and D'') demonstrate Wrm2 no colocalisation with Mega and an apical restricted localisation(white arrow and arrow head), in both hindgut and trachea. Adapted from (Konigsmann, Parfentev et al. 2020)

ii. Smooth Septate junction

Unlike the pSJ, very few studies address sSJ and, to date, only four proteins known to be exclusively present are described. As mentioned, most of the sSJ are found in endodermally derived tissues, such as the midgut and the gastric *caeca* but some ectodermally derived tissues also possess sSJs, such as the Malpighian tubules and the OELP. Notably, some of the proteins present at the pSJ are equally found at sSJs such as Dlg, Cora, Lgl and FasIII.

The first described at sSJ was the transmembrane protein **Snakeskin (Ssk)**. It is a four-transmembrane domains protein with two small extracellular loops and the N and C-terminal parts are intracellular. It is localized at the sSJ in the midgut and Malpighian tubules, which are revealed by the use of anti-Ssk antibody localizing at the parallel septa level using the TEM approach (Yanagihashi, Usui et al. 2012). Ssk is also essential for embryo development since only a few individuals hatch and develop to the first-instar larvae stage, even though midgut morphology and development are not impaired. Upon closer examination, the authors observe that the apical part of epithelial midgut cells protrudes following the loss of Ssk and that the parallel septa are missing with cell domains entirely lacking septa **(Figure 39).** They also demonstrated that the midgut barrier is disrupted using TRITC-labelled dextran in larvae food.

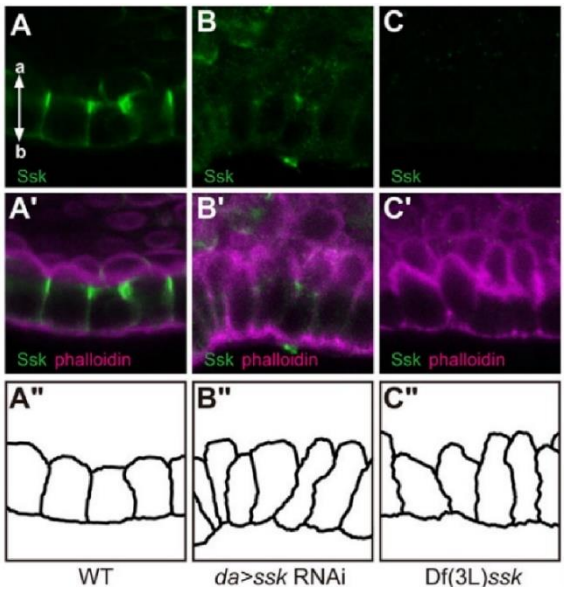

Figure 39. Drosophila embryo mutant for Snakeskin display abnormal anterior midgut cells morphology. A-C''. Late stage 17 embryos WT (A-A''), expressing a RNAi against Ssk (B-B'') or having a deficiency for the Ssk gene locus (C-C'') are stained for Ssk (green) and F-actin (Phalloidin, magenta). Loss of Ssk leads to apico-basally elongated cells associated with apical protrusions in the midgut lumen. Adapted from (Yanagihashi, Usui et al. 2012)

The same team then characterized another sSJ protein called **Mesh**. This is also a transmembrane protein with an extracellular part that contains a NIDO domain, an Ig-like E set domain, an AMOP domain, a vWD domain and a sushi domain. A GDPH autocatalytic cleavage site was identified in the vWD domain (Izumi, Yanagihashi et al. 2012). It is localised at sSJ level in the midgut, Malpighian tubules and gastric *caecum* and displays colocalisation with Ssk (Izumi, Yanagihashi et al. 2012). Loss of Mesh leads to Ssk apical accumulation and delocalisation as well as the spreading of Lgl, Dlg and Cora, but not FasIII, along the lateral membrane. Loss of Mesh also disrupts parallel septa and impairs the midgut barrier **(Figure 40).** Co-immunoprecipitation reveals interaction with Ssk. Ssk is required to ensure that Mesh is correctly localised and that the S2 cells expressing Mesh-GFP are adhering, suggesting that Mesh has an adhesive role (Izumi, Yanagihashi et al. 2012).

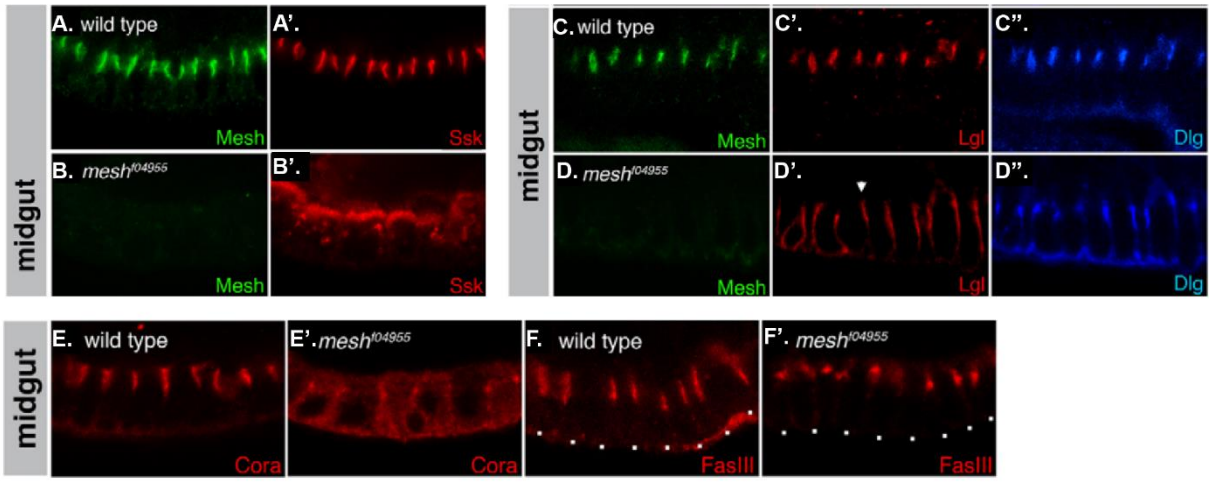

Figure 40. Smooth Septate Junction Protein Mesh is required to ensure Smooth Septate Junctions homeostasis. A-F'. First instar larvae midguts stained for sSJ proteins Mesh (green), Ssk (red) in A'-B', Lgl (red) in C'-D', Dlg (blue) in C''-D'', Cora (red) in E-E' and FasIII (red) in F-F'. WT larvae show colocalisation between Mesh and Ssk (A-A') and between Mesh, Lgl and Dlg (C-C''). Loss of Mesh leads to Ssk delocalisation and accumulation at apical level (B-B'), basal spreading of Lgl (D'), Dlg (D'') and Cora (E') but not FasIII (F'). Adapted from (Izumi, Yanagihashi et al. 2012)

Subsequently, the same team identified a new sSJ protein named **Tsp2A**. This is a tetraspanin family protein, composed of four transmembrane domains, two extracellular loops (one short and one big), one short intracellular loop and N and C-terminal part localised in the cell. Tsp2A localises with Mesh in the OELP and midgut (Izumi, Motoishi et al. 2016). Its loss results in the delocalisation of Mesh and Dlg and only minor defects are seen in the septa, the latter being less electron-dense. The

midgut barrier is also disrupted and Tsp2A needs Ssk and Mesh to be properly localised at sSJ (Izumi, Motoishi et al. 2016). Biochemical approaches highlight that Tsp2A forms a complex with Mesh and Ssk.

The last and novel sSJ protein discovered is **Hoka**. This is a transmembrane protein containing a very short extracellular part of 13 amino acids after cleavage of the signal peptide and with a rich threonine C-terminal region (Izumi, Furuse et al. 2021). Like the other sSJ compounds, it colocalises with sSJ proteins in the midgut, Malpighian tubules, gastric *caeca* and OELP. It forms a complex with Ssk, Mesh and Tsp2A and it is required to ensure the localisation of sSJ proteins, septa presence and midgut barrier integrity (Izumi, Furuse et al. 2021). In a similar manner, the localisation of Hoka requires the presence of the other sSJ proteins. Interestingly, Mesh and Tsp2A are delocalised in the cytoplasm and Ssk at the apical part in the case of sSJ defects, whereas, in *hoka* mutant cells, Mesh and Tsp2A are spread all along the lateral membrane. These results suggest that the core component of sSJ could be formed by Ssk, Mesh and Tsp2A and that Hoka regulates sSJ integrity at a different level (Izumi, Furuse et al. 2021).

c. Pleiotropic SJ proteins activities

During embryogenesis, different mechanisms occur in order to shape the future individual. In the *Drosophila*, two well described processes occur, namely the dorsal closure (DC) and the head involution (HI). Besides these main events, organogenesis also takes place with the establishment of the trachea, salivary glands (SG), the hindgut, the dorsal vessel (which is the equivalent to the heart in the *Drosophila*), imaginal discs, oogenesis and also the blood brain barrier (BBB), to name a few. In this section, I outline the current state of knowledge about the role of SJ proteins beyond their primary identified roles of establishing a paracellular permeability barrier.

i. The Blood Brain Barrier

I begin by describing the BBB since the decision was taken not to address it in the previous section. Therefore, the paracellular permeability role is briefly outlined below.

Insects, unlike their related living vertebrates, have their CNS exposed to the haemolymph, a fluid highly concentrated in K^+ and glutamate. In order to avoid any defects at neuronal level, such animals need to prevent the CNS from floating into this haemolymph. BBB starts to form at the end of embryogenesis (around 16h after the egg is laid)(Schwabe, Li et al. 2017) with the so-called polarised subperineurial glial cells (SPG) that elaborate SJs (Beckervordersandforth, Rickert et al. 2008, von Hilchen, Bustos et al. 2013) **(Figure 41).**

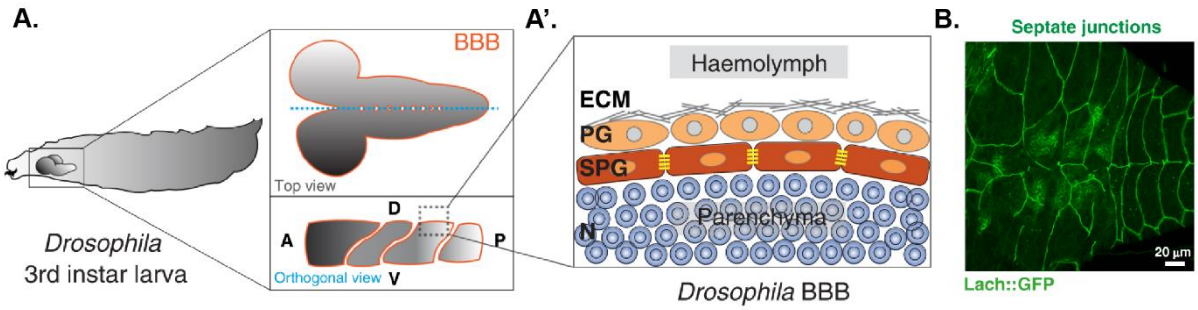

Figure 41. Drosophila third instar larva brain and associated blood brain barrier. A-A'. Schema of the larval brain surrounded by the BBB (dark orange in A) and close-up (A'). A: anterior, P: posterior, D: dorsal, V: ventral. ECM: extracellular matrix, PG: perineurial glia, PC: pericytes, SPG: subperineurial glia, E: endothelial cells, N: Neurons. SJs are representing in yellow. **B.** Confocal image of the BBB highlighted by the pSJ protein Lach::GFP. Adapted from (Benmimoun, Papastefanaki et al. 2020)

Most of the pSJ proteins are found at the BBB as well as certain G-protein signaling-related proteins, not previously discussed in this paper, namely **Moody** (a GPCR), the two heterotrimeric G proteins α subunits **Gαi-βγ** and **Gαo- βγ** and the regulator of G protein signaling **Loco**. Loss of any of these four proteins or other pSJ components leads to BBB defects associated with leakage, a phenotype highly similar to that observed in the trachea and SG (Limmer, Weiler et al. 2014).

Interestingly, the BBB needs to grow quickly during larval development which indicates a pSJ remodelling. However, pSJ proteins are found to be present at the embryonic stage, establishing highly stable complex proteins as mentioned before. In this case, it is hard to reconcile the need for a rapid cellular size adaptation and this quasi-fixed state of the pSJ complex. A study by (Babatz, Naffin et al. 2018) demonstrates how this process happens. The authors first highlight, using Nrv-2 Dendra-tagged, that pSJ compounds at the BBB are not recycled during larval growth, having being able to observe photoconverted Nrv-2::Dendra for up to three days after photoconversion **(Figure 42).** More interestingly, they observed that new pSJ material is added between the AJ and SJ level and that "old" SJ components are dragged to the basal side, analogous to the pSJ assembly in pupal notum described by the team (Daniel, Daude et al. 2018). Then using super-resolution microscopy, they show that pSJs are in a fold state at the beginning of larval stage and unfold across CNS growth during neuroblast divisions.

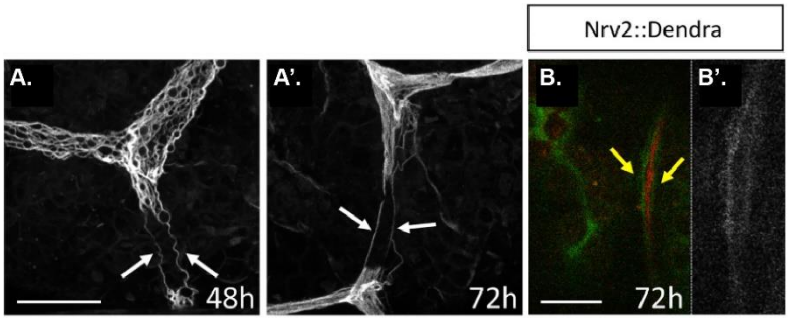

Figure 42. Pleated Septate Junction protein Nervana-2 forms the blood brain barrier and exhibits extremely slow turn over associated with an unfolding upon maturation. A-A'. Super-resolution images of second instar larvae (A) or third instar larvae (A') BBB via Nrx-IV::GFP signal. Between 48h and 72h after the bleaching of the area showed by white arrows, we could observe that strains of pSJs have been stretched, switching from a crumpled morphology to a straight one. **B.** Nrv-2 is fused to a photoconvertible probe Dendra (Nrv2::Dendra) and photoconversion reveals that old Nrv2 (red, photoconverted) is still present and newly added Nrv2 (green) is present on the lateral side of photoconverted Nrv2, 72h after the photoconversion. Adapted from (Babatz, Naffin et al. 2018)

Subsequently, the authors revealed that loss of Moody impairs pSJ organisation, as fragmented junction strands, including big Nrx-IV structures, are not incorporated correctly into the pSJs. Intriguingly, loss of the Wasp protein (an activator of the ARP2/3 nucleation complex of the actin) in the *moody* mutant context increases the

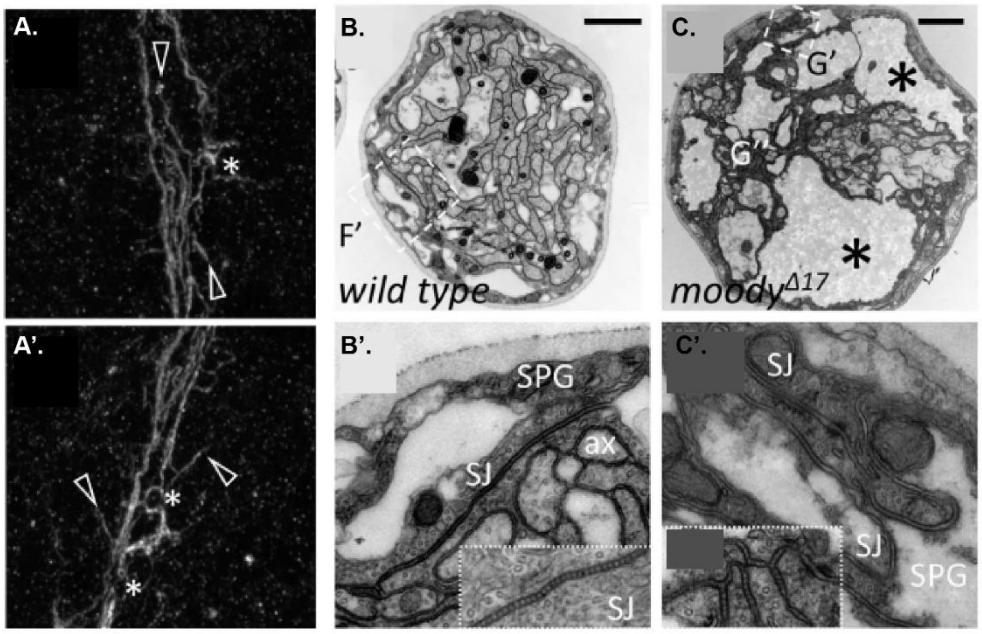

Figure 43. Defects in Pleated Septate Junctions assembly leads to interdigitated extension of the Drosophila blood brain barrier cells. **A-A'**. Confocal images of BBB cells moody mutant reveal Nrx-IV not integrating properly in pSJ strands associated with discontinued pSJ strands. **B-C'**. TEM analysis of third instar larvae BBB show that on the contrary of WT situation (B-B'), where SPG cells exhibit proper formed pSJ, moody SPG cells show no continuous stretch of pSJ strands, large number of interdigitated membranes as well as large liquid areas in the nerves (asterisks). Adapted from (Babatz, Naffin et al. 2018)

previous phenotype, suggesting that branched actin is playing a role in the pSJ arrangement. In addition, using TEM, they showed that loss of Moody (or Nrx-IV), which impairs the structural organisation of the pSJ, leads to cell-cell interdigitations, excessive membrane folds and large swelling inside nerves, arguing in favour of a somehow compensatory mechanism induced upon pSJ defects **(Figure 43).**

To conclude, pSJs are here shown to be of a capital importance for permeability barrier functions but also for the morphology and growth of the BBB, arguing for a more general role of pSJs, as further presented in the next section.

ii. Development and Morphogenesis

- **The trachea, the salivary glands and the hindgut**

Besides their well characterised phenotype of trachea and SG leakage, pSJ mutants display an over-elongated trachea phenotype **(Figure 44)**. The trachea is formed during embryogenesis starting from tracheal placodes around stage 9, localised on each side of the embryo at the level of thorax and abdomen and composed of around 40 cells. Then those cells divide once and give rise to tracheal metameres. Tracheal metameres are internalised and migrate to form future branches at stage 10. At stage 12, the primary branches start to form and migrate in order to begin to fuse by stage 14, thus making this interconnected tubular trachea. During late embryogenesis and until stage 17, the terminal branches continue to develop (Maruyama and Andrew 2012) **(Figure 45).**

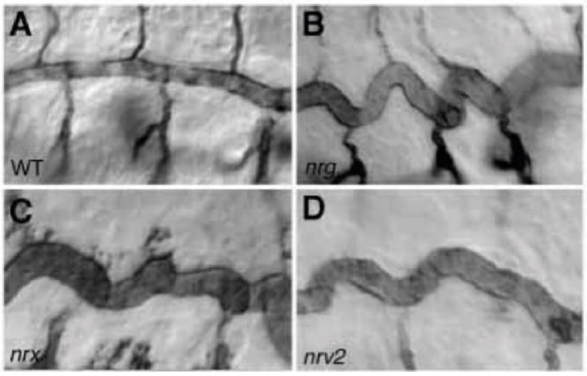

Figure 44. Drosophila embryo trachea classical Pleated Septate Junction mutant phenotype. On the contrary of WT (A) where the trachea is straight, loss of pSJ proteins such as Nrg (B), Nrx-IV (C) or Nrv2 (D) leads to over-elongated and undulated tracheas. Adapted from (Paul, Ternet et al. 2003)

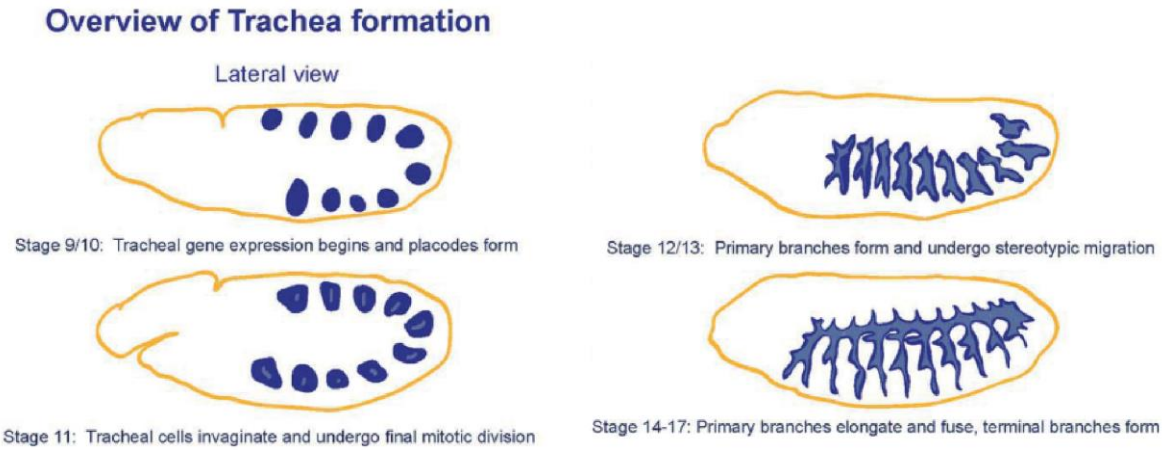

Figure 45. Scheme representing the trachea formation during Drosophila embryogenesis. Adapted from (Maruyama and Andrew 2012)

This development, particularly the regulation of the trachea length, relies on many proteins and pathways, including apico-basal polarity (Laprise, Paul et al. 2010), cell adhesion (Swanson, Yu et al. 2009), extracellular matrix integrity (Dong, Hannezo et

al. 2014), secretion of luminal matrix-modifying enzymes such as Serpentine (Serp) and Vermiform (Verm) (Luschnig, Batz et al. 2006, Wang, Jayaram et al. 2006) and the Hippo pathway (Robbins, Gbur et al. 2014). Any defects will lead to aberrant tracheal morphogenesis.

One example of the roles of pSJ in such mechanisms is the inability to accumulate Verm and Serp, two important proteins for the remodelling of the chitin matrix in the trachea, at the luminal part of the trachea epithelial cells, in pSJ mutants (Wu, Yu et al. 2007, Laprise, Paul et al. 2010, Nelson, Furuse et al. 2010, Tiklova, Senti et al. 2010, Ile, Tripathy et al. 2012, Batz, Forster et al. 2014, Konigsmann, Parfentev et al. 2020).Verm is trapped in tracheal cells mutant for ATP-α, Sinu and Lac (Wang, Jayaram et al. 2006). Another example is Cora, known for its role in regulating cell polarity with other pSJ components in the epidermis of embryos (Laprise, Lau et al. 2009). The same team shows that Cora and Yurt are needed to ensure pSJ integrity as well as apical membrane size, hence the trachea length, by regulating Crumbs at the apical level, which is known to regulate apical membrane size, as previously described (Laprise, Paul et al. 2010). Moreover, this pathway is independent of that involved in the regulation of the Verm and Serp secretion, suggesting multiple inputs and roles of the pSJ actors in regulating trachea length **(Figure 46).**

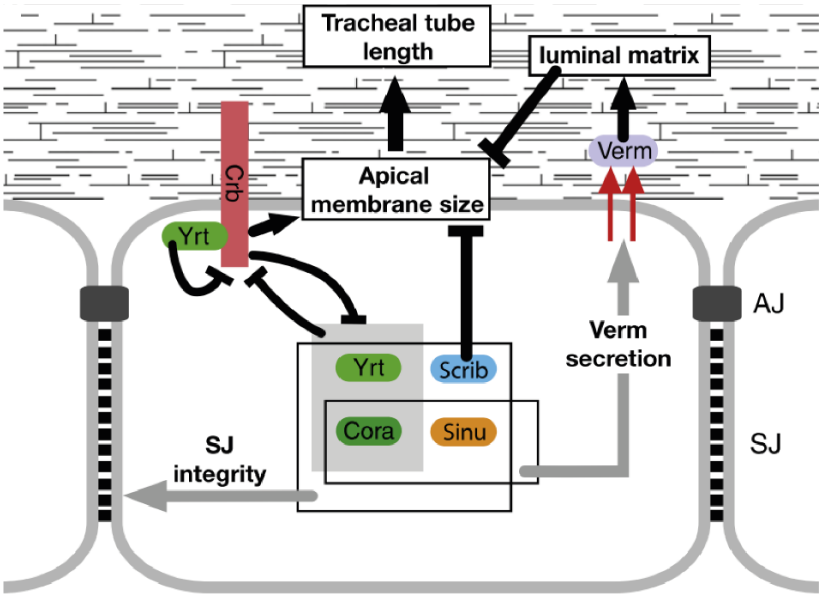

Figure 46. Pleated Septate Junction Proteins regulate the tracheal tube length via their interactions with Crumbs. Adapted from (Laprise, Paul et al. 2010)

The effects of Crumbs impairment in the trachea has also been demonstrated by the work of (Dong, Hannezo et al. 2014), in which depletion of the ESCRT-III component

Shrub leads to Crumbs apical accumulation associated with apical cell size increasing. It is interesting to note that this phenotype upon Shrub depletion is also associated with leakage, and Cora and Kune impaired localisation, indicating that pSJ components play regulatory roles in Shrub here.

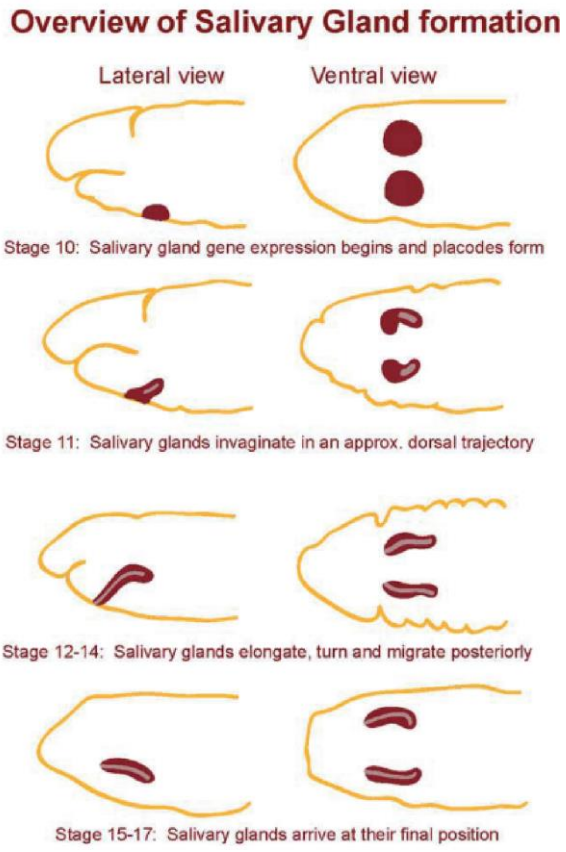

Figure 47. Scheme representing the salivary glands formation during Drosophila embryogenesis. Adapted from (Maruyama and Andrew 2012)

SGs are formed, like the trachea, of placodes composed of around 100 epithelial cells at stage 10. During embryo development, posterior cells of the placode start to constrict apically which induces tube internalisation around stage 11. The placode cells localised in a more anterior position also constrict apically, continuing to form the future tubes of the SG. The final most anterior non-internalised cells of the placode then begin to do so in a wrapping-type manner at the same time that posterior elongation occurs in the salivary tubes, starting at stage 12. The first internalised cells continue to push and migrate in the embryo until reaching their final destination around stage 17, forming the antero-posterior aligned tubes of the SG (Maruyama and Andrew 2012) **(Figure 47).**

During this process, epithelial cells have to rearrange both their contacts and their shapes in order to permit SG tubules antero-posterior elongation (Bradley, Myat et al. 2003, Vining, Bradley et al. 2005, Xu, Bagumian et al. 2011). Upon the loss of Nrv-2, Nrg, Cora, Nrx-IV, ATP-α or Mcr, abnormal deposits are observed as well as an abnormal morphology of the SGs (Ward IV, Lamb et al. 1998, Genova and Fehon 2003, Hall, Bone et al. 2014). A study performed by (Hall and Ward 2016), described in detail such phenotypes using *Mcr*, *Nrg*, *Cont* or *kune* mutant. The authors observed in abnormal SGs that cell morphologies are changed and look more cuboidal than the WT columnar ones **(Figure 48).** Moreover, cell rearrangement is defective and a

migration defect is suggested, based on the bent morphology of the SGs. Since such defects are observed as early as stage 13, the results once more indicate a “non-classical” pSJ proteins function, regardless of the role they play in paracellular permeability barrier.

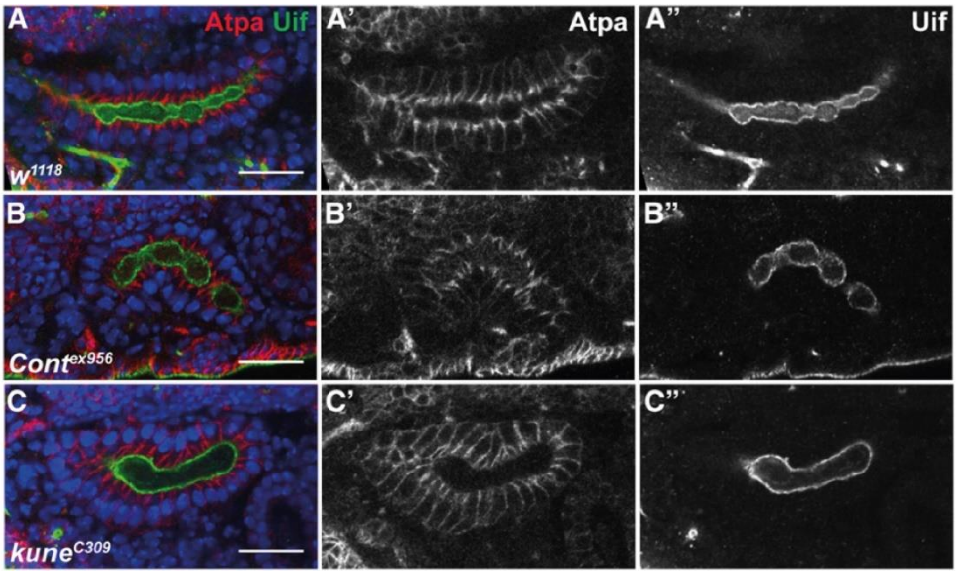

Figure 48. Pleated Septate Junction proteins ensure correct Drosophila salivary glands morphogenesis. A-C’’. Stage 16 Drosophila salivary glands are stained for ATP-α (red) and the apical marker Uif (green). Cont (B-B’’) or kune mutant (C-C’’) display shorter and fatter salivary glands compared to WT (A-A’’). Adapted from (Hall and Ward 2016)

The effect of pSJ proteins on hindgut morphogenesis is less clear. FasIII is considered as an associated pSJ protein since it is not strictly required to establish paracellular permeability or to ensure the localisation of other pSJ actors. Nevertheless, loss of FasIII results in a straightened hindgut curve and, given that it is a cell adhesion molecule, this effect could indeed be explained by its disappearance. The same phenotype is observed upon loss of Vari which highlights the pleiotropic effects of pSJ proteins as well (Wells, Barry et al. 2013).

- **The Imaginal discs**

Imaginal discs are ectodermally-derived tissues that grow and evolve during larvae stages in order to migrate and give rise to define adult parts (wings, legs, etc.), thanks to the metamorphosis processes. Most studies of the roles of pSJ during imaginal discs metamorphosis were carried out using hypomorphic mutations or specific tissues induction of RNAi against pSJ components, since embryos which are mutant for those proteins are not viable. Hypomorphic mutant *cora* displays malformed legs, defects in

the rotation of the ommatidia and genitalia (Ward IV, Lamb et al. 1998) and misoriented wing hairs (Venema, Zeev-Ben-Mordehai et al. 2004), which is also observed upon expression of an RNAi against Vari (Moyer and Jacobs 2008). Another study relates that heterozygous mutant *Mcr* in a *broad* (an ecdysone, hormone necessary to morphogenesis, inducible early gene) mutant background also results in abnormal legs (Ward, Evans et al. 2003).

A recent study by (Pannen, Rapp et al. 2020) showed the involvement of both retromer and ESCRT complex in pSJ proteins' intracellular traffic and that defects in this process lead to neoplasia growth. Having first knocked-down ESCRT-III's core component, Shrub, along with the expressing viral caspase inhibitor p35 in the posterior part of the wing disc, to prevent the apoptosis which is known to occur upon loss of ESCRT function, the authors observed neoplasia. This tissue showed no irregularities, or minimal ones at AJ level, compared to the WT anterior part of the wing disc. However, the authors noticed defects at pSJ level as demonstrated by TEM, showing a reduced number of septa. They also looked at Lac::GFP, which spread at the lateral membrane and was shown to be less stabilised when probed by FRAP analysis, displaying classical features of impaired pSJ complex. Moreover, there is a delocalisation of Mega at the basal side of the cell. Therefore, the authors claimed that Mega relies on Shrub

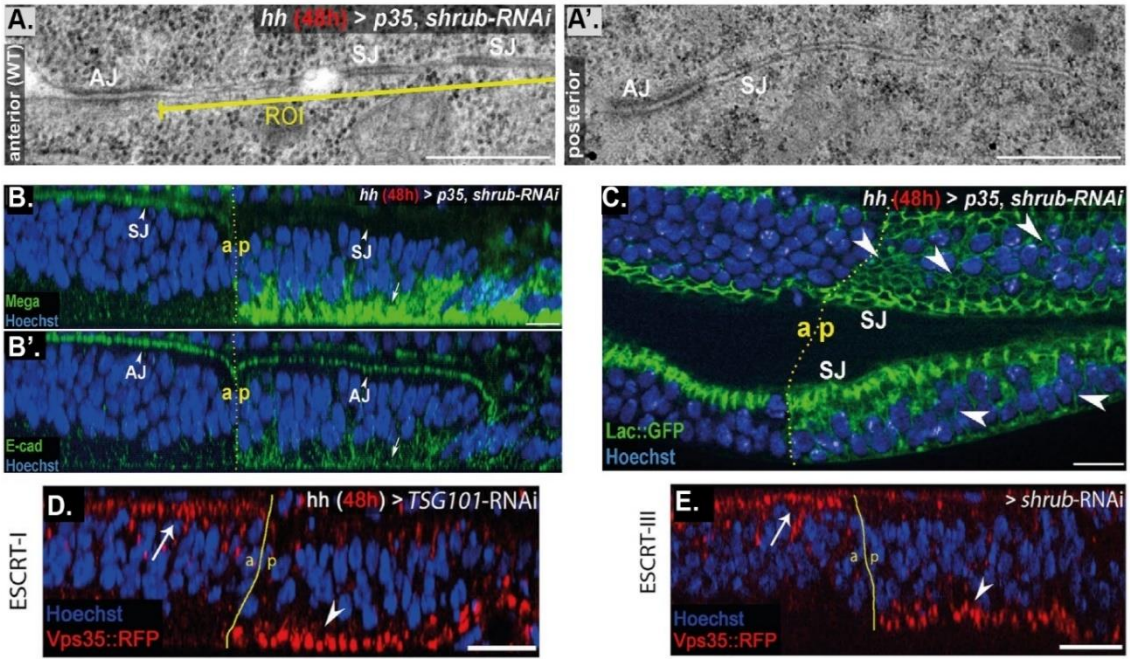

Figure 49. The ESCRT-III protein Shrub targets retromer at apical level in order to ensure the correct delivery of Pleated Septate Junction components in Drosophila wing discs. A-A'. TEM analysis of wing discs reveal that loss of Shrub along with expression of p35 strongly reduce the size of pSJ (A') compared to WT (A). **B-B'.** Confocal images of transversal view of wing discs showing basal delocalisation of Mega (green, B) or E-Cad (green, B') in the posterior region expressing RNAi against Shrub with p35 compared to control region in the WT anterior part (B-B'). **C.** Similar results are observed using Lac::GFP (green, C) probe, where this time, it spreads along lateral membrane rather than being trapped at the basal side. **D-E.** RNAi targeting ESCRT-I component TSG101 (D) or ESCRT-III Shrub (E) show delocalisation of the fluorescently tagged retromer protein Vsp35::RFP (red, D-E). Nuclei are marked by Hoechst (blue). Yellow dashed line shows the boundary between the anterior (a, control situation) and posterior (p, mutant situation) part of the wing discs. Adapted from (Pannen, Rapp et al. 2020)

for its localisation **(Figure 49).** The ESCRT complex localises the retromer complex, notably the retromer protein Vps35, at the apical level in epithelial wing discs cells in order to deliver Mega at pSJ. Indeed, Mega colocalises with the Vps26, another retromer component, and Vps35 proteins and the knock-out of Vps26 or Vps35 leads to a lower Mega signal at pSJ. This is, in fact, the first study showing the importance of both retromer and ESCRT complexes in regulating pSJ traffic. Interestingly, and as previously described, Shrub is also involved in pSJ homeostasis regulation (Dong, Hannezo et al. 2014). These results strongly indicate that pSJ is regulated by the ESCRT III protein Shrub, a subject I have explored during my PhD.

- **The Dorsal vessel** (*Drosophila* heart)

The dorsal vessel (DS) is an organ apparently devoid of any pSJs (Rugendorff, Younossi-Hartenstein et al. 1994, Yi, Johnson et al. 2008) and constituted of different types of cells, namely the contractile cardiomyocytes and non-myocytes which are the epicardial and endocardial cells. This organ could be seen as a linear tube made up of two inner rows of cardiomyocytes surround by two other rows of pericardial cells (Cripps and Olson 2002, Zaffran and Frasch 2002). Pericardial cells look like nephrocytes, particular cells involved in the filtration of toxins and proteins from the haemolymph (Das, Aradhya et al. 2008, Helmstadter, Huber et al. 2017, Lim, Bao et al. 2019). A screen for mutants with cardiac abnormalities performed by (Yi, Han et al. 2006) revealed that many actors are involved in the attachment of cardiomyocytes to the pericardial cells. Among these, the G protein γ subunit Gγ1, the HMG-CoA reductase and Nrx-IV are associated with the so-called "broken heart" phenotype. Another study by the same team shows that Sinu, Cora and Nrv2 are also involved in this phenotype (Yi, Johnson et al. 2008). More particularly, inducing mutations of the

former pSJ proteins in addition to Gγ1 shows that they are acting in the same pathway. For example, loss of Gγ1 leads to the impaired localisation of pSJ protein coupled with signal reduction. These studies indicate that pSJ proteins have adhesive properties in the context of DS.

A recent work by (Lim, Bao et al. 2019) demonstrates new properties of pSJ proteins in the context of DS. Normal cardiac function relies on reactive oxygen species activating p38-MAPK pathway in the pericardial cells that regulate cardiomyocytes' function (Lim, Wang et al. 2014). Here, the authors show that Cora and Kune are sensitive to reactive oxygen species level and act as downstream key players into the p38 signaling pathway. Cora also positively regulates Kune presence in the pericardial cells but loss of Kune has no effect on the Cora level. Moreover, the Kune levels in pericardial cells are sufficient to regulate Kune level in cardiomyocytes and vice versa, hence ensuring regular cardiac activity and DS diameter (Lim, Bao et al. 2019) **(Figure 50)**.

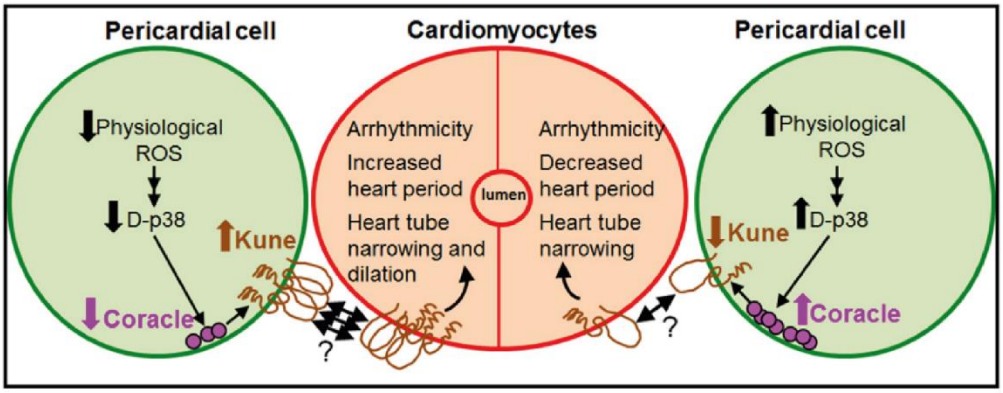

Figure 50. Model of the Pleated Septate Junction Proteins Coracle and Kune Kune roles in Dorsal vessel function regulation. Adapted from (Lim, Bao et al. 2019)

- **The Dorsal Closure (DC) and Head Involution (HI)**

The DC is a morphogenetic process which starts around stage 13 of embryogenesis. Just after the germband retraction around stage 12, the epidermis moves to cover the lateral and ventral parts of the embryo leaving a dorsal hole constituted of large, flat cells forming the amnioserosa. Epidermal cells have to cover this hole and this mechanism requires the accumulation of NMY-II and F-actin as well as the Jun N-

terminal kinase (JNK) signalling pathway. During this step, without any epidermal cell divisions, the dorsal-most epidermal cells, called leading edge cells (found at the purse strings), move and change their shape in order to progressively seal the amnioserosa part of the embryo. At the same time, amnioserosa cells are contracting thanks to their medial-apical network. When epidermal cells meet at the frontier formerly occupied by the amnioserosa, they initiate the zipping process which relies on cell actin-based protrusions combined with amnioserosa cell ingression and death **(Figure 51).** The DC event ends at stage 15 (Kiehart, Crawford et al. 2017).

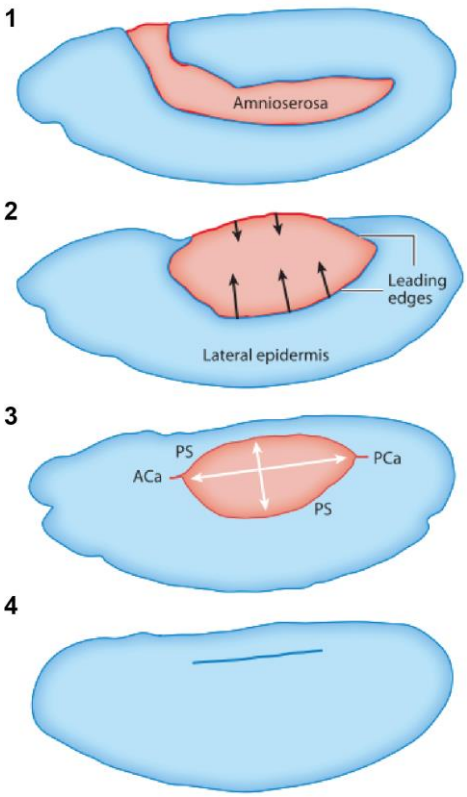

Figure 51. Scheme of Drosophila dorsal closure process during embryogenesis. 1. Extended germ band stage. **2.** End of germband retraction. **3.** Dorsal closure beginning. **4.** End of Dorsal closure. ACa: anterior canthus. PCa: Posterior canthus. PS: Purse string. Adapted from (Kiehart, Crawford et al. 2017)

The HI occurs parallel to the DC process and also starts at the germband retraction event. Three segments called procephalon and three others called gnathal segments, localised at the anterior part of the embryo, move in a dorsal and posterior way and start to form the dorsal ridge. This dorsal ridge then moves toward the anterior part and head segments are internalised all along the HI event. By stage 15, the HI is almost accomplished (VanHook and Letsou 2008).

One the first effects of pSJ component loss on the mechanisms outlined above was revealed by the phenotype of the *cora* mutant, which displays defective DC and HI (Fehon, Dawson et al. 1994). The DC defect is rescued in the *cora* mutant by the full-length Cora or just the N-terminal part containing the FERM domain, demonstrating the involvement of Cora during this event (Ward IV, Schweizer et al. 2001). Additional effectors give the same phenotype, namely Nrx-IV (Baumgartner, Littleton et al. 1996) and Mcr (Hall, Bone et al. 2014). Based on these results, (Hall and Ward 2016) decided to investigate the effect of other pSJ protein mutants. Mutants for Cora, Cont, Kune,

Lac, Mcr, Tsf2, Nrg, Nrv2 and Nrx-IV all display strong defects in HI and more heterogenous results for DC, with Mcr, Nrx-IV and Cora showing the strongest impact on DC. It is interesting to look at the paracellular barrier establishment timing compared to DC and HI. Stage 15 corresponds to the end of DC and HI but only to the beginning of SJ barrier integrity onset. Therefore, we could infer that the permeability role of the pSJ proteins is not involved in such morphogenetics events, showing further evidence of pSJ protein pleiotropic roles.

- **Oogenesis**

The *Drosophila* egg chamber has served as a very useful model to study epithelial morphogenesis. One eggshell is produced by an egg chamber, formed in the ovary in the part called the germarium. One egg chamber consists of 15 nurse cells and one oocyte, which are surrounded by a follicular epithelium. The egg chamber develops through 14 different stages (Osterfield, Berg et al. 2017, Popkova, Rauzi et al. 2021). Across the maturation of the egg chamber, different morphogenetics occur, such as the dorsal appendage formation, border cell migration, egg chamber elongation and

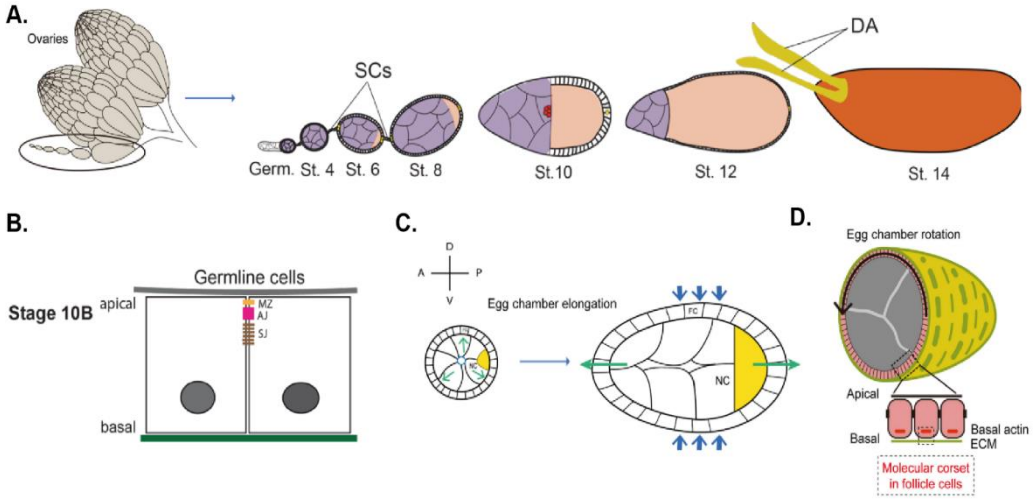

Figure 52. Overall view of Drosophila oogenesis. A. Drosophila ovary is composed of ovarioles which are composed of strings of egg chambers connected through stalk cells (SCs) showing different development stages. The final mature stage is stage 14 where dorsal appendices (DA) are present**. B-D.** Scheme of follicular cells (FC) surrounding nurse cells (NC) and the oocyte (yellow). SJ are formed at stage 10B (B). Egg chamber is elongated along green arrows axis and compressive forces are shown by blue arrows (C). During maturation, egg chamber starts to rotate as illustrated by the black arrow (D). Adapted from (Popkova, Rauzi et al. 2021) and (Alhadyian, Shoaib et al. 2021)

rotation. The maturation process also requires junctional establishment in the polarised follicular cells that build a mature pSJ beginning around stage 10B (Mahowald 1972) **(Figure 52).** The roles played by pSJ in the event of egg elongation have been shown

by (Alhadyian, Shoaib et al. 2021), who presented that RNAi against Lac, Sinu, Cont, Cora, Nrx-IV and Mcr induced in follicular cells leads to defects in egg shape, probably impairing the mechanism. Moreover, defects in bordel cell migrations, starting at stage 9 and ending at stage 10, are also observed upon knock-down of Cont, Cora or Nrx-IV at a time when pSJs are not fully mature. Those recent results, although heterogenous, suggest again that the core components of pSJ have additional functions, although off-target effects cannot be neglected here.

iii. Signalling pathways

As formerly mentioned, the midgut is a *Drosophila* tissue with an inverted polarity compare to other tissues, devoid of pSJ but with sSJ presence. However, many components present in pSJ are still found at the midgut level.

More precisely, the midgut shares remarkable similarities with the human intestine. It is composed of intestinal stem cells (ISCs), enterocytes (EC), EC progenitors which are enteroblasts (EB), secretory enteroendocrine cells (EE) and progenitors of EEs called enteroendocrine mother cells (EMC) (Micchelli and Perrimon 2006, Ohlstein and Spradling 2006, Guo and Ohlstein 2015) **(Figure 53).** It is known that during the aging of *Drosophila*, the midgut barrier declines and is associated with inflammatory and metabolic defects (Rera, Clark et al. 2012) as well as the reduction of many SJ components, such as Mega, Sinu, Kune and Dlg, observed by qPCR approaches from intestines (Clark, Salazar et al. 2015).

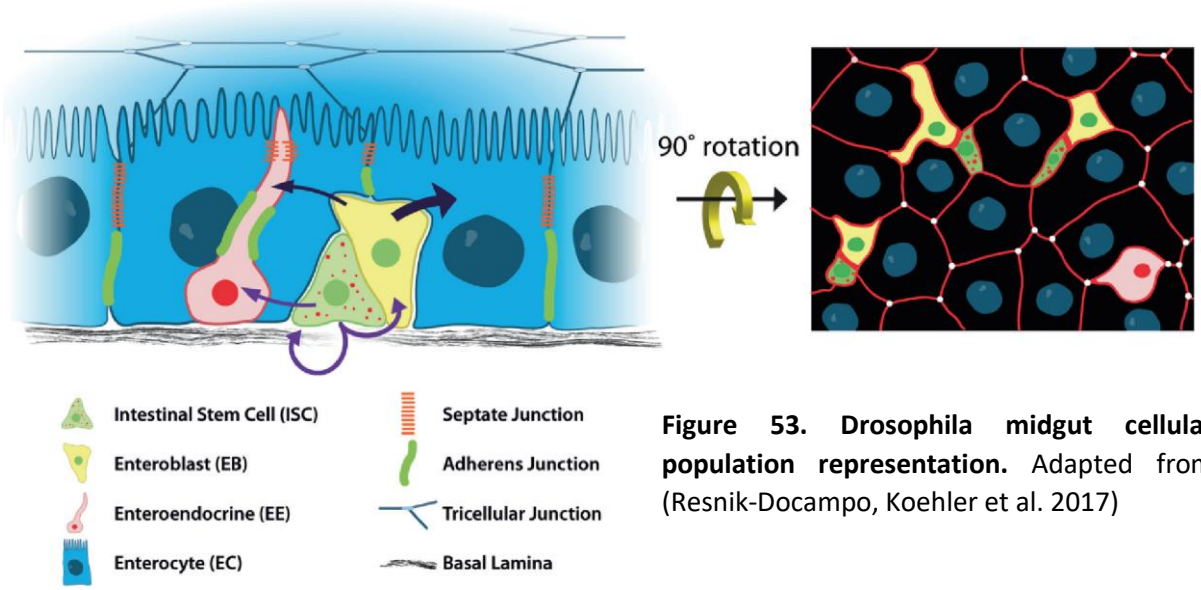

Figure 53. Drosophila midgut cellular population representation. Adapted from (Resnik-Docampo, Koehler et al. 2017)

Moreover, many research groups have reported defects in the midgut upon the knock-down of sSJ proteins. For example, loss of Ssk leads to altered gut morphology associated with ISC over-proliferation, impaired barrier function and dysbiosis (Salazar, Resnik-Docampo et al. 2018). In contrast, over-expressing Ssk rescues sSJ-mutant individuals and even extends lifespan by preventing barrier disruption and dysbiosis. One common point concerning the midgut defects upon sSJ impairment is the tissue hypertrophy associated with hyperproliferation. More precisely, different studies have described the complex interplay that exists between sSJ proteins and the signaling pathway controlling cell growth and proliferation. A key pathway involved in the regulation of cell growth is the previously described Hippo/YAP pathway.

A recent work by (Resnik-Docampo, Cunningham et al. 2021) revealed that Nrg could be involved in ISCs proliferation regulation. Indeed, the authors showed that Nrg is detected in ISCs and EBs but not in ECs, suggesting a probable independent role of a classic junctional protein for Nrg. Upon knock-out of Nrg in ISCs/EBs, the division rate is lower, whereas over-expression of Nrg provokes ISCs hyperproliferation. Moreover, suppression of Nrg is responsible for the loss of ISCs over the proliferation that occurs upon aging. The authors ended by demonstrating that epidermal growth factor receptor pathway, another key pathway of Midgut homeostasis regulation (Jiang and Edgar 2009, Biteau and Jasper 2011), acts downstream of Nrg in order to activate ISCs proliferation. This work revealed a previously undescribed role played by a pSJ protein in regulating ISC division.

To conclude this section, I wanted to present another context involving Hippo pathway and pSJ proteins is presented. Nrx-IV and Cora are reported to be necessary to establish the permeability barrier around the posterior signalling centre of the *Drosophila* lymph gland, an organ responsible for the production of immune cells called haemocytes. This permeability barrier is very important since it prevents signals from the posterior signaling centre from reaching the prohaemocytes and inducing development (Khadilkar, Vogl et al. 2017) **(Figure 54).**

The same authors showed that Nrx-IV and Cora act upstream of the Hippo/YAP pathway in the lymph glands context (Khadilkar and Tanentzapf 2019). As a matter of fact, loss of Cora or Nrx-IV induces over-proliferation of the immune subtype cells called crystal cells and the same phenotype is reported upon Hippo/YAP pathway inactivation. Genetic interaction studies have also revealed that Cora and Nrx-IV act upstream of two major Hippo/YAP pathway regulators, called Merlin and Expanded. Upon infection, an immune reaction is initiated and requires haemocytes proliferation via Hippo inactivation which is mediated by Cora downregulation in haemocytes. This work shows how pSJ proteins play a role in immune system homeostasis by modulating the Hippo/YAP signaling pathway and establishing a permeability barrier.

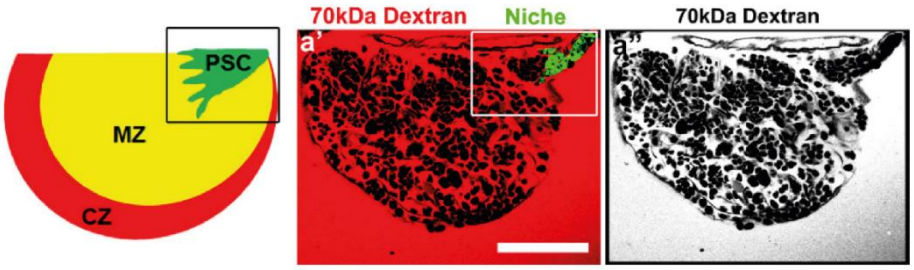

Figure 54. Drosophila lymph gland. CZ: Cortical zone. MZ: Medullary zone. PSC: Posterior Signalling Center (Niche). Injected Dextran (red) revealed impermeable niche highlighted in green. Adapted from (Khadilkar, Vogl et al. 2017)

iv. Adhesion and wound healing

A key feature of epithelia homeostasis regulation is the direction of cell division. Indeed, there are different outcomes, ranging from cell differentiation to death, depending on whether the daughter is included inside the plan of the tissue or left outside. Regulating the cell division orientation depends on orienting the cells' mitotic spindles. One interesting event during oogenesis is the fact that the follicular epithelial cells surrounding the egg chamber sometimes pop out during cell division. Upon mitosis, cells either WT or mutant for key proteins orienting the mitotic spindle (for example Mud, Inscuteable or Pins), round up and start to leave the layer of the follicular epithelium. However, they reintegrat into the tissue as the cytokinesis occurs (Bergstralh, Lovegrove et al. 2015). The authors observe the same property in different *Drosophila* tissues, such as the early embryonic ectoderm and the neuroepithelium of the optic lobe but not in the wing disc. Interestingly, this mechanism requires the presence of the homophilic adhesion protein FasII and the isoform Nrg^{167} but not, or to a minimal level, AJ integrity. Moreover, a recent work by (Cammarota, Finegan et al.

2020) has shown that FasIII is required for this reintegrating process, as well as the interaction with Ankyrin via the Nrg intracellular part. Nrx-IV is not needed during this event **(Figure 55).** It is interesting to note that this process happens at a time when pSJ are not mature and pSJ actors are spread along the lateral membrane, which again suggesting that pSJ p roteins play differential roles.

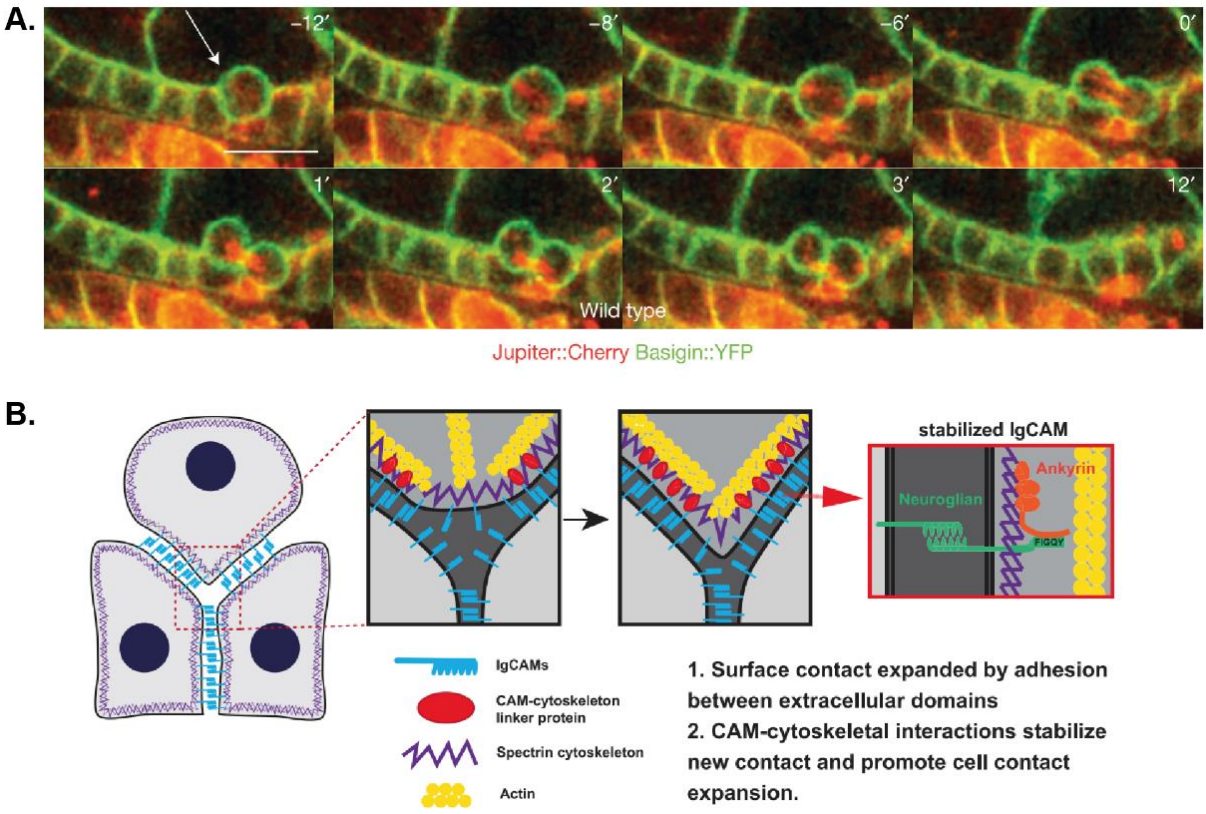

Figure 55. Reintegration of follicular cells into the layer upon mitosis in Drosophila egg chambers requires Pleated Septate Junction proteins. A. Time-lapse showing follicular cell expressing Jupiter::cherry (marking microtubules, red) and Basigin::YFP (highlighting cell membrane, green), reveals round up and pop-up mechanisms during mitosis followed by reintegration into the beneath cellular layer. Time is minutes. T=0 represents abscission onset. **B.** Scheme representing the reintegration model in the Drosophila egg chamber. The Nrg-Ankyrin interaction, via its link with the actin cytoskeleton, provides the necessary force to keep the cell into the layer during mitosis. Adapted from (Bergstralh, Lovegrove et al. 2015) and (Cammarota, Finegan et al. 2020)

Another key feature of epithelium homeostasis is its ability to repair upon injury, therefore preventing host invasion by pathogens. During wound healing repair, an actin cable is formed, as during the DC event. Formerly thought to be the major active driver of closure (Martin and Lewis 1992), the actin cable has been shown instead to protect part of the leading edge (Ducuing and Vincent 2016). It is coupled to the formation of filopodia and lamellipodia formed at the wound edge and shapes cell rearrangement (Razzell, Wood et al. 2014). It has only been recently revealed that pSJ proteins emerge as potential key players in the wound healing process. A screen using laser wounded embryos at late stage 15-16 and mutant for different pSJ actors revealed that wounds fail to close (Carvalho, Patricio et al. 2018). This is the case for the transmembrane proteins Nrg, Nrx-IV, Sinu, Kune, Mega but also the cytosolic Cora, Vari, Dlg and Ly6 family Cold and Crok. During the rest of the study, the authors used

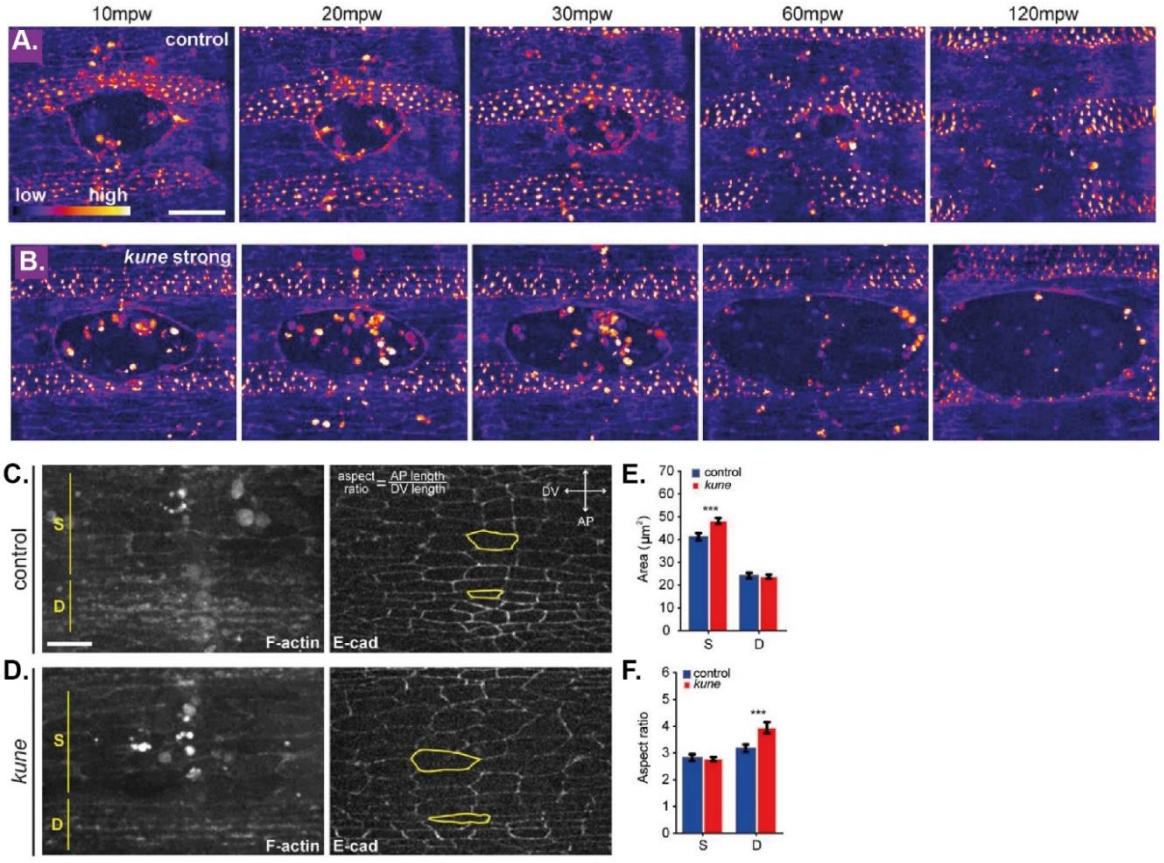

Figure 56. *kune* Drosophila embryos display defects during wound repair and atypical cell area and morphology. A-B. Embryos expressing Cherry::Moesin marking F-actin, are wounded using laser ablation (A-B). In kune conditions (B), the wound does not repair compared to WT situation (A) and shows elongated shape. C-D. Embryos expressing Cherry::Moesin and E-Cad::GFP show in kune cells (C), elongation in the dorso-ventral (DV) axis compared to WT cells (D) and display bigger area. antero-posterior (AP). E-F. Quantification of the cell area and aspect ratio (calculated as indicated in C). Smooth cells (S) are more prone to area augmentation upon loss of Kune whereas denticle cells (D) reveal extension in AP axis upon loss of Kune. S: Smooth cells. D: Denticle cells. Adapted from (Carvalho, Patricio et al. 2018)

Kune as a testimony of pSJ loss of function on wound healing since it displays a strong phenotype (more than 89% of embryos failed to heal the wound). Whereas it takes, on average, only 15 to 20 mins after hole induction to form the actin cable and 60 mins to resolve it in WT conditions, *kune* mutants able to fix the wound take 160 mins to do so. Moreover, this slower rate is associated many times with an increase of the wound hole size and a progressive disappearance of the acto-myosin cable, revealing impairment of the acto-myosin dynamics. Moreover, at the wounding edge, Nrx-IV and Nrg are gradually removed, but *kune* mutants show higher signals of Nrx-IV and Nrg with, sometimes, Nrx-IV spots associated with the actin cable, implying a probable turnover defect of pSJ proteins at the leading edge. Using RNAi against Kune in specific stripes of the *Drosophila* embryos (Engrailed), the authors showed that wounds localised either in the domain expressing RNAi or in the adjacent WT regions display defects similarly to *kune* mutants, demonstrating a tissue-level role for wound closure. In addition, *kune* mutants exhibit modified cell shapes and changes in mechanical tissue properties. Indeed, using laser ablation experiments, they demonstrated that *kune* mutant cells relax faster than WT cells with a similar general displacement of the adjacent vertex. Therefore, they stated, using the Kelvin-Void model of viscoelasticity and the fact that the apical area of *kune* mutant is bigger than WT, that it is most likely that *kune* mutants show reduced viscosity, making them less prone to handle membrane relaxation after laser ablation **(Figure 56).**

d. Septate Junctions conclusion

In this chapter, we have glimpsed the intricacy of the SJ complex. Firstly, most of the time SJ proteins rely on each other to form functional and stabilised SJs in order to provide their historical described role of paracellular permeability barrier. This is true in the case of ectodermally-derived tissues, forming mostly pSJs, but also of the endodermally-derived midgut with its inverted polarity, or the gastric *caeca*. This barrier

is a progressive mechanism which starts around stage 15, although many pSJ proteins are found to localise at membrane and vesicles prior to this, in order to be fully functional with mature SJs at stage 17. Furthermore, SJs are required in many other developmental processes, such as morphogenesis and polarity, and have also been found to be associated with signalling pathways regulating cell growth. Notwithstanding SJs have been heavily described and studied over the past decades, the focus on their pleiotropic effects has emerged only recently, calling for many new and exciting studies to be performed.

Chapter IV: Tricellular junctions

a. Generalities, ultrastructure and Embryonic development

i. Generalities

I have previously described the two main types of junctions found in the *Drosophila*, namely the AJ and SJ. I have deliberately avoided descriptions of additional junctions, such as hemidesmosomes, for reasons of clarity. Proteins that constitute AJs and SJs are found to be distributed almost equally around the cell perimeter, with some little heterogeneity from time to time. Moreover, I have mostly focused on describing the contacts that occur between two cells, here referred to as bicellular junctions (BCJ). However, contacts between three cells also exist. This peculiar point in the tissue is a site specially enriched in some proteins and displaying a particular morphology associated with special features. The three-cell point meeting is named the tricellular junction (TCJ) and was the starting point of my thesis work. TCJs are equally found in vertebrates and invertebrates but here in the introduction, I focus, as with the AJs and SJs, only on the arthropod case **(Figure 57)**. The importance of TCJs has become increasingly apparent over the past twenty years since they are key effectors in cell divisions and movements as well as hotspots for pathogens and metastatic cell invasion.

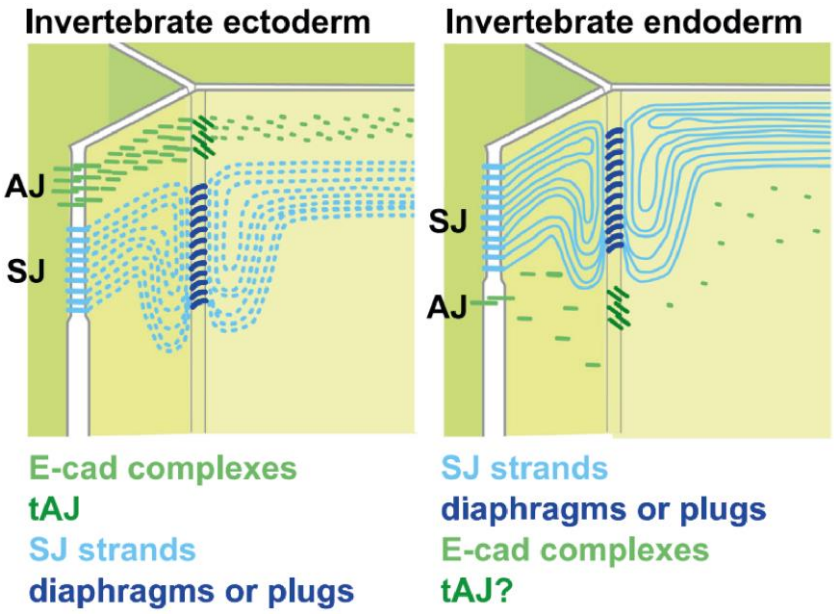

Figure 57. Junctional organisation in both ectodermally and endodermally derived tissues of Drosophila epithelial cells. tAJ: tricellular adherens junction. Adapted from (Higashi and Chiba 2020)

ii. Ultrastructure

Using the *caecum* of the small crustacean *Orchestia* and midgut of the cockroach *Blaberus* impregnated with lanthanum coupled with the freeze fracture technique and

TEM approaches, reveals TCJs as well-spaced diaphragms that span the extracellular space found at the three-cells vertex (Graf, Noirot-Timothee et al. 1982). More precisely, the bicellular septate junctions (BSJ) strands run along the cell perimeter and dive at the vertex occurrence, running in parallel to the TCJ and perpendicular to the cell surface **(Figure 58).** The depth of the BSJ increases with proximity to the TCJ, being 1.6 to 2 µm compare to 0.12 to 1µm (Graf, Noirot-Timothee et al. 1982).

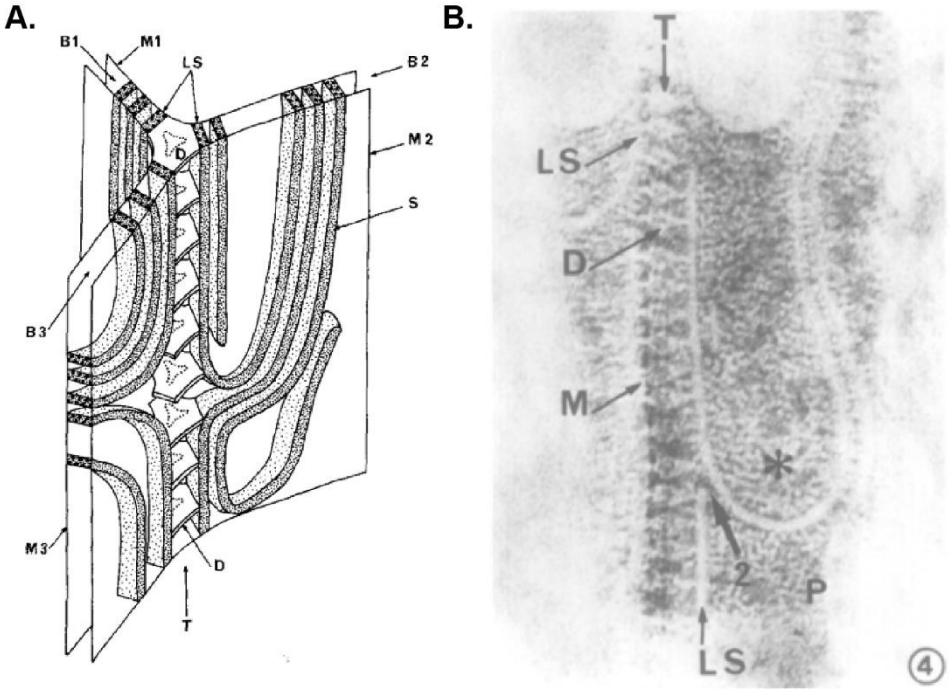

Figure 58. Tricellular junction ultrastructure in arthropod organisms. **A**. Scheme representing the general organisation of the TCJ. TCJ is a canal filled with diaphragms (D), connected to adjacent limiting septa (LS) running along and parallel to the TCJ. D are regularly spaced and connected to the three BCJs. S: septa. M: Membrane. **B.** TEM image of a tangential section of the caecum of Orchestia at TCJ area. D appeared as electron dense material regularly spaced and LS are seen in a negative contrast, running parallel to the TCJ where they dive at its contact. T: Tricellular junction. P: Pillar. Adapted from (Graf, Noirot-Timothee et al. 1982)

However, this is only reported in the *Orchestia caecum* context. The diaphragm has a bloated central part and a thin peripherical part linked to the BSJ strands that plunge. This is true for sSJs, as shown here, but also for pSJs as highlighted with the use of the hindgut of the firebrat *Thermobia domestica* and the epidermis of the mealworm *Tenebrio molitor* (Noirot-Timothee, Graf et al. 1982). In both cases, sSJs and pSJs, TCJs look similar and strands of SJ, when in close vicinity to TCJ, run parallel to it. The space between the diaphragms at TCJ were, respectively, 16.5, 19.5 and 20.5nm for *Orchestia*, *Blaberus* and *Thermobia domestica/Tenebrio molitor*. More particularly, diaphragms of both sSJ and pSJ contexts bind three doublets of particles, one pair corresponding to one adjacent cell, suggesting an anchoring point for diaphragms to

adjacent SJ strands. The septa of pSJs are known to be spaced by 20-22 nm, again indicating that diaphragms are connected to adjacent septa. Similar observations were made using the wing disc of *Drosophila* (Fristrom 1982). Interestingly, the morphology of TCJ in invertebrates is less prone to variations than SJ morphologies across different species, suggesting the robust organisational features of TCJ. Of note, the estimated size of the TCJ canal is around 25-30 nm, compared to less than 15nm for BCJ, and the regular angle made by the BCJ at the TCJ is around 120° in mature epithelia, similar to a honeycomb structure (Noirot-Timothée and Noirot 1980, Graf, Noirot-Timothee et al. 1982, Noirot-Timothee, Graf et al. 1982).

iii. Embryonic development

TCJ can be separated in two parts, albeit no studies of its ultrastructure have revealed differences as most works were interested in studying SJ level. Nonetheless, we know that at AJ level, one protein named Sidekick (Sdk) is specifically enriched and three other proteins are found to be specially enriched at SJ level, namely Gliotactin (Gli), Anakonda (Aka; also known as Bark Beetle) and M6. Therefore, two types or levels of TCJ exist: one referred as Tricellular Adherens Junction (tAJ) and other as the Tricellular Septate Junction (tSJ) **(Figure 59).**

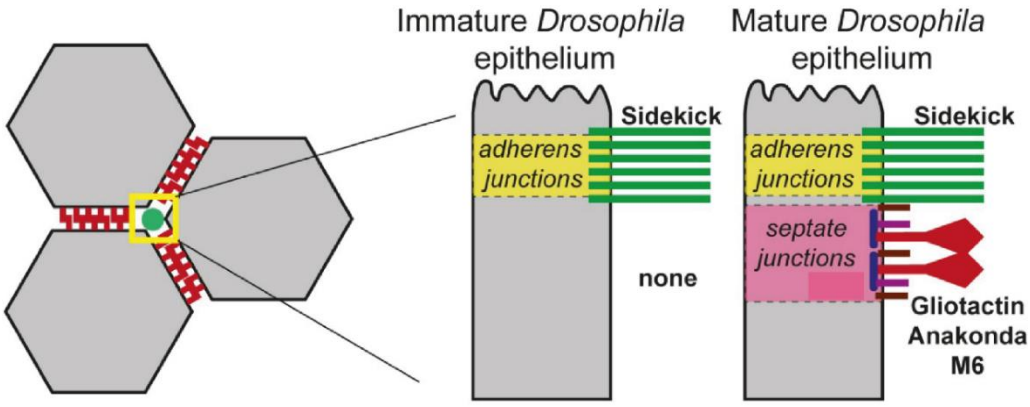

Figure 59. Sidekick presence during Drosophila embryogenesis. Scheme representing that Sdk is enriched at vertex (yellow square, top view, left side), and present at tAJ even at developmental stage where pSJs are not formed (transversal view, right side). Green: Sidekick. Tricellular Septate Junction proteins. Red: Anakonda, Black: Gliotactin and Blue: M6. Adapted from (Finegan, Hervieux et al. 2019)

Sdk is present as early as stage 7 of embryogenesis in the epidermal cells (Lye, Naylor et al. 2014, Finegan, Hervieux et al. 2019, Letizia, He et al. 2019). Sdk is present at the vertices in the dorsal epidermis but has also been found spread along the BCJ in the ventral epidermis and during germband extension in ectodermal cells, in the SG of

the stage 3 larvae and in the early-stage egg chamber (Finegan, Hervieux et al. 2019, Letizia, He et al. 2019, Isasti-Sanchez, Münz-Zeise et al. 2021). A common point

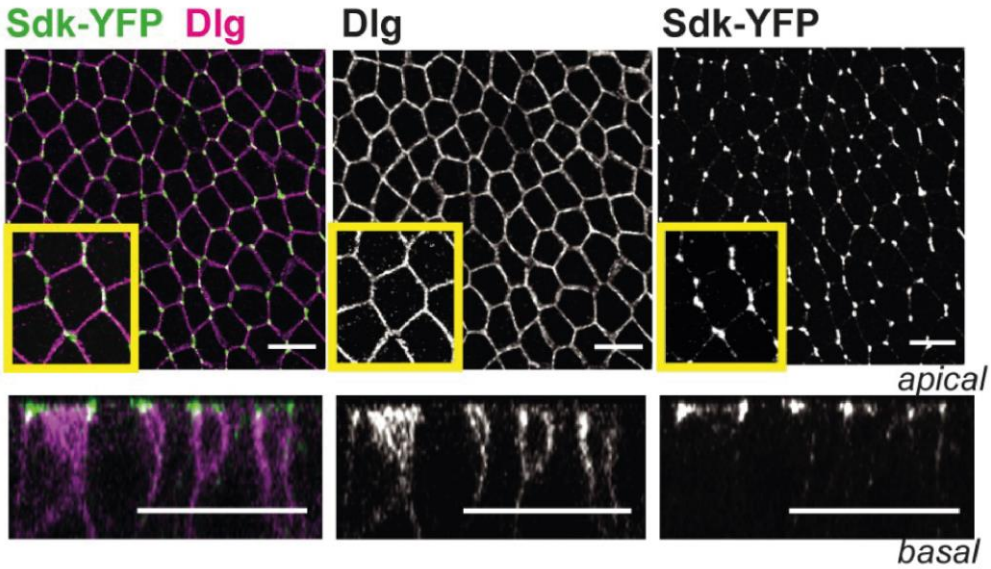

Figure 60. Sidekick is a specially enriched protein at Tricellular Adherens Junction. Stage 7 Drosophila embryos expressing Sdk-YFP and stained for Dlg show that Sdk is restricted and enriched at vertices in a top view (top panel). Transversal view (bottom panel) show Sdk-YFP apical localisation compared to Dlg. Adapted from (Finegan, Hervieux et al. 2019)

among these different tissues is that Sdk is expressed and localised at the vertex prior to the formation and maturity of SJs **(Figure 60).** Interestingly also, Sdk appears at BCJs when SJs are not formed and/or not mature, and no Sdk is detected in the midgut where the polarity is inverted (sSJ above AJ). Consequently, we can claim that tAJ is formed before tSJ during embryonic development, similarly to Bicellular Adherens Junctions (bAJs) compared to BSJ.

Hence, tSJs start to form later, in concordance with the onset of SJ formation. Indeed, Gli immunostaining has demonstrated its earlier presence at stage 11 in the epidermis, and it is found in the same tissues as Aka (Auld, Fetter et al. 1995, Schulte, Tepass et al. 2003). *In situ* hybridisation in *Drosophila* embryos has detected first Aka expression at stage 13, and its expression increases during stage 14 to 15 in the trachea, foregut, hindgut, epidermis and SG (Byri, Misra et al. 2015).

Aka expression is also detected at stage 16 in the CNS (Byri, Misra et al. 2015) and Gli at stage 13 in the peripheral glial tissue (Auld, Fetter et al. 1995), coinciding with the beginning of BBB formation. The same results have been observed for M6 using immunostaining, with an onset of expression around stage 11 (Wittek, Hollmann et al.

2020). Gli and M6 colocalise all around the cell perimeter at stage 11-13 in the embryo epidermis and start to localise at the vertices at late stage 13 during the onset of Aka expression (Schulte, Tepass et al. 2003, Byri, Misra et al. 2015, Wittek, Hollmann et al. 2020).

Gli also relocalises from the entire length of the apico-basal axis of the cell at stage 13 to a restricted half-apical area at stage 15, similarly to pSJ proteins (Schulte, Tepass et al. 2003). Aka, Gli and M6 exhibit a spaghetti shape once restricted at tSJs and also colocalise with pSJ proteins such as Mega, Cora, Dlg and Fas3 (Byri, Misra et al. 2015, Hildebrandt, Pflanz et al. 2015, Esmangart de Bournonville and Le Borgne 2020, Wittek, Hollmann et al. 2020). Aka and Gli also colocalise at stage 10B in the egg chamber (Isasti-Sanchez, Münz-Zeise et al. 2021). Of note, Aka and Gli are found in both endodermal-(sSJ) and ectodermal-(pSJ) derived tissues (Byri, Misra et al. 2015), supporting the fact that TCJ configuration and features are well maintained across tissues and species as mentioned in the ultrastructure section. In contrast, no Sdk has been detected in the adult midgut (Finegan, Hervieux et al. 2019).

Thus, the following model emerges: tAJs are probably assembled at the same time as the establishment and maturation of AJs, as Sdk is detected as early as stage 7 (which is after the cellularisation at stage 5, the onset of AJ assembly). Then, SJ proteins start to be expressed at stage 10 and are present at the lateral membrane around stage 11/12, similarly to the tSJ proteins Gli and M6. As SJ maturation occurs, SJ proteins start to be restricted more and more to the most apical half of the cell, like Gli, associated with Aka expression onset and presence at the vertex, coinciding with the restriction of M6 and Gli as well. This process continues in order to reach the final maturity of the tissue at stage 17, where tAJ and tSJ proteins are well restricted at the vertex, and SJs are fully functional and able to exert their role of permeability barrier.

b. Sidekick and the tAJ

Drosophila Sdk is a transmembrane protein from the Ig superfamily containing a large N-terminal extra-cellular part with six Ig domains and 13 fibronectin type III domains **(Figure 61).** In *Drosophila*, it was first discovered for its role in eye development, where mutant for Sdk showed abnormal organisation with extra photoreceptor cells (Nguyen, Liu et al. 1997).

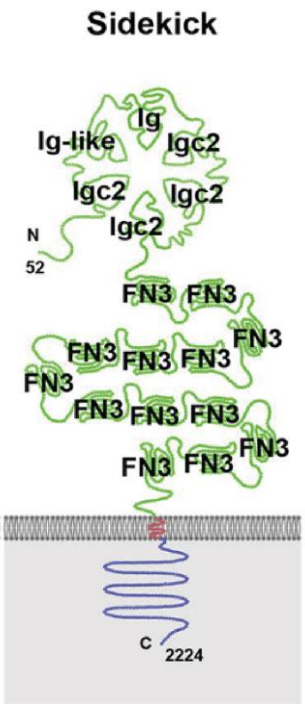

Figure 61. Sidekick structure. Ig: Immunoglobulin domain. FN3: Fibronectin type III domain. Adapted from (Higashi and Miller 2017)

Later, another work revealed that Sdk accumulates in specific synaptic layers, regulating the definite organisation of photoreceptors axons and the alignment of specific neurons involved in visual motion (Astigarraga, Douthit et al. 2018). Moreover, a screen of YFP-tagged proteins shows a Sdk-specific enriched position at the three-cell vertex (Lye, Naylor et al. 2014). Sdk has homophilic interaction properties, as demonstrated by (Uechi and Kuranaga 2019), where S2 cells expressing Sdk are aggregating, even though the authors suggested that the adhesive properties of Sdk are less strong than those of DE-Cad. Pull-down assays have reported that Sdk directly interacts, via its PDZ binding domain, with the PDZ domain of Pyd, an acting binding protein (Letizia, He et al. 2019). Albeit the authors did not show direct interactions of Sdk with Cno, the requirement of Sdk to enrich Cno at the vertex suggests at least an interaction (direct or indirect) between the two **(Figure 62)**. This interaction is probably independent of Pyd, since the depletion of Pyd when Sdk is present shows Cno enrichment at the vertex. Immunoprecipitation experiments have also revealed Sdk interaction with β-catenin and the intracellular part of Sdk expressed in S2 cell pulldowns NMY-II (Uechi and Kuranaga 2019).

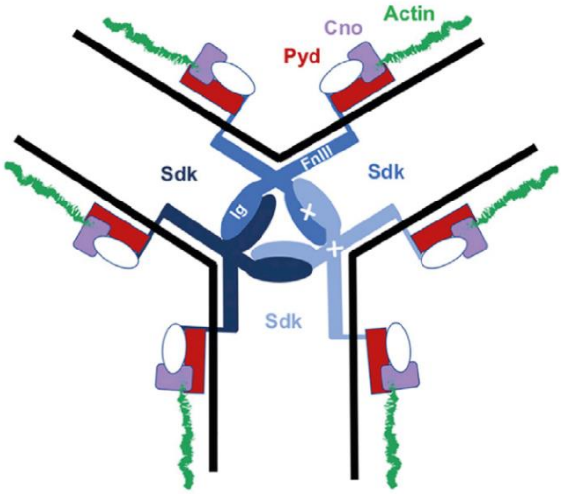

Figure 62. Sidekick binding partners at Tricellular Adherens Junction. Sdk Ig domains are binding in trans when FN3 bind in cis. Sdk is connected to F-actin via binding to Pyd and Cno. Adapted from (Letizia, He et al. 2019)

Another protein, named Shroom, an actin-associated protein which stabilises Rok at AJ level during planar-polarized cell rearrangements, is enriched at the vertices (Simoes Sde, Mainieri et al. 2014) in the same way as Rok in the *notum* (Curran, Strandkvist et al. 2017). NMY-II is also enriched at vertices during cell growth junction, playing an active role in this process, as shown in (Uechi and Kuranaga 2019) **(Figure**

63). This is to be seen in relation to the work of (Curran, Strandkvist et al. 2017), where the authors showed that NMY-II localised at the entire AJ in the *notum* is responsible for junctional shortening. These contradictory results could be explained by the differences in tissue and developmental context, but they could also be explained by the fact that NMY-II special enrichment at TCJ mediates junctional growth and NMY-II, targeted all along the AJ, shrinks the junction, suggesting a differential organisation of acto-myosin cytoskeleton in favour of regulating AJ length.

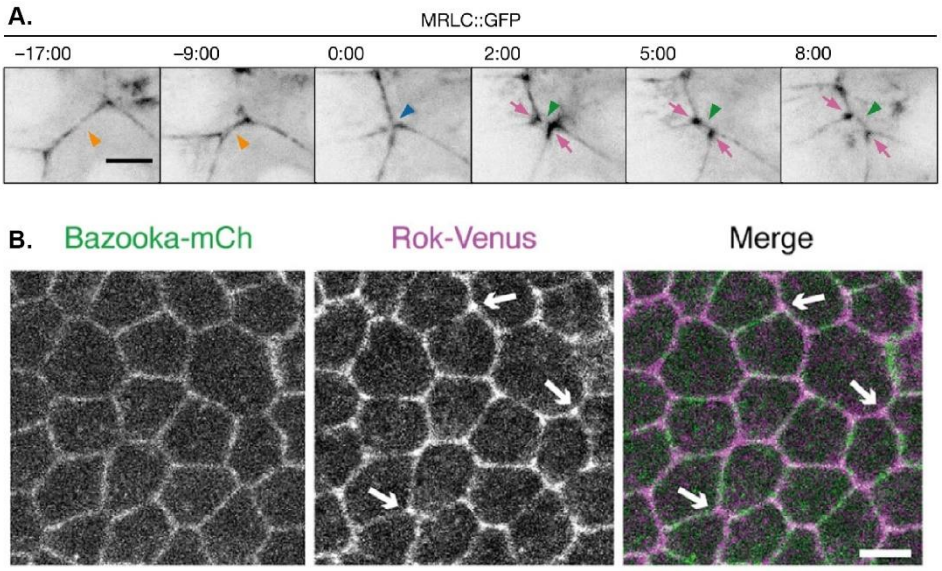

Figure 63. Tricellular Adherens Junctions are hotspots of components involved in mechanical properties of the tissue. A. Drosophila genitalia epithelial cells, expressing NMY-II tagged with GFP (MRLC::GFP), rearranging their junctions. Orange arrow shows the shrinkage of the junction, the blue one a four-way vertex, the green one the elongated junction and the pink ones highlight the enrichment of NMY-II at vertex which promotes junction elongation. Time is Min:Sec. **B**. Drosophila epithelial notum cells expressing Venus::Rok and Baz-mCherry, showing the enrichment of Rok at tAJs (white arrows). Adapted from (Uechi and Kuranaga 2019) and (Curran, Strandkvist et al. 2017)

It is worth noting that tAJ also shows enrichment of Enabled and Zyxin, two actin-binding proteins involved in Hippo/YAP pathway regulation (Grevengoed, Loureiro et al. 2001, Rauskolb, Pan et al. 2011, Gaspar, Holder et al. 2015). Therefore, the overall organisation and molecular composition of the tAJ in the *Drosophila* makes it very appealing for consideration as a key platform for both integrating mechanical information and inducing response for epithelial tissues growth, shape and general homeostasis.

c. Gliotactin, Anakonda and M6

- **Gliotactin**

Among the three proteins that form the tSJ, the first to be discovered was Gliotactin (Gli). Originally studied for its role during the formation of the BBB (Auld, Fetter et al. 1995), it is the first protein known to be specially enriched at TCJ (Schulte, Tepass et al. 2003). It is a transmembrane protein containing an extracellular non-catalytic active cholinesterase domain and an intracellular PDZ-binding domain and belongs to the family of the Neuroligin proteins **(Figure 64).**

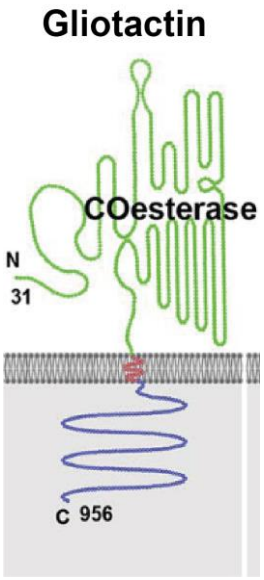

Figure 64. Gliotactin structure. COesterase: Cholinesterase domain. Adapted from (Higashi and Miller 2017)

As previously described, Gli appears during stage 11 of development, just after Nrx-IV. Upon loss of Gli, the SJ proteins Cora, Nrx-IV and Dlg are mislocalised at stage 15, spreading to the basal side of the cell. In a similar manner, in embryos mutant for Nrx-IV, Gli spreads at the BCJ and basally. In addition, TEM reveals less dense clusters of septa in *Gli* mutant associated with large regions of detached membranes and rhodamine-dextran analysis shows loss of permeability barrier looking at the SG (Schulte, Tepass et al. 2003) **(Figure 65).**

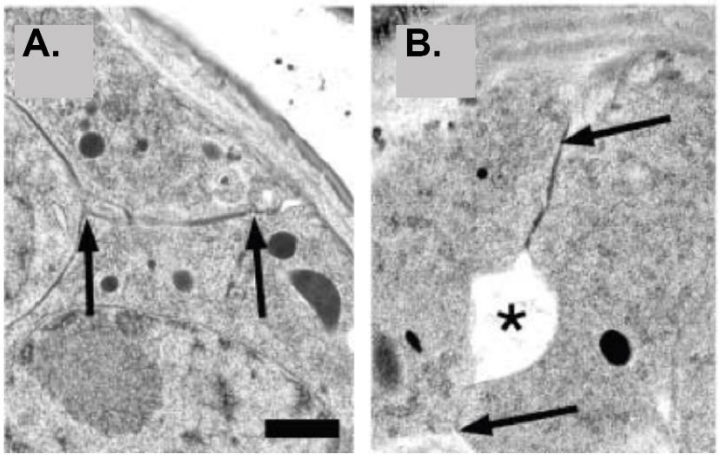

Figure 65. Gliotactin mutant displays detached membrane regions. **A-B.** TEM analysis of Drosophila embryo epidermis, showing large portions of detached membrane (asterisk) in Gli embryos (B) compared to WT (A). Arrows delimit pSJ domain. Adapted from (Schulte, Tepass et al. 2003)

Regarding Gli links with SJ proteins more specifically, another study by (Schulte, Charish et al. 2006) has shown that Gli is in specific interaction with Dlg, as highlighted by co-immunoprecipitation experiments and GST pull-down assays on adult tissues. Interestingly, overexpression of Gli in the wing discs leads to Gli spreading at the BCJ associated

with Dlg signal down regulation, suggesting some roles in controlling Dlg level **(Figure 66).** Still using wing discs, loss of Dlg by RNAi knock-down approach leads to the disappearance of Gli at the vertices (Padash-Barmchi, Charish et al. 2013). Moreover, Gli is phosphorylated at Tyrosine residues in its intracellular part, and this controls endocytosis and further targeting to the degradative pathway (Padash-Barmchi, Browne et al. 2010). Another level of Gli regulation appears to be at mRNA level, where a feedback loop mediated by the BMP signaling pathway activates a micro-RNA (miR-184) targeted degradation through the 3′ UTR of Gli mRNA (Sharifkhodaei, Padash-Barmchi et al. 2016).

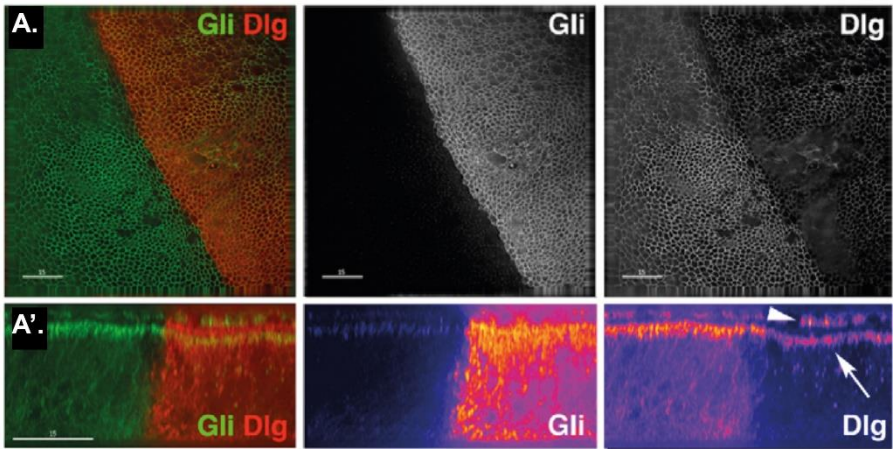

Figure 66. Gliotactin overexpression leads to Gliotactin presence all around cell perimeter associated with reduced level of Discs Large. **A-A'.** Drosophila wing discs expressing Gliotactin under the control of Apterous-GAL4 driver, leading to Gliotactin overexpression in this part of the tissue. Gli and Dlg are revealed by antibodies and show Gli (green) spreading at BCJ (A) which leads to Dlg (red) reduced signal, observed both in planar (A) and transversal view (A'). Enrichment of Gli in A' is highlighted using fire colour mode as well as Dlg diminished signal (white arrows). Adapted from (Schulte, Charish et al. 2006)

A version of Gli lacking the PDZ-binding domain displays a reduced level at the membrane and many vesicles positive for Gli staining **(Figure 67)**, suggesting higher rates of degradation/recycling of Gli, even though this study did not co-mark these mechanism players (Padash-Barmchi, Charish et al. 2013). Nonetheless, co-expressing a dominant negative form of the endosomal actor Rab5 along with Gli lacking PDZ-binding domain prevent the appearance of Gli positive structures and Gli is strictly present at the membrane. The authors concluded that Gli endocytosis is the mechanism that triggers Dlg reduction from the membrane when Gli is overexpressed, arguing for a co-regulation of Gli and Dlg.

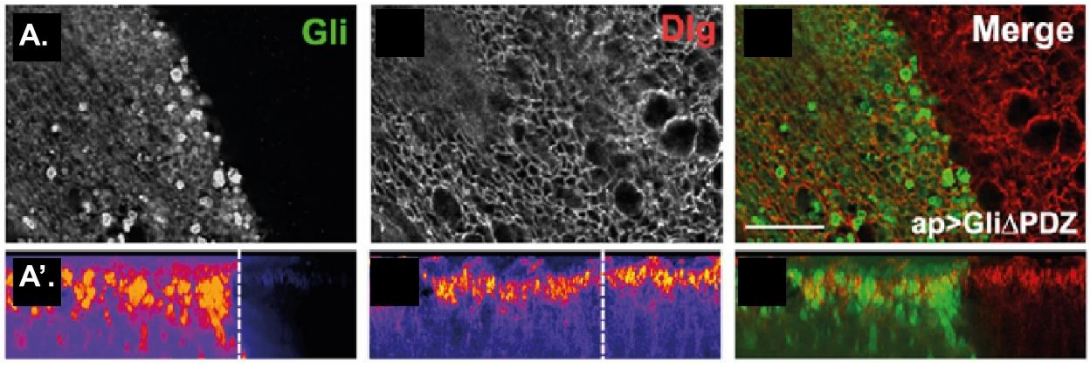

Figure 67. Overexpressing Gliotactin lacking its PDZ binding domain does not lead to Discs Large reduced level. A-A'. Drosophila wing discs expressing Gli lacking its PDZ binding domain (GliΔPDZ) under the control of Apterous-GAL4 driver. Gli (green) and Dlg (red) are revealed by antibodies. This leads to GliΔPDZ overexpression in a specific region of the tissue. Gli is localized into vesicular structures, suggesting higher rate of Gli endocytosis when it lacks PDZ binding domain. However, Dlg is not reduced at the cell junctions on the contrary of Gli full length overexpression. A and A' show respectively planar and transversal view of the wing discs cells. Adapted from (Padash-Barmchi, Charish et al. 2013)

However, those results are quite fragile, since authors looked at overexpressed and ectopically situated Gli (that is present all along the cell membrane). This could be problematic as Gli ectopic localisation upon overexpression leads to cell delamination, invasion, cell proliferation or even cell death via activation of the Jun N-terminal Kinase (JNK) pathway (Padash-Barmchi, Browne et al. 2010). Another level of complexity appears since overexpressing the C-terminal Src kinase (Csk) along with Gli, supresses the phenotype of cell extrusion/invasion and cell apoptosis (Samarasekera and Auld 2018). This could be explained by the intensified endocytosis of Gli upon Csk overexpression, where the tyrosine phosphorylation of Gli is enhanced, supposedly preventing Gli from acting at the BCJ. However, it is unclear whether Csk directly phosphorylates Gli, as *in vitro* studies of Csk phosphorylation of Gli and gold immunolabeling have shown no interactions of Gli and Csk whereas proximity ligation assay has done so.

Gli is also linked to intestinal stem cell regulation as observed in the posterior midgut of the *Drosophila* (Resnik-Docampo, Koehler et al. 2017). Unlike most of the epithelia tissues in the *Drosophila*, the midgut has sSJ, as previously mentioned. Still, Gli is present in differentiated EC, the absorptive cells of the gut. Upon aging, sSJ markers such as Ssk and Mesh are mislocalised in the cytoplasm and Dlg, Cora and Scrib signals are reduced at the membrane. Likewise, Gli is absent from TCJ upon aging. The integrity barrier of the midgut is impaired when Gli is knocked-down in the ECs,

and sSJ proteins signals are impaired, combined with an increased turnover of ISC and an increased expression of sSJ genes **(Figure 68).**

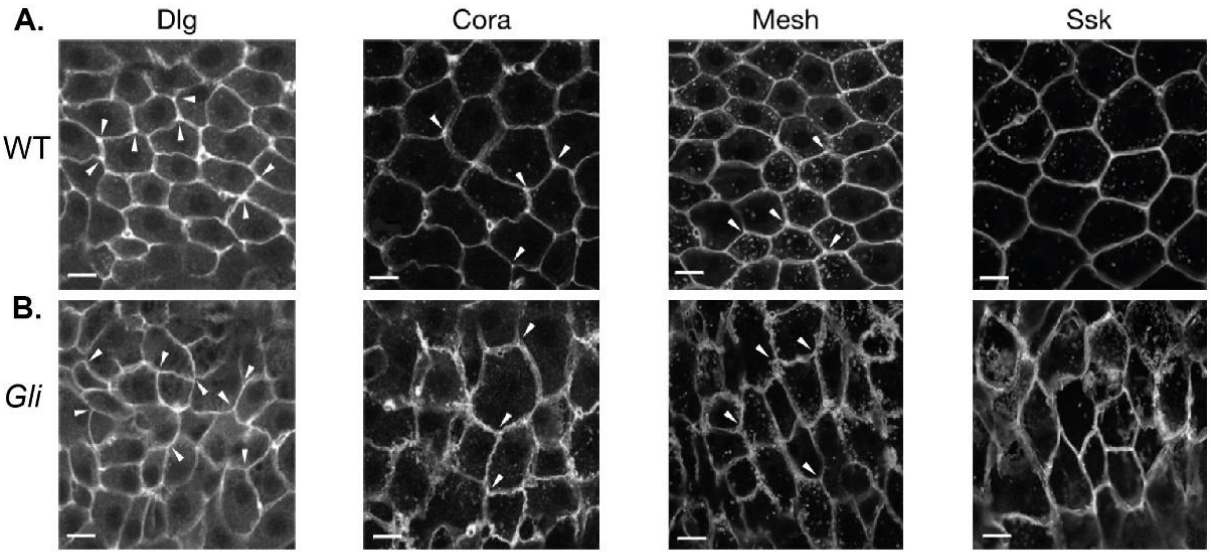

Figure 68. Loss of Gliotactin specifically in the Drosophila midgut leads to Smooth Septate Junctions defects. A-B. 23 days old adult Drosophila posterior part of midguts stained for Dlg, Cora, Mesh and Ssk in WT (A) and Gli knock down conditions (B). Knock down of Gli using RNAi leads to reduced and less restricted signals of sSJ proteins as well as the induction of deformations positives for sSJ proteins. White arrows head show TCJ. Adapted from (Resnik-Docampo, Koehler et al. 2017)

This enhanced proliferation of ISCs is controlled by the JNK pathway activated in the enterocytes upon loss of Gli. Interestingly, the opposite results are shown in the *Nrg* mutant context, as previously described, as loss of Nrg leads to a lower division rate and its overexpression and the over proliferation of ISCs (Resnik-Docampo, Cunningham et al. 2021).

- **Anakonda**

Anakonda (Aka; also known as Bark Beetle, Bark) is a large transmembrane protein with a tripartite repeated extracellular domain containing three scavenger receptors cysteine-rich domains (SR), a C-type lectin domain, one complement/UEGF/BMP1 (CUB) domain and 19 parallel beta helices as well as a C-terminal PDZ binding motif (ETAM) (Byri, Misra et al. 2015) **(Figure 69).**

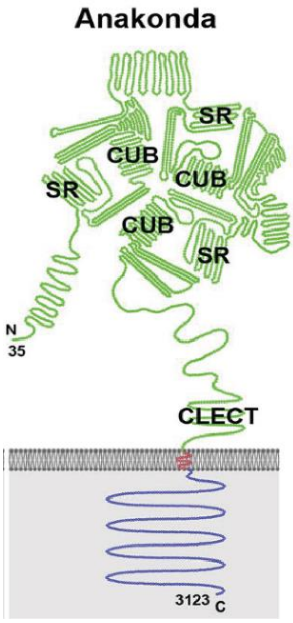

Figure 69. Anakonda structure. SR: Scavenger Receptors domain. CUB: Complement/UEGF/BMP1 domain. CLECT: C-type lectin domain. Adapted from (Higashi and Miller 2017)

Aka mutant displays the same phenotype of over-elongated trachea, as in the pSJ mutants associated with a disruption of the permeability barrier (Byri, Misra et al. 2015, Hildebrandt, Pflanz et al. 2015). Aka exhibits vertex enrichment, like Gli; furthermore, as suggested by the trachea and permeability defect barrier, loss of Aka shows pSJ defects such as basal spreading of Fas3 (Byri, Misra et al. 2015) but also of Mega, Kune, Nrx-IV and Nrg at stage 17 of embryonic development, which is not the case at stage 15 (Hildebrandt, Pflanz et al. 2015). The difference in the SJ defect observations in the two studies probably comes from the embryonic stage which the authors observed. At stage 15/16, the SJs and tSJs are not considered fully mature, which is not the case at stage 17, indicating differential roles for Aka in establishing *vs* maintaining SJ/tSJ integrity. TEM analysis reveals, as with Gli, that there are cavities between two adjacent membranes of epidermis cells (Byri, Misra et al. 2015, Hildebrandt, Pflanz et al. 2015) and denser septa clusters or equal situations compared to WT in (Byri, Misra et al. 2015). However, looking at stage 17, (Hildebrandt, Pflanz et al. 2015) show that there are defects in the septa, which are less present and disorganised in the trachea and epidermis. Those results further indicate that of Aka plays differential roles depending on the embryonic stage of development. They also suggest adhesive roles, based on the fact that the bubble's phenotype occurs between two cell membranes. Furthermore, Aka is required to localise and stabilise Gli at tSJ, and this effect is independent of the PDZ-binding motif (Byri, Misra et al. 2015). Aka needs to be present in all three cells adjacent to the vertex, since loss of Aka from only one cell present at the TCJ leads to Aka and,

therefore, the disappearance of Gli from the vertex. Co-marking with trafficking pathway components at stage 16 shows that Aka is recycled from the membrane via Clathrin-coated vesicles. Then, it colocalises into early endosomes, as shown by Rab5 co-staining, and into recycling endosomes via Rab11 colocalisation. Aka can also be found in late endosomes and lysosomes, co localising respectively with Rab7 and Lamp1 (Hildebrandt, Pflanz et al. 2015) **(Figure 70).** It is interesting to note that Aka, as indicated by the results of early and recycling endosomes, displays similar behaviour to pSJ proteins during embryonic development (Tiklova, Senti et al. 2010).

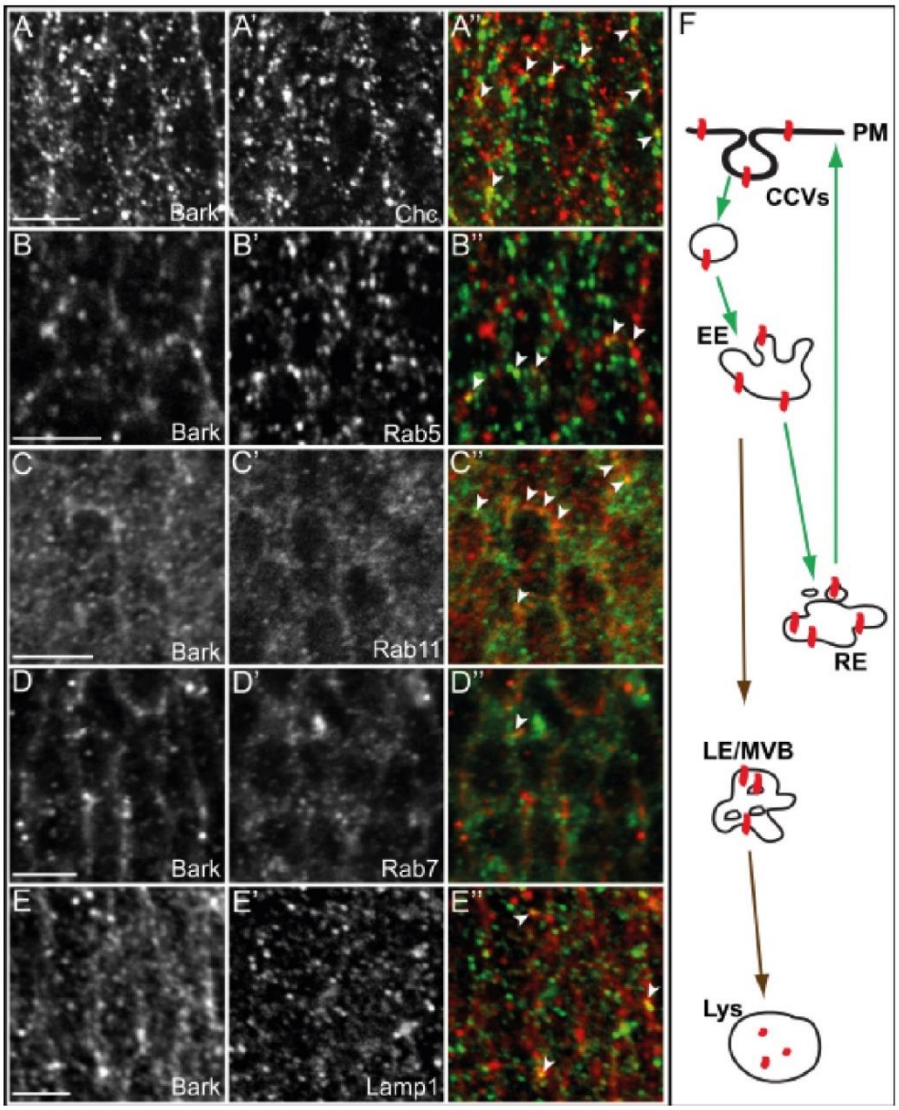

Figure 70. Anakonda intracellular trafficking. **A-E''**. Stage 16 Drosophila embryos stained for Aka (Bark, red, A-E''), Clathrin Heavy chain vesicular marker (Chc, green, A-A''), Rab5 early endosome marker (green, B-B''), Rab11 recycling endosome marker (green, C-C''), Rab7 late endosome marker (green, D-D'') and Lamp1 lysosomal marker (E-E''). **F.** Scheme representing Aka (red) intracellular trafficking, from its internalisation via Clathrin coated vesicle mechanisms (CCVs) toward early endosomes (EE), recycling endosomes (RE) but also late endosomes (LE), multivesicular bodies (MVB) and lysosomes (Lys) for degradation. Adapted from (Hildebrandt, Pflanz et al. 2015)

- **M6**

M6 is the only member of the family myelin proteolipid protein (PLP) in the *Drosophila* and the only tSJ protein which has a homologue in the vertebrates (M6a in the mouse). This is a small four-transmembrane-domain protein, with a small and a big extracellular loop and N- and C-terminal cytosolic parts **(Figure 71).**

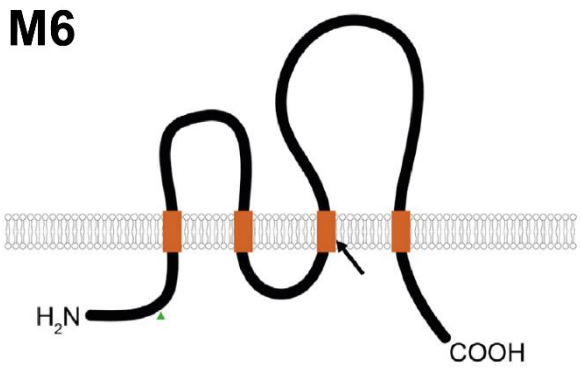

Figure 71. M6 structure. Orange represents transmembrane domains. Adapted from (Wittek, Hollmann et al. 2020)

Previously discovered for its requirement during oogenesis development and special enrichment at TCJ in the egg chamber (Zappia, Brocco et al. 2011), it is further described in the companion paper to the one I will present in the first part of the results. In this work, (Wittek, Hollmann et al. 2020) have shown, as we have done in the *notum*, that GFP::M6 colocalises with Aka and Gli at vertices at the SJ level in the epidermis of stage 16 embryos. They have also shown that M6 and Aka are upstream regulators of tSJ assembly, as we have also done, since they are required to recruit Gli at the vertex. Moreover, the M6 effect is cell-autonomous and depends on Aka: the loss of Aka leads to the loss of M6, but the opposite is also true, making Aka and M6 co-dependent for their specific enrichment at tSJ.

d. <u>Conclusion</u>

In this chapter, we have observed how tAJs and tSJs are established during development. tSJs behave in a similar way to pSJs although Aka acts differently, being expressed later at stage 13 and required to stabilise the overall tSJ at the vertex. Neither tAJs nor tSJs are disconnected from their adjacent neighbours BCJs, binding many proteins of both AJs and SJs and sometimes needed to enriched them at the vertex. Moreover, rather than only being needed for adhesive and permeability properties of the tissue, the roles of tAJs and tSJs expand beyond these primal determined functions, as briefly described in the case of Gli. We will see in the next chapter how diverse the roles of TCJs are in regulating key events during the epithelium's life.

Chapter V: Plasticity and robustness of epithelial (Tricellular) junctions

a. Cytokinesis, remodelling of junctions and cell division orientation

i. Cytokinesis and junctional remodelling

When an epithelial cell divides, it gives rise to two new daughter cells. In order to preserve the epithelium homeostasis, the cells need to maintain their junctional integrity during this process. A particular phase of the cell division is called the cytokinesis, which begins immediately after the anaphase onset and is characterised by the remodelling and establishment of both new bi- and tricellular junctions.

During this process, sister chromatids are separated equally into daughter cells thanks to the mitotic spindle which also activates signals in order to build a contractile ring of actomyosin that matures during cytokinesis and becomes the midbody (Cheffings, Burroughs et al. 2016). The midbody can be seen as the actomyosin ring associated with part of the microtubules of the central spindle and many other components, such as Septins (Founounou, Loyer et al. 2013) and Anillin (Guillot and Lecuit 2013), for example. The acto-myosin ring contracts asymmetrically, beginning at the basal level and moving toward the apical level. Its position is regulated via the central spindle. At the same time, DE-Cad is newly assembled at the new cell-cell interface when disassembled at neighbouring adjacent membranes (Guillot and Lecuit 2013). Another work by (Pinheiro, Hannezo et al. 2017) suggests that it is more likely to be a dilution of DE-Cad at the neighbouring junctions rather than a disassembly that triggers a flow of myosin toward the basis of the cell neighbouring membrane ingression. This in turn leads to a “tug of war” mechanism with the contractile activity of the midbody in order to ensure the correct length of the new AJ. The midbody is anchored at the apical level thanks to DE-Cad interaction with F-actin (Founounou, Loyer et al. 2013, Guillot and Lecuit 2013, Herszterg, Leibfried et al. 2013, Pinheiro, Hannezo et al. 2017).

Once the acto-myosin ring reaches the AJ position and its final state of constriction, it starts to detach and migrate, this time toward the basal side. At the pSJ level, the midbody is anchored to four cells, the two daughter cells and their neighbours via membrane protrusions with pre-existing pSJ, forming a “ménage à quatre” (Daniel, Daude et al. 2018, Wang, Bosveld et al. 2018). The basal midbody movement correlates with the establishment of pSJ just above it, showing a polarised assembly

of new pSJs. As the midbody continues to move basally and matures, tSJ components Gli and Aka start to appear close to the midbody at the level where it connects with the neighbour's protrusions **(Figure 72).** It has been proposed that the establishment of the new tSJ is a rate-limiting step regulating the midbody speed basal movement (Daniel, Daude et al. 2018) and disentanglement of cell protrusions from the midbody (Wang, Bosveld et al. 2018).

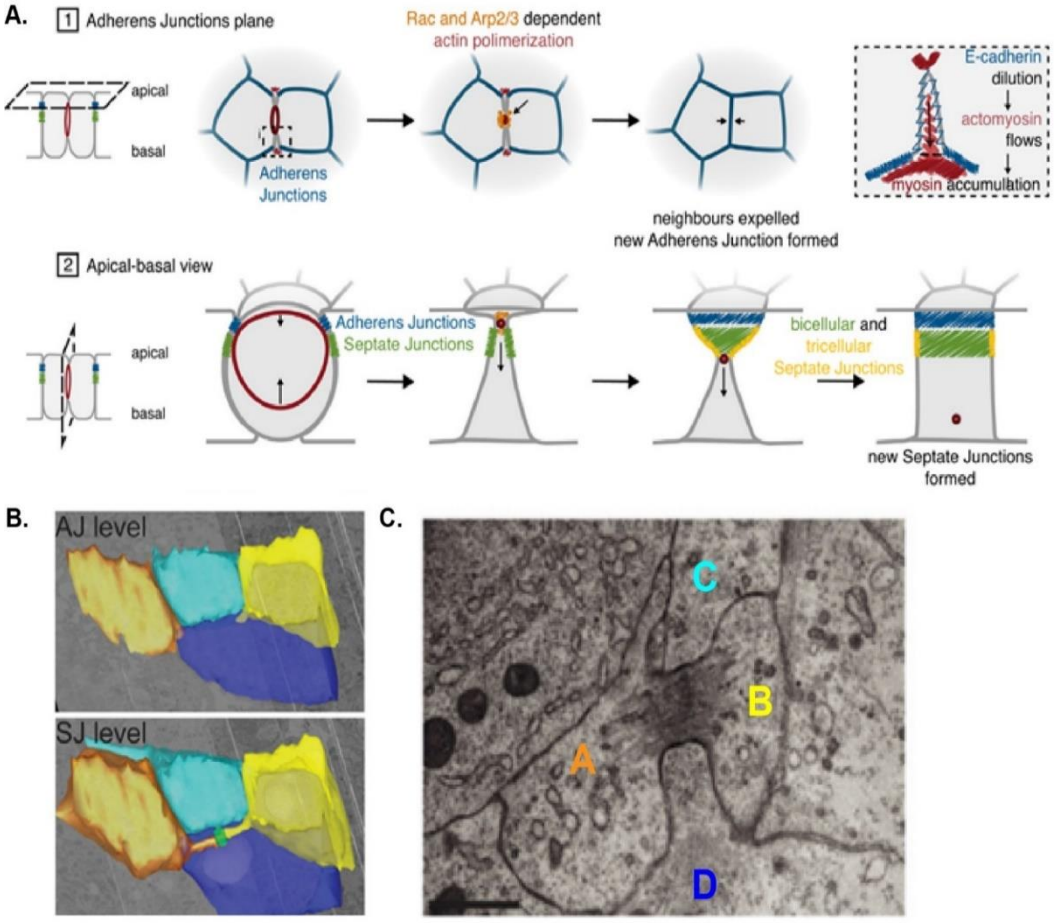

Figure 72. Cell junctional remodelling during Drosophila notum cytokinesis. A. 1) Planar and 2) transversal view of epithelial cell cytokinesis. As cytokinesis occurs, actomyosin ring contracts from basal side to the apical part of the cell. The midbody forms (dark red) and contracts thanks to NMY-II and F-actin polymerisation due to ARP2/3 and Rho GTPase activity. Membrane ingression induced by actomyosin ring contraction leads to DE-cad dilution. It activates actomyosin flows (red) in the neighbouring cell, where NMY-II (dark red) accumulates at the base of the invagination. After newly DE-Cad is added to the cell-cell interface, corresponding to the establishment of AJ (Blue), midbody starts to move basally after detachment. Polarized assembly of new pSJ (green) occurs in parallel to midbody basal displacement. Newly tSJ proteins (Yellow) are formed closed to the midbody and the midbody detaches once pSJ and tSJ have been established. **B.** 3D model based on SFB-scanning electron microscopy showing the contact between daughter cells (orange and yellow) and their neighbours (Cyan and Blue) at both AJ level and SJ level. Note the "ménage à 4" structure between the four cells at SJ level and highlighted in **C.** where TEM micrograph section shows the contacts between the four cells (labelled A to D). The scale bar represents 2µm in C. Adapted from (Osswald and Morais-de-Sa 2019) and (Daniel, Daude et al. 2018).

ii. Cell division orientation

Another key feature of cell division is the orientation, which defines whether the daughter cells will reside in the same plan as the dividing mother cell (called planar division) or outside the plan (called orthogonal division). Moreover, Hertwig's rule (named after the scientist Oscar Hertwig) states that cells, in a planar cell division context, tend to divide along their longer axis. However, tSJ proteins appear to play a role in cell division orientation. Indeed, (Bosveld, Markova et al. 2016) have shown that Gli is needed to recruit Mud, a dynein-associated protein, at the vertex and this position is inherited from the interphasic state of the cell. The astral microtubules contact Mud at the vertex and pull of the centrosomes to orient cell division. Loss of Gli diminishes the Mud signal at the TCJ and this is associated with defects in pulling forces mediated by astral microtubules on the mitotic spindle. These experimental results are confirmed by a model in which the anisotropy of the TCJs is a better predicter than cell shape of cell division orientation **(Figure 73).**

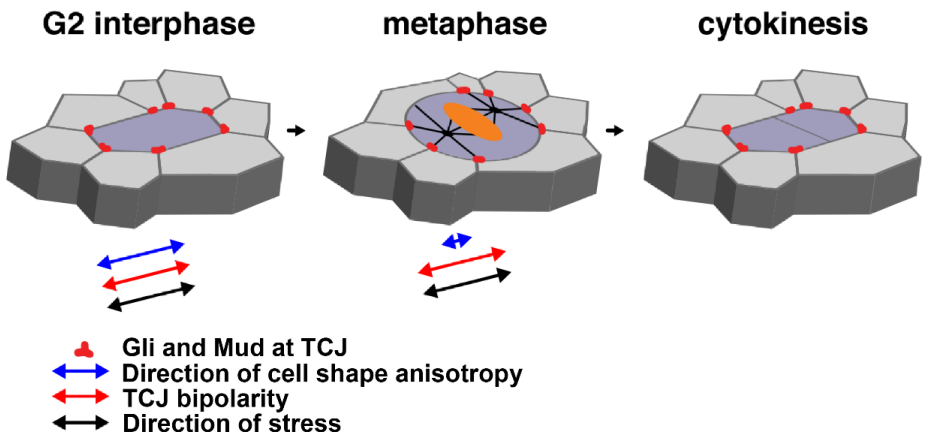

Figure 73. Cell division orientation relies on TCJ position. The dynein-associated protein Mud colocalizes with Gli (Red) during interphase as well as during metaphasis where it regulates mitotic spindle (Black lines), therefore, cell division. Cell shape anisotropy is lost during metaphasis but not the TCJ anisotropy, which allows the regulation of cell division orientation. Adapted from (Bosveld, Wang et al. 2018).

b. Mechanotransduction at Tricellular Adherens Junctions

- **Sidekick and cell-cell intercalation**

We previously saw that Sdk specifically organized the tAJ, acting as a platform to anchor F-actin, Pyd and Cno. In the same study, (Letizia, He et al. 2019) demonstrated Sdk BCJ localisation upon NMY-II inhibition mediated by NMY-II phosphatase,

suggesting that Sdk is present at lower tensed BCJ in the amniosera. In contrast, over-activated NMY-II leads to Sdk enrichment at tAJs. Moreover, when cells operate cell-cell intercalation during trachea formation, Sdk is enriched at the vertices and loss of Sdk prevents, in part, the formation of autocellular junctions from intercellular junctions. Loss of Sdk also impairs junctional rearrangement in retinal pigment cells, leading to extra cells or loss of bristles (Letizia, He et al. 2019).

Likewise, in *Drosophila* Germband expansion, epithelial cells operate intercalation thanks to T1 transition and a specific cell conformation called a rosette. During this process, Sdk is planar polarised and exhibits a different behaviour. In the case of dorso-ventral junction shrinkage, Sdk is more planar and looks like long strings; in the case of antero-posterior junction growth, however, it is shorter and looks more like vertical strings (Finegan, Hervieux et al. 2019). Loss of Sdk shows abnormal cell morphologies as well as an increased number of gaps associated with more time being necessary to resolve them **(Figure 74).** Experimental data and modelling have described how loss of Sdk prejudice polarises cell intercalation, diminishing the cell intercalation needed for antero-posterior elongation, impairing the orientation of T1 transition and their resolution and lowering intercellular adhesion.

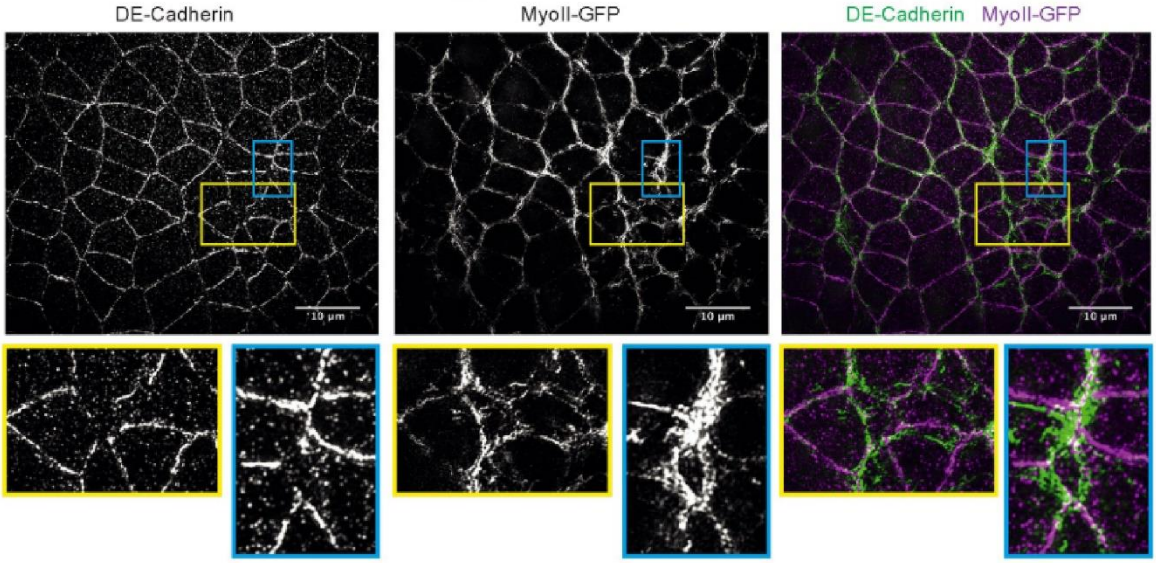

Figure 74. SIM super resolution microscopy showing holes upon loss of Sdk at stage 7 on fixed embryos during germband expansion. The discontinuities of DE-Cad signal reveal gaps surrounded by NMY-II like illustrated in the close-up images. Adapted from (Finegan, Hervieux et al. 2019).

Furthermore, during the rotation of the male genitalia, (Uechi and Kuranaga 2019) have shown that Sdk recruits NMY-II at the vertex to promote cell junction growth and, at the same time, prevents DE-Cad from accumulating.

- **Other tAJ components and cell-cell intercalation**

During convergent extension, Sdk is not the only actors specifically acting at the tAJ. A key player appears to be Cno. We have already seen in the AJ and acto-myosin cytoskeleton chapter that it was especially enriched at TCJ, along with F-actin and β-catenin, at different development stages of the *Drosophila* embryos (Sawyer, Harris et al. 2009). Recently, (Yu and Zallen 2020) have demonstrated that Cno is recruited to vertices in a mechano-sensible way via its phosphorylation by Abl tyrosine kinase. Once present at the vertex, Cno stabilises tAJs and it has to be removed from this position in order to allow cell-cell contact rearrangement.

- **Cell size scaling, Hippo/YAP pathway regulation and tAJs**

In a recent work, (Lopez-Gay, Nunley et al. 2020) characterised the formation of apical stress fibres (aSFs) during *notum* development when anisotropic stress increases. Those aSFs are made of NMY-II and display the typical stress fibres proteins Zyxin, Enabled and α-actinin enrichment at their tips. Interestingly, Ajuba and Warts are also enriched at the tip of the aSFs. Moreover, aSFs form at tAJs, move along the cell membrane and break apart when they encounter a new vertex. Rather, a tAJ will become a nucleating aSF or a breaking one, depending on its orientation in regard to stress direction. Using both modelling and experimental data, the authors determined that tAJs are the main regulators for the scaling between cell area and aSF numbers, where bigger cells with a higher number of tAJs also display a higher number of aSFs. Since the Hippo/YAP pathway actors Jub and Warts are both found to be enriched at the tip of aSFs and that increased tension correlates with the appearance of aSFs, this study shows how tAJs by linking cell size area to number of aSFs, regulate the proliferative state of the cell upon stress induction **(Figure 75).** This study once more indicates that TCJs play a specific role as a platform to integrate mechanical cues and transduce them into biochemical responses.

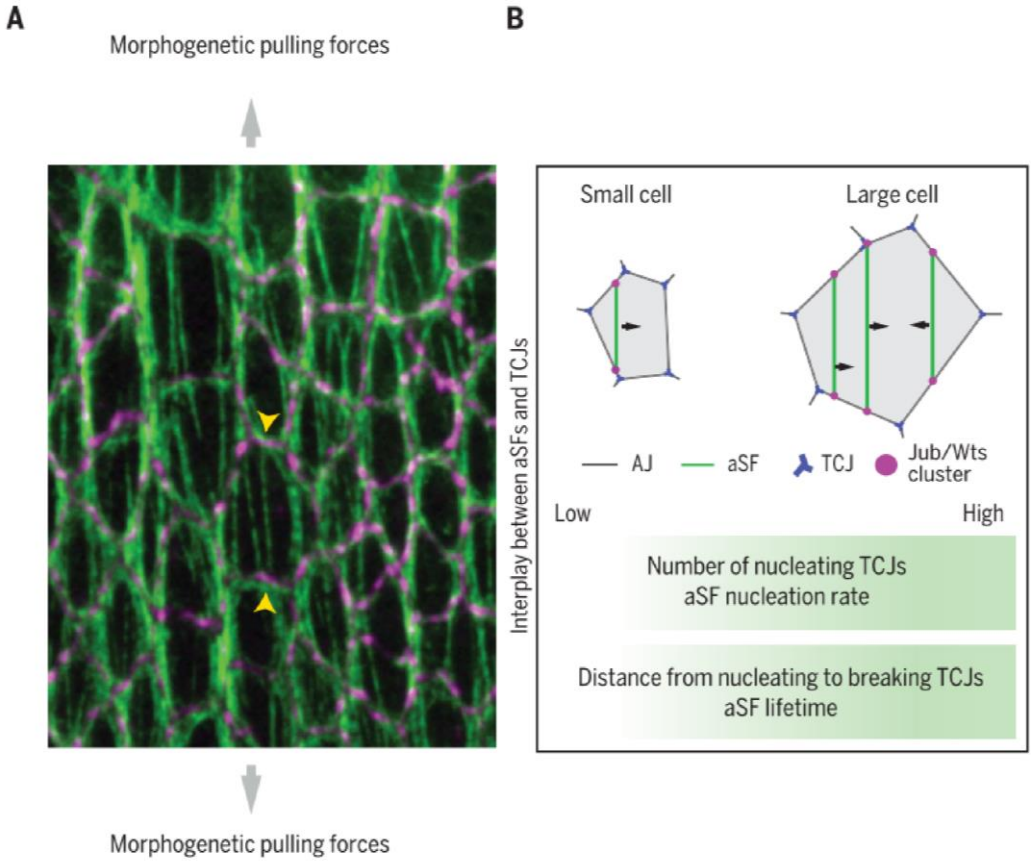

Figure 75. Apical Stress Fibres (aSFs) along with TCJs couple cell area and mechanical response under stress conditions. A. Epithelial cells of the notum display aSFs characterized here by NMY-II (green) at AJ level marked by DE-Cad (magenta) upon stress induced by morphogenetic movements during notum development. **B.** Representation of the coupling between apical cell size area and number of aSFs that accumulate Hippo/YAP pathway proteins at their tips (Ajuba and Warts). aSFs both nucleate and break apart at TCJ level. By doing so, apical cell size, via TCJ, regulates cell divisions because Ajuba/Warts captured at aSFs tips means an increased rate of cell proliferation. Adapted from (Lopez-Gay, Nunley et al. 2020)

c. Apical cell delamination upon loss of M6

Another unmentioned role of TCJ in epithelia homeostasis is its ability to mediate apical cell delamination. Indeed, (Dunn, Rush et al. 2018) studied the effect of loss of M6 in an oncogenic Ras^{V12} background using the *Drosophila* eye disc. They observed M6 mutant/Ras^{V12} cell invasion of the ventral nerve cord upon induction of mutant cells in the eye disc. Those migrated cells originated in an apical cell delamination, which is unusual, and detached totally from their original tissue to localise into the lumen present in the eye disc. Apical delamination needs active NMY-II, Rho-A activity but and also Cno, since knock-down of these proteins in the M6/Ras^{V12} mutant context prevents cell delamination. The authors also looked at loss of M6 in the cell junction

by TEM and observed holes at the vertices. Therefore, the authors argued that M6, by regulating cell cytoskeleton organisation along with cellular junction, is a leading actor of cell delamination in oncogenic background once absent.

d. Conclusion

This chapter ends the introduction, in which we have had the opportunity to sense how TCJs, placed at crucial positions in the tissue, display a great variety of roles, ranging from cell-cell rearrangement to cell division and regulating signalling pathways involved in proliferation.

Objectives

Despite the growing number of TCJs studies which start to unravel their roles, ranging from orienting cell division, to regulating cell-cell contact rearrangement or being involved in tissue invasiveness, little is known about the TCJ itself. Moreover, previous studies in the lab focus on how cellular junctions were remodelled upon cytokinesis in order to preserve epithelium integrity. They notably showed how AJ kept its mechanical barrier function and how pSJ proteins allowed connections between the dividing cells and their neighbours, forming a “ménage-à-quatre” at the midbody level. Also, they highlighted how the abscission process, the ultimate step of cell separation, is tightly linked to midbody basal displacement and how this displacement relied on adding new pSJ proteins at the new cell-cell junction. During pSJ protein studies, they characterised the onset of tSJ formation, looking at Gli and Aka, at midbody level as well. Still, further descriptions of TCJ assembly are required since the Sdk tAJ protein and the tSJ protein M6 were not characterised at this moment.

Hence, like AJ and SJ, do tAJ and tSJ remodel one after another and if so, do they execute this process in the same amount of time? Moreover, are the TCJ components specifically target to the new TCJ? Still looking at the cell division, is the loss of TCJ components somehow involve with cytokinesis defects?

The few studies focusing on TCJ components interplay were done most of the time in epithelium devoid of mature pSJ. Therefore, it was important to decipher if TCJ proteins behaviours were similar in a mature epithelium. pSJ proteins are not only playing roles in permeability barrier but like we previously saw, display a wide range of activities. Moreover, both pSJ and bAJ are in contact with the TCJ. This requires to probe if any defects at TCJ level could interfere with BCJ homeostasis. On the contrary, will defects at BCJ level trigger impairment of the TCJ proteins? Also, can proteins present at different junctional plans, such as tAJ and tSJ, interact directly or indirectly, leading to defects when removing one actor from a different level?

Therefore, describing and characterising the role of these different TCJ proteins, both at TCJ and BCJ level, will start to unravel the cellular processes involved in the general homeostasis of the epithelium, both during anaphase and cell division.

Results part 1:

Publication

Report

Current Biology

Interplay between Anakonda, Gliotactin, and M6 for Tricellular Junction Assembly and Anchoring of Septate Junctions in *Drosophila* Epithelium

Graphical Abstract

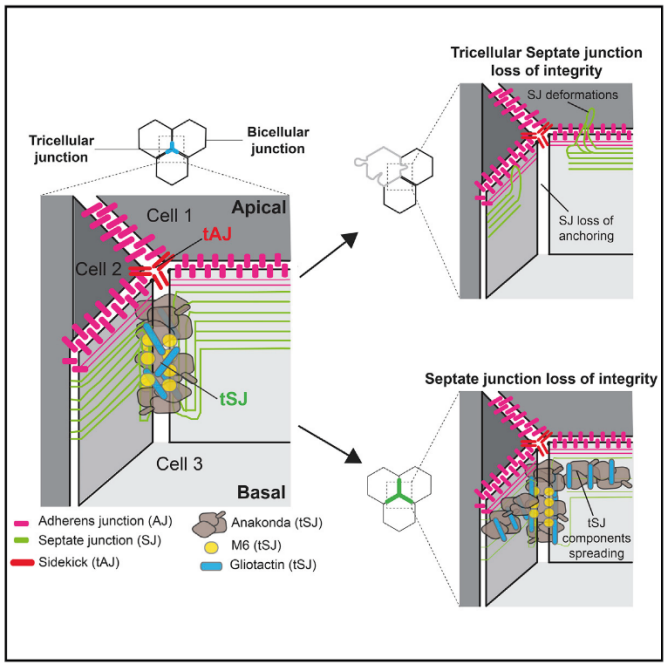

Highlights

- Tricellular adherens junction and tricellular septate junction (tSJ) are independent
- Aka and M6 are upstream regulators of tSJ assembly while Gli stabilizes Aka
- tSJs anchor bicellular septate junctions at vertex and ensure epithelium integrity
- Bicellular septate junction components restrict tSJ components to the vertex

Authors

Thomas Esmangart de Bournonville, Roland Le Borgne

Correspondence

roland.leborgne@univ-rennes1.fr

In Brief

Esmangart de Bournonville and Le Borgne characterize the assembly and interactions of tricellular junction components in *Drosophila* epithelial cytokinesis. Tricellular septate junctions (tSJs) ensure the anchoring and morphology of bicellular septate junctions (bSJs). In turn, bSJ integrity restricts the localization of tSJ components at vertices.

Esmangart de Bournonville & Le Borgne, 2020, Current Biology *30*, 4245–4253
November 2, 2020
https://doi.org/10.1016/j.cub.2020.07.090

CellPress

Current Biology

CellPress

Report

Interplay between Anakonda, Gliotactin, and M6 for Tricellular Junction Assembly and Anchoring of Septate Junctions in *Drosophila* Epithelium

Thomas Esmangart de Bournonville[1,2] and Roland Le Borgne[1,2,3,*]
[1]Univ Rennes, CNRS, IGDR (Institut de Génétique et Développement de Rennes), UMR 6290, 2 Avenue du Professeur Leon Bernard, 35000 Rennes, France
[2]Equipe Labellisée Ligue Nationale contre le Cancer, 14 Rue Corvisart, 75013 Paris, France
[3]Lead Contact
*Correspondence: roland.leborgne@univ-rennes1.fr
https://doi.org/10.1016/j.cub.2020.07.090

SUMMARY

In epithelia, tricellular junctions (TCJs) serve as pivotal sites for barrier function and integration of both biochemical and mechanical signals [1–3]. In *Drosophila*, TCJs are composed of the transmembrane protein Sidekick at the adherens junction (AJ) level, which plays a role in cell-cell contact rearrangement [4–6]. At the septate junction (SJ) level, TCJs are formed by Gliotactin (Gli) [7], Anakonda (Aka) [8, 9], and the Myelin proteolipid protein (PLP) M6 [10, 11]. Despite previous data on TCJ organization [12–14], TCJ assembly, composition, and links to adjacent bicellular junctions (BCJs) remain poorly understood. Here, we have characterized the making of TCJs within the plane of adherens junctions (tricellular adherens junction [tAJ]) and the plane of septate junctions (tricellular septate junction [tSJ]) and report that their assembly is independent of each other. Aka and M6, whose localizations are interdependent, act upstream to localize Gli. In turn, Gli stabilizes Aka at tSJ. Moreover, tSJ components are not only essential at vertex, as we found that loss of tSJ integrity induces micron-length bicellular SJ (bSJ) deformations. This phenotype is associated with the disappearance of SJ components at tricellular contacts, indicating that bSJs are no longer connected to tSJs. Reciprocally, SJ components are required to restrict the localization of Aka and Gli at vertex. We propose that tSJs function as pillars to anchor bSJs to ensure the maintenance of tissue integrity in *Drosophila* proliferative epithelia.

RESULTS

TCJ *De Novo* Assembly and SJ Regulation during Cytokinesis

The notum of the *Drosophila melanogaster* is a proliferative monolayer epithelium, allowing the study of cell division in time and space. Epithelial cytokinesis is a multicellular process during which a new bicellular junction (BCJ) interface and two new tricellular junctions (TCJs) are established (Figures 1A and 1C). To decipher the *de novo* assembly of TCJ (tricellular adherens junction [tAJ] and tricellular septate junction [tSJ]) that takes place in cytokinesis, we imaged the adherens junction (AJ) and the midbody using the non-muscle Myosin II light chain tagged with red fluorescent protein (Spaghetti Squash, Sqh::RFP) [15] together with the tAJ marker Sdk::GFP [16] or tSJ markers GFP::M6 [17] and Anakonda (Aka)::GFP [8]. All fluorescent markers are inserted at the locus, giving rise to functional reporters expressed at physiological level. In telophase, following actomyosin ring constriction, Sqh is recruited at the new cell-cell interface and in neighboring cells at AJ level as reported (Figure 1A) [18–20]. In all cases, the transition from metaphase to anaphase, defined by the frame just before the onset of cell elongation, was considered to be t0 (time is indicated in min:sec). Initiation of the formation of new adhesive contacts between daughter cells occurs at t10 (Figure 1B; Video S1) [18, 19, 21]. Concomitantly, the first signal of Sdk::GFP appears at the new vertex around t10–t13 (Figures 1B and 1F; Video S1). Basal to AJ, as previously described [15, 22], the contractile ring remains anchored to the plasma membrane at the septate junction (SJ) level, connecting the divided cells to their neighbors and resulting in the formation of finger-like protrusions (FLPs) upon midbody formation (Figures 1C and S1A–S1B′; Video S2). tSJ markers GFP::M6 (Video S3) and Aka::GFP first appear in the form of puncta adjacent to the midbody at t15 and t17, respectively (Figures 1D’ and 1E’) [15]. Their signals then spread laterally until they form a continuous tSJ strand (t50; Figures 1D–1F; Video S3). Thus, assembly of the tAJ and tSJ are spatially and temporally independent (Figure 1G).

The presence of tSJ components along the FLP connected to the midbody during cytokinesis raises the question of the role of tSJ in FLP maintenance. In wild-type conditions, FLPs labeled with the core SJ component ATP-α::GFP [15] formed 1 μm below AJ at t5 as the result of actomyosin cytokinetic ring constriction (Figures S1A–S1B’) and displayed a characteristic “U” shape between t5 and t10 (Figures S1A′–S1B′; Video S1). Midbody was centered in 71% of the cases, resulting in the formation of two FLPs of similar length (Figures S1A′, S1B, and S1E). Upon

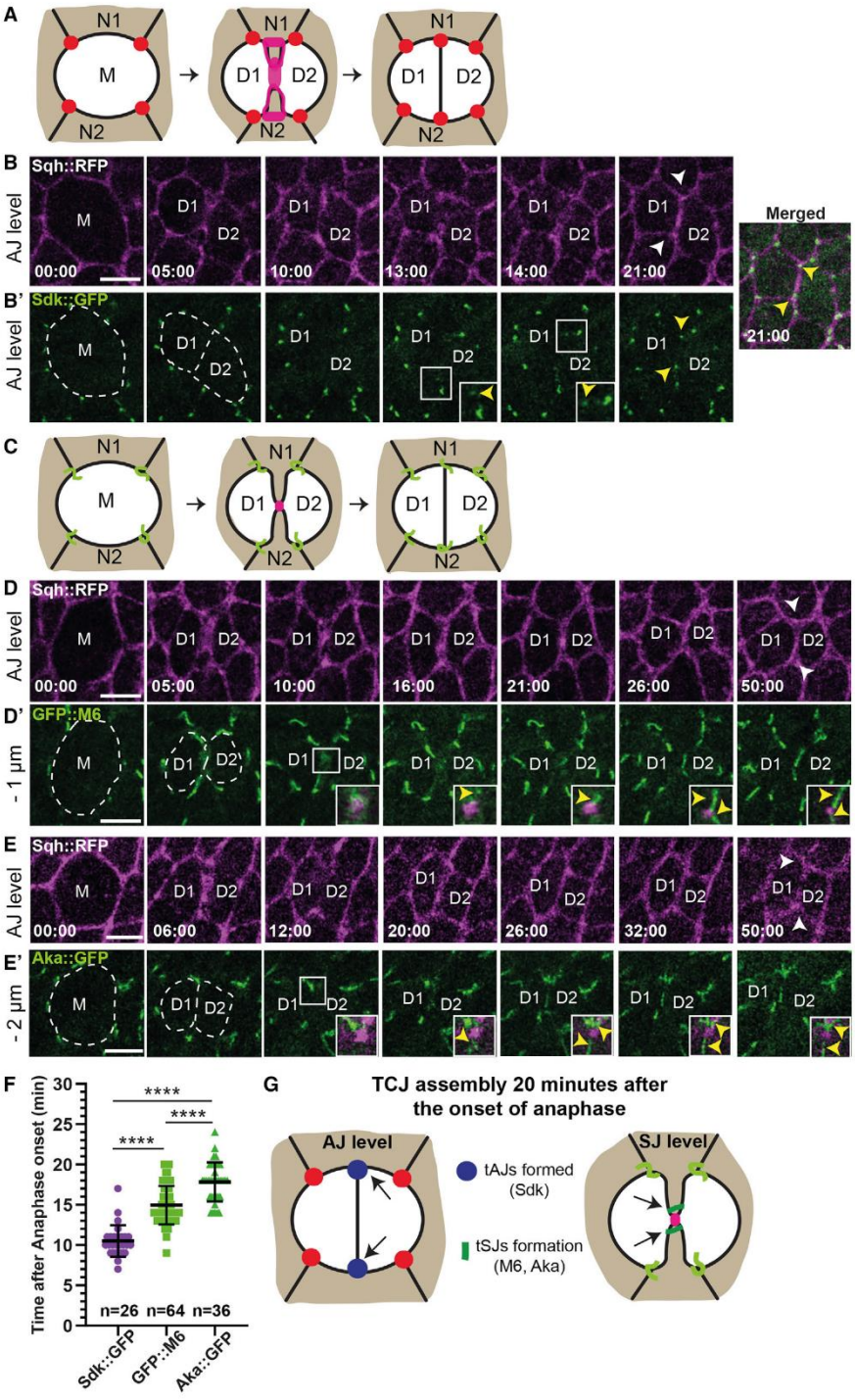

(legend on next page)

loss of Aka using the aka^{L200} null mutant [8], the midbody is off-centered, leading to two FLPs of unequal length (62% of cases compare to only 29% for wild-type cells; Figures S1C–S1E; Video S4). In addition, we observed that ATP-α::GFP signal is inhomogeneous in those FLPs compared to wild-type conditions (Figures S1C′–S1D; Video S4). These results indicate that Aka ensures the symmetry in FLP formation as well as the SJ components distribution, suggesting a role for Aka in regulating bicellular septate junction (bSJ) (Figure S1F; see below).

The fact that the recruitment of Sdk and Aka/M6 are spatially and temporally independent during cytokinesis (Figure 1) suggests that tSJ and tAJ assembling, and perhaps functioning, are independent.

Interplay between tAJ and tSJ Components

In order to analyze the relationship between tAJ and tSJ, we next analyzed the consequence of loss of Sdk on tSJ. We used the homozygous viable null allele $sdk^{\Delta 15}$ [23] and observed no differences of Aka signals (Figures S2A and S2B'). Conversely, we studied the loss of tSJ integrity using the aka^{L200} mutant on Sdk localization. No differences in the localization of Sdk were observed between wild-type and aka^{L200} cells (Figures S2C and S2C'). These data indicate that the localization, recruitment, and/or stabilization of Sdk and Aka at TCJ are independent of each other.

Then, we investigated the relationship between the three tSJ components. Loss of Aka leads to Gliotactin (Gli) (Figures S2D and S2D') and GFP::M6 (Figures 2A and 2A') disappearance from tSJ. This is true even when only one cell contributing to the vertex is mutant for Aka, thereby confirming that Aka is an upstream regulator in the notum, as described in *Drosophila* embryo [8]. We next studied the role of M6 on Aka and Gli localization and found that loss of M6, using $M6^{w186}$ null mutant [11], leads to Aka (Figures 2B and 2B') and Gli (Figures S2E and S2E') no longer accumulating at vertex. Therefore, M6 and Aka are both upstream regulators of tSJ assembly. However, unlike Aka, loss of M6 from one cell contributing to the vertex triggers the reduction in Aka signal (Figures 2B–2B'') rather than a complete disappearance. Gli signal is still detectable in that case, too (Figure S2E).

Because Gli activity is dispensable for Aka localization at tSJ in *Drosophila* embryo [8], we tested whether this was also the case in the pupal notum. Unexpectedly, we found a decrease in the intensity of Aka signal in Gli^{dv3} mutant cells (Figures 2C and 2C'). We next tested the possibility that the stabilization of Aka at tSJ is modified upon loss of Gli using FRAP. Our experiments revealed that upon loss of Gli, immobile fraction of Aka::GFP drastically dropped to 0.30, compared to 0.75 in wild-type conditions, 20 min after photobleaching (Figures S2F and S2G) with a mild reduction of the rate of fluorescence recovery ($t_{1/2}$ = 318 s in Gli^{dv3} and $t_{1/2}$ = 361 s in wild type).

Therefore, while being dispensable to localize Aka at tSJ, Gli influences the time of residency of Aka, revealing an interplay between Aka, Gli, and M6 (Figure 2D).

Loss of tSJ Disrupts SJ Integrity at Both bSJs and Vertices and Induces SJ Deformations

In addition to defects in tSJ assembly, our time-lapse analyses also revealed defects in the integrity of bSJ in interphase upon loss of Aka. Indeed, it caused the appearance of 1-μm to 3-μm-long membrane deformations labeled using GAP43::mCherry (Figures S3A and S3B). These membrane deformations are located within the plane of SJ, positive for the SJ core components including Cora (Figure 3A), ATP-α::GFP (Figure 3B), and Nrx-IV (Figure 3C), as well as Dlg (Figure 3D). This phenotype was not only observed using several *aka* mutant alleles (data not shown) upon silencing of Aka (Figures S3A and S3B), but also upon loss of Gli (Figure S3C), indicating that loss of Aka or its stability at tSJ is associated with SJ membrane deformations. Using Nrx-IV, we observed that many deformations are found apical, close to and/or within the plane of DE-cad, albeit not colocalizing with it (Figures 3E–3H'). We also observed Nrx-IV signal disappearance or drastic decrease from vertices in aka^{L200} cells (Figures 3I and 3I'). While similar results were observed for ATP-α::GFP (data not shown), in contrast, Dlg (Figures 3I and 3I') and GAP43::mCherry (Figures S3A and S3B) remained present at the vertex. These data argue for a depletion of SJ core components from the vertex. The loss of Gli induced similar results on Nrx-IV presence at vertex (data not shown). These results raise the question of how and why loss of tSJ integrity causes SJ deformations (Figure 3D') and prevents the presence of SJ core components at the vertex (Figure 3J).

Since SJ-containing membrane deformations localize in part at AJ level and AJs are the sites of actomyosin-driven mechanical forces of the tissue [24, 25], we probed whether forces were involved in the stabilization of these deformations. Using two-photon laser-based nano ablation, we cut the tips of deformations to reveal possible pulling or pushing forces (Figure S3D). No significant recoil or changes in the shape of deformations were observed upon ablation. Then, we probed lateral forces by cutting the bSJ close to the deformation and again revealed no deformation shape changes after ablation (Figure S3E). In accordance with those results, neither Sqh nor Actin marked by phalloidin were enriched in those deformations, excluding the possibility that AJ components (DE-cad; Figures 3E–3H') or

Figure 1. TCJ Assembly during Epithelial Cytokinesis

(A and C) Schematic of tAJ (A) and tSJ (C) assembly during cytokinesis. In this and the following panels, M, D, and N represent mother, daughter, and neighboring cells, respectively. Magenta signal represents Sqh::RFP enrichment at the new interface and in neighboring cells (A) or the midbody between the FLP forming at SJ level (C). Red dots show tAJ (A) and green lines show tSJ (C).

(B, D, and E) Time-lapse imaging of Sqh::RFP (magenta), Sdk::GFP (B'), GFP::M6 (D'), and Aka::GFP (E') in dividing cells. The dashed line highlights the divided cell and the two new cells. Yellow arrowheads show the first appearance of GFP signal. White arrowheads show the two new TCJs formed at AJ level. White squares show high magnifications of Sdk::GFP (B') arrival at new vertex or GFP::M6 (D') or Aka::GFP (E') first appearance close to the midbody (magenta).

(F) Plot of the mean times of the first appearance after anaphase onset of Sdk::GFP (purple dots, n = 26 divisions, 4 pupae), GFP::M6 (green squares, n = 64 divisions, >5 pupae), and Aka::GFP (dark green triangles, n = 36 divisions, >5 pupae). Bars show mean ± SD, ****p < 0.0001, unpaired t test.

(G) Schematic of tAJ and tSJ assembly 20 min after anaphase onset. Magenta signal represents the midbody between the FLP forming at SJ level. Dark blue dots show new tAJs characterized by Sdk::GFP, and dark green lines show the formation of new tSJs characterized by GFP::M6 and Aka::GFP below tAJs.

In these and all other panels, time is min:sec (B, D, and E) with t0 corresponding to the anaphase onset, and scale bars are 5 μm. Distances correspond to the position relative to tAJ labeled with Sqh::RFP. See also Figure S1 and Videos S1–S4.

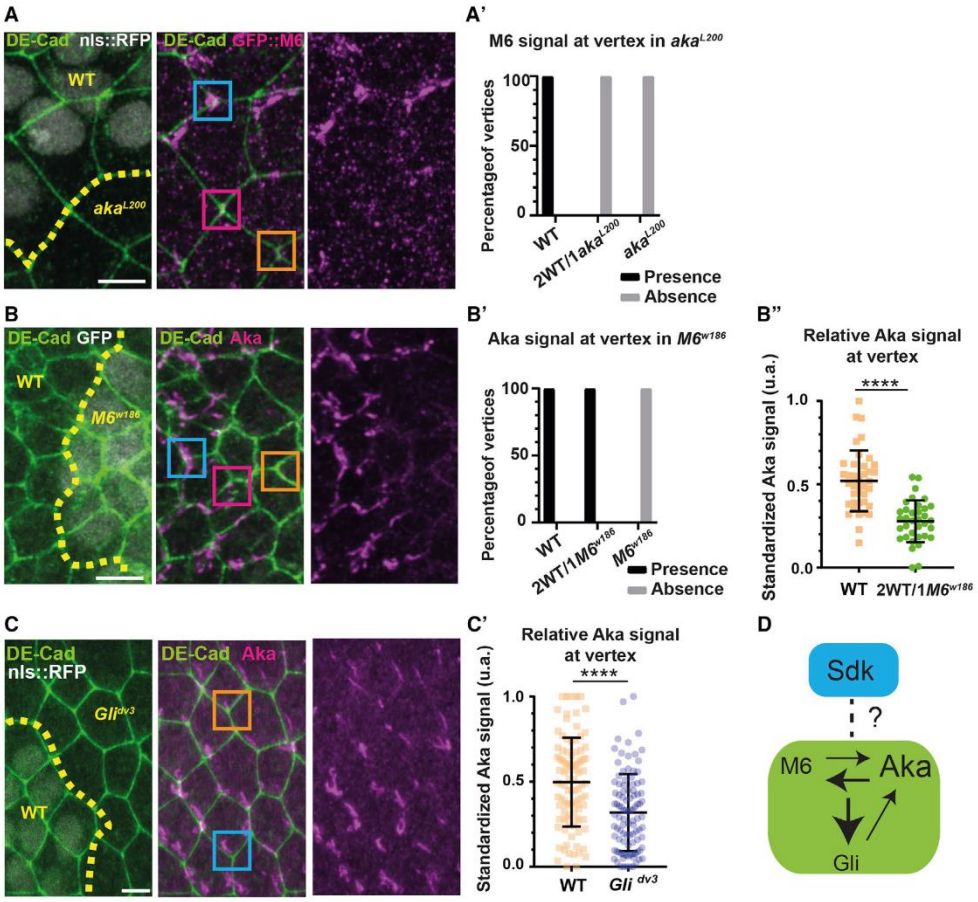

Figure 2. Aka and M6 Are Upstream Regulators of tSJ

(A–C) Nota stained for DE-cad (anti-DE-cad, green) after heat-shock to induce clone of wild-type (A and C nls::RFP positive; B, GFP negative) and mutant cells (A and C nls::RFP negative; B, GFP positive) for tSJ components. (A) Localization of M6 (GFP::M6 + anti-GFP, magenta). Wild-type and aka^{L200} cells are separated by the dashed yellow line. M6 is enriched at the TCJ at wild-type vertex (blue square) and is no longer detected at vertex upon loss of Aka from one cell adjacent to the vertex (pink square) or at a vertex of three aka^{L200} cells (orange square). (B) Localization of Aka (anti-Aka, magenta). Wild-type and $M6^{w186}$ mutant cells are separated by the dashed yellow line. Aka is enriched at the TCJ at wild-type vertex (blue square) and upon loss of M6 from one cell adjacent to the vertex (pink square), but the accumulation disappears at vertex of three $M6^{w186}$ mutant cells (orange square). (A' and B') Histograms representing the percentage of presence (black) or absence (gray) of M6 and Aka accumulation at the vertex between three wild-type cells, two wild-type and one aka^{L200} cell (A'), one $M6^{w186}$ cell (B'), three aka^{L200} cells (A'), or three $M6^{w186}$ cells (B') (n = 100 vertices, >5 pupae for each experiment). (B'') Plot of the standardized Aka signal at a wild-type vertex (orange squares) and a vertex of two wild-type and one $M6^{w186}$ cells (green circles). (n = 39 and 35 vertices respectively, 3 pupae). Bars show mean ± SD, ****p < 0.0001, unpaired t test. (C) Localization of Aka (anti-Aka, magenta). Wild-type and Gli^{dv3} cells are separated by the dashed yellow line. Orange and blue squares show Aka signal in *Gli* and wild-type conditions, respectively. (C') Plot of the standardized Aka signal at vertex in wild-type (orange squares) and Gli^{dv3} cells (blue circles). (n = 100 vertices each, >5 pupae). Bars show mean ± SD, ****p < 0.0001, unpaired t test.

(D) Schematic of the interplay of TCJ components.

The scale bars represent 5 μm. All images are maximum projection. See also Figure S2.

actomyosin (Figures S3F and S3G) stabilized them. Next, we tested whether changes in SJ component dynamics could be responsible for the induction of those deformations by FRAP approach on ATP-α::GFP (Figures S3H–S3J). Wild-type cells exhibited slow turnover at bSJ ($t_{1/2}$ = 280 s) with an immobile fraction of 0.67 at 18 min after photobleaching (Figures S3H and S3K). In aka^{L200} cells, the kinetics of recovery were similar to wild-type condition ($t_{1/2}$ = 294 s) but exhibited a slight increase of the immobile fraction of 0.76 at 18 min after photobleaching (Figures S3I and S3K). Moreover, SJ-containing membrane deformations revealed a higher immobile fraction of 0.82 at 18 min after photobleaching, while the $t_{1/2}$ = 296 s remained similar (Figures S3J and S3L). Therefore, loss of tSJ led to an increased residency time of ATP-α::GFP. This might explain why the steady-state levels of ATPα::GFP signal are higher in membrane deformations (Figures 3B, 3C, 3G, and S3D–S3F).

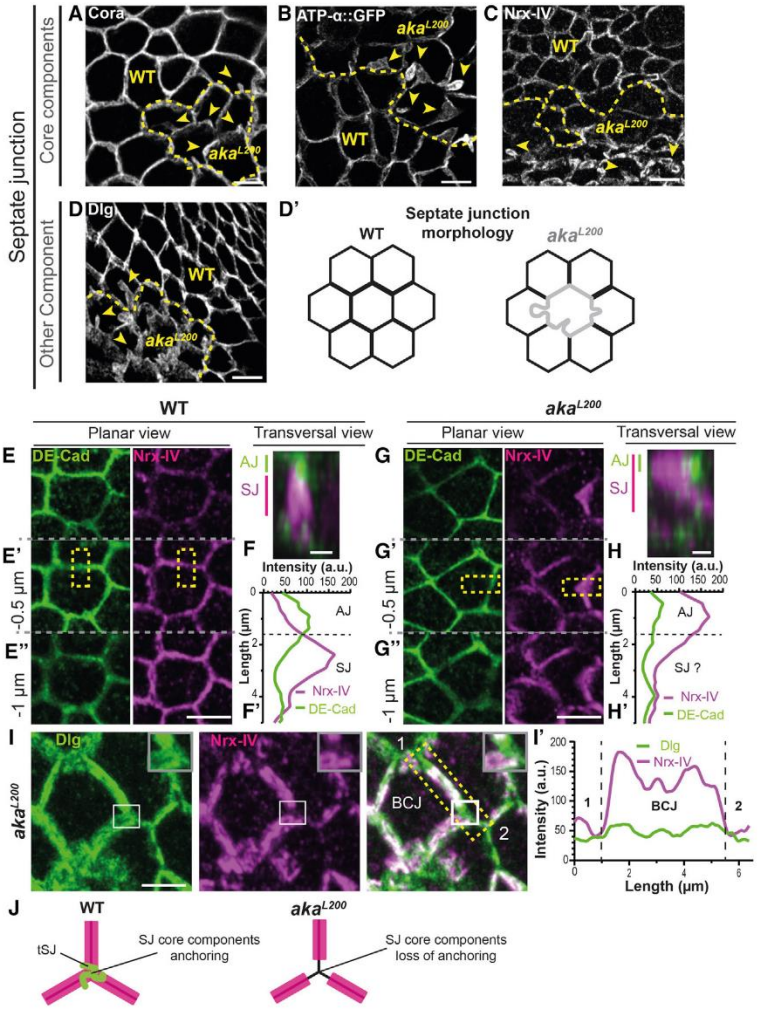

Figure 3. tSJs Regulate the Shape of SJ and Ensure the Anchoring of SJ Core Components at the Vertex

(A–D) SJ morphology visualized with Cora (anti-Cora), ATP-α (ATP::GFP), and Nrx-IV (anti-Nrx-IV) or other SJ component Dlg (anti-Dlg) in wild-type and *aka*^{L200} cells, separated with the dashed yellow line. Yellow arrowheads indicate micrometric size deformations of SJ. (D') Schematic of the bSJ membrane deformations observed upon loss of Aka.

(E–H) Localization of Nrx-IV (anti-Nrx-IV, magenta) in notum marked by DE-cad (anti-DE-cad, green). (E–E''' and G–G''') Different planar sections separated by 0.5 µm in wild-type and *aka*^{L200} cells. (F and H) Maximum projection of the transversal section depicted by the yellow rectangles. (F' and H') Plots representing DE-cad (green line) and Nrx-IV (magenta line) signals as a function of cell transversal length represented in transverse sections. Black dashed lines show the presumptive boundary between AJ and SJ.

(I) Localization of Dlg (anti-Dlg, green) and Nrx-IV (anti-Nrx-IV, magenta) in *aka*^{L200} cells after maximal projection. White squares show high magnification of a vertex in *aka*^{L200} cells. Yellow dashed rectangle shows the line scan used between two vertices represented by 1 and 2 (I). Plot representing Dlg (green line) and Nrx-IV (magenta line) signals as a function of the length of cell-cell boundary (I').

(J) Scheme showing the loss of *aka*^{L200} effect on SJ core component. Magenta lines show SJ core component, green lines the tSJ, and black lines the membrane as well as Dlg protein.

The scale bars represent 5 µm or 1 µm in (F and H). See also Figure S3.

bSJs Restrict the Localization of tSJ Components at Vertices

Loss of tSJ leads to detachment of bSJ from vertex and changes in the dynamics of recovery of SJ core components in membrane deformations, suggesting a possible physical connection between tSJ and bSJ. This prompted us to study the consequence of loss of function of bSJ on the localization of tSJ proteins. We found that depletion of the SJ core component Cora leads to the spreading of Aka along bSJ (Figures 4A–4C'). The lateral spreading of Aka was not due to an increase in the length of BCJ adjacent to the vertex (Figures 4D and 4E). Similar results were obtained upon depletion of Nrx-IV (Figures S4A–S4C'). Finally, the spreading of Gli was equally observed in Nrx-IV RNAi context (Figures S4D–S4F') and Cora RNAi (data not shown). Together, our results demonstrate that bSJ integrity is required to confine tSJ components localization at the vertex.

DISCUSSION

Here, we provided evidence that the recruitment, localization, and stabilization of tAJ and tSJ are spatially and temporally independent. Among tSJ, Aka and M6 were found to be upstream regulators of tSJ while Gli stabilized Aka at tSJs. Moreover, we uncovered that tSJ components are essential to maintain SJ homeostasis both in interphase and during mitosis. Conversely, SJ integrity is required for tSJ components to be confined at vertices. Based on these results, we propose a model of mutual dependence in which tSJs act as pillars to anchor SJ strands at vertices while SJ core components act to restrict tSJ components at the vertices (Figures 4F–4H).

Our study of TCJ assembly showed that, like AJ and SJ, tAJ is established first, prior to tSJ. *De novo* formation of AJ occurs concomitantly to Sdk recruitment at vertices (this study) [18, 19, 21], suggesting a coupled mechanism to ensure AJ mechanical integrity at both BCJs and TCJs. Once tAJs are formed, tSJ components begin to be recruited at FLP level, with GFP::M6 detected before Aka::GFP. It is interesting to note that, during cytokinesis in vertebrates, Tricellulin and Lipolysis-stimulated lipoprotein receptor LSR, the main

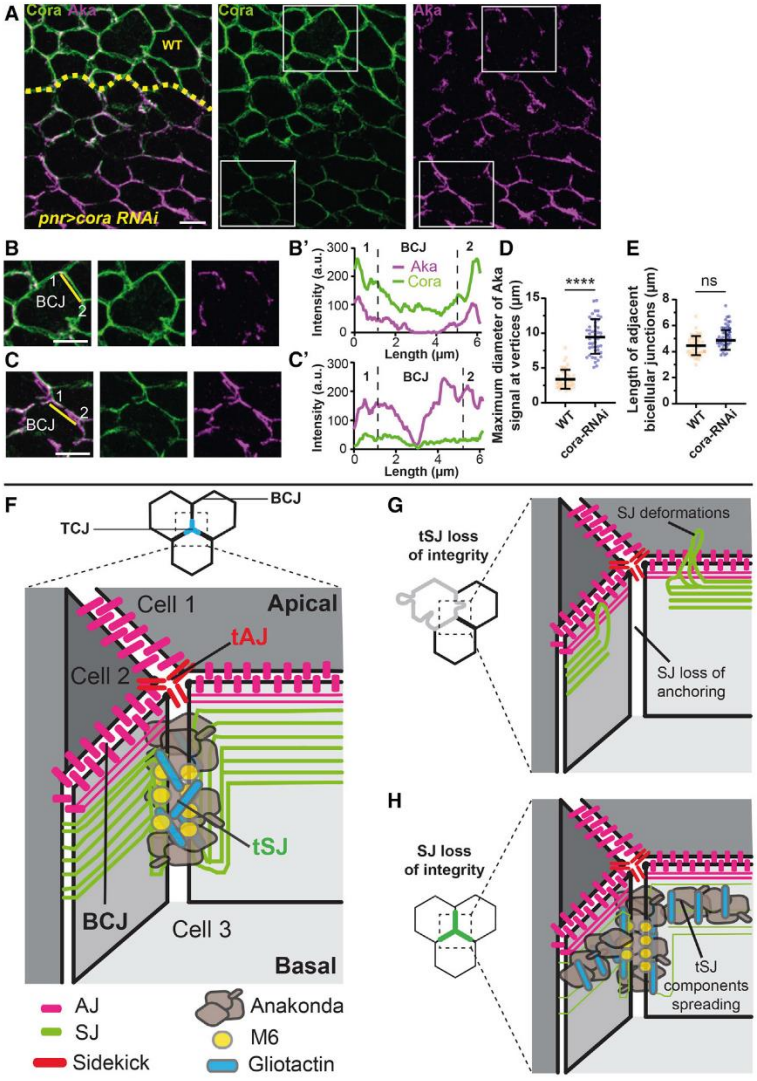

Figure 4. SJ Integrity Is Required to Confine tSJ Components at Vertex

(A–C) Localization of Aka (anti-Aka, magenta) in cells marked by Cora (anti-Cora, green) in wild-type and cells expressing UAS::Cora-RNAi under *pnr*-Gal4 control. The dashed yellow line separates wild-type and Cora-RNAi cells. Aka spreads at the BCJ upon knockdown of Cora (A). White squares show magnification of wild-type and knockdown cells for Cora (B and C). Yellow lines show the line scan used to obtain plots representing Cora (green line) and Nrx-IV (magenta line) signals as a function of the length of cell-cell boundary in wild type and Cora-RNAi cells respectively (B' and C').

(D) Plot of the diameters (μm) of circles including maximal Aka signal at vertex in wild-type (orange squares) and Cora-RNAi cells (blue circles) (n = 50 vertices, >5 pupae).

(E) Plot of the length (μm) of BCJ adjacent of wild-type vertices (orange squares) and Cora-RNAi vertices (blue circles) (n = 50 BCJ, >5 pupae). Bar show mean ± SD, ****p < 0.0001, ns: non-significant, unpaired t test.

(F) Schematic of the TCJ general organization in *Drosophila* notum.

(G) Upon loss of tSJ integrity, SJ strands are no longer anchored on tSJ complex, leading to loss of SJ components presence at vertex and SJ deformations inductions in both AJ and SJ level.

(H) Upon silencing of SJ core components, Aka and Gli spread at BCJ and are no longer restricted at the vertex.

The scale bars represent 5 μm. See also Figure S4.

components of tight tricellular junction (tTJ) [26–28], are also recruited with different timing [29]. Although we cannot exclude that the difference in stoichiometry at tSJ could account for the delay in Aka::GFP appearance compared to GFP::M6, these results suggest similarities for tSJ and tTJ assembly.

Here, we show that Aka and M6 are interdependent for their localization at tSJ and are acting upstream of Gli in the tSJ assembly pathway. Nonetheless, our analyses of clone borders suggest some differences in the requirement of Aka and M6 in tSJ assembly. Structure function analyses and mode of subcellular localization of M6, a small four-pass transmembrane proteolipid protein, will help in understanding its activity, stoichiometry, and relationship with Aka. In addition, it will be interesting to determine whether the mammalian ortholog of M6, enriched in CNS [30, 31], also localizes at TCJ and exerts similar function in vertebrates. Our study also revealed that Gli is required for the maintenance of Aka localization at tSJ. Thus, Gli is not simply a downstream effector of Aka and M6, indicating an interplay between Aka, M6, and Gli in regulating tSJ assembly, stability, and function. Loss of LSR in vertebrates leads to the spreading of Tricellulin, resembling the loss of Aka on Gli [27]. Whether or not Tricellulin plays a role on LSR stability remains to be determined.

Transmission electron microscopy (TEM) revealed that vertices in invertebrates are intercellular-space-spanned vertically with diaphragms [12–14]. SJs were also characterized by TEM as belt-like strands of septa [12–14, 32]. Moreover, SJ proteins partially colocalize with tSJ proteins (this study) [33], suggesting that SJs and tSJs are physically connected. Our results are compatible with a model in which Gli interacts directly with SJ proteins. Another hypothesis could state that the loss of Aka stability by loss of Gli triggers SJ core components exclusion from the vertex. If so, the effect of loss of Gli on Aka stability might be indirectly mediated since they are not reported to co-immunoprecipitate [8]. Gli is part of the Neuroligin family [34], a set of proteins involved in synapse formations [35] and synaptic

transmission [36, 37]. Moreover, recent studies highlighted physical interaction between MGDA proteins and Neuroligin [38–40]. MGDA proteins are composed of six N-terminal Ig domains and one fibronectin type III domain [41] that looks like Neuroglian (Nrg) organization, a SJ core component also displaying six N-terminal Ig domains followed by five fibronectin type III domains [42]. MGDAs are reported interacting with Neuroligin via their first two Ig domains [38–40]. Knowing that Nrg formed a complex with Cora, ATP-α; and Nrx-IV [43, 44], the link between tSJ and SJ could be Gli binding Nrg, making tSJ the pillar required to anchor SJ strands.

Epithelial cells lacking CrebA showed excess of membrane and SJ components [45]. Also, another recent study [46] highlighted that subperineurial glial cells lacking SJ integrity compensate by overexpressing SJ components and making more cellular membrane. It is conceivable that the loss of SJ anchorage at tSJs could result in a permeability defect that is detected at the cell level. In an attempt to compensate for the lack of permeability, more SJ proteins and membrane components would be targeted to the plasma membrane. Such an excessive amount of SJ proteins combined with their slow turnover would cause the local enrichment, resulting in BCJ elongation and thus in membrane deformations. However, how cells could sense SJ permeability defects and the molecular processes leading to SJ deformations remains elusive at present.

The mutual exclusion of bSJ and tSJ components combined with the pillar model proposed above raise the question about origins of tSJ protein localization. Inducing loss of SJ integrity leads to Aka and Gli spreading along BCJ, as shown here upon Cora or Nrx-IV depletion. The space freed up by the loss of SJ may allow tSJ components to move to this location [47]. Another explanation could be that tSJ component roles are multiple. One is to anchor SJ strands at vertices to ensure their shape and integrity. Another could be that they also play a role in permeability function, localizing SJ components in close vicinity of the vertex or playing a filter role themselves. Therefore, their spreading at BCJ upon SJ loss of integrity could be a compensatory mechanism.

Since permeability barrier function is essential for the maintenance of epithelial integrity in both invertebrates and vertebrates, it will be interesting to determine whether these relationships between TCJs and BCJs are conserved.

STAR★METHODS

Detailed methods are provided in the online version of this paper and include the following:

- KEY RESOURCES TABLE
- RESOURCE AVAILABILITY
  - Lead Contact
  - Materials Availability
  - Data and Code Availability
- EXPERIMENTAL MODEL AND SUBJECT DETAILS
  - Experimental model
  - Genotypes
- METHOD DETAILS
  - Immunostaining
  - Live-imaging and image analyses
  - Fluorescence recovery after photobleaching
  - Nanoablation
- QUANTIFICATION AND STATISTICAL ANALYSIS
  - Signal recovery upon photobleaching
  - Fluorescence vertex analysis
  - Line scan fluorescence analysis
  - Statistical tests

SUPPLEMENTAL INFORMATION

Supplemental Information can be found online at https://doi.org/10.1016/j.cub.2020.07.090.

ACKNOWLEDGMENTS

We thank Drs. Luschnig, Klämbt, Martin, Treisman, Uv, and Xu; the Bloomington *Drosophila* Stock Center; the Vienna Drosophila Resource Center; InDroso; and the Developmental Studies Hybridoma Bank for providing fly stocks and antibodies. We also thank the Microscopy Rennes Imaging facility. We thank S. Luschnig, M. Hollmann, and members of R.L.B.'s laboratory for critical reading of the manuscript. This work was supported in part by the ARED program from the Région Bretagne, France to T.E.d.B., La Ligue contre le Cancer-Equipe Labelisée, France, and Agence Nationale de la Recherche CytoSIGN (ANR-16-CE13-004-01), France to R.L.B.

AUTHOR CONTRIBUTIONS

Conceptualization, Methodology, Investigation, Formal Analysis, Visualization, Writing – Original Draft and Review & Editing, T.E.d.B. and R.L.B.; Funding Acquisition, R.L.B.; Supervision, R.L.B.

DECLARATION OF INTERESTS

The authors declare no competing interests.

Received: April 22, 2020
Revised: July 27, 2020
Accepted: July 29, 2020
Published: August 27, 2020

REFERENCES

1. Bosveld, F., Wang, Z., and Bellaïche, Y. (2018). Tricellular junctions: a hot corner of epithelial biology. Curr. Opin. Cell Biol. *54*, 80–88.
2. Higashi, T., and Miller, A.L. (2017). Tricellular junctions: how to build junctions at the TRICkiest points of epithelial cells. Mol. Biol. Cell *28*, 2023–2034.
3. Furuse, M., Izumi, Y., Oda, Y., Higashi, T., and Iwamoto, N. (2014). Molecular organization of tricellular tight junctions. Tissue Barriers *2*, e28960.
4. Finegan, T.M., Hervieux, N., Nestor-Bergmann, A., Fletcher, A.G., Blanchard, G.B., and Sanson, B. (2019). The tricellular vertex-specific adhesion molecule Sidekick facilitates polarised cell intercalation during Drosophila axis extension. PLoS Biol. *17*, e3000522.
5. Uechi, H., and Kuranaga, E. (2019). The Tricellular Junction Protein Sidekick Regulates Vertex Dynamics to Promote Bicellular Junction Extension. Dev. cell *50*, 327–338.e5.
6. Letizia, A., He, D., Astigarraga, S., Colombelli, J., Hatini, V., Llimargas, M., and Treisman, J.E. (2019). Sidekick Is a Key Component of Tricellular Adherens Junctions that Acts to Resolve Cell Rearrangements. Dev. cell *50*, 313–326.e5.
7. Schulte, J., Tepass, U., and Auld, V.J. (2003). Gliotactin, a novel marker of tricellular junctions, is necessary for septate junction development in Drosophila. J. Cell Biol. *161*, 991–1000.

8. Byri, S., Misra, T., Syed, Z.A., Bätz, T., Shah, J., Boril, L., Glashauser, J., Aegerter-Wilmsen, T., Matzat, T., Moussian, B., et al. (2015). The Triple-Repeat Protein Anakonda Controls Epithelial Tricellular Junction Formation in Drosophila. Dev. Cell *33*, 535–548.

9. Hildebrandt, A., Pflanz, R., Behr, M., Tarp, T., Riedel, D., and Schuh, R. (2015). Bark beetle controls epithelial morphogenesis by septate junction maturation in Drosophila. Dev. Biol. *400*, 237–247.

10. Zappia, M.P., Brocco, M.A., Billi, S.C., Frasch, A.C., and Ceriani, M.F. (2011). M6 membrane protein plays an essential role in Drosophila oogenesis. PLoS ONE *6*, e19715.

11. Dunn, B.S., Rush, L., Lu, J.Y., and Xu, T. (2018). Mutations in the *Drosophila* tricellular junction protein M6 synergize with *Ras* ^{V12} to induce apical cell delamination and invasion. Proc. Natl. Acad. Sci. USA *115*, 8358–8363.

12. Fristrom, D.K. (1982). Septate junctions in imaginal disks of Drosophila: a model for the redistribution of septa during cell rearrangement. J. Cell Biol. *94*, 77–87.

13. Graf, F., Noirot-Timothée, C., and Noirot, C. (1982). The specialization of septate junctions in regions of tricellular junctions. I. Smooth septate junctions (=continuous junctions). J. Ultrastruct. Res. *78*, 136–151.

14. Noirot-Timothée, C., Graf, F., and Noirot, C. (1982). The specialization of septate junctions in regions of tricellular junctions. II. Pleated septate junctions. J. Ultrastruct. Res. *78*, 152–165.

15. Daniel, E., Daude, M., Kolotuev, I., Charish, K., Auld, V., and Le Borgne, R. (2018). Coordination of Septate Junctions Assembly and Completion of Cytokinesis in Proliferative Epithelial Tissues. Curr. biol. *28*, 1380–1391.e4.

16. Bellen, H.J., Levis, R.W., He, Y., Carlson, J.W., Evans-Holm, M., Bae, E., Kim, J., Metaxakis, A., Savakis, C., Schulze, K.L., et al. (2011). The Drosophila gene disruption project: progress using transposons with distinctive site specificities. Genetics *188*, 731–743.

17. Buszczak, M., Paterno, S., Lighthouse, D., Bachman, J., Planck, J., Owen, S., Skora, A.D., Nystul, T.G., Ohlstein, B., Allen, A., et al. (2007). The carnegie protein trap library: a versatile tool for Drosophila developmental studies. Genetics *175*, 1505–1531.

18. Founounou, N., Loyer, N., and Le Borgne, R. (2013). Septins regulate the contractility of the actomyosin ring to enable adherens junction remodeling during cytokinesis of epithelial cells. Dev. Cell *24*, 242–255.

19. Herszterg, S., Leibfried, A., Bosveld, F., Martin, C., and Bellaiche, Y. (2013). Interplay between the dividing cell and its neighbors regulates adherens junction formation during cytokinesis in epithelial tissue. Dev. Cell *24*, 256–270.

20. Pinheiro, D., Hannezo, E., Herszterg, S., Bosveld, F., Gaugue, I., Balakireva, M., Wang, Z., Cristo, I., Rigaud, S.U., Markova, O., and Bellaïche, Y. (2017). Transmission of cytokinesis forces via E-cadherin dilution and actomyosin flows. Nature *545*, 103–107.

21. Guillot, C., and Lecuit, T. (2013). Adhesion disengagement uncouples intrinsic and extrinsic forces to drive cytokinesis in epithelial tissues. Dev. Cell *24*, 227–241.

22. Wang, Z., Bosveld, F., and Bellaïche, Y. (2018). Tricellular junction proteins promote disentanglement of daughter and neighbour cells during epithelial cytokinesis. J. Cell Sci. *131*, https://doi.org/10.1242/jcs.215764.

23. Astigarraga, S., Douthit, J., Tarnogorska, D., Creamer, M.S., Mano, O., Clark, D.A., Meinertzhagen, I.A., and Treisman, J.E. (2018). *Drosophila* Sidekick is required in developing photoreceptors to enable visual motion detection. Development *145*, https://doi.org/10.1242/dev.158246.

24. Lecuit, T., and Yap, A.S. (2015). E-cadherin junctions as active mechanical integrators in tissue dynamics. Nat. Cell Biol. *17*, 533–539.

25. Harris, T.J., and Tepass, U. (2010). Adherens junctions: from molecules to morphogenesis. Nat. Rev. Mol. Cell Biol. *11*, 502–514.

26. Ikenouchi, J., Furuse, M., Furuse, K., Sasaki, H., Tsukita, S., and Tsukita, S. (2005). Tricellulin constitutes a novel barrier at tricellular contacts of epithelial cells. J. Cell Biol. *171*, 939–945.

27. Masuda, S., Oda, Y., Sasaki, H., Ikenouchi, J., Higashi, T., Akashi, M., Nishi, E., and Furuse, M. (2011). LSR defines cell corners for tricellular tight junction formation in epithelial cells. J. Cell Sci. *124*, 548–555.

28. Higashi, T., Tokuda, S., Kitajiri, S., Masuda, S., Nakamura, H., Oda, Y., and Furuse, M. (2013). Analysis of the 'angulin' proteins LSR, ILDR1 and ILDR2–tricellulin recruitment, epithelial barrier function and implication in deafness pathogenesis. J. Cell Sci. *126*, 966–977.

29. Higashi, T., Arnold, T.R., Stephenson, R.E., Dinshaw, K.M., and Miller, A.L. (2016). Maintenance of the Epithelial Barrier and Remodeling of Cell-Cell Junctions during Cytokinesis. Curr. Biol. *26*, 1829–1842.

30. Yan, Y., Narayanan, V., and Lagenaur, C. (1996). Expression of members of the proteolipid protein gene family in the developing murine central nervous system. J. Comp. Neurol. *370*, 465–478.

31. Lagenaur, C., Kunemund, V., Fischer, G., Fushiki, S., and Schachner, M. (1992). Monoclonal M6 antibody interferes with neurite extension of cultured neurons. J. Neurobiol. *23*, 71–88.

32. Gilula, N.B., Branton, D., and Satir, P. (1970). The septate junction: a structural basis for intercellular coupling. Proc. Natl. Acad. Sci. USA *67*, 213–220.

33. Sharifkhodaei, Z., Gilbert, M.M., and Auld, V.J. (2019). Scribble and Discs Large mediate tricellular junction formation. Development *146*, https://doi.org/10.1242/dev.174763.

34. Gilbert, M., Smith, J., Roskams, A.J., and Auld, V.J. (2001). Neuroligin 3 is a vertebrate gliotactin expressed in the olfactory ensheathing glia, a growth-promoting class of macroglia. Glia *34*, 151–164.

35. Zhang, C., Milunsky, J.M., Newton, S., Ko, J., Zhao, G., Maher, T.A., Tager-Flusberg, H., Bolliger, M.F., Carter, A.S., Boucard, A.A., et al. (2009). A neuroligin-4 missense mutation associated with autism impairs neuroligin-4 folding and endoplasmic reticulum export. J. Neurosci. *29*, 10843–10854.

36. Chanda, S., Hale, W.D., Zhang, B., Wernig, M., and Südhof, T.C. (2017). Unique versus Redundant Functions of Neuroligin Genes in Shaping Excitatory and Inhibitory Synapse Properties. J. Neurosci. *37*, 6816–6836.

37. Zhang, B., Chen, L.Y., Liu, X., Maxeiner, S., Lee, S.J., Gokce, O., and Südhof, T.C. (2015). Neuroligins Sculpt Cerebellar Purkinje-Cell Circuits by Differential Control of Distinct Classes of Synapses. Neuron *87*, 781–796.

38. Kim, J.A., Kim, D., Won, S.Y., Han, K.A., Park, D., Cho, E., Yun, N., An, H.J., Um, J.W., Kim, E., et al. (2017).). Structural Insights into Modulation of Neurexin-Neuroligin Trans-synaptic Adhesion by MDGA1/Neuroligin-2 Complex. Neuron *94*, 1121–1131.e6.

39. Gangwar, S.P., Zhong, X., Seshadrinathan, S., Chen, H., Machius, M., and Rudenko, G. (2017). Molecular Mechanism of MDGA1: Regulation of Neuroligin 2:Neurexin Trans-synaptic Bridges. Neuron *94*, 1132–1141.e4.

40. Elegheert, J., Cvetkovska, V., Clayton, A.J., Heroven, C., Vennekens, K.M., Smukowski, S.N., Regan, M.C., Jia, W., Smith, A.C., Furukawa, H., et al. (2017). Structural Mechanism for Modulation of Synaptic Neuroligin-Neurexin Signaling by MDGA Proteins. Neuron *96*, 242–244.

41. Litwack, E.D., Babey, R., Buser, R., Gesemann, M., and O'Leary, D.D. (2004). Identification and characterization of two novel brain-derived immunoglobulin superfamily members with a unique structural organization. Mol. Cell. Neurosci. *25*, 263–274.

42. Bieber, A.J., Snow, P.M., Hortsch, M., Patel, N.H., Jacobs, J.R., Traquina, Z.R., Schilling, J., and Goodman, C.S. (1989). Drosophila neuroglian: a member of the immunoglobulin superfamily with extensive homology to the vertebrate neural adhesion molecule L1. Cell *59*, 447–460.

43. Genova, J.L., and Fehon, R.G. (2003). Neuroglian, Gliotactin, and the Na+/K+ ATPase are essential for septate junction function in Drosophila. J. Cell Biol. *161*, 979–989.

44. Banerjee, S., Sousa, A.D., and Bhat, M.A. (2006). Organization and function of septate junctions: an evolutionary perspective. Cell Biochem. Biophys. *46*, 65–77.

45. Fox, R.M., and Andrew, D.J. (2015). Changes in organelle position and epithelial architecture associated with loss of CrebA. Biol. Open *4*, 317–330.

46. Babatz, F., Naffin, E., and Klambt, C. (2018). The Drosophila Blood-Brain Barrier Adapts to Cell Growth by Unfolding of Pre-existing Septate Junctions. Dev. cell *47*, 697–710.3.

47. Schmid, E.M., Bakalar, M.H., Choudhuri, K., Weichsel, J., Ann, H., Geissler, P.L., Dustin, M.L., and Fletcher, D.A. (2016). Size-dependent protein segregation at membrane interfaces. Nat. Phys. *12*, 704–711.

48. Auld, V.J., Fetter, R.D., Broadie, K., and Goodman, C.S. (1995). Gliotactin, a novel transmembrane protein on peripheral glia, is required to form the blood-nerve barrier in Drosophila. Cell *81*, 757–767.

49. Stork, T., Thomas, S., Rodrigues, F., Silies, M., Naffin, E., Wenderdel, S., and Klämbt, C. (2009). Drosophila Neurexin IV stabilizes neuron-glia interactions at the CNS midline by binding to Wrapper. Development *136*, 1251–1261.

50. Martin, A.C., Gelbart, M., Fernandez-Gonzalez, R., Kaschube, M., and Wieschaus, E.F. (2010). Integration of contractile forces during tissue invagination. J. Cell Biol. *188*, 735–749.

51. Claret, S., Jouette, J., Benoit, B., Legent, K., and Guichet, A. (2014). PI(4,5)P2 produced by the PI4P5K SKTL controls apical size by tethering PAR-3 in Drosophila epithelial cells. Curr. Biol. *24*, 1071–1079.

52. Calleja, M., Moreno, E., Pelaz, S., and Morata, G. (1996). Visualization of gene expression in living adult Drosophila. Science *274*, 252–255.

53. Schindelin, J., Arganda-Carreras, I., Frise, E., Kaynig, V., Longair, M., Pietzsch, T., Preibisch, S., Rueden, C., Saalfeld, S., Schmid, B., et al. (2012). Fiji: an open-source platform for biological-image analysis. Nat. Methods *9*, 676–682.

54. Koulouras, G., Panagopoulos, A., Rapsomaniki, M.A., Giakoumakis, N.N., Taraviras, S., and Lygerou, Z. (2018). EasyFRAP-web: a web-based tool for the analysis of fluorescence recovery after photobleaching data. Nucleic Acids Res. *46* (W1), W467–W472.

55. Gho, M., Lecourtois, M., Géraud, G., Posakony, J.W., and Schweisguth, F. (1996). Subcellular localization of Suppressor of Hairless in Drosophila sense organ cells during Notch signalling. Development *122*, 1673–1682.

56. Gho, M., Bellaïche, Y., and Schweisguth, F. (1999). Revisiting the Drosophila microchaete lineage: a novel intrinsically asymmetric cell division generates a glial cell. Development *126*, 3573–3584.

STAR★METHODS

KEY RESOURCES TABLE

REAGENT or RESOURCE	SOURCE	IDENTIFIER
Antibodies		
Mouse anti-Cora (1:200)	DSHB	C615.16, RRID: AB_1161644
Rat anti-DE-cad (1:500)	DSHB	DCAD2; AB_528120
Mouse anti-Dlg (1:500)	DSHB	4F3; AB_528203
Mouse anti-GFP (1:200)	Roche	Clone 7.1
Rabbit anti-Aka (1:2000)	[8]	Gift from Anne Uv
Mouse anti-Gli (1:200)	[48]	1F61D4
Guinea pig Anti-Sdk (1:200)	[23]	Gift from Jessica Treisman
Rabbit anti-Nrx-IV (1:1000)	[49]	Gift from Christian Klämbt
Cy2-, Cy3- and Cy5-coupled secondary antibodies (1:300)	The Jackson Laboratory	N/A
Alexa Fluor™ 647 Phalloidin (1:500)	Thermo Fisher Scientific	Cat#A22287
Chemicals, Peptides, and Recombinant Proteins		
Paraformaldehyde	EMS	19340-72
Triton X-100	Euromedex	2000B
Phosphate Buffered Saline	Lonza	BE17-515F
Voltalef	VWR	24627.188
Experimental Models: Organisms/Strains		
D.melanogaster: Sqh::GFP^{crispr}	InDroso	N/A
D.melanogaster: Sqh::RFP^{crispr}	[15]	N/A
D.melanogaster: Aka::GFP	[8]	N/A
D.melanogaster: Aka::GFP, *Gli^{dv3}*, FRT40A / CyO	This study	N/A
D.melanogaster: GFP::M6	[17]	CA 06602
D.melanogaster: Sdk::GFP	[17]	RRID: BDSC_ 60169
D. melanogaster:; ubi-RFP nls, FRT40A / (CyO); ATP-α::GFP, sqh-Sqh::mCherry / (TM6, *Tb^{1}*)	This study	N/A
D. melanogaster: sqh-GAP43::mCherry	[50]	Gift from Adam Martin
D.melanogaster: hs-FLP; *aka^{L200}*, FRT40A / CyO	This study	Gift from Stefan Luschnig
D.melanogaster: sdk^{Δ15}	[23]	Gift from Jessica Treisman
D.melanogaster: Gli^{dv3}, FRT40A/CyO	[7]	Gift from Vanessa Auld
D.melanogaster: w*; UAS-Ras^{V12}; *M6^{w186}*, FRT79E / TM6, *Tb^{1}*	[11]	Gift from Tian Xu
D.melanogaster: hs-FLP; If/CyO; *M6^{w186}*, FRT79E / TM6, *Tb^{1}*	This study	Gift from Tian Xu
D.melanogaster: yw, *ey*-FLP; Act > y+Gal4, UAS-GFP; *tub*-Gal80, FRT79E	[11]	Gift from Tian Xu
D.melanogaster: yw, *hs*-FLP; *ubi*-RFP nls, FRT40A / (CyO)	[51]	N/A
D.melanogaster: UAS-Cora-RNAi	VDRC	RRID: BDSC_9788
D.melanogaster: UAS-Nrx-IV-RNAi	VDRC	108 128
D.melanogaster: pnr-Gal4 / TM6, *Tb^{1}*	[52]	RRID: BDSC_3039
Software and Algorithms		
Fiji	[53]	https://imagej.net/Fiji
Illustrator	Adobe Systems	Adobe Illustrator CS6

(*Continued on next page*)

Continued

REAGENT or RESOURCE	SOURCE	IDENTIFIER
Prism 8	GraphPad	GraphPad
EasyFRAP-web	[54]	https://easyfrap.vmnet.upatras.gr/
Others		
Confocal Microscope	Leica	LSM TCS SPE, TCS SP5 and TCS SP8

RESOURCE AVAILABILITY

Lead Contact

Further information and requests for resources and reagents should be directed to and will be fulfilled by the Lead Contact, Roland Le Borgne (roland.leborgne@univ-rennes1.fr)

Materials Availability

This study did not generate new unique reagents.

Data and Code Availability

This study did not generate/analyze [datasets/code].

EXPERIMENTAL MODEL AND SUBJECT DETAILS

Experimental model

Drosophila *strains*

Drosophila melanogaster stocks were maintained and crossed at 25°C. The following strains were obtained as follow: Aka::GFP, Gli^{dv3}, FRT40A / CyO was obtained by recombining Aka::GFP [8] with Gli^{dv3}, FRT40A / CyO [7]; *hs*-FLP; aka^{L200}, FRT40A / CyO was obtained by crossing aka^{L200}, FRT40A / CyO [8] with *hs*-FLP; If / CyO and appropriate flies were selected; *hs*-FLP; If / CyO; $M6^{w186}$, FRT79E / TM6, Tb^{1} was obtained by crossing w*; UAS-Ras^{V12}; $M6^{w186}$, FRT79E / TM6, Tb^{1} [11] with *hs*-FLP; If / CyO; MKRS / TM6, Tb^{1} and appropriate flies were selected; *ubi*-RFP nls, FRT40A / (CyO); ATP-α::GFP, *sqh*-Sqh::mCherry/(TM6, Tb^{1}) was constructed by crossing ATP-α::GFP, *sqh*-Sqh::mCherry / (TM6, Tb^{1}) [15] with *ubi*-RFP nls, FRT40A / (CyO); MKRS / TM6, Tb^{1} and appropriate flies were selected. Somatic clones were induced using the FLP-FRT technique using the hs-FLP and by two to three heat shocks (60 min at 37°C) at second and third instar larvae.

Genotypes

Figure 1

(B) Sqh::RFP^{crispr} / Sdk::GFP obtained by crossing Sqh::RFP^{crispr} with Sdk::GFP
(D) Sqh::RFP^{crispr};; GFP::M6 obtained by crossing Sqh::RFP^{crispr} with GFP::M6
(E) Sqh::RFP^{crispr}; Aka::GFP obtained by crossing Sqh::RFP^{crispr} with Aka::GFP

Figure 2

(A) *hs*-FLP; aka^{L200}, FRT40A / *ubi*-RFP nls, FRT40A obtained by crossing aka^{L200}, FRT40A / CyO with yw, *hs*-FLP; *ubi* -RFP nls, FRT40A / (CyO)
(B) *hs*-FLP; Act > y+Gal4, UAS-GFP; $M6^{w186}$, FRT79E / *tub* -Gal80, FRT79E obtained by crossing yw, *ey*-FLP; Act > y+Gal4, UAS-GFP; *tub*-Gal80, FRT79E with *hs*-FLP; If/CyO; $M6^{w186}$, FRT79E / TM6, Tb^{1}
(C) *hs*-FLP; Gli^{dv3}, FRT40A/ *ubi*-RFP nls, FRT40A obtained by crossing Gli^{dv3}, FRT40A/CyO with yw, *hs*-FLP; *ubi*-RFP nls, FRT40A / (CyO)

Figure 3

(A, C, D, E, G and I) *hs*-FLP; aka^{L200}, FRT40A / *ubi* -RFP nls, FRT40A obtained by crossing aka^{L200}, FRT40A / CyO with yw, *hs*-FLP; *ubi* -RFP nls, FRT40A / (CyO)
(B) *hs*-FLP; aka^{L200}, FRT40A / *ubi*-RFP nls, FRT40A; ATP-α::GFP, sqh-Sqh::mCherry/ + obtained by crossing; *ubi*-RFP nls, FRT40A/(CyO); ATP-α::GFP, *sqh*-Sqh::mCherry / (TM6, Tb^{1}) with *hs*-FLP; aka^{L200}, FRT40A / CyO

Figure 4

(A-C) UAS-Cora-RNAi / *pnr*-Gal4 obtained by crossing UAS-Cora-RNAi with *pnr*-Gal4 / TM6, Tb^{1}

METHOD DETAILS

Immunostaining

Pupae were collected at puparium formation (0 h After Puparium Formation, 0 h APF) and were dissected at 16 h30 APF using Cannas microscissors (Biotek, France) in 1X Phosphate-Buffered Saline (1X PBS, pH 7.4) and fixed 15 min in 4% paraformaldehyde at room temperature [55]. Following fixation, dissected nota were permeabilized using 0.1% Triton X-100 in 1X PBS (PBT), incubated with primary antibodies diluted in PBT for 2 h at room temperature. The following primary antibodies were used: Cora (mouse, 1:200, DSHB, C615.16), DE-Cad (rat, 1:500, DSHB, DCAD2), Dlg (mouse, 1:500, DSHB, 4F3), GFP (mouse, 1:200, Roche, clone 7.1), Aka (rabbit, 1:2000, a gift from A. Uv) [8], Gli (mouse, 1:200, a gift from V. Auld) [48], Sdk (guinea pig, 1:200, a gift from J. Treisman) [23], Nrx-IV (rabbit, 1:1000, a gift from C. Klämbt) [49].

After 3 washes of 5 min in PBT, nota were incubated with secondary antibodies (Jackson ImmunoResearch Laboratories) diluted at 1:1000 in PBT for 1 h, followed by 2 washes in PBT, and one wash in PBS, prior mounting in 0,5% N-propylgallate dissolved in 90% glycerol/PBS 1X final.

Live-imaging and image analyses

Live imaging was performed on pupae aged for 16 h30 APF at 25°C. Pupae were adhered on a glass slide with a double-sided tape, and the brown pupal case was removed over the head and dorsal thorax using microdissecting forceps. Pillars made of 4 and 5 glass coverslips were positioned at the anterior and posterior side of the pupae, respectively. A glass coverslip covered with a thin film of Voltalef 10S oil is then placed on top of the pillars such that a meniscus is formed between the dorsal thorax of the pupae and the glass coverslip [56]. Images were acquired with a LSM Leica SPE, SP5 or SP8 equipped with a 63X N.A. 1.4. and controlled by LAS AF software. Confocal sections (z) were taken every 0.5 μm. For figures representation, images were processed with Gaussian Blur σ = 1.1. All images were processed and assembled using Fiji software [53] and Adobe Illustrator.

Fluorescence recovery after photobleaching

FRAP experiments were performed in pupae expressing Aka::GFP with RFP-nls used as a marker of *Gli*^{dv3} cells. Aka::GFP was bleached (488 nm laser at 60% power, 2 iterations of 1.293 s, square ROI of 2μm*1.5μm) using a LSM Leica SP5 or SP8 equipped with a 63X N.A. 1.4 PlanApo objective. Confocal stacks were acquired every 30 s or 2 min before and after photobleaching on 13 z steps to compensate for movement in z during acquisition.

FRAP experiments were performed in pupae expressing ATP-α::GFP with Sqh::RFP^{crispr} to localize AJ level and RFP-nls used as a marker of *aka*^{L200} cells. ATP-α::GFP was bleached (488 nm laser at 60% power, 2 iterations of 1.293 s, 2.5μm*1.5μm) using a LSM Leica SP5 or SP8 equipped with a 63X N.A. 1.4 PlanApo objective. Confocal stacks were acquired every 30 s or 2 min before and after photobleaching on 6 or 14 z steps to compensate for movement in z during acquisition.

Nanoablation

Laser ablation was performed on live pupae aged for 16 h to 19 h APF using a Leica SP5 confocal microscope equipped with a 63X N.A. 1.4 PlanApo objective. Ablation was carried out on epithelial cell membranes at SJ/AJ level with a two-photon laser-type Mai-Tai HP from Spectra Physics set to 800 nm and a laser power of 2.9W. LAS AF parameters are laser trans 50%, gain 70%, offset 35% and 1 iteration of 1.293 s.

QUANTIFICATION AND STATISTICAL ANALYSIS

Signal recovery upon photobleaching

In all FRAP experiments, ROI 1 corresponds to the photobleached area, ROI 2 to the area used as a control for general photobleaching of the sample across time and ROI 3 to the background. ROI 1 and ROI 3 had the same dimensions in all FRAP experiments (2μm*1.5μm for Aka::GFP; 2.5μm*1.5μm for ATP-α::GFP).

For Aka::GFP, a sum slice of 8 z (4μm in total) was applied in order to collect the entire signal. ROI 2 was considered as the fluorescence of the entire field.

For ATP-α::GFP, a sum slice, of 2 z (1μm in total) of the plan just below AJ marked by Sqh::RFP^{crispr} and the one below, was applied to avoid z movements. ROI 2 was considered as the fluorescence of the entire field.

Then, we used EasyFRAP-web [54] for all data processing and to extract normalized values. The I(t) which correspond to the fluorescence intensity across time was calculated as described:

First, the fluorescence intensity is corrected by subtracting the background:

$$I(t)_{ROI1'} = I(t)_{ROI1} - I(t)_{ROI3}$$

$$I(t)_{ROI2'} = I(t)_{ROI2} - I(t)_{ROI3}$$

Then, values of fluorescence intensity are normalized in this way:

$$I(t)_{\text{double norm}} = \left(\frac{\frac{1}{n_{pre}} \times \sum_{t=1}^{n_{pre}} I(t)_{ROI2'}}{I\,(t)_{ROI2'}}\right) \times \left(\frac{I(t)_{ROI1'}}{\frac{1}{n_{pre}} \times \sum_{t=1}^{n_{pre}} I(t)_{ROI1'}}\right)$$

We decided to take value from full scale normalization in order to have a curve starting from 0:

$$I(t)_{\text{fullscale norm}} = \frac{I(t)_{\text{double norm}} - I(t_{\text{postbleach}})_{\text{double norm}}}{1 - I(t_{\text{postbleach}})_{\text{double norm}}}$$

Recovery curves were then fitted assuming a one-phase exponential association equation using the GraphPad Prism 8.0 software:

$$I(t)_{\text{fullscale norm}} = I(t)_{\text{maxfullscale norm}} \times \left(1 - e^{-K \times t}\right)$$

We admitted that $I(t)_{\text{maxfullscale norm}}$ is the maximum value based on the fitted curve for the post-bleach time (20 min for Aka::GFP and 18 min for ATP-α::GFP) and it is considered as the immobile fraction. $t_{1/2}$ was deduced when $I(t)_{\text{fullscale norm}} = 0,5 \times I(t)_{\text{maxfullscale norm}}$ which occurred at $t = \frac{-\ln(0,5)}{K}$.

Fluorescence vertex analysis

Sum slices were applied to different experiments. A segmented line of 10 pixels width was used to measure Aka signal in WT and *Gli*^{dv3}*/M6*^{W186} mutant vertex. Using the same width, lines were drawn to extract background fluorescence signal and the background signal was subtracted to each vertex quantification. After, data were standardized between 0 and 1 to allow visual representation with 1 corresponding to the highest signal of Aka at vertex in each experiment analyzed and 0 the lowest.

Line scan fluorescence analysis

Maximal projection were applied and a 20 pixels width line was drawn from apical part to basal part (Figures 3E–3H') or from vertex 1 to vertex 2, spanning the BCJ (Figures 3I', 4B', 4C', S4B', S4C', S4E' and S4F'). Then gray value was plotted across length of the line.

Statistical tests

All information concerning the statistical details are provided in the main text and in figure legends, including the number of samples analyzed for each experiment. Scattered plots use the following standards: thick line indicate the means and errors bars represent the standard deviations. Boxplots with connected line use the following standards: dots represent mean and the total colored areas show SD.

Statistical analyses were performed using the GraphPad Prism 8.0 software. The Shapiro-Wilk normality test was used to confirm the normality of the data and the F-test to verify the equality of SD. The statistical difference of Gaussian datasets was analyzed using the Student unpaired two-tailed t test. For contingency analysis (Figure S1E), a Fisher's exact test was used. Statistical significances were represented as follow: p value > 0.05 NS (not significant) and p value $\leq$ 0.0001 ****.

Current Biology, Volume *30*

Supplemental Information

Interplay between Anakonda, Gliotactin, and M6 for Tricellular Junction Assembly and Anchoring of Septate Junctions in *Drosophila* Epithelium

Thomas Esmangart de Bournonville and Roland Le Borgne

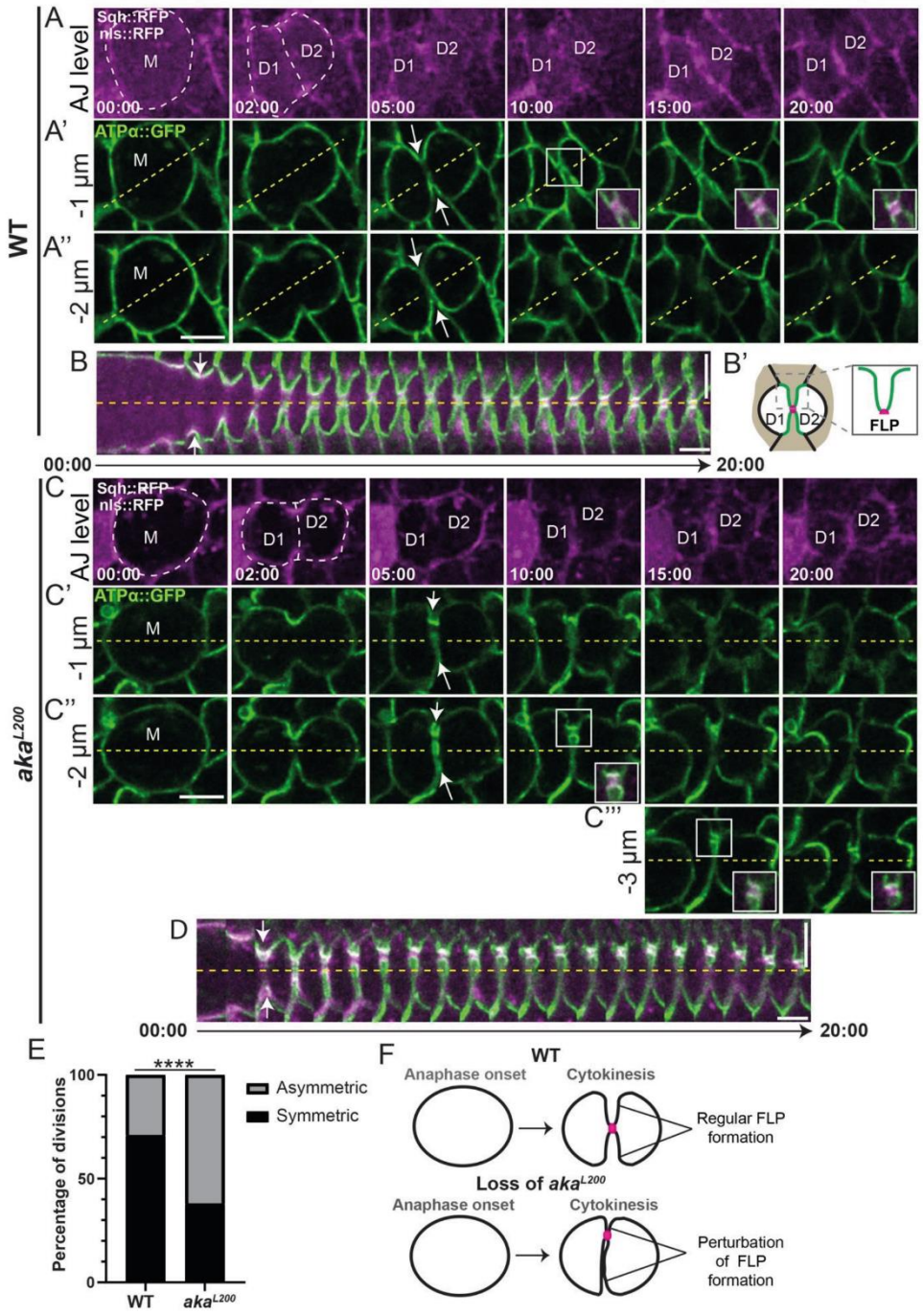

Figure S1: tSJ integrity is required to ensure FLP formation during cytokinesis. Related to Figure 1.

(A-D) Time-lapse imaging of FLP using Sqh::RFP^{crispr} (magenta, AJ) and ATPα::GFP (green, SJ) in wild type (marked by nls::RFP; A-B) and *aka*^{L200} (loss of nls::RFP; C-D) dividing cells, from plane view (A-A'' and C-C''') and with a kymograph representation (B and D). The mother cell is represented by the M and the daughters by D1 and D2. The white dashed lines highlight the divided cell and daughters. White arrows indicate FLP formation at SJ level. Yellow dashed lines define symmetry axis of the cell. White squares show high magnification of midbody (magenta) linking FLP. (B') Graphical representation of a FLP linking the two dividing cells and the adjacent neighbor cell. (E) Histogram representing the number of symmetric (black) and asymmetric (grey) FLP formation during cytokinesis in wild type (n = 14 divisions, 3 pupae) and *aka*^{L200} cells (n = 21 divisions, > 5 pupae). **** $p < 0.0001$, Fisher's exact test. (F) Schematic representation of the FLP formation upon cytokinesis. Loss of tSJ integrity leads to abnormal FLP shape and asymmetrical midbody formation at the new cell-cell interface. The horizontal scale bars represent 5µm (A and C), the vertical scale bars represent 5µm (B and D) and the horizontal scale bars represent 1min (B and D).

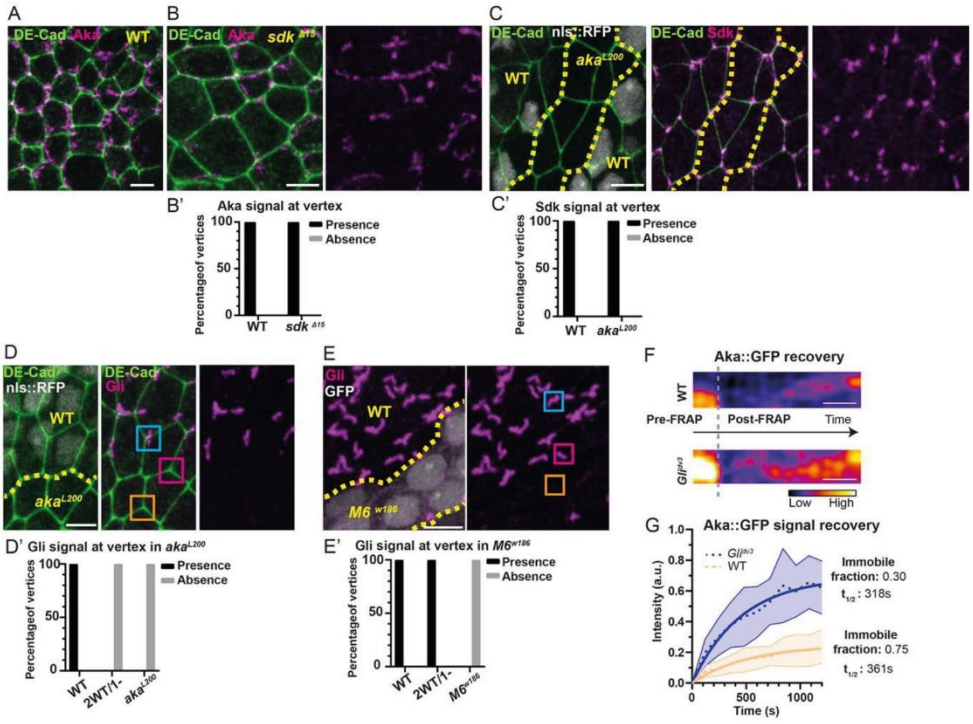

Figure S2: Aka, M6 and Gli are required for tSJs and dispensable for tAJs integrity. Related to Figure 2.

(A-B) Localization of Aka (anti-Aka, magenta) in wild type and *sdk*$^{\Delta 15}$ pupa. (B') Histogram representing the percentage of presence (black) or absence (gray) of Aka accumulation at the vertex in wild type (presence n = 100%, absence n = 0%) and *sdk*$^{\Delta 15}$ (presence n = 100, absence n = 0) (n = 100 vertices, 3 pupae). (C-E) show nota between 16h-18h APF stained for DE-cad (C and D ; anti-DE-cad, green) after heat-shock to induce clone of wild type (C and D nls::RFP positive; E, GFP negative) and mutant cells (C and D, nls::RFP negative; E, GFP positive) for tSJ components. (C) Localization of Sdk (anti-Sdk, magenta). The dashed yellow line separates wild type and *aka*^{L200} cells. (C') Histogram representing the percentage of presence (black) or absence (gray) of Sdk accumulation at the vertex in wild type (n presence n = 100%, absence n = 0%) and *aka*^{L200} (presence n = 100%, absence n = 0%) (n = 100 vertices, > 5 pupae). (D-E') Localization of Gli (anti-Gli, magenta). The dashed yellow line separates wild type and *aka*^{L200} (mutant) cells (D) or wild type and *M6*^{w186} (mutant) cells (E). Gli is enriched at the TCJ at wild-type vertex (blue square) and is no longer detected at a vertex of three *aka* mutant cells (D; orange square) or *M6* (E; orange

square) but also when Aka is lost in only one of the three cells participating in the vertex (D; pink square) but not for M6 (E; pink square). (D' and E') Histograms representing the percentage of presence (black) or absence (gray) of Gli accumulation at the vertex between 3 wild type cells (D' and E'; presence n = 100%, absence n = 0%), 2 wild type and 1 aka^{L200} cell (D'; presence n = 0%, absence n = 100%) or 1 $M6^{w186}$ cell (E'; presence n = 100%, absence n = 0%) or 3 aka^{L200} cells (D'; presence n = 0%, absence n = 100%) or 3 $M6^{w186}$ cells (E'; presence n = 0%, absence n = 100%) (n = 100 vertices, > 5 pupae for each experiment). (F) Kymograph of the bleached region for Aka::GFP in wild type and Gli^{dv3} cells. A calibration bar shows LUT for gray value range. Scale bars show 5min. (G) Plot of Aka::GFP fluorescence recovery as a function of time for the conditions described in (F). Wild type: n = 11 FRAP experiments, 4 pupae; Gli^{dv3}: n = 12 FRAP experiments, 5 pupae. Data are mean ± SD. Solid line shows a simple exponential fit.

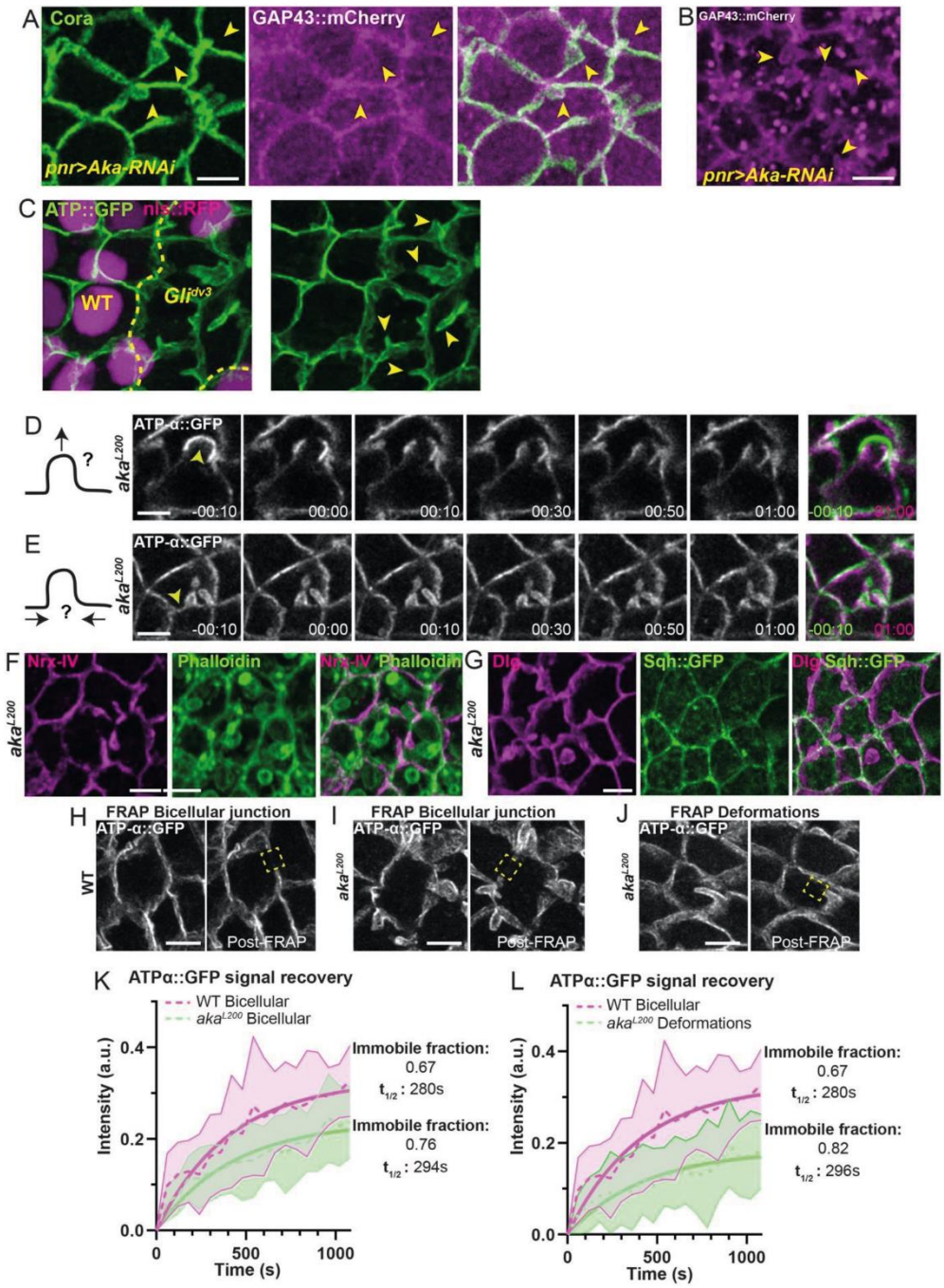

Figure S3: SJ deformations stabilization does not rely on mechanicals forces and SJ proteins exhibits increased stability within SJ deformations. Related to Figure 3.

(A-C) SJ and membrane morphology analysis using core components Cora (anti-Cora; A), GAP43::mCherry (A-B), or ATP-α::GFP (C) in wild type and upon knockdown of *aka* by RNAi approach (A-B) or in Gli^{dv3} cells (C). (A, B) GAP43::mCherry tagged membrane after fixation or in living samples (B) in *aka* RNAi area. (C) Localization of ATP-α::GFP in Gli^{dv3} cells. Yellow arrowheads indicate micrometric size SJ/membrane deformations. (D and E) Bi-photonic laser-based nanoablation of SJ deformations in aka^{L200} cells expressing ATP-α::GFP (white). Green and magenta pictures represent SJ deformations 10s before and 1min after ablation respectively. Yellow arrowheads show the ablation area. (F and G) Notum between 16h and 18h APF stained for Nrx-IV (anti-Nrx-IV, magenta; F), Dlg (anti-Dlg, magenta; G), Phalloidin (green; F) or expressing Sqh::GFP (green; G) in aka^{L200} cells. (H-J) Example of FRAP experiment of ATP-α::GFP at wild-type bicellular junction, aka^{L200} bicellular junction or SJ deformations in aka^{L200} cells. Yellow dashed rectangles show FRAP area. (K and L) Plot of ATP-α::GFP fluorescence recovery as a function of time for the conditions described in (H-J). Wild type bicellular junction: n= 8 FRAP experiments, 4 pupae; aka^{L200} bicellular junction: n= 6 FRAP experiments, 4 pupae. aka^{L200} SJ deformations: n= 9 FRAP experiments, 4 pupae. Data are mean ± SD. Solid line shows a simple exponential fit. The scale bars represent 5µm.

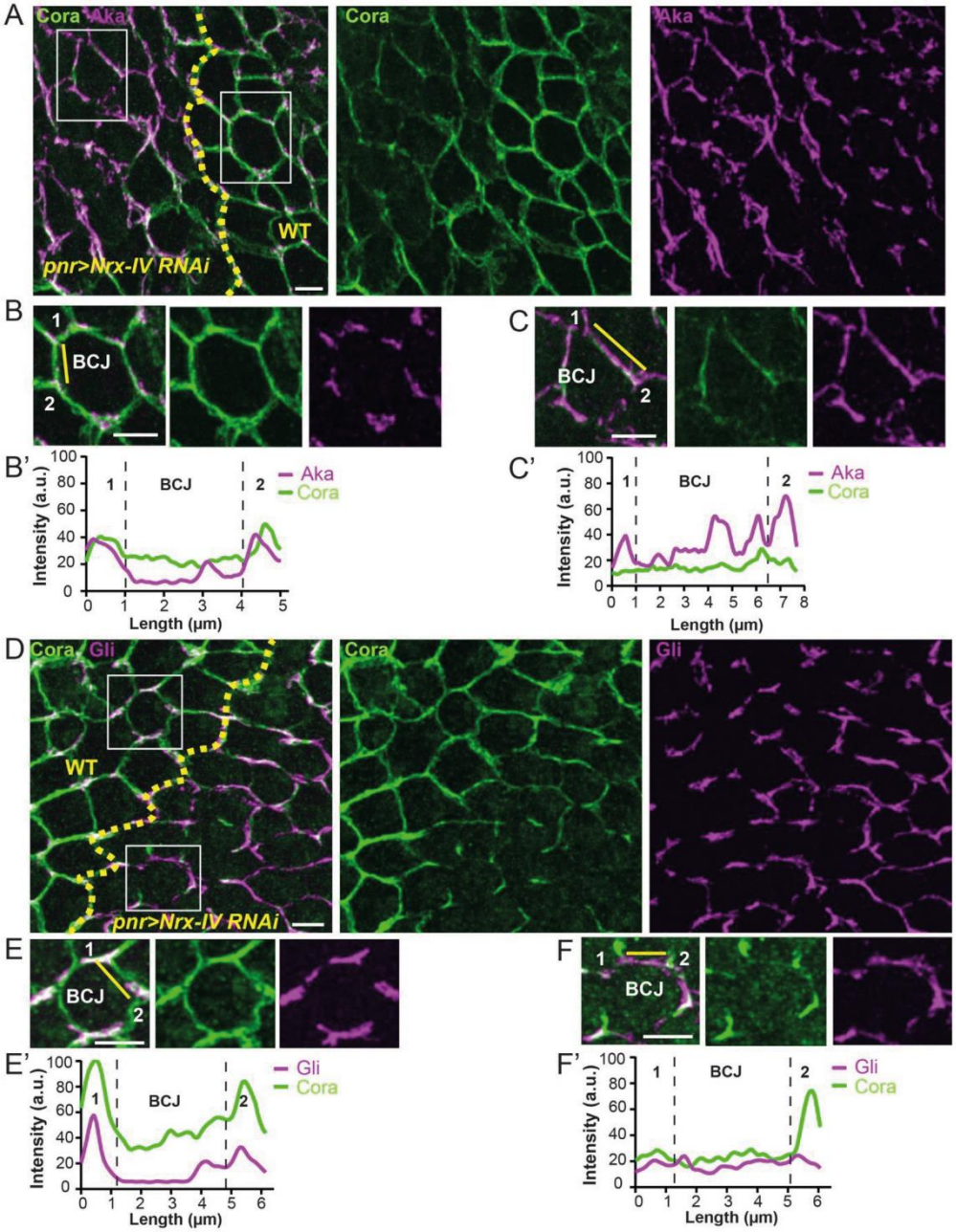

Figure S4: The presence of SJ core component is required to restrict Aka and Gli localization at vertex. Related to Figure 4.

(A-C, D-F) Localization of Aka (anti-Aka, magenta; A-C) or Gli (anti-Gli, magenta; D-F) in cells marked by Cora (anti-Cora, green) in wild type and cells expressing UAS::Nrx-IV RNAi under *pnr*-Gal4 control. The dashed yellow line separates wild type and Nrx-

IV-RNAi cells. Aka and Gli spread at the BCJ upon knockdown of Nrx-IV. White squares (A and D) show magnification (B-C and E-F) of wild type and knockdown cells for Nrx-IV. White dashed rectangles show the line scan used to obtain (B'-C' and E'-F') between two vertices represented by number 1 and 2. (B'-C' and E'-F') Plots representing Cora (green line) and Aka/Gli (magenta line) signals as a function of the length of cell-cell boundary in wild type and Nrx-IV-RNAi cells respectively. The scale bars represent 5μm.

Results part 2: Loss of tSJ and bSJ proteins lead to AJ and associated acto-myosin defects

Material and Methods

KEY RESOURCES TABLE

REAGENT or RESOURCE	SOURCE	IDENTIFIER
Antibodies		
Mouse anti-Coracle (1:200)	DSHB	C615.16, RRID: AB_1161644
Guinea pig Anti-Sdk (1:200)	(Astigarraga, Douthit et al. 2018)	Gift from Jessica Treisman
Mouse anti-HRS (1:100)	DSHB	27-4
Rabbit anti-Nrx-IV (1:1000)	(Stork, Thomas et al. 2009)	Gift from Christian Klämbt
Goat anti-GFP (1:1000)	Abcam	Cat#ab5450
Mouse anti-FK2 (1:1000)	Sigma-Aldrich	Cat#04-263
Rabbit anti-Aka (1:2000)	(Byri, Misra et al. 2015)	Gift from Anne Uv
Rat anti-Crb (1:1000)	(Richard, Grawe et al. 2006)	Gift from Elisabeth Knust
Rabbit anti-Cno (1:1000)	(Matsuo, Takahashi et al. 1999)	Gift from Mark Peifer
Cy2-, Cy3- and Cy5-coupled secondary antibodies (1:300)	The Jackson Laboratory	N/A
Alexa Fluor™ 647 Phalloidin (1:1000)	Thermo Fisher Scientific	Cat#A22287
Chemicals, Peptides, and Recombinant Proteins		
Paraformaldehyde	EMS	19340-72
Triton X-100	Euromedex	2000B
Phosphate Buffered Saline	Lonza	BE17-515F
Voltalef	VWR	24627.188
Experimental Models: Organisms/Strains		
D.melanogaster: Sdk::GFP	(Nagarkar-Jaiswal, Lee et al. 2015)	RRID: BDSC 60169
D.melanogaster: NMY-II::GFP^{crispr}	InDroso	N/A
D.melanogaster: mNG::Rok ;;	(Sidor, Stevens et al. 2020)	Gift from Katja Röper
D.melanogaster: hs-FLP ; *aka*^{L200}, FRT40A / CyO	(Esmangart de Bournonville and Le Borgne 2020)	N/A
D.melanogaster: ; DE-Cad::GFP;	(Huang, Zhou et al. 2009)	N/A
D.melanogaster: ; *nrv2*^{k13315}, FRT40A / CyO	(Chen, Call et al. 2005)	DGRC 114351
D.melanogaster: ; Shrb::GFP ;	N/A	Gift from Juliette Mathieu
D.melanogaster: w ;; UAS-KAEDE	BDSC	RRID: BDSC 26161
D.melanogaster: ;; Crb::GFP	(Huang, Zhou et al. 2009)	Crb::GFP-A GE24
D.melanogaster: ;; Jub::GFP	(Sabino, Brown et al. 2011)	Gift from Renata Basto
D.melanogaster: ;; Vinc::GFP	(Kale, Yang et al. 2018)	Gift from Thomas Lecuit
D.melanogaster: w^{1118} ;; Karst ::YFP	Kyoto Stock Center	Stock: 115 518
D.melanogaster: y, w^{1118}, ey-FLP ; *cold*^{f05607}, FRT40A / CyO	Kyoto Stock Center	Stock: 114 662
D.melanogaster: hs-FLP ; *ubi*-RFP nls, FRT40A / (CyO)	(Claret, Jouette et al. 2014)	Gift from Antoine Guichet
D.melanogaster: ;; UAS-Cora-RNAi	VDRC	Stock: 9788
D.melanogaster: UAS-Nrx-IV-RNAi	VDRC	Stock: 108 128
D.melanogaster: ;; UAS-Cora-RNAi-TRiP	(Perkins, Holderbaum et al. 2015)	RRID: BDSC 51845

D.melanogaster: ; UAS-Aka-RNAi-TRiP ;	(Perkins, Holderbaum et al. 2015)	RRID: BDSC 67014
D.melanogaster: ;; *pnr*-Gal4 / TM6, *Tb*^{1}	(Calleja, Moreno et al. 1996)	
Software and Algorithms		
Fiji	(Schindelin, Arganda-Carreras et al. 2012)	https://imagej.net/Fiji
Illustrator	Adobe Systems	Adobe Illustrator CS6
Prism 8	GraphPad	GraphPad
EasyFRAP-web	(Koulouras, Panagopoulos et al. 2018)	https://easyfrap.vmnet.upatras.gr/
Others		
Confocal Microscope	Leica	LSM TCS SPE, TCS SP5 and TCS SP8
Confocal Microscope	Zeiss	Confocal LSM 880 Airyscan

Drosophila genotypes

Figure 1

(A-C) *hs*-FLP / Sdk::GFP ; *aka*^{L200}, FRT40A / *ubi*-RFP nls, FRT40A obtained by crossing Sdk::GFP; *ubi*-RFP nls, FRT40A / CyO ; with *hs*-FLP ; *aka*^{L200}, FRT40A / CyO

Figure 2

(A-A') *hs*-FLP / NMY-II::GFP ; *aka*^{L200}, FRT40A / *ubi*-RFP nls, FRT40A obtained by crossing NMY-II::GFP; *ubi*-RFP nls, FRT40A / CyO ; with *hs*-FLP ; *aka*^{L200}, FRT40A / CyO

(C-C') *hs*-FLP / mNG::Rok ; *aka*^{L200}, FRT40A / *ubi*-RFP nls, FRT40A obtained by crossing mNG::Rok ; *ubi*-RFP nls, FRT40A / CyO ; with *hs*-FLP ; *aka*^{L200}, FRT40A / CyO

(E-E') *hs*-FLP ; *aka*^{L200}, FRT40A / *ubi* -RFP nls, FRT40A obtained by crossing *hs*-FLP ; *aka*^{L200}, FRT40A / CyO with *hs*-FLP ; *ubi*-RFP nls, FRT40A / (CyO)

Figure 3

(A-A') *hs*-FLP ; *nrv2*^{k13315}, FRT40A / *ubi* -RFP nls, FRT40A, DE-Cad::GFP ; obtained by crossing *hs*-FLP ; *nrv2*^{k13315}, FRT40A / CyO with *hs*-FLP ; *ubi*-RFP nls, FRT40A, DE-Cad::GFP / CyO ;

(C-C') *hs*-FLP / NMY-II::GFP ; *nrv2*^{k13315}, FRT40A / *ubi*-RFP nls, FRT40A obtained by crossing NMY-II::GFP; *ubi*-RFP nls, FRT40A / CyO ; with *hs*-FLP ; *nrv2*^{k13315}, FRT40A / CyO ;

(E-E') *hs*-FLP ; *nrv2*^{k13315}, FRT40A / *ubi* -RFP nls, FRT40A ; obtained by crossing *hs*-FLP ; *nrv2*^{k13315}, FRT40A / CyO with *hs*-FLP ; *ubi*-RFP nls, FRT40A / CyO ;

Figure 4

(A-C) UAS-cora-RNAi / *pnr*-Gal4 obtained by crossing UAS-cora-RNAi with *pnr*-Gal4 / TM6, *Tb*^{1}

(D-F) *hs*-FLP ; *nrv2*^{k13315}, FRT40A / *ubi* -RFP nls, FRT40A ; obtained by crossing *hs*-FLP ; *nrv2*^{k13315}, FRT40A / CyO with *hs*-FLP ; *ubi*-RFP nls, FRT40A / CyO ;

Figure 5

(A-G) Shrub::GFP ; UAS-cora-RNAi / UAS-KAEDE, *pnr*-Gal4 obtained by crossing ;; UAS-cora-RNAi with ; Shrub::GFP ; UAS-KAEDE, *pnr*-Gal4 / SM5-TM6, *Tb*^{1}

Figure 6

(A-A') *hs*-FLP ; *aka*^{L200}, FRT40A / *ubi* -RFP nls, FRT40A obtained by crossing *hs*-FLP ; *aka*^{L200}, FRT40A / CyO with *hs*-FLP ; *ubi*-RFP nls, FRT40A / (CyO)

(B-B' and D) *hs*-FLP ; *aka*^{L200}, FRT40A / *ubi*-RFP nls, FRT40A ; Crb::GFP / + obtained by crossing ; *ubi*-RFP nls, FRT40A / CyO ; Crb::GFP / TM6, *Tb*^{1} with *hs*-FLP ; *aka*^{L200}, FRT40A / CyO

Figure 7

(A-B; D-E) *hs*-FLP ; *aka*^{L200}, FRT40A / *ubi* -RFP nls, FRT40A, DE-Cad::GFP ; obtained by crossing *hs*-FLP ; *aka*^{L200}, FRT40A / CyO with *hs*-FLP ; *ubi*-RFP nls, FRT40A, DE-Cad::GFP / CyO ;

Figure 8

(A-A') *hs*-FLP ; *aka*^{L200}, FRT40A / *ubi*-RFP nls, FRT40A ; Jub::GFP / + obtained by crossing ; *ubi*-RFP nls, FRT40A / CyO ; Jub::GFP / TM6, *Tb*^{1} with *hs*-FLP ; *aka*^{L200}, FRT40A / CyO

(C-C'; E-E') *hs*-FLP ; *aka*^{L200}, FRT40A / *ubi*-RFP nls, FRT40A ; Vinc::GFP / + obtained by crossing ; *ubi*-RFP nls, FRT40A / CyO ; Vinc::GFP / TM6, *Tb*^{1} with *hs*-FLP ; *aka*^{L200}, FRT40A / CyO

Figure S1

(A-A') *hs*-FLP ; *aka*^{L200}, FRT40A / *ubi* -RFP nls, FRT40A, DE-Cad::GFP ; obtained by crossing *hs*-FLP ; *aka*^{L200}, FRT40A / CyO with *hs*-FLP ; *ubi*-RFP nls, FRT40A, DE-Cad::GFP / CyO ;

Figure S2

(A-A') *hs*-FLP ; *aka*^{L200}, FRT40A / *ubi*-RFP nls, FRT40A ; Karst::YFP / + obtained by crossing ; *ubi*-RFP nls, FRT40A / CyO ; Karst::YFP / TM6, *Tb*^{1} with *hs*-FLP ; *aka*^{L200}, FRT40A / CyO

Figure S3

(A-A') NMY-II::RFP ; UAS-KAEDE ; UAS-cora-RNAi / *pnr*-Gal4 obtained by crossing UAS-cora-RNAi with NMY-II::RFP ; UAS-KAEDE ; *pnr*-Gal4 / TM6, *Tb*^{1}

(B-B') *hs*-FLP / NMY-II::GFP ; *cold*^{f05607}, FRT40A / *ubi*-RFP nls, FRT40A obtained by crossing NMY-II::GFP; *ubi*-RFP nls, FRT40A / CyO ; with *hs*-FLP ; *cold*^{f05607}, FRT40A / CyO

(C-C') *hs*-FLP ; *cold*^{f05607}, FRT40A / *ubi* -RFP nls, FRT40A, DE-Cad::GFP ; obtained by crossing *hs*-FLP ; *cold*^{f05607} / FRT40A / CyO with *hs*-FLP ; *ubi*-RFP nls, FRT40A, DE-Cad::GFP / CyO ;

Figure S4

(A-B'') Shrub::GFP, UAS-cora-RNAi; + / *pnr*-Gal4 obtained by crossing UAS-cora-RNAi with Shrub::GFP ; *pnr*-Gal4 / TM6, *Tb*^{1}

(C-D'') Shrub::GFP ; UAS-Nrx-IV-RNAi / *pnr*-Gal4 obtained by crossing UAS-Nrx-IV-RNAi with Shrub::GFP ; *pnr*-Gal4 / TM6, *Tb*^{1}

Figure S5

(A-A') *hs*-FLP ; *nrv2*^{k13315}, FRT40A / *ubi* -RFP nls, FRT40A ; obtained by crossing *hs*-FLP ; *nrv2*^{k13315}, FRT40A / CyO with *hs*-FLP ; *ubi*-RFP nls, FRT40A / CyO ;

(B-B') *hs*-FLP ; *nrv2*^{k13315}, FRT40A / *ubi*-RFP nls, FRT40A ; Crb::GFP / + obtained by crossing ; *ubi*-RFP nls, FRT40A / CyO ; Crb::GFP / TM6, *Tb*^{1} with *hs*-FLP ; *nrv2*^{k13315}, FRT40A / CyO

Figure S6

(A-A') *hs*-FLP ; *aka*^{L200}, FRT40A / *ubi* -RFP nls, FRT40A obtained by crossing *hs*-FLP ; *aka*^{L200}, FRT40A / CyO with *hs*-FLP ; *ubi*-RFP nls, FRT40A / (CyO)

(B-B') *hs*-FLP ; *nrv2*^{k13315}, FRT40A / *ubi* -RFP nls, FRT40A ; obtained by crossing *hs*-FLP ; *nrv2*^{k13315}, FRT40A / CyO with *hs*-FLP ; *ubi*-RFP nls, FRT40A / CyO ;

(C-C') *ubi*-RFP nls , *w**, *hs*-Flp, FRT19A / *Nrg*^{G0488b}, FRT19A ; ; obtained by crossing *ubi*-RFP nls , *w**, *hs*-Flp, FRT19A ; ; with *Nrg*^{G0488b}, FRT19A ; ;

Figure S7

hs-FLP / NMY-II::GFP ; *aka*^{L200}, FRT40A / *ubi*-RFP nls, FRT40A obtained by crossing NMY-II::GFP; *ubi*-RFP nls, FRT40A / CyO ; with *hs*-FLP ; *aka*^{L200}, FRT40A / CyO

Experimental model

Drosophila strains

The following strains were constructed as follow : Sdk::GFP; *ubi*-RFP nls, FRT40A / CyO was obtained by crossing Sdk::GFP with *ubi*-RFP nls, FRT40A / CyO and appropriate flies were selected; *hs*-FLP ; NMY-II::GFP; *ubi*-RFP nls, FRT40A / CyO ; was obtained by crossing NMY-II::GFP ; If / CyO ; with *ubi*-RFP nls, FRT40A / CyO and appropriate flies were selected mNG::Rok ; *ubi*-RFP nls, FRT40A / CyO was obtained by crossing mNG::Rok ; If / CyO ; with *ubi*-RFP nls, FRT40A / CyO and appropriate flies were selected ; *hs*-FLP ; *ubi*-RFP nls, FRT40A, DE-Cad::GFP / CyO ; was constructed by recombining DE-Cad::GFP with *hs*-FLP ; *ubi*-RFP nls, FRT40A / CyO ; and recombined flies were selected. UAS-KAEDE, *pnr*-Gal4 / SM5-TM6, *Tb*^{1} was obtained by recombining w ;; UAS-KAEDE with *pnr*-Gal4 / SM5-TM6, *Tb*^{1} and recombined flies were selected. Shrub::GFP ; UAS-KAEDE, *pnr*-Gal4 / SM5-TM6, *Tb*^{1} was obtained by crossing ; Shrub::GFP / (CyO) ; with UAS-KAEDE, *pnr*-Gal4 / SM5-TM6, *Tb*^{1} and appropriate flies were selected. *ubi*-RFP nls, FRT40A / CyO ; Jub::GFP / TM6, *Tb*^{1} was obtained by crossing ; *ubi*-RFP nls, FRT40A / CyO ; MKRS / TM6, *Tb*^{1} with ;; Jub::GFP and appropriate flies were selected. *ubi*-RFP nls, FRT40A / CyO ;

Vinc::GFP / TM6, *Tb*^{1} was obtained by crossing ; *ubi*-RFP nls, FRT40A / CyO ; MKRS / TM6, *Tb*^{1} with ;; Vinc::GFP and appropriate flies were selected. *ubi*-RFP nls, FRT40A / CyO ; Karst::YFP / TM6, *Tb*^{1} was obtained by crossing ; *ubi*-RFP nls, FRT40A / CyO ; MKRS / TM6, *Tb*^{1} with ;; Karst::YFP and appropriate flies were selected.

Method details

Immunofluorescence

Pupae aged for 16h30 to 19h after puparium formation (APF) were dissected using Cannas microscissors (Biotek, France) in 1X Phosphate-Buffered Saline (1X PBS, pH 7.4) and fixed 15 min in 4% paraformaldehyde at room temperature (Gho, Lecourtois et al. 1996). Following fixation, dissected nota were permeabilized using 0.1% Triton X-100 in 1X PBS (PBT), incubated with primary antibodies diluted in PBT for 2 hours at room temperature. After 3 washes of 5 minutes in PBT, nota were incubated with secondary antibodies diluted in PBT for 1 hour, followed by 2 washes in PBT, and one wash in PBS, prior mounting in 0,5% N-propylgallate dissolved in 90% glycerol/PBS 1X final.

Live-imaging and image analyses

Live imaging was performed on pupae aged for 16h30 APF at 25°C. Pupae were sticked on a glass slide with a double-sided tape, and the brown pupal case was removed over the head and dorsal thorax using microdissecting forceps. Pillars made of 4 and 5 glass coverslips were positioned at the anterior and posterior side of the pupae, respectively. A glass coverslip covered with a thin film of Voltalef 10S oil is then placed on top of the pillars such that a meniscus is formed between the dorsal thorax of the pupae and the glass coverslip (Gho, Bellaiche et al. 1999). Images were acquired with a LSM Leica SPE, SP5 or SP8 equipped with a 63X N.A. 1.4. objective and controlled by LAS AF software or by LSM Zeiss 880 AiryScan equipped with a 63X N.A.1.4. objective and controlled by ZEN software. Confocal sections (z) were taken every 0.5 µm or 1µm. For figures representation, images were processed with Gaussian Blur σ = 1.1. All images were processed and assembled using Fiji software (Schindelin, Arganda-Carreras et al. 2012) and Adobe Illustrator.

Fluorescence recovery after photobleaching

FRAP experiments were performed only in female pupae expressing Sdk::GFP together with RFP-nls used as a marker of *aka*^{L200} cells. Sdk::GFP was bleached (488 nm laser at 60% power, 2 iterations of 1.293s, square ROI of 1.5µm*1.5µm) using a LSM Leica SP8 equipped with a 63X N.A. 1.4 objective. Confocal stacks were acquired every minute, 3 min before and 10 min after photobleaching on 13z steps of 0.5µm to compensate for movement in z during acquisition.

FRAP experiments were performed in pupae expressing Crb::GFP with RFP-nls used as a marker of *aka*^{L200} cells. Crb::GFP was bleached (488 nm laser at 95% power, 2 iterations of 943.72 ms) using a LSM Zeiss 880 AiryScan equipped with a 63X N.A. 1.4 objective. Frames were acquired every seconds, 5s before and 55s after photobleaching at the best Crb::GFP signal level.

Nanoablation

Laser ablation was performed on live pupae aged for 16h to 19h APF using a Leica SP5 confocal microscope equipped with a 63X N.A. 1.4 objective or a LSM Zeiss 880 AiryScan equipped with a 63X N.A. 1.4 objective. Ablation was carried out on epithelial cell membranes at AJ level with a two-photon laser-type Mai-Tai HP from Spectra Physics set to 800 nm and a laser power of 2.9W.

Quantification and statistical analysis

Signal recovery upon photobleaching

In all FRAP experiments, ROI1 corresponds to the photobleached area, ROI2 to the area used as a control for general photobleaching of the sample across time and ROI3 to the background.

For Crb::GFP, the entire signal was collected at the level of the best signal plan. ROI2 was considered as the fluorescence of the entire field.

Then, we used EasyFRAP-web (Koulouras, Panagopoulos et al. 2018) for all data processing and to extract normalized values. The I(t) which correspond to the fluorescence intensity across time was calculated as described:

First, the fluorescence intensity is corrected by subtracting the background:

$$I(t)_{ROI1'} = I(t)_{ROI1} - I(t)_{ROI3}$$
$$I(t)_{ROI2'} = I(t)_{ROI2} - I(t)_{ROI3}$$

Then, values of fluorescence intensity are normalized in this way:

$$I(t)_{\text{double norm}} = \left(\frac{\frac{1}{n_{pre}} \times \sum_{t=1}^{n_{pre}} I(t)_{ROI2'}}{I(t)_{ROI2'}} \right) \times \left(\frac{I(t)_{ROI1'}}{\frac{1}{n_{pre}} \times \sum_{t=1}^{n_{pre}} I(t)_{ROI1'}} \right)$$

We decided to take value from full scale normalization in order to have a curve starting from 0:

$$I(t)_{\text{fullscale norm}} = \frac{I(t)_{\text{double norm}} - I(t_{\text{postbleach}})_{\text{double norm}}}{1 - I(t_{\text{postbleach}})_{\text{double norm}}}$$

Recovery curves were then fitted assuming a one-phase exponential association equation using the GraphPad Prism 8.0 software:

$$I(t)_{\text{fullscale norm}} = I(t)_{\text{max fullscale norm}} \times (1 - e^{-K \times t})$$

We admitted that $I(t)_{\text{max fullscale norm}}$ is the maximum value based on the fitted curve for the post-bleach time (55s after the photobleaching for Crb::GFP) and it is considered as the immobile fraction. $t_{1/2}$ was deduced when $I(t)_{\text{fullscale norm}} = 0{,}5 \times I(t)_{\text{max fullscale norm}}$ which occurred at $t = \frac{-\ln(0{,}5)}{K}$.

Fluorescence signal analysis

Sum slices were applied to different experiments. A circular ROI of 2µm*2µm was drawn to measure signal at vertices, a circular ROI of 3µm*3µm for the medial network and centered in the measured cells and a segmented line of 10 pixels width was used to measure signals at bicellular junctions. Using the same width or diameter, lines and circular ROI were drawn to extract background fluorescence signals and the

background signal was subtracted to each quantification. After, data were standardized between 0 and 10 to allow visual representation with 10 corresponding to the highest signal in each experiment analyzed and 0 the lowest. Standardization was operated on data of cells belonging to the same *notum* in every experiments.

Line scan fluorescence analysis

Sum slices projection were applied and a 20 pixels width line was drawn from vertex 1 to vertex 2, spanning the BCJ (Figures 1B, 4A-4C and 4D-4F). Then gray value was plotted across length of the line.

Length establishment measurement

The time T = 0 was set according to the frame just before the beginning of the contraction of the cell. Each frame was separated by 2 mins. The maximal expected size of the junction was inferred at the beginning of the contraction with the expected localization of the two future vertices. Then, each frame, the length was measured at the new vertices formed and standardized to the initial maximal expected size.

Statistical tests

All information concerning the statistical details are provided in the main text and in figure legends, including the number of samples analyzed for each experiment. Scattered plots use the following standards: thick line indicate the means and errors bars represent the standard deviations. Boxplots with connected line use the following standards: dots represent mean and the total-colored areas show SD.

Statistical analyses were performed using the GraphPad Prism 8.0 software. The Shapiro-Wilk normality test was used to confirm the normality of the data and the F-test to verify the equality of SD. The statistical difference of data sets was analyzed using the Student unpaired two-tailed t test or the non-parametric Mann-Whitney test. Statistical significances were represented as follow: p value > 0.05 NS (not significant) and p value $\leq$ 0.0001 ****.

Results

Loss of Anakonda leads to Sidekick enrichment at the bicellular junction

Using anti-Sdk antibody, we previously reported that Sdk localisation at the vertex was unaffected by the loss of Aka (Esmangart de Bournonville and Le Borgne 2020). Strikingly, using the Sdk::GFP probe, we were able to observe Sdk enrichment at the BCJ of *aka*^{L200} cells (Figure 1A-1A'). A close up and a line scan analysis of a representative bicellular *aka*^{L200} cell showed Sdk::GFP signal enrichment at the BCJ or loss of restriction at the TCJ compared to WT cell (Figure 1B-1B'). We sought if differences in Sdk::GFP localisation might be due to changes in its dynamics at the membrane. Using FRAP analysis at vertex level (Figure 1C-1C'), no differences were observed in terms of immobile fraction, which is equal to 0.50 and 0.51 for both WT and *aka*^{L200} conditions respectively as well as no significative changes in the rate of fluorescence recovery ($t_{1/2}$=322s in WT and $t_{1/2}$=340s in *aka*^{L200}). Previous work of (Letizia, He et al. 2019) highlights the fact that Sdk spreads at BCJ upon reduced tension in the tissue. Therefore, these results prompted us to investigate into more details eventual defects at AJ level upon loss of tSJ component.

Mutant cells for Anakonda display enrichment of DE-Cadherin and underlying acto-myosin components at both BCJ and TCJ

First, we started to probe DE-Cadherin tagged with GFP (DE-Cad::GFP) behaviour in the *aka*^{L200} cells since it is the most iconic component of AJs. Surprisingly, loss of Aka led to a 2 fold enrichment of DE-Cad::GFP at vertices and 1.5 fold enrichment at BCJ (Figure S1A-1B). This phenotype was not restricted to mutant/mutant junctions since enrichment was also reported at the BCJ between one WT and one *aka*^{L200} cell or at a vertex shared by both WT and *aka*^{L200} cells. Hence, this suggested that only one vertex defective for tSJ integrity is enough to trigger AJ remodelling. The enrichment of DE-Cad::GFP was accompanied by Non muscle Myosin-II tagged with GFP (NMY-II::GFP) enrichment both at vertices (1.7 fold enrichment) and BCJ (1.8 fold enrichment; Figure 2A-2B). Again, this effect was not restricted to mutant/mutant interfaces. These two pools act in synergy in order to transmit forces exerted by the medial-apical network onto the junctional pool. Interestingly, medial-apical network was also stronger in NMY-II::GFP signal in *aka*^{L200} cells compared to WT situation (1.5 fold enrichment; Figure

2A-2B). To test if NMY-II was active in this mutant context, we made use of the Rho-kinase N-terminally tagged with the mNeon-Green fluorophore (mNG::Rok), one of the most prominent NMY-II activator (Sidor, Stevens et al. 2020). We confirmed that NMY-II was activated since mNG::Rok signal was higher at both BCJs and vertices (1.5 fold enrichment) level in *aka*^{L200} cells (Figure 2C-2D), suggesting presence of higher forces at this localisation. Again, this was true both at mutant/mutant junctions and WT/mutant interfaces. However, mNG::Rok did not show clear signal at medial-apical network, making the study of this pool's activation not possible. Using a phospho-NMY-II antibody could solve the problem. In addition to DE-Cad::GFP, NMY-II::GFP and its activator mNG::Rok enrichment in *aka*^{L200} cells, we probed F-actin via Phalloidin coupled to the fluorophore Alexa Fluor®647 (Phalloidin 647) and revealed enrichment at both BCJ (1.9 fold enrichment) and TCJ (2.5 fold enrichment) levels, phenocopying previous results (Figure 2E-2F). The F-actin crosslinker Karst was also reported enriched both at BCJs (1.4-fold enrichment), TCJs (1.6-fold enrichment) and at the apical medial part of the cell (1.2-fold enrichment; Figure S2A-2B). Overall, those result showed that tSJ impairment via loss of Aka had an impact on AJ organisation and its associated acto-myosin cytoskeleton. Both DE-Cad, NMY-II, Rok and F-actin were enriched in homozygous mutant cells and at boundaries between *aka*^{L200} and WT cells.

Impairment of Septate Junctions integrity recapitulates phenotype observed at Adherens Junction level upon depletion of Anakonda

We knew from our previous work that tSJ impairment could not be dissociated from pSJ defects in the *notum*. In order to decipher if the AJ level impairments upon loss of Aka were specific to the tSJ proteins, we used a hypomorphic mutant version of the pSJ core component Nrv2 named *nrv2*^{k13315}. We observed in a similar manner to the loss of Aka, DE-Cad::GFP (Figure 3A-3B), NMY-II::GFP (Figure 3C-3D) and F-actin (Figure 3E-3E') enrichment at both BCJ and TCJ levels in *nrv2*^{k13315} cells compared to WT cells. Since in *nrv2*^{k13315} cells, Aka signal was sometimes higher or sometimes reduced (data not shown), probably due to pSJs being too much impacted, we further confirmed those results using known situation where Aka is spread at the BCJ, therefore excluding the idea that absence of Aka is the main driver of the effects observed in *nrv2*^{k13315} cells. Depleted another pSJ core component Cora via expression of RNAi-Cora under the control of pannier (pnr) promoter driving GAL4

expression, we observed NMY-II::GFP enrichment in cells knocked-down for Cora (Figure S3A-S3A'). Another approach using a mutant version of the Ly6 protein Cold, referred as *cold*^{f05607}, known to control pSJ proteins trafficking, exhibited similar outcomes for both NMY-II::GFP (Figure S3B-S3B') and DE-Cad::GFP (Figure S3C-S3C'). Therefore, those results argued in favour of pSJ defects mediating AJ and acto-myosin enrichment at apical level.

Because the phenotype of pSJ depletion was similar to what happened upon loss of Aka, we next wondered if the effects were restricted to bicellular AJ components or also applied to the tAJ component Sdk. Using first a situation where Aka is not absent but rather enriched at BCJ, we observed a striking enrichment of Sdk at the BCJ of Cora depleted cells (Figure 4A and 4C-4C') compared to its restriction at vertex in the wild type area (Figure 4A and 4B-4B'). Those outcomes were further confirmed looking at *nrv2*^{k13315} cells (Figure 4D-4F') or using another RNAi against the core component protein Nrx-IV (data not shown). These results showed how similar were pSJ and tSJ defects mediating AJ and acto-myosin irregularities observed at apical level.

How can defective pSJs impact AJ proteins located at different plan? A possible precedent in the literature has been observed upon loss of ESCRT-III component Shrub which caused Kune/Cora mislocalisation and ESCRT-0 component HRS as well as Crb aggregates associated with growth of cell apical domains leading to elongated trachea. This elongated trachea phenotype is reminiscent of pSJ and tSJ mutants. Moreover, internal lab data showed that mutant cells for Shrub in the *notum* displayed loss or reduction of pSJ and tSJ component signals. Also, Crb has been reported to regulate Rok localisation in *Drosophila* epithelial cells. This prompted us to investigate if defects at pSJ or tSJ levels were somehow impairing Shrub activity, therefore leading to defects at Crb level, which could explained in part the apical level defects of mNG::Rok observed upon loss of pSJ/tSJ proteins.

Impairment of Septate Junctions leads to defective ESCRT-dependent degradation

In the control situation, Shrub::GFP and HRS localized in small punctate structures (Figure 5A-5C) and often colocalized as depicted in the close-up section (Figure 5B). Those punctate structures were mostly situated at pSJ level like demonstrated using Nrx-IV signal as a reference (Figure 5B'). Silencing of Cora induced the formation of

large Shrub::GFP-positive aggregates associated with increased numbers and larger HRS-positive punctae (Figure 5D-5G). Those Shrub::GFP aggregates were not specifically colocalizing with HRS punctae (Figure 5E-E') and were found sometimes basally (Figure 5E' and 5F') but also apically (data not shown). Some Shrub::GFP vesicles were still colocalizing with HRS but only when exhibiting a WT situation shape, meaning not aggregated. Therefore, those results somehow gave evidence of Shrub and HRS defects.

Another way to probe potential ESCRT problems in those cells is to look at the poly-ubiquitinylated proteins targeted for degradation since ESCRT complex is involved in the degradative pathway control.

Therefore, we looked at both Shrub::GFP and poly-ubiquitinylated proteins using FK2 antibody marker in WT conditions, showing similar results as mentioned before (Figure S4A). Then, in the area knocked-down for Cora, we observed again induction of Shrub::GFP aggregates but also of FK2 (Figure S4B-4B''). Shrub::GFP aggregates were partially colocalizing with FK2 accumulations while being sometimes disposed around FK2 structures (Figures S4B'-4B''). Similar outcomes were observed upon knock-down of Nrx-IV (Figures S4C-4D''). Those results added another clue to the fact that pSJ defects impaired ESCRT proteins HRS and Shrub activity in those cells.

Loss of Bicellular and Tricellular Septate Junction components leads to Crumbs accumulation at apical level

Defective ESCRT-dependent endosomal pathway may be reminiscent of loss of Shrub activity in which not only localisation of SJ components was impacted, but also Crb degradation leading to accumulation of Crb in intracellular organelles. This prompted us to investigate the localisation of Crb upon depletion of bSJ or tSJ components.

Using Crb tagged with a GFP in its extracellular part (Crb::GFP), we observed Crb::GFP signal both at junctions and at the medial part of the WT cells (Figure S5B-5B'). Then, we were able to see in *nrv2*^{k13315} cells an increased number and brighter HRS punctae (Figure S5A-5A') as well as increased signal of Crb::GFP signal at the medial apical part of the cell (Figure S5B-5C). Concerning the Crb::GFP signal found at the junction, the phenotype was much more intricate. We observed either enrichment associate with small aggregated structures or less well-defined signal

(Figure S5B-5B'). Moreover, using a Crb antibody targeting its N-terminal extracellular part, we were able to see again the medial apical part enrichment of Crb but not at the junction level, showing mostly disappearance at this site (Figure S6B-6B'). Similar results were reported using a mutant for another pSJ protein named Neuroglian (Nrg, Figure S6C-6C'). Still, pSJ defects triggered Crb irregularities at apical level (Figure S6B-C).

We then investigated the *aka*^{L200} situation. Again, we noted enrichment of HRS punctae which were bigger and brighter, similarly to pSJ defects case (Figure 6A-6A'). Looking at Crb::GFP, we reported increased signal of Crb::GFP both at medial apical part as well as the junction (Figure 6B-6C). Again, this phenotype was complex as some junctions were enriched when at the same time some were not. Using Crb antibody, we noticed similar defects upon loss of Aka even though this time, the Crb junctional enrichment was less pronounced that when using Crb::GFP (Figure S6A-S6A'). Still, this confirmed previous differences observe between loss of pSJ and tSJ proteins on Crb::GFP. This Crb enrichment could be explained at least by a potential trafficking defects since it relies on Shrub for correct localisation and amount at the apical level (Dong, Hannezo et al. 2014). Using FRAP analysis like for Sdk::GFP (Figure 6D-6E), no significative differences were reported looking at the immobile fraction of junctional Crb::GFP, equal to 0.57 and 0.62 for both WT and *aka*^{L200} conditions respectively and no changes in the rate of fluorescence recovery either ($t_{1/2}$=18s in WT and $t_{1/2}$=16s in *aka*^{L200}). Collectively those results argued in favour of pSJ/tSJ defects leading to Crb higher level at apical level albeit not having significative differences in terms of junctional stability.

Tricellular Septate Junction defects are associated with increased tension upon Adherens Junction and acto-myosin cytoskeleton remodelling

We saw that pSJ/tSJ defects triggered AJ and acto-myosin remodelling, leading to higher amount of those components. One could reasonably infer that increased quantity of NMY-II, Rok and F-actin at the junction might be linked to increased tension. This is why we decided to probe junctional tension using classical two-photon laser-based nano ablation and the DE-Cad::GFP as a junctional marker (Figure 7A-7B). Intriguingly, no significative differences of recoil velocities were observed upon ablation of WT cells versus *aka*^{L200} mutant junctions *(*Mean = 0.19 +/-0.08 µm/s in WT vs Mean

= 0.20 +/- 0.07 µm/s in *aka*^{L200}) or *nrv2*^{k13315} cells (Mean = 0.15 +/-0.07 µm/s in WT vs Mean = 0.16 +/- 0.08 µm/s in *nrv2*^{k13315}) (Figure 7C). However, we did observe significative differences comparing WT cells and *cold*^{f05607} cells (Mean = 0.24 +/-0.07 µm/s in WT vs Mean = 0.15 +/- 0.07 µm/s in *cold*^{f05607}). This suggested that even if the remodelling of AJ and acto-myosin were restricted to mutant areas, global defects at tissue level could be at play here. Still, we could not exclude defects in heterozygous cells and this will be investigated soon.

Another way to look at mechanical properties defects in epithelium tissue is to look at cell cytokinesis. When a cell divides and starts to form its new cell/cell interface at AJ level, neighbouring cells respond by recruiting NMY-II at the boundary. This causes the tug of war mechanism that counterbalances the contractile activity of the midbody, hence regulating the length of the new cell/cell interface (Founounou, Loyer et al. 2013, Guillot and Lecuit 2013, Herszterg, Leibfried et al. 2013). We chose to look at epithelial cell cytokinesis using DE-Cad::GFP to decipher if mechanical defects could be revealed in *aka*^{L200} cells. A typical WT cell established a long interface upon cytokinesis with few variations across time during the next 30 minutes after the Anaphase onset (Figure 7D and 7F). In the opposite, *aka*^{L200} cells showed impairment of this junctional length regulation as highlighted by the extreme case of shrinkage in (Figure 7E-7F). This change in *aka*^{L200} cells started to be significant around 10 minutes after the anaphase onset, which correlated surprisingly with the onset of tAJ establishment like described in our previous paper (Esmangart de Bournonville and Le Borgne 2020). As expected, knowing that loss of Aka from one cell impacts the two neighbours, when a WT cell was dividing and having only one neighbour mutant for Aka, this cell displayed similar defects, even though the differences started to occur later around 20 minutes after anaphase onset (Figure 7F).

Then, we observed what was happening at NMY-II level. Typical case is depicted in (Figure S7A), where NMY-II::GFP enrichment at neighbouring boundaries started to happen around 3 min after anaphase onset, then continuing to increase across time. This recruitment was symmetrical and cells rarely displayed strong inequalities in term of NMY-II::GFP signal at neighbouring boundaries. Moreover, we studied the situation where a WT dividing cell was doing so with one WT and one *aka*^{L200} neighbours. In this situation, the boundary between the mutant and the wild type cell displayed strong

NMY-II::GFP enrichment compared to the WT side (Figure S7B). Then looking at *aka*^{L200} cells dividing with one WT and one mutant neighbours, we observed again stronger NMY-II::GFP enrichment at the mutant/mutant side compared to mutant/WT side (Figure S7C). Therefore, cell cytokinesis further unravelled mechanical defects occurring upon loss of Aka.

Loss of Anakonda reveals mechano-effector proteins Ajuba and Vinculin enrichment at junctional level

Still looking at the defects in mechanical tension, we chose to examine known markers of increased mechanical tension in *Drosophila* epithelium. One of them is the Hippo/YAP partner named Jub, recruited to AJ upon increased cytoskeleton tension in wings discs (Rauskolb, Sun et al. 2014). We used the Jub tagged GFP (Jub::GFP) and looked at *aka*^{L200} cells. We observed higher level of Jub::GFP both at BCJ and TCJ compared to WT situation, confirming that tension was increased in those cells (Figure 8A-8B). Another protein known to be tension dependent recruited is the F-actin binding partner Vinc (Kale, Yang et al. 2018). Using Vinc tagged with GFP (Vinc::GFP), we did observe Vinc::GFP higher level at TCJ and BCJ in *aka*^{L200} cells compared to WT cells (Figure 8C-8D). Even more interestingly, Vinc::GFP was found all along lateral membrane as clusters but also at the basal part of mutant cells (Figure 8E-8F'), suggesting a reorganisation of F-actin anchored point at the membrane associated with increased tension at these localisations. Those results confirmed our primary hypothesis that AJ and acto-myosin remodelling upon loss of Aka were associated with changing in the mechanical properties of the cells.

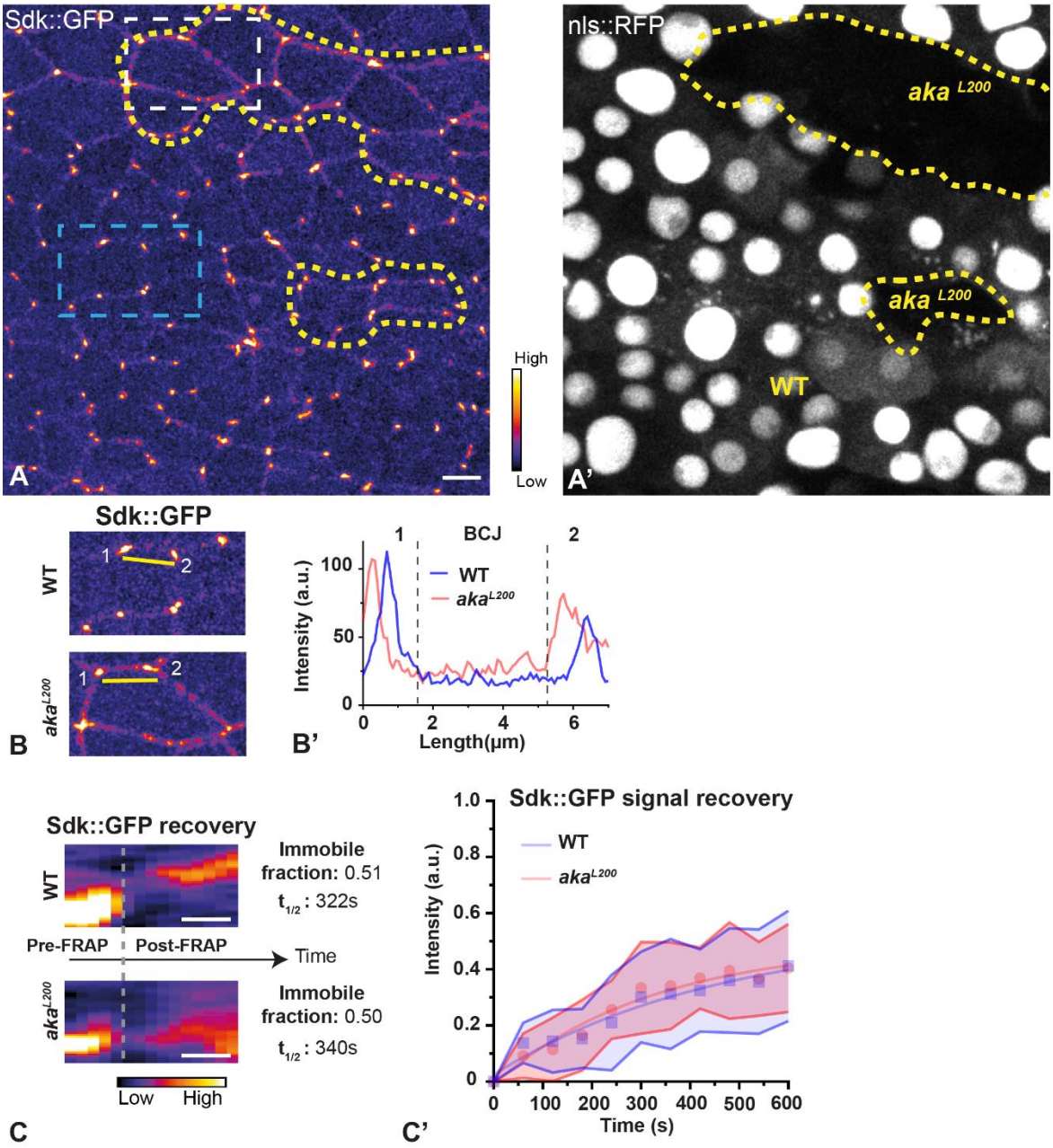

Figure 1. **Sidekick is enriched at the bicellular junction upon loss of Anakonda**.(A-A') show *nota* expressing Sdk::GFP (A, fire color) between 16h-18h APF, after heat-shock to induce clone of wild type (A', nls::RFP positive) and mutant cells for Aka (A', nls::RFP negative). (A) Localisation of Sdk::GFP (fire color) in both WT and *aka*^{L200} cells, separated by the dashed yellow line. (A') Clones of WT and *aka*^{L200} cells revealed by nls::RFP marking. Blue dashed square and white dashed square show magnification of respectively WT and *aka*^{L200} cells (B). (B) Yellow lines show the line scan used to obtain (B'), a plot representing Sdk::GFP signals as a function of the length of cell-cell boundary in WT and *aka*^{L200} cells respectively. (C) Kymographs of the bleached region for Sdk::GFP in wild type and *aka*^{L200} cells. Scale bars show 5min. (C') Plot of Sdk::GFP fluorescence recovery as a function of time for the conditions described in (C). WT: n = 8 FRAP experiments, 4 pupae; *aka*^{L200}: n = 10 FRAP experiments, 4 pupae. Data are mean ± SD. Solid line shows a simple exponential fit. Blue square and red circles represent WT and *aka*^{L200} time point values. A calibration bar shows LUT for grey value range. The scale bar represents 5µm.

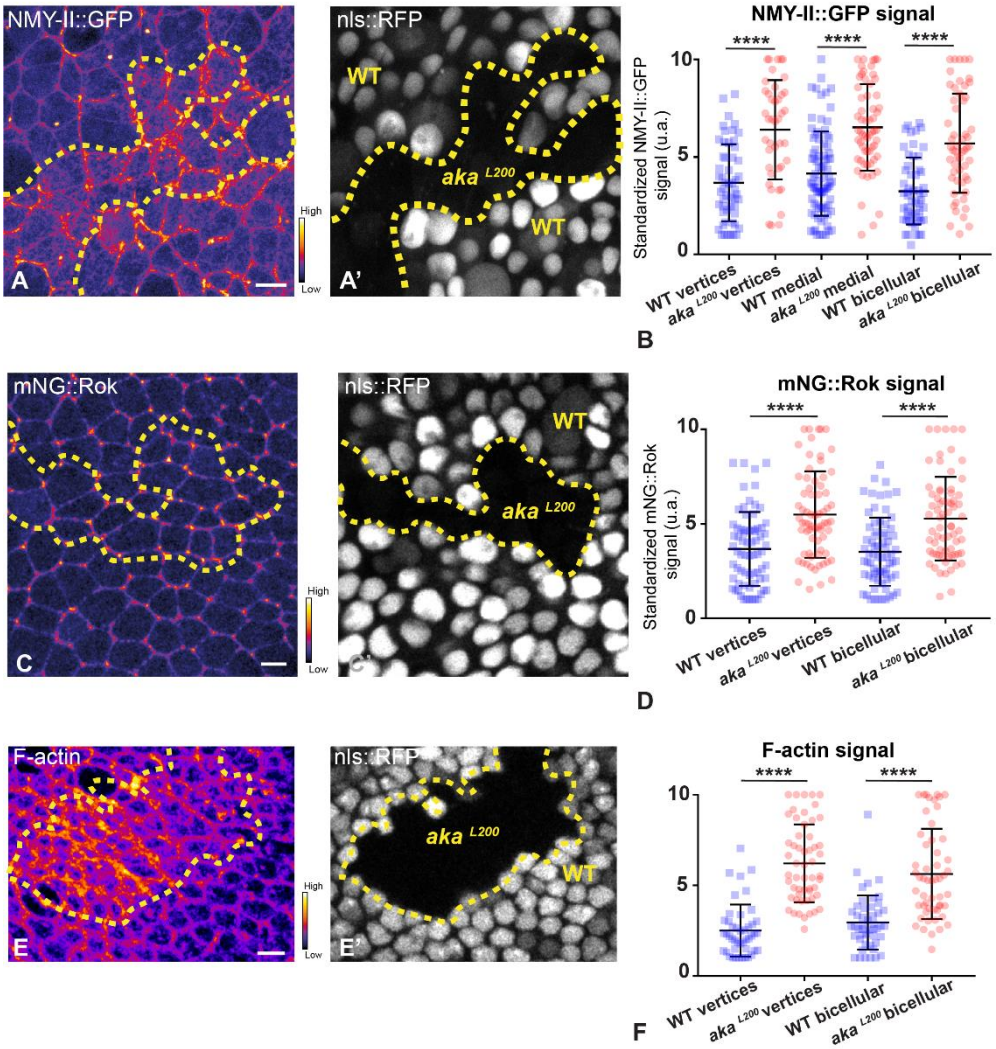

Figure 2: Loss of Anakonda triggers Non-muscle Myosin II and its activator Rho Kinase as well as F-actin enrichment at both bicellular and tricellular junctions. (A-A' and C-C') show *nota* expressing NMY-II::GFP (A, fire color) and mNG::Rok (C, fire color) or stained for F-actin (E, 647 Phalloidin , fire color) between 16h-19h APF, after heat-shock to induce clone of wild type (A' and C', nls::RFP positive) and mutant cells for Aka (A' and C', nls::RFP negative). (A) Localisation of NMY-II::GFP (fire color) in both WT and *aka*^{L200} cells, separated by the dashed yellow line. (A') Clones of WT and *aka*^{L200} cells revealed by nls::RFP marking. (B) Plot of the standardized NMY-II::GFP signal at tricellular and bicellular junctions as well as medial network in wild type (blue squares) and *aka*^{L200} cells (red circles). (n = 54 and 42 vertices and n = 84 and 61 cellular medial networks and n = 55 and 56 bicellular junctions for WT and *aka*^{L200} respectively, n = 5 pupae for each condition). (C) Localisation of mNG::Rok (fire color) in both WT and *aka*^{L200} cells, separated by the dashed yellow line. (C') Clones of WT and *aka*^{L200} cells revealed by nls::RFP marking. (D) Plot of the standardized mNG::Rok signal at tricellular and bicellular junctions in WT (blue squares) and *aka*^{L200} cells (red circles). (n = 70 vertices and bicellular junctions for WT and *aka*^{L200}, n = 5 pupae for each condition). (E) Localisation of F-actin (fire color) in both WT and *aka*^{L200} cells, separated by the dashed yellow line. (E') Clones of WT and *aka*^{L200} cells revealed by nls::RFP marking. (F) Plot of the standardized F-actin signal at tricellular and bicellular junctions in wild type (blue squares) and *aka*^{L200} cells (red circles). (n = 45 and 55 vertices and n = 47 and 54 bicellular junctions for WT and *aka*^{L200} respectively, n = 5 pupae for each condition). Bars show Mean ± SD, **** $p < 0.0001$, Mann-Whitney test. A calibration bar shows LUT for grey value range. The scale bars represent 5µm.

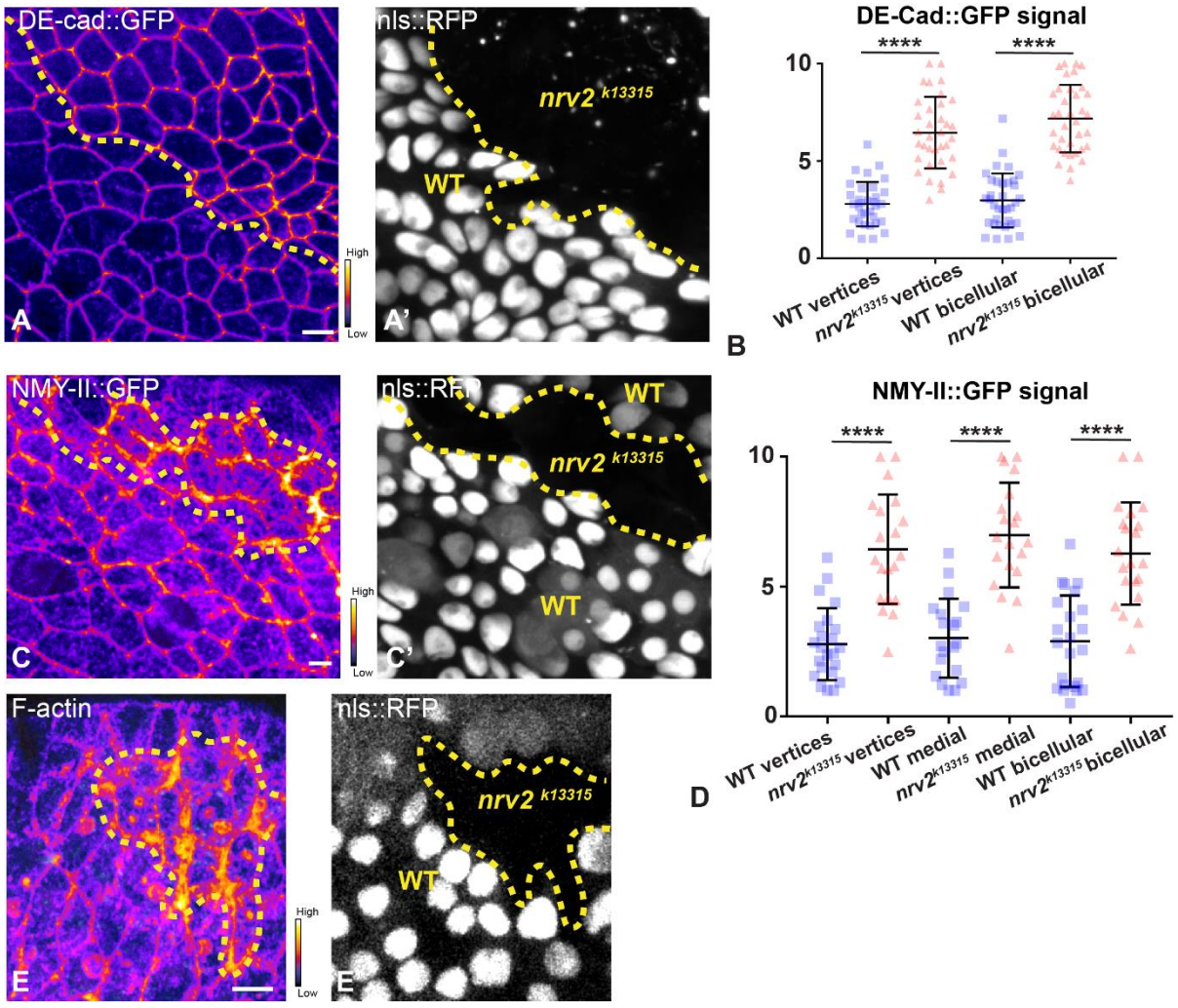

Figure 3: Loss of Nervana 2 phenocopies loss of Anakonda on DE-Cadherin and acto-myosin cytoskeleton enrichment. (A/A', C/C', E-E') show *nota* expressing DE-Cad::GFP (A, fire color), NMY-II::GFP (C, fire color) or stained for F-actin (E, 647 Phalloidin , fire color) between 16h-19h APF, after heat-shock to induce clone of wild type (A', C' and E', nls::RFP positive) and mutant cells for Nrv2 (A', C' and E', nls::RFP negative). (A) Localisation of DE-Cad::GFP (fire color) in both WT and *nrv2*^{k13315} cells, separated by the dashed yellow line. (A') Clones of WT and *nrv2*^{k13315} cells revealed by nls::RFP marking. (B) Plot of the standardized DE-Cad::GFP signal at tricellular and bicellular junctions in wild type (blue squares) and *nrv2*^{k13315} cells (red triangles). (n = 33 and 35 vertices and n = 35 and 36 bicellular junctions for WT and *nrv2*^{k13315} respectively, 2 pupae for each condition). (C) Localisation of NMY-II::GFP (fire color) in both WT and *nrv2*^{k13315} cells, separated by the dashed yellow line. (C') Clones of WT and *aka*^{L200} cells revealed by nls::RFP marking. (D) Plot of the standardized NMY-II::GFP signal at tricellular and bicellular junctions as well as medial network in wild type (blue squares) and *nrv2*^{k13315} cells (red triangles). (n = 23 and 20 vertices and n = 20 cellular medial networks and n = 23 and 21 bicellular junctions for WT and *nrv2*^{k13315} respectively, n = 2 pupae for each condition). (E) Localisation of F-actin (fire color) in both WT and *nrv2*^{k13315} cells, separated by the dashed yellow line. (E') Clones of WT and *nrv2*^{k13315} cells revealed by nls::RFP marking. Bars show Mean ± SD, **** $p < 0.0001$, unpaired t test. A calibration bar shows LUT for grey value range. The scale bars represent 5µm.

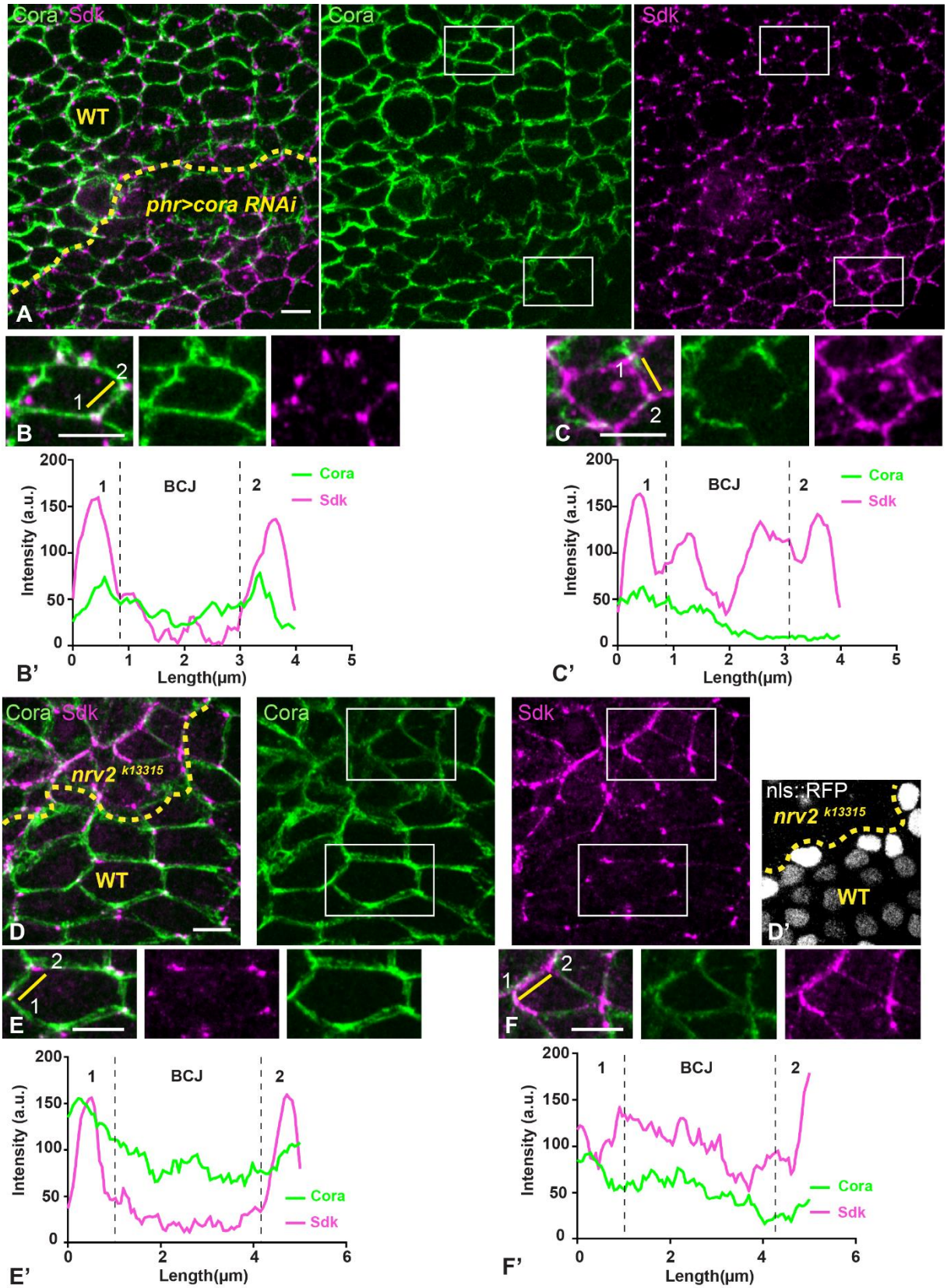
Cora Sdk
WT
phr>cora RNAi
A
Cora
Sdk
B
C
1
2
BCJ
Intensity (a.u.)
Length(μm)
Cora
Sdk
B'
C'
nrv2 k13315
D
D'
nls::RFP
E
F
E'
F'

Figure 4: Septate junction defects lead to Sidekick enrichment at the bicellular junction. (A-C and D-F) Localisation of Sdk (anti-Sdk, magenta) in cells marked by Cora (anti-Cora, green) in wild type and cells expressing UAS::*cora*-RNAi under *pnr*-Gal4 control (A-C) or in *nrv2*^{k13315} cells obtained after heat-shock to induce clones (D-F). The dashed yellow line separates WT and Cora-RNAi cells (A) or WT and *nrv2*^{k13315} cells as revealed by (D and D', nls::RFP negative). Sdk is highly enriched at the BCJ upon knock-down of Cora (A and C) or loss of Nrv2 (D and F). White squares show (B and C) magnification of wild type and knock-down cells for Cora as well as (E and F) magnification of WT and *nrv2*^{k13315} cells. Yellow lines show the line scan used to obtain (B'/C' and E'/F'), plots representing Cora (green line) and Sdk (magenta line) signals as a function of the length of cell-cell boundary in wild type and *cora*-RNAi cells (B' and C') or WT and *nrv2*^{k13315} cells (E' and F'). The scale bars represent 5µm.

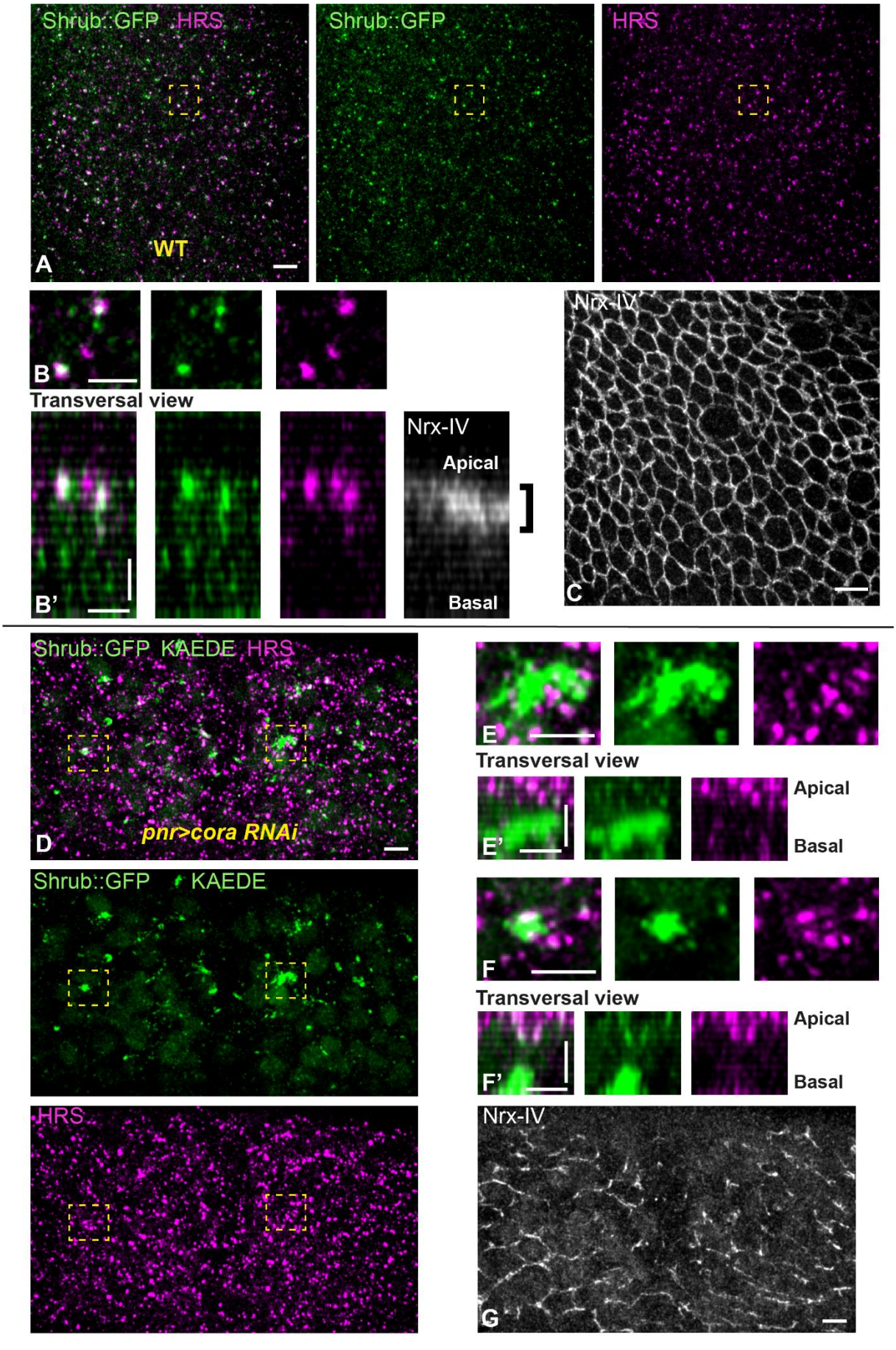
Shrub::GFP HRS
Shrub::GFP
HRS
WT
A
B
Transversal view
B'
Nrx-IV
Apical
Basal
C
Shrub::GFP KAEDE HRS
pnr>cora RNAi
D
Shrub::GFP KAEDE
HRS
E
Transversal view
E'
Apical
Basal
F
Transversal view
F'
Apical
Basal
Nrx-IV
G

Figure 5: Septate junction defects are associated with increased number of HRS positives vesicles and ESCRT III protein Shrub aggregates. (A-G) Localisation of Shrb::GFP + GFP antibody (green), KAEDE (D) in cells marked by Nrx-IV (anti-Nrx-IV, grey) and HRS (anti-HRS, magenta) in wild type and cells expressing UAS::*cora*-RNAi and UAS::KAEDE under *pnr*-Gal4 control. (A-C) Localisation of Shrb::GFP + GFP antibody and HRS in a WT area (KAEDE negative and regular Nrx-IV signal in (C)) in a planar view (A, B and C) or in a transversal view (B'). Yellow dashed square shows (B and B') magnification of wild type cell with colocalisation between Shrb::GFP and HRS at SJ level showed by Nrx-IV in the transversal view. (D-G) Localisation of Shrb::GFP + GFP antibody and HRS in cells expressing UAS::*cora*-RNAi and UAS::KAEDE under *pnr*-Gal4 control (KAEDE positives and Nrx-IV reduced signal in (G)) in a planar view (D, E, F and G) or in a transversal view (E' and F'). Yellow dashed squares show (E-F') magnification of cells with partial or no colocalisation between Shrb::GFP and HRS as well as aggregates of Shrb::GFP surrounded by HRS staining. The scale bar represents 5µm (A, B, C, D, E, F and G) and 2.5µm in (B', E' and F').

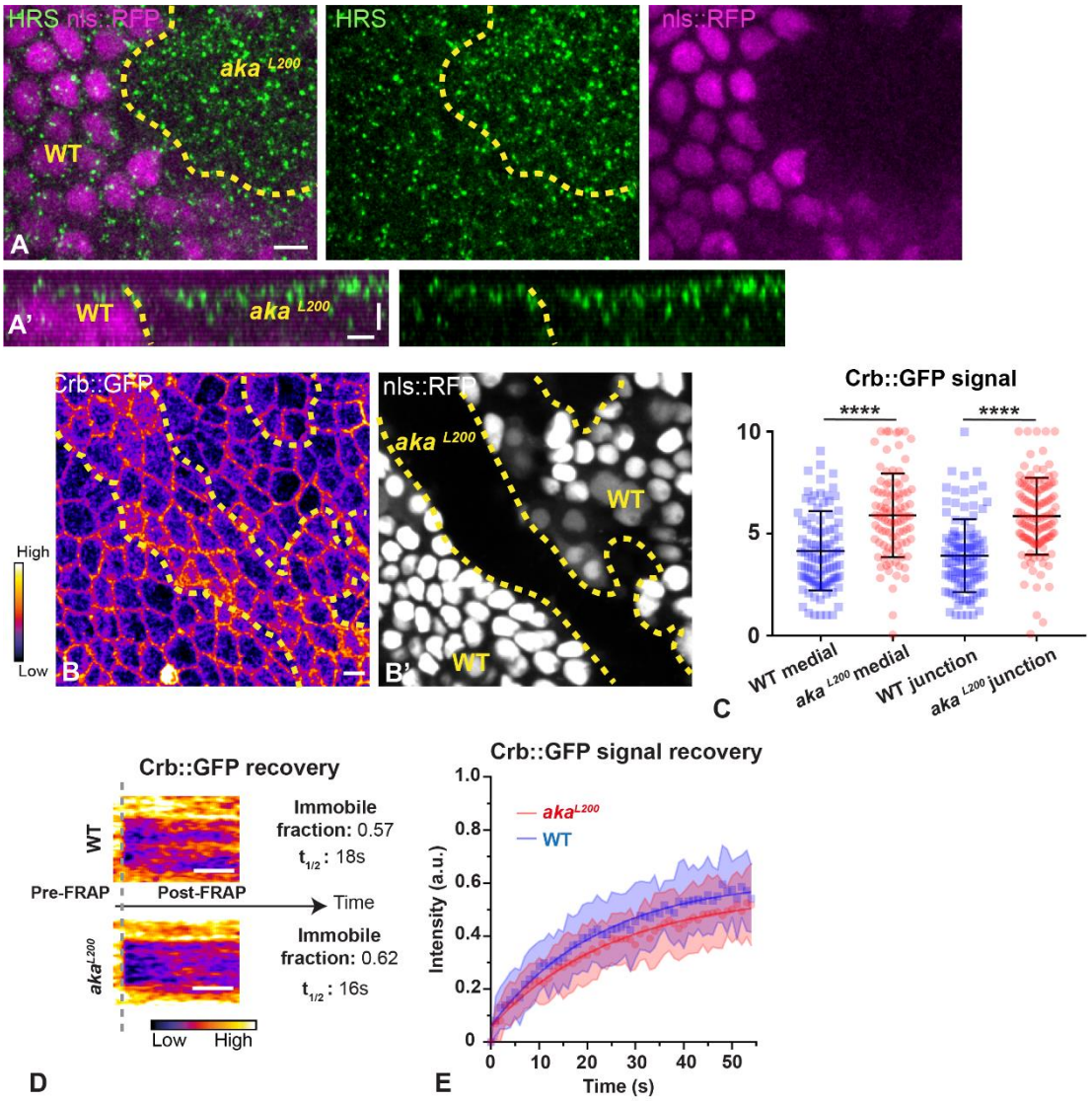

Figure 6: Loss of Anakonda triggers increased number of HRS positives vesicles associated with higher level of Crumbs at both junctional and medial part of the cell. (A-B') show *nota* stained for HRS (A-A', anti-HRS, green) or expressing Crb::GFP (B fire color), between 16h-19h APF, after heat-shock to induce clone of wild type (A, A' and B', nls::RFP positive) and mutant cells for *aka*^{L200} (A, A' and B', nls::RFP negative). (A) Localisation of HRS (green) in both WT and *aka*^{L200} cells, separated by the dashed yellow line. Clones of WT and *aka*^{L200} cells revealed by nls::RFP marking (magenta). (A') Transversal view of (A). (B) Localisation of Crb::GFP (fire color) in both WT and *aka*^{L200} cells, separated by the dashed yellow line. (B') Clones of WT and *aka*^{L200} cells revealed by nls::RFP marking. (C) Plot of the standardized Crb::GFP signal at the medial and junctional part of the cell in wild type (blue squares) and *aka*^{L200} cells (red circles). (n = 100 and 96 cellular medial networks and n = 110 and 119 junctions for WT and *aka*^{L200} respectively, n = 5 pupae for each condition). Bars show Mean ± SD, **** $p < 0.0001$, Mann-Whitney test. (D) Kymographs of the bleached region for Crb::GFP in wild type and *aka*^{L200} junction's cells. Scale bars show 20s. (E) Plot of Crb::GFP fluorescence recovery as a function of time for the conditions described in (D). WT: n = 23 FRAP experiments, 3 pupae; *aka*^{L200}: n = 24 FRAP experiments, 3 pupae. Data are mean ± SD. Solid line shows a simple exponential fit. Blue square and red circles represent WT and *aka*^{L200} time point values. A calibration bar shows LUT for grey value range. The scale bar represents 5µm (A and B) and 2.5µm in (A').

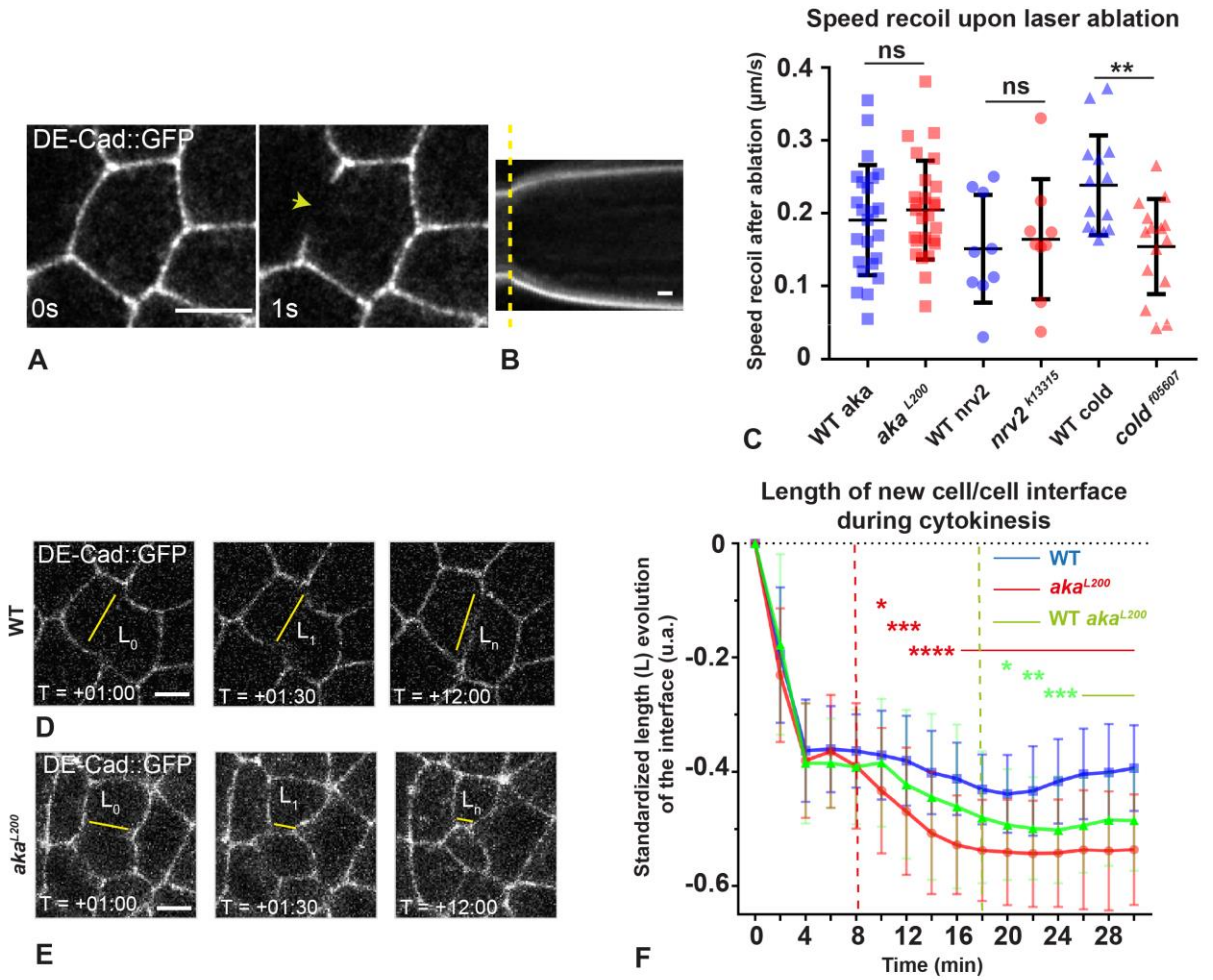

Figure 7: Mechanical forces are perturbed upon bSJ and tSJ junction defects. (A) Bi-photonic laser-based nano ablation example of AJ in cells expressing DE-Cad::GFP (white). Yellow arrowheads show the ablation area. (B) Kymograph of the ablation area depicted in (A) showing vertices recoil upon ablation. Scale bar shows 5s. (C) Plot of the mean recoil speed upon laser-based nano ablation for wild type (blue squares, circles and triangles) and *aka*^{L200} (red squares), *nrv2*^{k13315} (red circles) and *cold*^{f05607} (red triangles) cells respectively. (D-E) Cytokinesis of *notum* cells expressing DE-Cad::GFP at 16h APF, after heat-shock to induce clone of wild type (D) and mutant cells for *aka*^{L200} (E). Time is min:sec with T=0 corresponding to the Anaphase onset. L represents the length of the new cell/cell interface. (F) Plot of the mean length interface at each corresponding time points. Wild type situation is represented by blue squares, a WT cell dividing with one WT neighbour and one *aka*^{L200} is represented by green triangles and a complete *aka*^{L200} situation is represented by red circles. Bars show Mean ± SD, * $p < 0.05$, ** $p < 0.005$, *** $p = 0.0001$, **** $p < 0.0001$, unpaired t test and Mann-Whitney test. The scale bars represent 5µm.

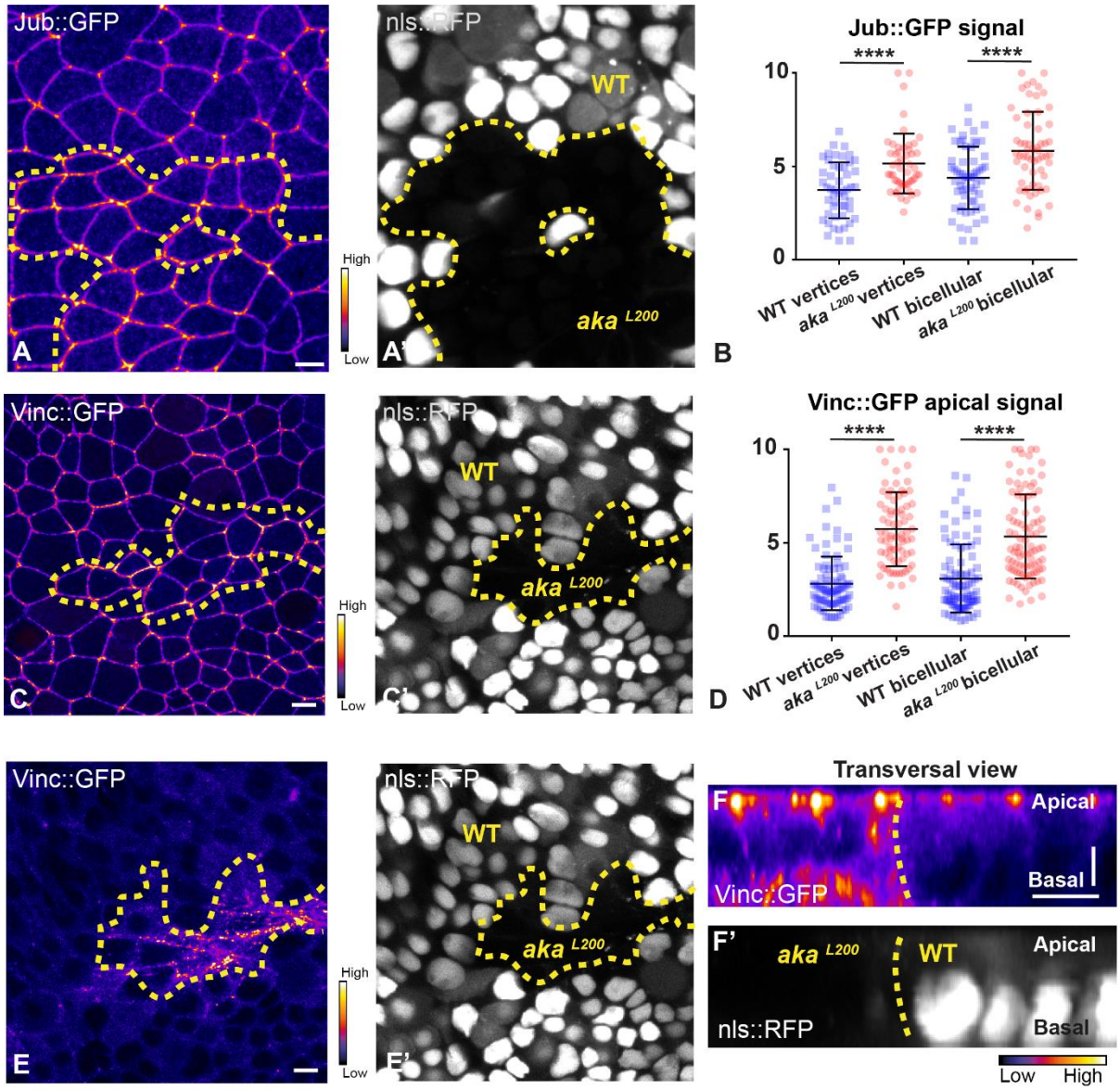

Figure 8: Loss of Anakonda leads to Hippo/YAP pathway component Ajuba and the tension sensible protein Vinculin enrichment at the bicellular and tricellular junctions. (A/A', C/C', E-F') show *nota* expressing Jub::GFP (A, fire color) or Vinc::GFP (C, E and F, fire color) between 16h-19h APF, after heat-shock to induce clone of wild type (A', C', E' and F', nls::RFP positive) and mutant cells for Aka (A', C', E' and F', nls::RFP negative). (A) Localization of Jub::GFP (fire color) in both wild-type and *aka*^{L200} cells, separated by the dashed yellow line. (A') Clones of wild-type and *aka*^{L200} cells revealed by nls::RFP marking. (B) Plot of the standardized Jub::GFP signal at tricellular and bicellular junctions in wild type (blue squares) and *aka*^{L200} cells (red circles). (n = 50 vertices and n = 60 bicellular junctions for wild-type and *aka*^{L200} respectively, n = 2 pupae for each condition). (C, E and F) Localization of Vinc::GFP (fire color) in both wild-type and *aka*^{L200} cells, at apical (C) and basal level (E) in a planar view or in a transversal view (F), separated by the dashed yellow line. (C', E' and F') Clones of wild-type and *aka*^{L200} cells revealed by nls::RFP marking. (D) Plot of the standardized Vinc::GFP signal at tricellular and bicellular junctions in wild type (blue squares) and *aka*^{L200} cells (red circles). (n = 84 and 76 vertices and n = 92 bicellular junctions for wild-type and *aka*^{L200} respectively, n = 4 pupae for each condition). Bars show Mean ± SD, **** $p < 0.0001$, unpaired t test and Mann-Whitney test. A calibration bar shows LUT for grey value range. The scale bars represent 5µm.

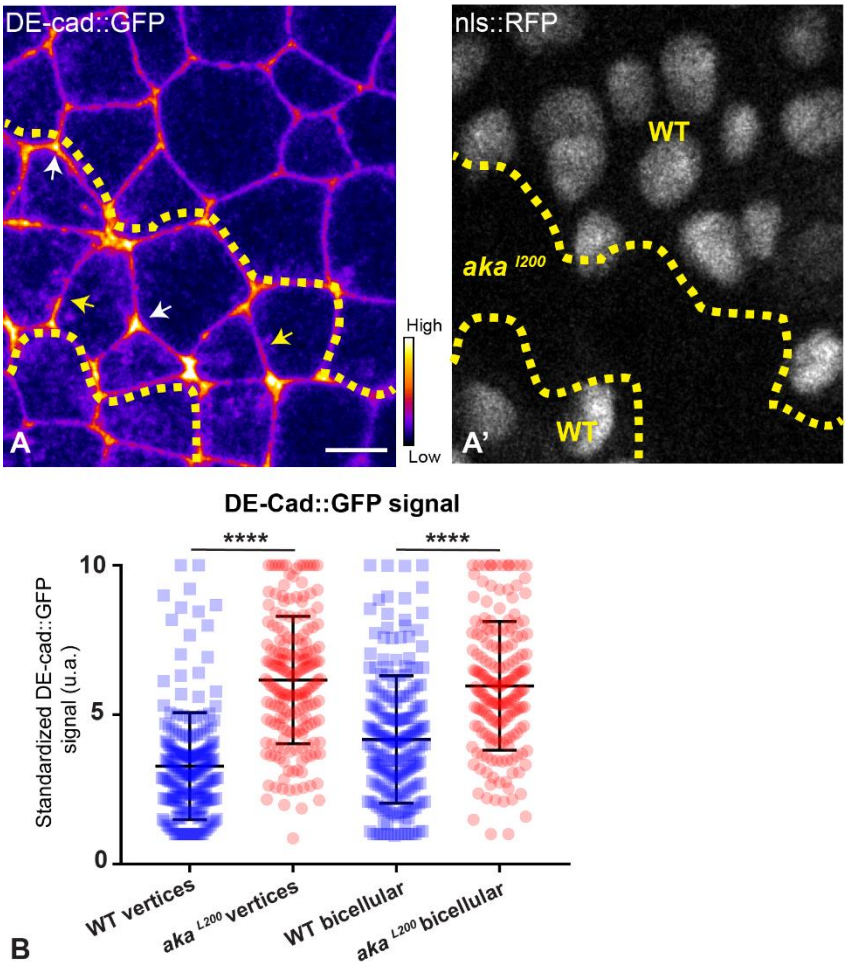

Figure S1: Loss of Anakonda triggers DE-Cadherin enrichment at both bicellular and tricellular junctions. (A-A') show *nota* expressing DE-Cad::GFP (A, fire color) between 16h-19h APF, after heat-shock to induce clone of wild type (A', nls::RFP positive) and mutant cells for Aka (A', nls::RFP negative). (A) Localisation of DE-Cad::GFP (fire color) in both WT and *aka*^{L200} cells, separated by the dashed yellow line. White and yellow arrows show DE-Cad::GFP enrichment at both vertices and bicellular level. (A') Clones of WT and *aka*^{L200} cells revealed by nls::RFP marking. (B) Plot of the standardized DE-Cad::GFP signal at tricellular and bicellular junctions in wild type (blue squares) and *aka*^{L200} cells (red circles). (n = 201 and 193 vertices and n = 208 and 188 bicellular junctions for WT and *aka*^{L200} respectively, > 5 pupae for each condition). Bars show Mean ± SD, **** $p < 0.0001$, Mann-Whitney test. A calibration bar shows LUT for grey value range. The scale bar represents 5µm.

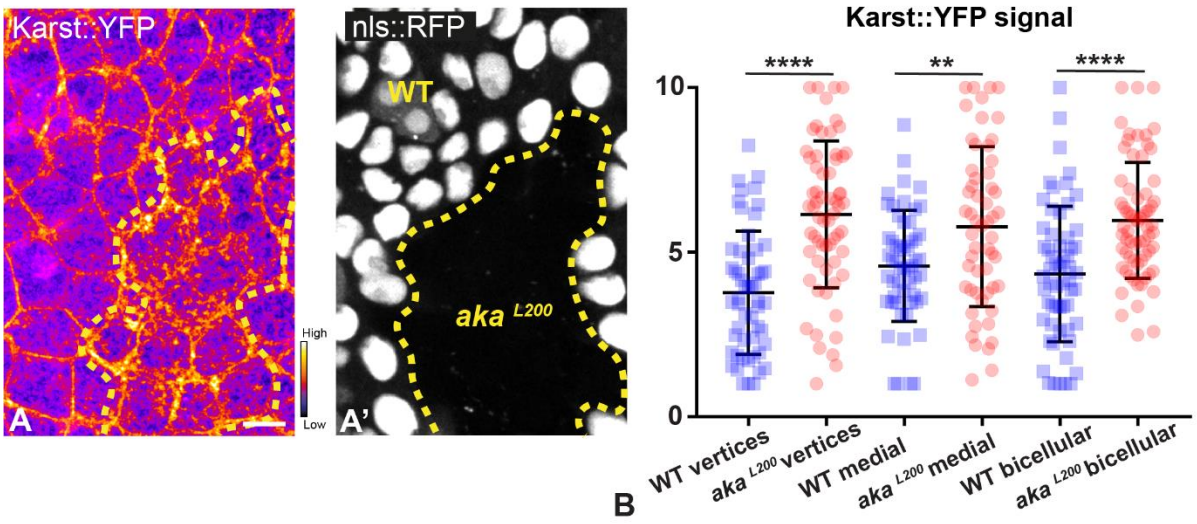

Figure S2: Loss of Anakonda leads to the scaffold protein β-Heavy Spectrin Karst enrichment at the bicellular and tricellular junctions. (A/A', C/C') show *nota* expressing Karst::YFP (A, fire color) or stained for Cno (C, anti-Cno) between 16h-19h APF, after heat-shock to induce clone of wild type (A' and C', nls::RFP positive) and mutant cells for Aka (A' and C', nls::RFP negative). (A) Localisation of Karst::YFP (fire color) in both WT and *aka*^{L200} cells, separated by the dashed yellow line. (A') Clones of WT and *aka*^{L200} cells revealed by nls::RFP marking. (B) Plot of the standardized Karst::YFP signal at tricellular and bicellular junctions as well as medial network in wild type (blue squares) and *aka*^{L200} cells (red circles). (n = 54 and 64 vertices and n = 55 and 56 cellular medial networks and n = 59 and 68 bicellular junctions for WT and *aka*^{L200} respectively, n = 4 pupae for each condition). Bars show Mean ± SD, ** $p < 0.005$, **** $p < 0.0001$, unpaired t test and Mann-Whitney test. A calibration bar shows LUT for grey value range. The scale bars represent 5µm.

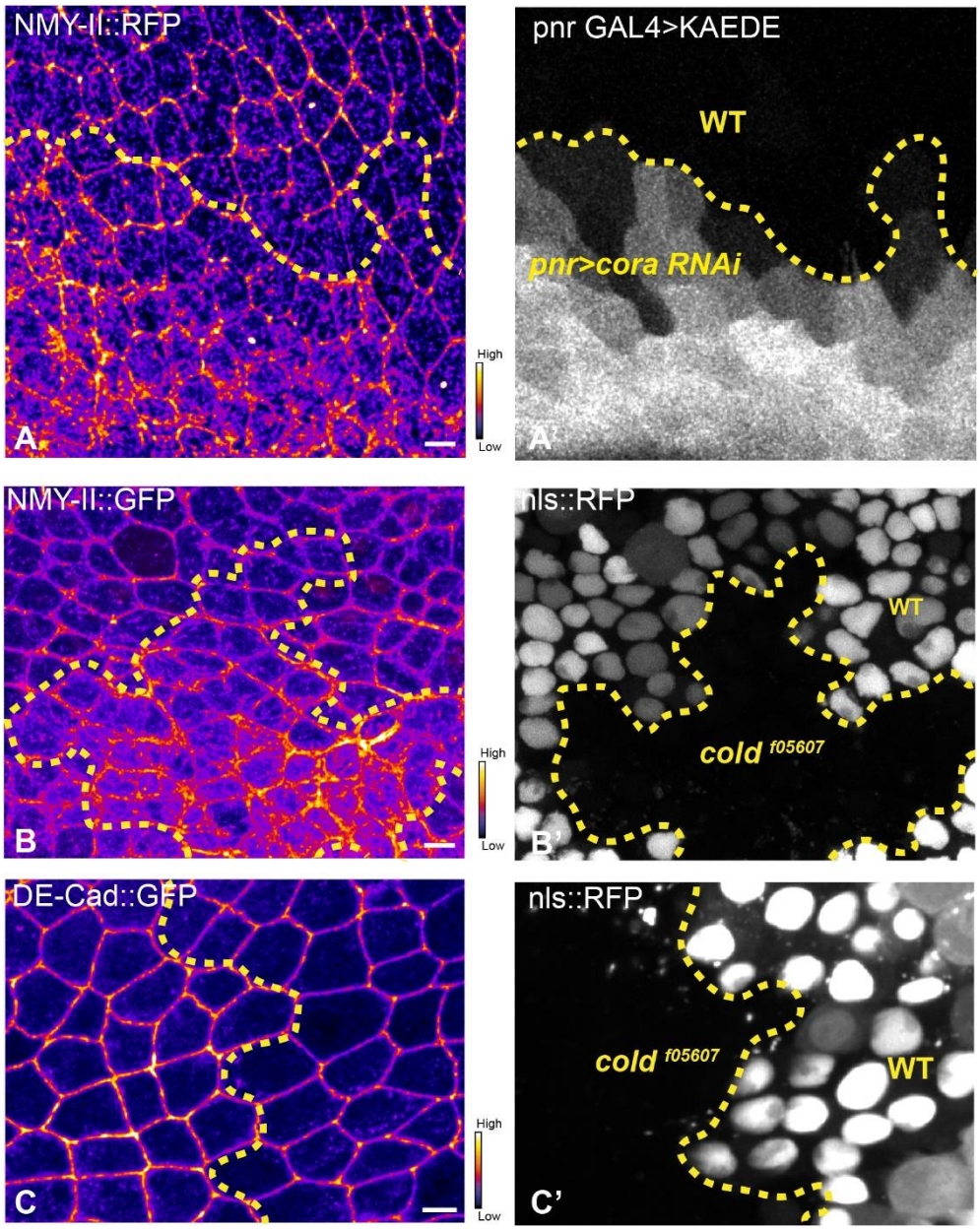

Figure S3: Septate junction defects phenocopy loss of Anakonda and Nervana 2 on DE-Cadherin and Non-muscle Myosin II enrichment. (A, B and C) Localisation of NMY-II::RFP (A, fire color), KAEDE (A', grey), NMY-II::GFP (B, fire color) and DE-Cad::GFP (C, fire color) in cells expressing UAS::*cora*-RNAi under *pnr*-Gal4 control (A) or in *cold*^{f05607} cells obtained after heat-shock to induce clones of wild type (B' and C', nls::RFP positive) and mutant cells for Cold (B' and C', nls::RFP negative). The dashed yellow line separates WT (A', KAEDE negative) and Cora-RNAi cells (A', KAEDE positive) or WT and *cold*^{f05607} cells (B-C'). (A) Localisation of NMY-II::RFP (fire color) in both WT and Cora-RNAi cells, separated by the dashed yellow line. (A') Cells expressing UAS::*cora*-RNAi and UAS::KAEDE under *pnr*-Gal4 control (KAEDE positives) separated by the yellow dashed line from the WT cells (KAEDE negative). (B) Localisation of NMY-II::GFP (fire color) in both WT and *cold*^{f05607} cells, separated by the dashed yellow line. (B') Clones of WT and *cold*^{f05607} cells revealed by nls::RFP marking. (C) Localisation of DE-Cad::GFP (fire color) in both WT and *cold*^{f05607} cells, separated by the dashed yellow line. (C') Clones of WT and *cold*^{f05607} cells revealed by nls::RFP marking. A calibration bar shows LUT for grey value range. The scale bars represent 5µm.

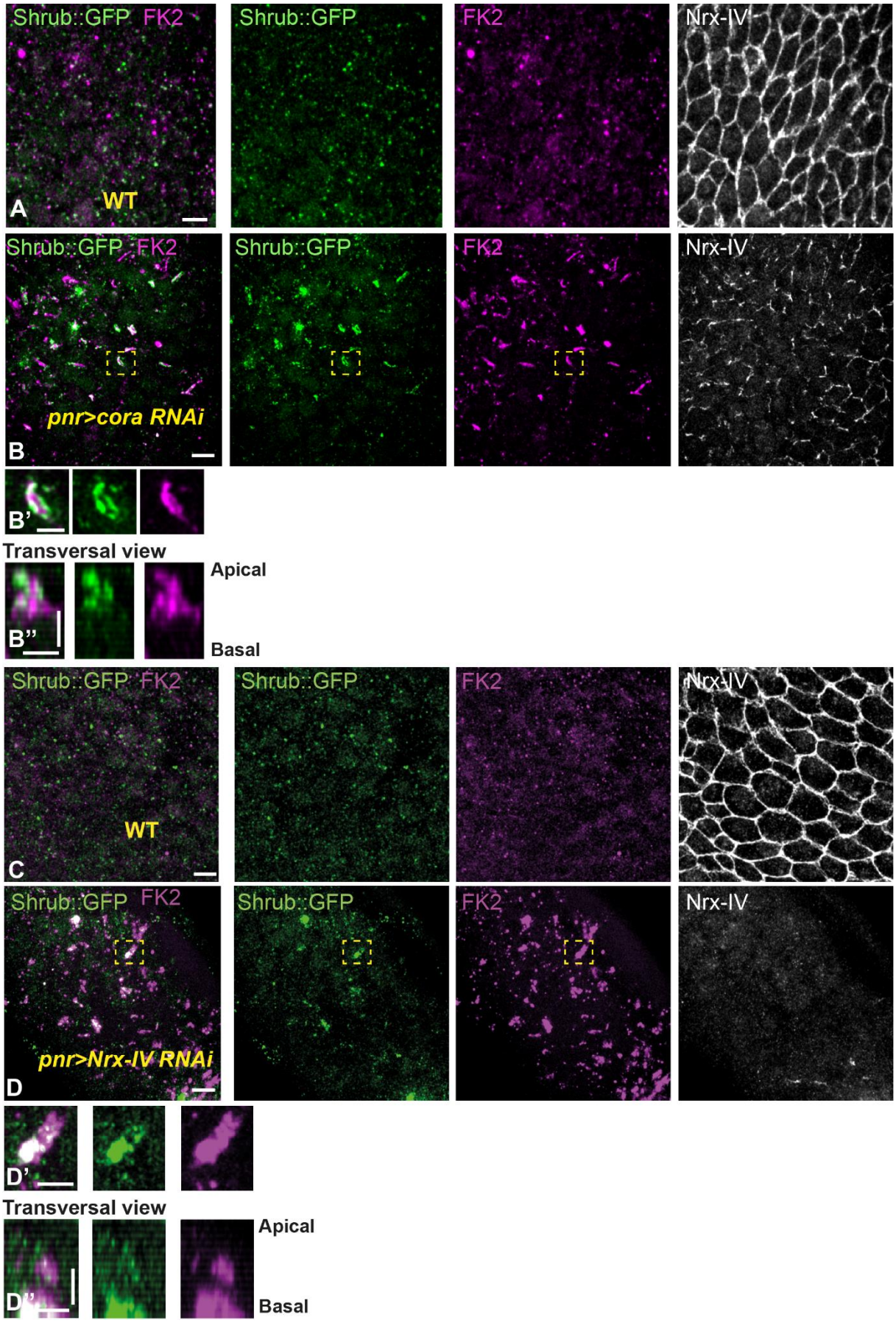
Shrub::GFP FK2
Shrub::GFP
FK2
Nrx-IV
A
WT
Shrub::GFP FK2
Shrub::GFP
FK2
Nrx-IV
pnr>cora RNAi
B
B'
Transversal view
Apical
B''
Basal
Shrub::GFP FK2
Shrub::GFP
FK2
Nrx-IV
WT
C
Shrub::GFP FK2
Shrub::GFP
FK2
Nrx-IV
pnr>Nrx-IV RNAi
D
D'
Transversal view
Apical
D''
Basal

Figure S4: Septate junction defects lead to ESCRT III protein Shrub and ubiquitinylated proteins aggregates. (A-G) Localisation of Shrb::GFP + GFP antibody (green), KAEDE (D) in cells marked by Nrx-IV (anti-Nrx-IV, grey) and FK2 (anti ubiquitinylated proteins, magenta) in wild type and cells expressing UAS::*cora*-RNAi and UAS::KAEDE or only UAS::*Nrx-IV*-RNAi under *pnr*-Gal4 control. (A-B'') Localisation of Shrb::GFP + GFP antibody and FK2 in a WT area (KAEDE negative and regular Nrx-IV signal in (A)) or in cells expressing UAS::*cora*-RNAi and UAS::KAEDE under *pnr*-Gal4 control (KAEDE positives and Nrx-IV reduced signal in (B)). Yellow dashed square shows (B' and B'') magnification of cells with partial or no colocalisation between Shrb::GFP and FK2 as well as aggregates of FK2 surrounded by Shrb::GFP staining in a planar view (B') and transversal view (B''). (C-D'') Localisation of Shrb::GFP + GFP antibody and FK2 in a WT area (regular Nrx-IV signal in (C)) or in cells expressing UAS::*Nrx-IV*-RNAi under *pnr*-Gal4 control (Nrx-IV signal disappearance in (D)). Yellow dashed square shows (D' and D'') magnification of cells with partial or no colocalisation between Shrb::GFP and FK2 in a planar view (D') and transversal view (D''). The scale bar represents 5µm (A, B, B', C, D and D') and 2.5µm in (B'' and D').

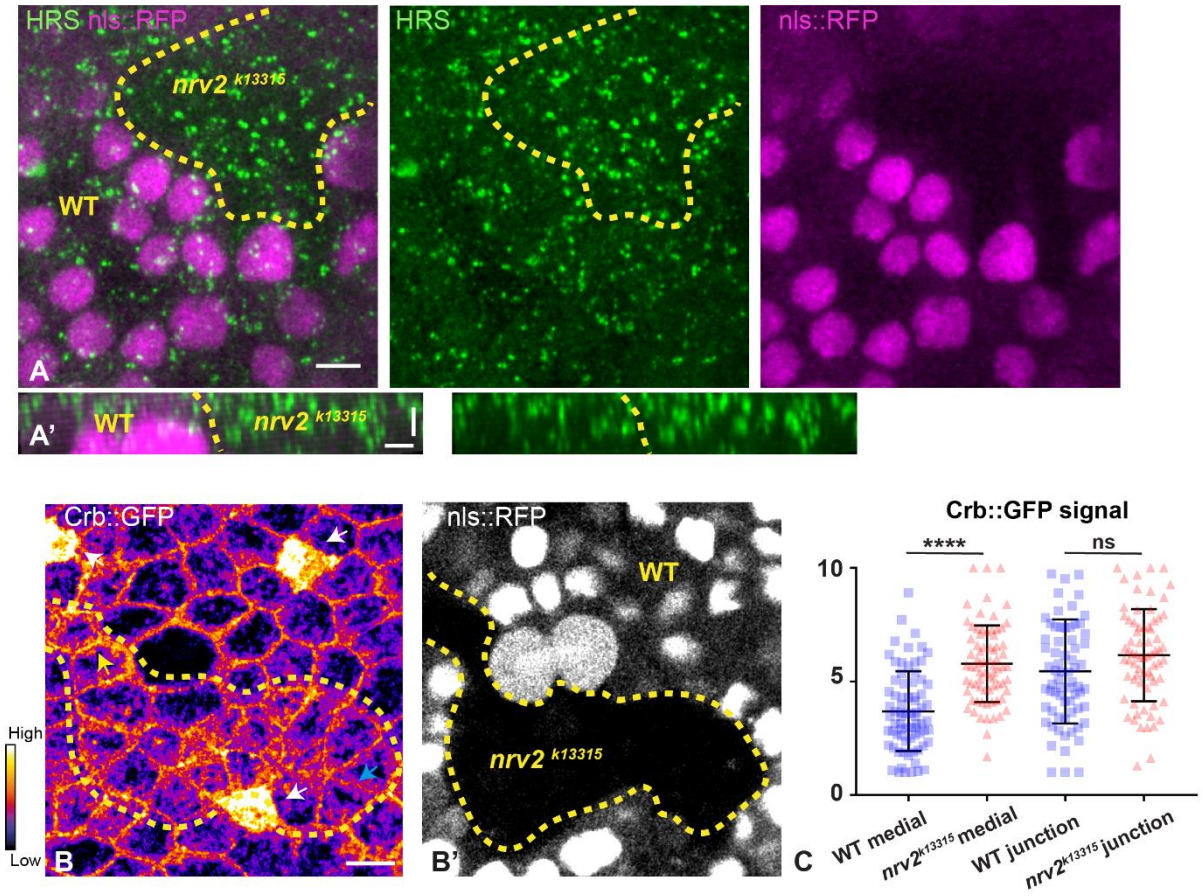

Figure S5: Loss of Nervana 2 triggers increased number of HRS positives vesicles associated with higher level of Crumbs at the medial part of the cell. (A-B') show *nota* stained for HRS (A-A', anti-HRS, green) or expressing Crb::GFP (B fire color), between 16h-19h APF, after heat-shock to induce clone of wild type (A, A' and B', nls::RFP positive) and mutant cells for *nrv2*^{k13315} (A, A' and B', nls::RFP negative). (A) Localisation of HRS (green) in both WT and *nrv2*^{k13315} cells, separated by the dashed yellow line. Clones of WT and *nrv2*^{k13315} cells revealed by nls::RFP marking (magenta). (A') Transversal view of (A). (B) Localisation of Crb::GFP (fire color) in both WT and *nrv2*^{k13315} cells, separated by the dashed yellow line. (B') Clones of WT and *nrv2*^{k13315} cells revealed by nls::RFP marking. White arrows show the strong Crb::GFP enrichment observed in the SOP daughter cells, pIIa and pIIb. Yellow arrow shows enrichment of Crb associate with aggregates. Blue arrow shows less well-defined Crb signal at the junction. (C) Plot of the standardized Crb::GFP signal at the medial and junctional part of the cell in wild type (blue squares) and *nrv2*^{k13315} cells (red circles). (n = 75 cellular medial networks and n = 70 junctions for WT and *nrv2*^{k13315} respectively, n = 3 pupae for each condition). Bars show Mean ± SD, **** $p < 0.0001$, unpaired t test and Mann-Whitney test.

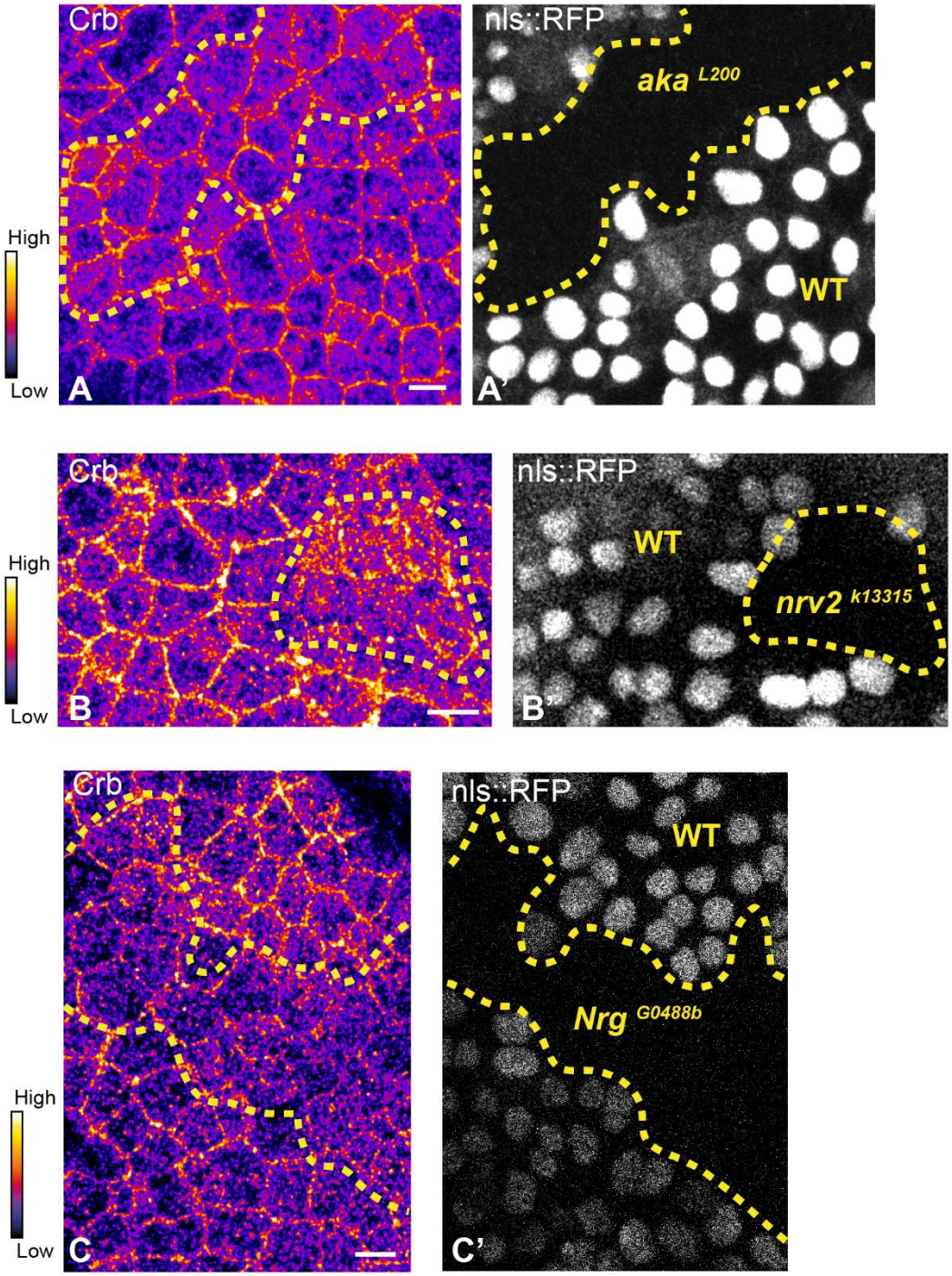

Figure S6: Septate junction defects phenocopy loss of Anakonda and Nervana 2 on Crumbs medial cell network enrichment. (A-C') show *nota*, stained for Crb (anti-Crb, fire color), between 16h-19h APF, after heat-shock to induce clone of wild type (A', B' and C', nls::RFP positive) and mutant cells for *aka*^{L200} (A', nls::RFP negative), *nrv2*^{k13315} (B', nls::RFP negative) and *Nrg*^{G0488b} (C', nls::RFP negative). A calibration bar shows LUT for grey value range. The scale bars represent 5µm.

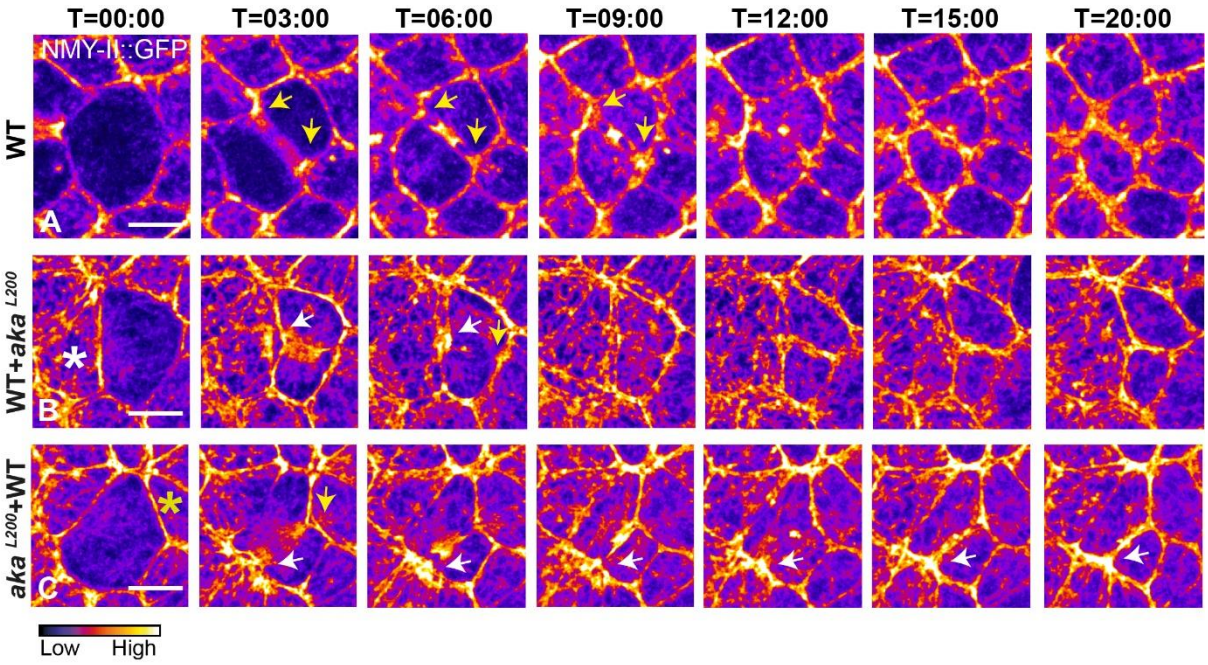

Figure S7: Differential recruitment of Non-muscle Myosin II during cytokinesis in cells mutant for Anakonda. (A-C) Cytokinesis of *notum* cells expressing NMY-II::GFP between 16h-19h APF, after heat-shock to induce clone of wild type and mutant cells for aka^{L200}. (A) Representation of WT cell cytokinesis with recruitment of NMY-II::GFP at the contact between the dividing cell and its neighbours like showed by the yellow arrows. NMY-II::GFP recruitment is symmetrical and synchronous looking at the minute time scale. (B) Representation of a WT cell cytokinesis with recruitment of a higher amount of NMY-II::GFP at the contact with aka^{L200} cell (marked by the asterisk, white arrow for NMY-II::GFP signal) compared to the WT one (yellow arrow). NMY-II::GFP recruitment is asymmetrical in terms of NMY-II::GFP signal intensity.(C) Representation of a aka^{L200} cell cytokinesis with recruitment of a higher amount of NMY-II::GFP at the contact with aka^{L200} cell (white arrow) compared to the WT one (marked by green asterisk, yellow arrow for NMY-II::GFP signal). NMY-II::GFP recruitment is asymmetrical in terms of NMY-II::GFP signal intensity. Time is min:sec with T=0 corresponding to the Anaphase onset. A calibration bar shows LUT for grey value range. The scale bars represent 5µm.

Discussion

Part I. Effect of loss of pSJ on SJ compartment

a. TCJ assembly and tSJ proteins interplay

During my PhD, I have been able to investigate many subjects ranging from deciphering general organisation, remodelling and roles of both pSJs and tSJs on the epithelium integrity with TCJ study as a starting point. All began by describing in time and space the remodelling of both tAJs and tSJs upon cytokinesis, describing similar processes for both AJs and pSJs. Indeed, tAJs are formed prior to the onset of tSJs formation. tSJ proteins are added in close vicinity of the midbody as cytokinesis is occurring and pSJs forming and maturating. In the vertebrates, the analogous of tSJ proteins called Tricellulin and Lipolysis-stimulated lipoprotein receptor (LSR), are also recruited with different timing at the newly formed TCJ (Higashi, Arnold et al. 2016). However, I cannot decipher if these differences between Aka, Gli and M6 are due to stoichiometry divergences at this moment.

Then, I have highlighted the intricate interplay that exists between all three tSJ components. Aka and M6 are referred as the “key” players of tSJ integrity since loss of one of the two leads to the disappearance to every actor from the vertex. However, Aka is required from the three cells adjacent to the vertex which is not the case for M6. Indeed, using the mosaic clonal analysis, I showed that removal of Aka from only one cell adjacent to the vertex leads to total disappearance of M6 enrichment at TCJ but not the opposite. Those results are confirmed by a companion paper (Wittek, Hollmann et al. 2020), where authors demonstrate a cell-autonomous mechanism for M6 restriction activity on Aka at the vertex. Moreover, they show that Aka is still present at BCJ level upon loss of M6, arguing in favour of M6 not being required to target Aka at the plasma membrane but rather to keep it within bounds. Similar results are reported for M6 when Aka is absent. Still, the reason to explain why those proteins target precisely vertex remains unresolved. One explanation suggested by (Byri, Misra et al. 2015) states that vertex selection by Aka could be due to its characteristic morphology with the three repeated domains. Here, one Aka protein from one cell adjacent to the vertex could be in touch with the two other cells with each rerepeated domain apposing to one cell membrane surface. Those contacts would be required and needed to stabilize Aka molecules between them. Therefore, this could be a way to explain differences observe upon loss of Aka *vs* loss of M6 where the last one due to its

relatively small size, could not display such conformational properties. Another explanation might involve specific lipidic composition of the TCJ. Indeed, the cholesterol is known to be required for membrane bending (Evans and Needham 2002). Moreover, the vertebrate orthologous of M6 called GPM6a, is a protein recognized to be associated with lipid-rich domain, which is curved, and to induce filopodia or neurites formation (Lagenaur, Kunemund et al. 1992, Scorticati, Formoso et al. 2011, Formoso, Garcia et al. 2015). Concerning M6 structure, it displays similarities with the family of tetraspanins proteins and those latter target specifically cholesterol enriched domains (van Deventer, Arp et al. 2021). Interestingly, cholesterol enriched domains targeting requires palmitoylation of tetraspanins (van Deventer, Arp et al. 2021) and both *Drosophila* M6 (Strassburger, Kang et al. 2019) and mouse M6a (Honda, Ito et al. 2017) are palmitoylated. Tetraspanins are binding many other different tetraspanins but also other proteins such as integrins or signalling molecules. Hence, vertex might be a specific cholesterol enriched domain which traps M6 and then stabilizes Aka and Gli at TCJ.

I also discover that Gli, although non-essential for Aka recruitment at the vertex, stabilizes Aka and therefore the tSJ complex. Also, LSR is described to be palmitoylated and this lipidic modification is required to specify it at vertex level. In the opposite, depletion of cholesterol in cells leads to LSR disappearance at the vertex (Oda, Sugawara et al. 2020). Hence, it could be interesting to probe if Aka and/or Gli can be palmitoylated and to identify potential cysteine residues, in order to remove them and observe their localisation at the cell membrane. Furthermore, we could not exclude specific trafficking toward vertex. Interesting candidates could be the members of the Ly6 family, such as Crok, Cold and Bou since they have been demonstrated to be involved in pSJ components membrane delivery (Nilton, Oshima et al. 2010). Preliminary data I obtained revealed that Aka spreads at BCJ in *cold* mutant cells, similarly to what I obtained upon knock-down of Cora and Nrx-IV. Therefore, intracellular trafficking could be a way for the cell to directly address tSJ proteins at vertex.

b. tSJ and pSJ proteins interplay

One major question that came to us during this work was to elucidate what could be the impact of the loss of tSJ on pSJ general organisation. I saw that loss of tSJ components is first associated with huge membrane deformations positive for pSJ proteins. I also observed depletion of pSJ proteins from the vertex. In the opposite, impairing pSJ by RNAi knock-down approaches reveal that tSJ actors are no longer restricted at the TCJ and expanded at the BCJ.

Additional results characterize the consequences of loss of Gli on Aka and I observed Aka destabilisation at the vertex probed by FRAP approaches. Gli is a member of the of Neuroligin family (Gilbert, Smith et al. 2001), a set of proteins involved in synapse formations (Zhang, Milunsky et al. 2009) and synaptic transmission (Zhang, Chen et al. 2015, Chanda, Hale et al. 2017). Moreover, recent studies highlight physical interaction between MGDA proteins and Neuroligin (Elegheert, Cvetkovska et al. 2017, Gangwar, Zhong et al. 2017, Kim, Kim et al. 2017). MGDA proteins are composed of six N-terminal Ig domains and one fibronectin type III domain (Litwack, Babey et al. 2004), which look like Nrg organisation, displaying also six N-terminal Ig domains followed by five fibronectin type III domain (Bieber, Snow et al. 1989). MGDA are reported interacting with Neuroligin via their first two Ig domains (Elegheert, Cvetkovska et al. 2017, Gangwar, Zhong et al. 2017, Kim, Kim et al. 2017). Based on these results and knowing that Nrg forms a complex with Cora, ATP-α and Nrx-IV (Genova and Fehon 2003, Banerjee, Sousa et al. 2006), the link between tSJ and pSJ could be Gli binding Nrg. However, which partner of tSJ is binding another one remains a mystery.

Moreover, expressing prematurely Aka and M6 in a tissue devoid of pSJ, (Wittek, Hollmann et al. 2020) highlight the fact that M6 and Aka can still associate at TCJs, which argues in favour of a tSJ complex establishment independent of pSJ proteins. Still, these data reveal the potential link between pSJ and tSJ proteins, where tSJ complex could emerge thanks to its own components but once present at vertex, require interactions with neighbouring pSJ proteins. Hence, tSJ can be imagined as pillar to anchor pSJ strands at vertices.

c. *Drosophila notum* cells reveal sensing of pSJ defects

At this point of my work, I am prone to propose a hypothesis. A striking phenotype that emerges upon loss of tSJ proteins is the pSJ positive membrane deformations. This defect is reminiscent of what has been observed in the context of CrebA mutant in the *Drosophila* salivary glands (Fox and Andrew 2015). CrebA is a transcriptional factor known to regulate secretory pathway component genes as well as cell specific genes involved in the secretion of the cuticle (Fox, Hanlon et al. 2010). Upon loss of CrebA, salivary glands cells display membrane deformations at pSJ level associated with less secreted material in the lumen, displaced organelles and elevated expression of tetraspanins such as Tsp66E. Adding a chromosomal deficiency spanning nine tetraspanin genes to the CrebA mutant, partially rescues the phenotype, suggesting a role for tetraspanins in inducing or maintaining those deformations. Authors state that apically relocalisation of organelles might be a way to compensate for secretory defects upon loss of CrebA. Moreover, they claim that extra-membrane adding specifically at pSJ level could be a way for the cell to cope with the dilution of secretory proteins in the organelles. Sending extra membrane elsewhere allows organelles to concentrate secretory proteins and to maintain their function as much as they could. Then, sending membranes precisely at pSJ provokes deformations without impairing the apical or basal side of the cell, which would be much more deleterious. Therefore, pSJs appear as a membrane supply in the cell which can adapt upon cell deformations.

Later, another study shows similar phenotypes at the level of the BBB (Babatz, Naffin et al. 2018). First, they reveal that the BBB is forming during larval growth thanks to the unfolding of the pre-existing pSJs. Those results are in accordance with the fact that pSJs are the site of large amount of cellular membranes that could adapt during morphogenesis. Secondly, larvae mutant for the protein Moody, which is needed to establish proper pSJ at BBB level, or Nrx-IV, are displaying extra-cellular membranes similarly to the CrebA mutant as well as over-expression of the pSJ protein Nrx-IV in the case of Moody mutant. This argues strongly in favour of cells being able to sense defects either in permeability barrier or pSJ complex defective establishment, leading to compensatory mechanism. This is why I suggest the following hypothesis.

In the tSJ mutant conditions, cells have defective permeability barrier at vertex level where pSJ proteins are no longer present, therefore needed to be repaired. Hence,

cells start to produce more and more pSJ strands in order to add them at the precise localisation. Due to the slow turnover of pSJ proteins like previously described, pSJ components are accumulating at the membrane and start to form aggregates thanks to their *cis/trans* interactions properties. FRAP analysis on these deformations reveal higher immobile fraction which goes hand in hand with increased stability. This compensatory mechanism could be under the control of CrebA and this leads to focus activity of CrebA on pSJ proteins expression.

In order to demonstrate this hypothesis, it could be interesting to check if pSJ genes are over expressed upon loss of tSJ and if CrebA is a binding factor of pSJ genes promoters. However, why only tSJ defects and not pSJ defects lead to such a phenotype stays a mystery. One plausible explanation could be that missing part in pSJ complexes prevent them to form stabilized structures, as shown by FRAP analysis (Oshima and Fehon 2011, Daniel, Daude et al. 2018), which is not the case upon loss of tSJ proteins. Hence, pSJ positive membrane deformations appear only upon loss of tSJ proteins. An alternative explanation could be the fact that pSJs are anchoring at tSJs level and since they look like a fold corrugated layer and since they seem to be a position of high amount of cellular membrane, loss of adhesion at vertex removes the stretching and they appear as membrane deformations upon movements. In this situation, one would predict equivalent quantity of pSJ proteins in both WT anchored context or detached context. However, this explanation seems unlikely based on the observation of their appearance. It takes around 90 min to establish such a deformation and during the process, I did not detect special cell moves. Moreover, I frequently saw strong enrichment of ATP-α or Nrx-IV in those deformations, suggesting higher protein quantities. Quantifying pSJ compounds signal relatively to the pSJ length in WT and tSJ defective cells can be a mean to probe if the overall amount of pSJ proteins is changed.

d. Sensing and continuous reparation of pSJ impair ESCRT machinery functions in pSJ/tSJ mutant cells

Previous studies show similarities between mutant for pSJ/tSJ proteins and the ESCRT-III protein Shrub. Mutant embryos for those proteins display over elongated trachea. Moreover, *Shrub* mutant have defects at pSJ level, both in the trachea and in the *notum* like noticed in the past by our team. Also, *Shrub* mutant cells have Crb

cytoplasmic aggregates, reported responsible for the apical area growth observed in the tracheal cells (Dong, Hannezo et al. 2014). Because we observe Rok and Karst enrichment in *aka* mutant and knowing that Crb regulates Rok (Sidor, Stevens et al. 2020) and is a binding partner of Karst (Medina, Williams et al. 2002), we hypothesize that pSJ/tSJ defects are impairing Shrub activity, leading therefore to Crb defects at apical level.

Still concerning the compensatory mechanism hypothesis, it could be the cause of the ESCRT complex defects observe in this situation. Like mentioned earlier, a recent work demonstrates that pSJ proteins traffic to the apico-lateral membrane requires both the activity of the Retromer and ESCRT complexes (Pannen, Rapp et al. 2020). In the wing discs, they observe upon loss of Shrub, disappearance of the pSJ protein Mega from the lateral membrane. It is found stuck in baso-lateral endosomal compartment along with Retromer component Vps35. Indeed, retromer complex apical localisation and mobility are under the control of Shrub. Moreover, blocking the Clathrin Heavy Chain, they report Mega accumulation at the basal part of the lateral membrane, showing that pSJ component are dragged basally prior to their internalisation for endocytosis. Coupled to the fact that pSJ proteins are delivered apically, these results argue in favour of transcytosis of pSJ components, similarly to what have been described in (Tiklova, Senti et al. 2010) and in accordance with the model of pSJ proteins operating treadmill mechanism in the *notum* like showed in (Daniel, Daude et al. 2018). Therefore, one could imagine ESCRT-III protein Shrub highjacked by the need of addressing continuously new pSJ proteins, therefore being unable to fulfil its entire role in the cell. In return, this can triggers Retromer complex defects, therefore Crb irregularities at apical level since it relies on Retromer activity in *Drosophila* wing discs to be properly addressed (Pocha, Wassmer et al. 2011). However, this does not explain clearly why Shrub and polyubiquitinylated proteins aggregates appear as well as higher number of HRS positives vesicles.

HRS is a member of the complex ESCRT-0 and resides on early endosomes thanks to Phosphatidylinositol-3-phosphate link. When ubiquitinylated cargoes arrive at early endosomes, HRS recognizes and clusters them at this location, followed by the recruitment of ESCRT-I and ESCRT-II components which also recognize ubiquitinylated cargoes, conducting to the creation of Multivesicular Bodies (MVBs).

Then, ESCRT-III components perceive ESCRT-II density, establish spiralling filaments and perform the scission of the membrane, leading to the creation of intraluminal vesicles which contain the cargoes destined to lysosomal degradation. During this process, HRS and other ESCRT-I/II proteins are relieved from the maturating bud (Cullen and Steinberg 2018). Hence, we could imagine that if Shrub is not able to execute its scission roles at MVBs level, HRS could not leave the degradative vesicles and this could explain the increased amount and bigger size of HRS vesicles observed in pSJ/tSJ mutant cells. Even more, we could imagine that increased amount of pSJ proteins is associated with higher degradative rate, therefore more numerous HRS positive vesicles. Based on this hypothesis of continuous and sustained degradation, endo-lysosomes could be under pressure as well, accumulating protein aggregates. This might be due to the specific organisation of the pSJ components which establish particularly stable complexes. Protein aggregates gathering in endo-lysosomes are a known cause of endo-lysosomes damages (Bohannon and Hanson 2020). Those damages are compensated by the action of the ESCRT complex proteins, notably the ESCRT-III protein CHMPB4, the vertebrate orthologous of Shrub (Skowyra, Schlesinger et al. 2018). Therefore, in SJ defects case, endo-lysosomes are accumulating huge number of poly-ubiquitinylated proteins targeted for degradation, disrupting integrity of the degradative compartments and leading to the recruitment of Shrub for vesicular membrane reparation. Reparation of endo-lysosomes is analogous to plasma membrane repair in a way that they are both relying on ESCRT machinery (Jimenez, Maiuri et al. 2014, Scheffer, Sreetama et al. 2014). However, I did not detect specific Shrub enrichment at pSJ level, arguing more in favour of repairing endo-lysosomes rather than plasma membrane. Still, all those data suggest defects of ESCRT machinery which might explain the defects observe on Crb signal.

e. Crb irregularities are responsible for part of apical domain remodelling of the cell in pSJ/tSJ mutant cells

We looked at Crb in both pSJ/tSJ mutant cells and observed increased signal of Crb at apical level. This enrichment is shown similarly at the medial part of the cell in pSJ and tSJ mutants but only *aka* mutant cells display significative Crb enrichment at the junctional level. However, Crb dynamics is unchanged in tSJ mutant cells. Still, Crb enrichment prompted us to hypothesize Crb stability or trafficking defects, although not

revealed by FRAP analysis. Those Crb defects are quite interesting since they could be a good reason for explaining enrichment of mNG-Rok and Karst in the pSJ/tSJ mutant cells. Indeed, like previously mentioned, Crb is required for mNG-Rok turnover control at cell junctions and is a known binding partner of the β-heavy Spectrin Karst. Moreover, mNG-Rok activates the ERM protein Moesin which linked the cell membrane to the actin cortex (Matsui, Maeda et al. 1998). Moesin is binding Crb via its FERM domain (Thompson, Pichaud et al. 2013). Because Moesin is implied in constructing a rigid cortical actin, leading for example to the rounding of the cell during mitosis (Carreno, Kouranti et al. 2008, Kunda, Pelling et al. 2008), the enrichment of both Crb and mNG-Rok could explain why F-actin enrichment is observed in those mutant cells. Therefore, looking directly at Moesin in *aka* mutant situation would be really informative. Another link between Crb and the acto-myosin cytoskeleton might be explained thanks to its interaction with the RhoGEF Cysts (Silver, Wirtz-Peitz et al. 2019). Indeed, loss of Cysts leads to AJ integrity disruption like observed upon loss of Crb in *Drosophila* embryos. Authors then show that Cysts is recruited at the apical membrane via Crb complex and Baz and then, activates Rho1 which can stabilise acto-myosin cytoskeleton at the AJ level. Therefore, Crb enrichment in tSJ/pSJ mutant situation might stabilise acto-myosin as well in the *notum*.

One last hypothesis to explain Crb defects in pSJ/tSJ mutant cells is based on its links with pSJ proteins. Indeed, Yurt at late stage of embryogenesis is binding Crb in order to regulate its activity and preventing apical domain overgrowth (Laprise, Beronja et al. 2006, Laprise, Lau et al. 2009, Gamblin, Hardy et al. 2014). This could be a potential explanation for the differences observed in Crb enrichment at junctional level between pSJ and tSJ mutants. In the case of *aka* mutants, they are large membrane deformations associated with enrichment of pSJ components. Yurt is also enriched in these deformations (data not shown). Also, I demonstrated that these deformations can be found apically. Hence, enriched Yurt at apical level could explain the Crb enrichment observed in *aka* mutant. Looking at potential colocalisation between the two will reveal if such events are occurring. On the contrary, in pSJ mutants, pSJ proteins signals are reduced at membrane and this could lead to less Crb at the junction. However, this does not explain the Crb accumulation in the medial part of the cell in both pSJ/tSJ defects context. This is why I propose the model where defects into trafficking machinery explain Crb accumulation, at least in part, in the medial part

of the cell. That would mean different subpopulations of Crb that do not behave in the same manner at apical level.

Then, I continued to explore links and roles that could exist between tSJ components and their upper neighbours from AJ.

Part II. Effect of loss of SJ on AJ compartment / cell mechanics

The principal tAJ protein Sdk is not disappearing from the vertex upon loss of Aka but rather enriched at the BCJ. tSJ impairments are not dissociated from pSJ defects. This is why I tested if Sdk enrichment at BCJ is only due to loss of Aka. In a similar manner to tSJ defects, pSJ deficiencies lead to Sdk enrichment at BCJ. To our knowledge, it is the first time that loss of pSJ/tSJ is shown to trigger such defects in *Drosophila notum*. This prompts us to explore potential AJ defects upon loss of both tSJ or pSJ proteins. Hence, upon loss of Aka, I showed enrichment of DE-Cad, NMY-II and its activator Rok, F-actin, Karst, the Hippo/YAP pathway protein Jub and Vinc enrichment at BCJ and TCJ levels. I observed similar DE-Cad, NMY-II and F-actin enrichment upon loss of pSJ proteins, giving credit to the idea that pSJ defects might be a cornerstone for AJ remodelling. However, I cannot discriminate clearly now if AJs defects are direct consequences of tSJ or pSJ impairments.

a. Putative roles of Sdk during cell cytokinesis

A study in *Drosophila* male genitalia reveals the defect of four ways junction's resolution and subsequent junction growth upon loss of Sdk (Uechi and Kuranaga 2019). Interestingly, they look at cases where one vertex is mutant for Sdk and not the other and demonstrate the defect on junctional growth. Even more interestingly, the Sdk presence at vertex is required to accumulate NMY-II responsible for the junctional growth. In my first paper, I showed that Sdk signal appearance at new tAJ is around 10 min after anaphase onset. Curiously, defects on length of new cellular junctions in *aka* mutant context start to be significative around 10 minutes after the anaphase onset. I did not observe absence of Sdk upon loss of Aka but its enrichment at BCJ, suggesting at least some defects. Since Sdk seems to be required to promote junctional growth during cellular contact rearrangement, we could infer that loss of Aka

impairs proper functions of Sdk, leading to cell-cell shrinkage. However, qualitative preliminary results show higher NMY-II signal at neighbouring side mutant for Aka compare to the WT side during cytokinesis. Since the beginning of NMY-II recruitment is around 3 min after anaphase onset and that Sdk arrives only at 10 min, the cell-cell reduced interface might be only due to uncoordinated NMY-II activity in neighbouring cells. It could also be that Sdk adds another layer of resistance to pulling forces during cytokinesis when it appears at forming tAJs. One way to explore a possible explanation for this shrinkage defect might be to look at Sdk recruitment in time and space upon loss of Aka. Even if it is present at vertex and shows no dynamic differences in *aka* mutant context, it still could be impaired specifically during cytokinesis. Hence, I predict an active role of Sdk, calling for the analysis of cytokinesis in *sdk* mutant cells. Another hypothesis could infer that the contraction of the acto-myosin ring is increased in this situation, exerting higher pulling forces which prevents neighbouring cells to respond properly, therefore leading to the new interface shrinkage. Why such extra pulling forces can occur remain unknown at the time being.

b. tAJs are hot spots of tension in the *notum*

Additional results I did not mentioned, show differences in the establishment of new tAJs in *aka* mutant conditions. The typical case leads to the formation of two new tAJs at a certain distance from pre-existing vertices. On the contrary, a significant proportion of the new tAJs in *aka* mutant cells formed in close vicinity or almost directly at the position of a previously formed tAJ. Furthermore, both my work and previous studies have highlighted enrichment of acto-myosin and its regulators at vertices. Mathematical models qualify TCJ as tension hot spots too (Farhadifar, Roper et al. 2007, Trichas, Smith et al. 2012). In vertebrates, the F-actin binding protein Vinc is enriched at vertices and its amount increased upon raised tension (Yonemura, Wada et al. 2010, Higashi, Arnold et al. 2016). Also, during *notum* epithelial cell cytokinesis, if the cleavage furrow is facing a neighbouring vertex, the neighbouring cell deformation controlled by the acto-myosin ring contraction is less strong than in the opposite side devoid of vertex. In this situation, the acto-myosin ring is flattened which is not the case in “regular” situation, suggesting that vertices are resisting strongly to the pulling forces of the ring (Founounou, Loyer et al. 2013). All of that argue strongly in favour of TCJ being a high-tension location in the tissue. Hence, we could imagine

that cells deficient for Aka try somehow to compensate the ring extra pulling forces or the less strong neighbouring response during cytokinesis by creating new tAJs directly at positions known to respond efficiently to forces, namely TCJs. A good way to justify this mechanism would be to observe if the junctional length of the new cell-cell interface is restored in this situation. However, because TCJs are also known to orient cell division in the *Drosophila notum* (Bosveld, Markova et al. 2016), I cannot exclude the possibility that loss of Aka impairs Mud presence at vertex, leading to cell division troubles.

c. SJ proteins display adhesive roles

Last but not least, cell cytokinesis defects could occur thanks to pSJ defects observed in *aka* mutant cells. During the cytokinesis, cell must keep their adhesion while at the same time remodelling the AJ. However, looking at pSJ components, such as ATP-α like I did, reveals that cells are still connected at pSJ level, both below the midbody and at the level of finger-like protrusions connected to it. Those finger-like protrusions have their shape, size and pSJ proteins distribution perturbed upon loss of Aka. In the vertebrate *Xenopus*, the equivalent of pSJ, the Tight Junction (TJ), is still connected to the contractile ring during cytokinesis (Higashi, Arnold et al. 2016). This time and on the contrary of *Drosophila*, AJs are also continuously connected to the midbody. Still, impairing the specific TJ protein ZO-1 (Pyd in the *Drosophila*) leads to defects in cytokinesis mechanism due to increased tension at AJ level (Hatte, Prigent et al. 2018). Moreover, works performed by (Bergstralh, Lovegrove et al. 2015) and (Cammarota, Finegan et al. 2020) show that pSJ components such as Nrg, FasII and FasIII promote cell-cell adhesive contact, thanks to *trans* interactions between Nrg and its link to actin cytoskeleton via interactions with Ankyrin and β-Spectrin. Those adhesives contacts are really important in order to keep the cell in the tissue during cell division. Based on this index cluster, we could imagine that pSJ proteins are required for proper cell-cell adhesion, especially during cell cytokinesis. Defects at pSJ level might push the cell to compensate for defects in adhesion forces and reorganizing its acto-myosin cytoskeleton according to the situation. Therefore, looking at Ankyrin and β-Spectrin in the *notum* first in a WT situation and comparing it with *aka* mutant situation can be a good start to probe potential adhesive defects. Then, observing if removing Ankyrin or

β-Spectrin triggers pSJ defects both during interphase and cytokinesis, would be really informative.

d. Cell shape irregularities are mediated by Cno and Sdk upon loss of Aka

Sdk has been reported to interact with different proteins, notably the scaffold protein Cno (Letizia, He et al. 2019). Cno is also showed to be specifically enriched at TCJ level with F-actin during gastrulation (Sawyer, Harris et al. 2009). It is also recruited at vertex upon NMY-II contractile activity via phosphorylation by the Abl tyrosine kinase like described in (Yu and Zallen 2020). During their study, they trap specifically Cno at the vertex and observe a drastic reduction into cell-cell contact rearrangement via T1 transitions and stretching of the cell area as well as many four ways junction events. Once at the vertex, Cno stabilizes it, preventing the cell-cell neighbour exchange that occurs during epithelia remodelling. Interestingly, similar results are observed but this time in *sdk* mutant context (Finegan, Hervieux et al. 2019). Indeed, loss of Sdk leads to atypical apical cell shape, reduced level of T1 transition and formation of four ways junctions or even rosettes (more than four cells). Here, authors provide arguments in favour of Sdk activity being required to disentangle the four ways junctions or rosettes. Each time, the defects in cell-cell contact exchange is associated with abnormal apical cell shape. What is puzzling here is the fact that Cno seems to be important to recruit Sdk and Sdk activity is needed to operate cell-cell rearrangement. In the case of Cno being blocked at vertex, Sdk should be there too, therefore operating the junctional rearrangement, which seems not to be the case according to (Yu and Zallen 2020). Also, the PDZ domain of Cno is not required for its activity at TCJ whereas at the same time, the C-terminal PDZ binding domain of Sdk is required for its proper function. However, Sdk direct binding to Cno has not been demonstrated, only the Pyd direct binding has been (Letizia, He et al. 2019). Therefore, it is hard now to decipher which actor is the main driver of the cellular junction's rearrangement.

During my work, I observed enrichment of F-actin, DE-Cad and Vinc at vertices upon loss of Aka. Some preliminary results that I recently obtained, described also Cno enrichment at vertex in *aka* mutant cells. Moreover, I observed regular events of four ways junctions or rosette formation in the *notum* upon loss of Aka associated with stretched shape cells even though I have not characterized it properly at the moment. The higher amount of NMY-II and Rok activity in mutant cells could also explained

rosettes formation as NMY-II is required for junction shrinkage and rosette formation (Simoes Sde, Blankenship et al. 2010). Still, my data suggest defects in T1 transition resolution and this defect is associated with higher amount of Cno at the vertex, arguing in favour of Cno stabilizing vertex. Therefore, Sdk might be required to resolve T1 transition only in immature tissues lacking SJ which could explain differences between our tissue and the others. Another explanation could be that even though Cno is a probable binding partner of Sdk and might logically recruits it at TCJ, trapping Cno at vertex differs from Cno recruiting Sdk in WT conditions. Indeed, their dynamics could be totally different in this context, therefore impairing the correct activity of Sdk. Still, nothing argues against the fact that Sdk might also be involved in stabilizing the vertex. The FRAP analysis I performed on Sdk::GFP, reveals a recovery of 40% around 10min after photobleaching compared to a recovery of 40% in only 3min in the case of DE-Cad::GFP at vertex (data not shown), suggesting a much more stable complex, therefore a potential stabilizing role of Sdk at the vertex.

e. Increased tension upon loss of tSJ/pSJ components

Another key result of my work is the enrichment of Sdk at BCJ upon loss of tSJ or pSJ components. At first glance, it might seem that Sdk enrichment at the BCJ is due to reduced tension like demonstrated by (Letizia, He et al. 2019). In the *Drosophila* embryonic amnioserosa, they express a constitutive non-activated form of NMY-II and observe reduced signal of Sdk at vertex while expanding at the BCJ at the same time. However, my results show no diminution of Sdk signal at vertex upon loss of tSJ/pSJ proteins.

Moreover, I reported enrichment of NMY-II, Rok, DE-Cad and F-actin in this situation. Likewise, I noticed an enrichment of Vinc, one of the best indications in favour of increased tension. Indeed, upon increased load tension on AJ, conformational changes occur which lead to α-cat recruitment of Vinc, reinforcing connection between AJs and acto-myosin cytoskeleton (Hoffman and Yap 2015, Charras and Yap 2018). Interestingly, like mentioned before, I started to describe Cno enrichment. (Yu and Zallen 2020) show Cno specific enrichment at TCJ thanks to Abl kinase activity. The same kinase is known to phosphorylate Vinc upon increased tension on DE-Cad complexes, therefore recruiting Vinc at AJ level (Bays, Peng et al. 2014). We could argue that one plausible explanation in favour of increased tension in the tSJ mutant

situation is the fact that two known targets of Abl kinase, which is previously activated by increased tension at AJ level, are enriched in the *notum*. F-actin enrichment also suggests long time scale response to continuous mechanical load (Charras and Yap 2018). Looking at F-actin polymerase such as Enabled or ARP2/3 can be informative to decipher if the Vinc enrichment is due to short or long-time mechanical responses.

Furthermore, a work involving M6 shows that its loss in an oncogenic background Ras^{V12} mutant leads to apical cell delamination in the *Drosophila* eye disc (Dunn, Rush et al. 2018). Authors report increased quantity of activated NMY-II in mutant cells for both M6 and Ras compared to only *Ras* mutant. Moreover, they observe the Rho-GTPase RhoA, regulating NMY-II activity, as well as Cno mislocalisation in the cytoplasm. Hence, loss of M6 seems to display similar phenotype of the one from *aka* mutant. This is expected since loss of M6 leads to loss of Aka at TCJ. But more interestingly, those results suggest the idea that localisation rather than the loss of tSJ proteins dictates remodelling of acto-myosin cytoskeleton and therefore, the probable increased tension.

f. Hippo/YAP pathway is perturbed upon loss of Aka

One more argument in favour of increased tension in *aka* mutant context is the accumulation of the Hippo/YAP protein Jub at both TCJs and BCJs. This protein has been reported to be recruited upon higher tension at AJs in *Drosophila* wing discs (Rauskolb, Sun et al. 2014). Likewise, apical stress fibres that form upon mechanical stress occurring during *Drosophila notum* morphogenesis, recruit Jub at their tips (Lopez-Gay, Nunley et al. 2020). Moreover, Jub restricted at the AJ level keeps Warts here, preventing him to induce Yorkie degradation. Additional results I did not present in the manuscript seem to highlight that *aka* mutant cells divide more than their counterpart during *notum* development. Similar phenotype is observed upon loss of Nrv2 (Daniel, Daude et al. 2018).Those results remain speculative now since they deserve to be well characterized. Also, I have not been able to observe Warts::GFP stronger signal in those mutant cells (data not shown) on the contrary of Jub. Hence, it remains elusive if Jub higher amount at cell junctions upon loss of Aka could lead to Yorkie boosted activity but this idea needs to be explored into more details, especially in the context of not only loss of tSJ proteins but also pSJ proteins.

g. Increased friction or reduced viscosity counteract acto-myosin dependent tension in pSJ/tSJ mutant cells

Another counterintuitive result is the fact that I did not observe differences of recoil velocity upon laser ablation in the cells mutant for Aka or Nrv2 despite every other clue pointing toward increased tension situation. A plausible explanation is the fact that among mutant cells, all cells have their acto-myosin and linked AJs remodelled. Therefore, the pulling forces might be equal on both side of the junctions, leading to similar recoil velocity in WT and mutant conditions. Hence, only boundary between WT and mutant might be informative to observe potential increased tension thanks to differences between the two populations. Unfortunately, this cannot be done. Indeed, we saw that only one cell contributing to the TCJ mutant for Aka led to entire disruption of tSJ. Moreover, boundaries between WT and mutant cells, both in *aka and nrv2* context, display enrichment of DE-Cad, NMY-II and F-actin. Still, why Cold mutant shows differences compared to WT cells remains unsolved.

Also, we could not rule out that cell heterozygote for *aka* and *nrv2* mutant alleles is impaired, even if I did not observe the AJ and acto-myosin remodelling in those cells. Another explanation can be that higher amount of DE-Cad and associated acto-myosin enhanced the friction at junctional level, therefore reducing eventual extra pulling forces. Such example for DE-Cad linked to acto-myosin cytoskeleton to account for higher friction has been provided in (Pinheiro, Hannezo et al. 2017). One possible experiment to test it is to use optic trap of lipid droplets present in cells cytoplasm. However, such measurements will not provide precise information about friction itself but rather on the overall cell viscosity.

An argument in favour of similar tension in both WT/heterozygous and mutant cells is that clones of mutant cells are compacted and not dispersed among WT cells (or the opposite situation). One would have expected mixing of cells upon differential tension at boundaries like highlighted in (Levayer, Hauert et al. 2015).

To end with this part, I would like to mention that *Drosophila* embryos mutant for Kune display mechanical defects characterized by a reduced effective viscosity, seeing there as faster recoil upon laser ablation (Carvalho, Patricio et al. 2018). Accordingly, those results are in favour of mechanical tissue irregularities upon loss of pSJ/tSJ components

h. Loss of Aka leads to putative Focal Adhesion points formation

Speaking about tension, I not only reported Vinc enrichment at AJ level but also along lateral membranes and at the basal side. The presence of Vinc along the apico-basal axis can be a sign toward actin reorganisation such as apico-basal contractile cable, a way for the cell to stabilize its links with its surrounding. Still, using F-actin marker and NMY-II::GFP, I have not been able to observe such events. A partner of Vinc is Rhea (the Fly Talin), an established protein of the integrin-based adhesions, called Focal Adhesion (FA) linking extra-cellular matrix to the actin cytoskeleton. It is known that contractile activity of the acto-myosin cytoskeleton induces FA contacts (Klapholz and Brown 2017). Probing Rhea in the situation where Vinc is enriched at lateral and basal membrane places could unravel if FA contacts are created. This is conceivable that reinforced Vinc/Rhea contacts can be a way for the cell to compensate adhesive defects, both at lateral and basal sides of the cell. By doing so and knowing that forces at FAs are transmitted to the apical level of the cell in the *Drosophila* embryos (Goodwin, Ellis et al. 2016), increased mechanical forces can be experienced upon loss of tSJ proteins. However, no studies report presence of FAs in the *notum* at the time being. This is why describing first potential FAs in the *notum* and then probing their appearance/remodelling upon loss of tSJ proteins can be a way to test if FAs are indeed a way for the cell to compensate mechanical properties impairment.

Part III. Vertebrate vs Invertebrate comparison

a. Vertebrates pSJs equivalent Tight Junctions (TJ) show similar interplay with AJs

In the vertebrate's model, TJ defects similarly show impairment of AJ and acto-myosin cytoskeleton. First of all, TJ on the contrary of SJ in *Drosophila* is found above AJ. Like its counterpart, TJ regulates permeability barrier of the tissue and acts as a fence to prevent merging between apical and baso-lateral domain. It is constituted of transmembrane proteins Claudins which interact with cytoplasmic zonula occludens family protein members, junctional adhesion molecules, MARVEL domain proteins such as Occludin and the specially enriched at vertex Tricellulin and also Angulins (Angulin 1: also known as LSR; Angulin 2: known as Ig-like domain-containing receptor ILDR1; Angulin3: known as ILDR2) (Higashi and Miller 2017, Otani and Furuse 2020).

Former studies report that increased macromolecules flux at TJ are associated with actin cytoskeleton enrichment (Hopkins, Walsh et al. 2003, Van Itallie, Tietgens et al. 2015). Another example reveals that in MDCK cells knocked down for ZO proteins, cells are recruiting higher amount of Shroom3 at junctions and thus ROCK, which leads to the formation of a more contractile acto-myosin network associated with higher amount of E-Cad. Moreover, the vertebrates Cno homologue Afadin, when depleted along with ZO in MDCK, conduct those cells to display less dense E-Cad and acto-myosin network at TCJ, revealing Afadin importance in order to anchor those proteins at vertex level (Choi, Acharya et al. 2016). Similar results are observed in (Odenwald, Choi et al. 2018, Otani, Nguyen et al. 2019). Also, Afadin is a known binding partner of ZO-1 as showed in (Yamamoto, Harada et al. 1997, Ooshio, Kobayashi et al. 2010). Tuba, which is a GEF regulating Cdc-42 activity, is localizing with ZO-1 in Caco2 cells where it regulates cells morphology (Otani, Ichii et al. 2006). ZO-1 has among its numerous partners the GEF ARHGEF11 which mediates RhoA-NMY-II signaling in order to establish correct TJ and acto-myosin cytoskeleton in EpH4 cells (Itoh, Tsukita et al. 2012). Extracellular matrix and FAs are similarly linked to forces exerted on ZO-1 at TJ level (Haas, Zihni et al. 2020).

b. Vertebrate cells sense TJ defects and trigger reparatory mechanism

Another recent example of the interlinked relationship between TJ and acto-myosin cytoskeleton has been observed in (Stephenson, Higashi et al. 2019). Using *Xenopus laevis* embryos, authors demonstrate using a Zn^{2+} sensible probe, leakage defects at the level of TJ occurring spontaneously during development. Occludin and ZO-1 are reduced or quasi absent at leaking areas. They describe a specific recruitment of the small GTPase Rho-A, a regulator of both actin polymerisation and ROCK activity that activates NMY-II. Concomitantly, membrane protrusion spans the breach and after reaching maximal signal of F-actin and NMY-II, specific ZO-1 and Occludin enrichment occur. This study states that cells detect leakage defects and recruit specifically acto-myosin cytoskeleton in order to contract TJ and promote membrane protrusion to seal this transient hole. Similar events are observed in the *notum*. During my first work, I used laser nano-ablation at pSJ level to decipher potential forces occurring in order to explain membrane deformations, and observed recruitment of NMY-II at holes followed by cell-cell contraction (data not shown). Therefore, cells seem to sense leakage defects and react in a similar manner both in vertebrate and invertebrate organisms.

General conclusion:

This work has highlighted how intricate are links between junctional complexes. Here, I not only pinpoint the interplay between TCJ and BCJ but more generally between apical and basal junctions in a mature epithelium. Few studies have started now to focus on how SJ/TJ are playing roles beyond their primary identified filtering one. What emerges here is that pSJ are probably involved in adhesive properties of the cell and in the regulation of acto-myosin cytoskeleton. Moreover, my results propose a sensing property of the cell to detect junctional defects and to compensate it. Because the study of pSJ proteins has only been oriented toward their permeability barrier role and because the study of TCJ at molecular level has only emerged recently, further exciting works will reveal us the multiple functions provide by these proteins.

Bibliography

Abbott, L. A. and Natzle, J.E. (1992). "Epithelial polarity and cell separation in the neoplastic l(1)dlg-1 mutant of Drosophila." Mech Dev **37**: 43-56.
Abedin, M. and N. King (2010). "Diverse evolutionary paths to cell adhesion." Trends Cell Biol **20**(12): 734-742.
Alegot, H., C. Markosian, C. Rauskolb, J. Yang, E. Kirichenko, Y. C. Wang and K. D. Irvine (2019). "Recruitment of Jub by alpha-catenin promotes Yki activity and Drosophila wing growth." J Cell Sci **132**(5).
Alhadyian, H., D. Shoaib and R. E. Ward (2021). "Septate junction proteins are required for egg elongation and border cell migration during oognesis in Drosophila." bioRxiv.
Astigarraga, S., J. Douthit, D. Tarnogorska, M. S. Creamer, O. Mano, D. A. Clark, I. A. Meinertzhagen and J. E. Treisman (2018). "Drosophila Sidekick is required in developing photoreceptors to enable visual motion detection." Development **145**(3).
Auld, V., R. D. Fetter, K. Broadie and C. S. Goodman (1995). "Gliotactin, a Novel Transmembrane Protein on Peripheral Gila, Is Required to Form the Blood-Nerve Barrier in Drosophila." Cell **81**: 757-767.
Babatz, F., E. Naffin and C. Klambt (2018). "The Drosophila Blood-Brain Barrier Adapts to Cell Growth by Unfolding of Pre-existing Septate Junctions." Dev Cell **47**(6): 697-710 e693.
Bachmann, A., M. Draga, F. Grawe and E. Knust (2008). "On the role of the MAGUK proteins encoded by Drosophila varicose during embryonic and postembryonic development." BMC Dev Biol **8**: 55.
Bachmann, A., M. Schneider, E. Theilenberg, F. Grawe and E. Knust (2001). "Drosophila Stardust is a partner of Crumbs in the control of epithelial cell polarity." Nature **414**: 638-643.
Bachmann, A., M. Timmer, J. Sierralta, G. Pietrini, E. D. Gundelfinger, E. Knust and U. Thomas (2004). "Cell type-specific recruitment of Drosophila Lin-7 to distinct MAGUK-based protein complexes defines novel roles for Sdt and Dlg-S97." J Cell Sci **117**(Pt 10): 1899-1909.
Banerjee, S., A. D. Sousa and M. A. Bhat (2006). "Organization and function of septate junctions: an evolutionary perspective." Cell Biochem Biophys **46**(1): 65-77.
Bastiani, M. J., A. L. Harrelson, P. M. Snow and C. S. Goodman (1987). "Expression of fasciclin I and II glycoproteins on subsets of axon pathways during neuronal development in the grasshopper." Cell **48**: 745-755.
Batz, T., D. Forster and S. Luschnig (2014). "The transmembrane protein Macroglobulin complement-related is essential for septate junction formation and epithelial barrier function in Drosophila." Development **141**(4): 899-908.
Baumgartner, S., J. T. Littleton, K. Broadie, M. A. Bhat, R. Harbecke, J. A. Lengyel, R. Chiquet-Ehrismann, A. Prokop and H. J. Bellen (1996). "A Drosophila Neurexin Is Required for Septate Junction and Blood-Nerve Barrier Formation and Function." Cell **87**(6): 1059-1068.
Bays, J. L., X. Peng, C. E. Tolbert, C. Guilluy, A. E. Angell, Y. Pan, R. Superfine, K. Burridge and K. A. DeMali (2014). "Vinculin phosphorylation differentially regulates mechanotransduction at cell-cell and cell-matrix adhesions." J Cell Biol **205**(2): 251-263.
Beckervordersandforth, R. M., C. Rickert, B. Altenhein and G. M. Technau (2008). "Subtypes of glial cells in the Drosophila embryonic ventral nerve cord as related to lineage and gene expression." Mech Dev **125**(5-6): 542-557.
Behr, M., D. Riedel and R. Schuh (2003). "The Claudin-like Megatrachea Is Essential in Septate Junctions for the Epithelial Barrier Function in Drosophila." Dev Cell **5**: 611-620.
Benmimoun, B., F. Papastefanaki, B. Perichon, K. Segklia, N. Roby, V. Miriagou, C. Schmitt, S. Dramsi, R. Matsas and P. Speder (2020). "An original infection model identifies host lipoprotein import as a route for blood-brain barrier crossing." Nat Commun **11**(1): 6106.
Bergstralh, D. T., H. E. Lovegrove and D. St Johnston (2015). "Lateral adhesion drives reintegration of misplaced cells into epithelial monolayers." Nat Cell Biol **17**(11): 1497-1503.
Bhat, M. A., J. C. Rios, Y. Lu, G. P. Garcia-Fresco, W. Ching, S. St. Martin, J. Li, S. Einheber, M. Chesler, J. Rosenbluth, J. L. Salzer and H. J. Bellen (2001). "Axon-Glia Interactions and the Domain Organization of Myelinated Axons Requires Neurexin IV Caspr Paranodin." Neuron **30**: 369-383.

Bieber, A. J., P. M. Snow, M. Hortsch, N. H. Patel, J. R. Jacobs, Z. R. Traquina, J. Schilling and C. S. Goodman (1989). "Drosophila neuroglian A member of the immunoglobulin superfamily with extensive homology to the vertebrate neural adhesion molecule L1." Cell **59**: 447-460.
Bieber, A. J., P. M. Snow, M. Hortsch, N. H. Patel, J. R. Jacobs, Z. R. Traquina, J. Schilling and C. S. Goodman (1989). "Drosophila neuroglian: a member of the immunoglobulin superfamily with extensive homology to the vertebrate neural adhesion molecule L1." Cell **59**(3): 447-460.
Bilder, D., M. Li and N. Perrimon (2000). "Cooperative regulation of cell polarity and growth by Drosophila tumor suppressors." Science **789**: 113-115.
Bilder, D. and N. Perrimon (2000). "Localization of apical epithelial determinants by the basolateral PDZ protein Scribble." Nature **403** 676-680.
Bilder, D., M. Schober and N. Perrimon (2003). "Integrated activity of PDZ protein complexes regulates epithelial polarity." Nat Cell Biol **5**(1): 53-58.
Biteau, B. and H. Jasper (2011). "EGF signaling regulates the proliferation of intestinal stem cells in Drosophila." Development **138**(6): 1045-1055.
Blankenship, J. T., M. T. Fuller and J. A. Zallen (2007). "The Drosophila homolog of the Exo84 exocyst subunit promotes apical epithelial identity." J Cell Sci **120**(Pt 17): 3099-3110.
Boettner, B., P. Harjes, S. Ishimaru, M. Heke, H. Qing Fan, Y. Qin, L. Van Aelst and U. Gaul (2003). "The AF-6 Homolog Canoe Acts as a Rap1 Effector During Dorsal Closure of the Drosophila Embryo." Genetics **165**: 159-169.
Bohannon, K. P. and P. I. Hanson (2020). "ESCRT puts its thumb on the nanoscale: Fixing tiny holes in endolysosomes." Curr Opin Cell Biol **65**: 122-130.
Bonello, T. T. and M. Peifer (2019). "Scribble: A master scaffold in polarity, adhesion, synaptogenesis, and proliferation." J Cell Biol **218**(3): 742-756.
Bonello, T. T., K. Z. Perez-Vale, K. D. Sumigray and M. Peifer (2018). "Rap1 acts via multiple mechanisms to position Canoe and adherens junctions and mediate apical-basal polarity establishment." Development **145**(2).
Bosveld, F., O. Markova, B. Guirao, C. Martin, Z. Wang, A. Pierre, M. Balakireva, I. Gaugue, A. Ainslie, N. Christophorou, D. K. Lubensky, N. Minc and Y. Bellaiche (2016). "Epithelial tricellular junctions act as interphase cell shape sensors to orient mitosis." Nature **530**(7591): 495-498.
Bosveld, F., Z. Wang and Y. Bellaiche (2018). "Tricellular junctions: a hot corner of epithelial biology." Curr Opin Cell Biol **54**: 80-88.
Bradley, P. L., M. M. Myat, C. A. Comeaux and D. J. Andrew (2003). "Posterior migration of the salivary gland requires an intact visceral mesoderm and integrin function." Developmental Biology **257**(2): 249-262.
Bulgakova, N. A., O. Kempkens and E. Knust (2008). "Multiple domains of Stardust differentially mediate localisation of the Crumbs-Stardust complex during photoreceptor development in Drosophila." J Cell Sci **121**(Pt 12): 2018-2026.
Byri, S., T. Misra, Z. A. Syed, T. Batz, J. Shah, L. Boril, J. Glashauser, T. Aegerter-Wilmsen, T. Matzat, B. Moussian, A. Uv and S. Luschnig (2015). "The Triple-Repeat Protein Anakonda Controls Epithelial Tricellular Junction Formation in Drosophila." Dev Cell **33**(5): 535-548.
Calleja, M., E. Moreno, S. Pelaz and G. Morata (1996). "Visualization of Gene Expression in Living Adult Drosophila." Science **274**: 252-255.
Cammarota, C., T. M. Finegan, T. J. Wilson, S. Yang and D. T. Bergstralh (2020). "An Axon-Pathfinding Mechanism Preserves Epithelial Tissue Integrity." Curr Biol **30**(24): 5049-5057 e5043.
Campbell, K., E. Knust and H. Skaer (2009). "Crumbs stabilises epithelial polarity during tissue remodelling." J Cell Sci **122**(Pt 15): 2604-2612.
Caria, S., C. M. Magtoto, T. Samiei, M. Portela, K. Y. B. Lim, J. Y. How, B. Z. Stewart, P. O. Humbert, H. E. Richardson and M. Kvansakul (2018). "Drosophila melanogaster Guk-holder interacts with the Scribbled PDZ1 domain and regulates epithelial development with Scribbled and Discs Large." J Biol Chem **293**(12): 4519-4531.

Carreno, S., I. Kouranti, E. S. Glusman, M. T. Fuller, A. Echard and F. Payre (2008). "Moesin and its activating kinase Slik are required for cortical stability and microtubule organization in mitotic cells." J Cell Biol **180**(4): 739-746.
Carvalho, L., P. Patricio, S. Ponte, C. P. Heisenberg, L. Almeida, A. S. Nunes, N. A. M. Araujo and A. Jacinto (2018). "Occluding junctions as novel regulators of tissue mechanics during wound repair." J Cell Biol **217**(12): 4267-4283.
Chanda, S., W. D. Hale, B. Zhang, M. Wernig and T. C. Sudhof (2017). "Unique versus Redundant Functions of Neuroligin Genes in Shaping Excitatory and Inhibitory Synapse Properties." J Neurosci **37**(29): 6816-6836.
Charras, G. and A. S. Yap (2018). "Tensile Forces and Mechanotransduction at Cell-Cell Junctions." Curr Biol **28**(8): R445-R457.
Cheffings, T. H., N. J. Burroughs and M. K. Balasubramanian (2016). "Actomyosin Ring Formation and Tension Generation in Eukaryotic Cytokinesis." Curr Biol **26**(15): R719-R737.
Chen, J., G. B. Call, E. Beyer, C. Bui, A. Cespedes, A. Chan, J. Chan, S. Chan, A. Chhabra, P. Dang, A. Deravanesian, B. Hermogeno, J. Jen, E. Kim, E. Lee, G. Lewis, J. Marshall, K. Regalia, F. Shadpour, A. Shemmassian, K. Spivey, M. Wells, J. Wu, Y. Yamauchi, A. Yavari, A. Abrams, A. Abramson, L. Amado, J. Anderson, K. Bashour, E. Bibikova, A. Bookatz, S. Brewer, N. Buu, S. Calvillo, J. Cao, A. Chang, D. Chang, Y. Chang, Y. Chen, J. Choi, J. Chou, S. Datta, A. Davarifar, P. Desai, J. Fabrikant, S. Farnad, K. Fu, E. Garcia, N. Garrone, S. Gasparyan, P. Gayda, C. Goffstein, C. Gonzalez, M. Guirguis, R. Hassid, A. Hong, J. Hong, L. Hovestreydt, C. Hu, F. Jamshidian, K. Kahen, L. Kao, M. Kelley, T. Kho, S. Kim, Y. Kim, B. Kirkpatrick, E. Kohan, R. Kwak, A. Langenbacher, S. Laxamana, C. Lee, J. Lee, S. Y. Lee, T. H. Lee, T. Lee, S. Lezcano, H. Lin, P. Lin, J. Luu, T. Luu, W. Marrs, E. Marsh, S. Min, T. Minasian, A. Misra, M. Morimoto, Y. Moshfegh, J. Murray, C. Nguyen, K. Nguyen, E. Nodado, 2nd, A. O'Donahue, N. Onugha, N. Orjiakor, B. Padhiar, M. Pavel-Dinu, A. Pavlenko, E. Paz, S. Phaklides, L. Pham, P. Poulose, R. Powell, A. Pusic, D. Ramola, M. Ribbens, B. Rifai, D. Rosselli, M. Saakyan, P. Saarikoski, M. Segura, R. Singh, V. Singh, E. Skinner, D. Solomin, K. Soneji, E. Stageberg, M. Stavchanskiy, L. Tekchandani, L. Thai, J. Thiyanaratnam, M. Tong, A. Toor, S. Tovar, K. Trangsrud, W. Y. Tsang, M. Uemura, M. Unkovic, E. Vollmer, E. Weiss, D. Wood, S. Wu, W. Wu, Q. Xu, K. Yackle, W. Yarosh, L. Yee, G. Yen, G. Alkin, S. Go, D. M. Huff, H. Minye, E. Paul, N. Villarasa, A. Milchanowski and U. Banerjee (2005). "Discovery-based science education: functional genomic dissection in Drosophila by undergraduate researchers." PLoS Biol **3**(2): e59.
Cho, K. O., C. A. Hunt and M. B. Kennedy (1992). "The Rat Brain Postsynaptic Density Fraction Contains a Homolog of the Drosophila Discs-large Tumor Suppressor Protein." Neuron **9**: 929-942.
Choi, W., B. R. Acharya, G. Peyret, M. A. Fardin, R. M. Mege, B. Ladoux, A. S. Yap, A. S. Fanning and M. Peifer (2016). "Remodeling the zonula adherens in response to tension and the role of afadin in this response." J Cell Biol **213**(2): 243-260.
Choi, W., N. J. Harris, K. D. Sumigray and M. Peifer (2013). "Rap1 and Canoe/afadin are essential for establishment of apical-basal polarity in the Drosophila embryo." Mol Biol Cell **24**(7): 945-963.
Chow, C. Y. and L. T. Reiter (2017). "Etiology of Human Genetic Disease on the Fly." Trends Genet **33**(6): 391-398.
Chugh, P. and E. K. Paluch (2018). "The actin cortex at a glance." J Cell Sci **131**(14).
Claret, S., J. Jouette, B. Benoit, K. Legent and A. Guichet (2014). "PI(4,5)P2 produced by the PI4P5K SKTL controls apical size by tethering PAR-3 in Drosophila epithelial cells." Curr Biol **24**(10): 1071-1079.
Clark, K. A., A. S. McElhinny, M. C. Beckerle and C. C. Gregorio (2002). "Striated muscle cytoarchitecture: an intricate web of form and function." Annu Rev Cell Dev Biol **18**: 637-706.
Clark, R. I., A. Salazar, R. Yamada, S. Fitz-Gibbon, M. Morselli, J. Alcaraz, A. Rana, M. Rera, M. Pellegrini, W. W. Ja and D. W. Walker (2015). "Distinct Shifts in Microbiota Composition during Drosophila Aging Impair Intestinal Function and Drive Mortality." Cell Rep **12**(10): 1656-1667.
Clarke, D. N. and A. C. Martin (2021). "Actin-based force generation and cell adhesion in tissue morphogenesis." Curr Biol **31**(10): R667-R680.
Cripps, R. M. and E. N. Olson (2002). "Control of cardiac development by an evolutionarily conserved transcriptional network." Dev Biol **246**(1): 14-28.

Cullen, P. J. and F. Steinberg (2018). "To degrade or not to degrade: mechanisms and significance of endocytic recycling." Nat Rev Mol Cell Biol **19**(11): 679-696.
Curran, S., C. Strandkvist, J. Bathmann, M. de Gennes, A. Kabla, G. Salbreux and B. Baum (2017). "Myosin II Controls Junction Fluctuations to Guide Epithelial Tissue Ordering." Dev Cell **43**(4): 480-492 e486.
Daniel, E., M. Daude, I. Kolotuev, K. Charish, V. Auld and R. Le Borgne (2018). "Coordination of Septate Junctions Assembly and Completion of Cytokinesis in Proliferative Epithelial Tissues." Curr Biol **28**(9): 1380-1391 e1384.
Das, D., R. Aradhya, D. Ashoka and M. Inamdar (2008). "Macromolecular uptake in Drosophila pericardial cells requires rudhira function." Exp Cell Res **314**(8): 1804-1810.
Davies, A., D. L. Simmons, G. Hale, R. A. Harrison, H. Tighe, P. J. Lachmann and H. Waldmann (1989). "CD59, an LY-6-like protein expressed in human lymphoid cells, regulates the action of the complement membrane attack complex on homologous cells." J Exp Med **170**: 637-654.
Davis, J. Q. and V. Bennett (1994). "Ankyrin binding activity shared by the neurofascin/L1/NrCAM family of nervous system cell adhesion molecules." Journal of Biological Chemistry **269**(44): 27163-27166.
de la Cova, C., M. Abril, P. Bellosta, P. Gallant and L. A. Johnston (2004). "Drosophila Myc Regulates Organ Size by Inducing Cell Competition." Cell **117**: 107-116.
Deligiannaki, M., A. L. Casper, C. Jung and U. Gaul (2015). "Pasiflora proteins are novel core components of the septate junction." Development **142**(17): 3046-3057.
Denisenko-Nehrbass, N., K. Oguievetskaia, L. Goutebroze, T. Galvez, H. Yamakawa, O. Ohara, M. Carnaud and J. A. Girault (2003). "Protein 4.1B associates with both Caspr/paranodin and Caspr2 at paranodes and juxtaparanodes of myelinated fibres." Eur J Neurosci **17**(2): 411-416.
Dong, B., E. Hannezo and S. Hayashi (2014). "Balance between Apical Membrane Growth and Luminal Matrix Resistance Determines Epithelial Tubule Shape." Cell Reports **7**(4): 941-950.
Dongre, A. and R. A. Weinberg (2019). "New insights into the mechanisms of epithelial-mesenchymal transition and implications for cancer." Nat Rev Mol Cell Biol **20**(2): 69-84.
Dubreuil, R. R., G. MacVicar, S. Dissanayake, C. Liu, D. Homer and M. Hortsch (1996). "Neuroglian-mediated Cell Adhesion Induces Assembly of the membrane skeleton at Cell contact sites." J Cell Biol **133**(3): 674-655.
Dubreuil, R. R., P. B. Maddux, T. A. Grushko and G. MacVicar (1997). "Segregation of two spectrin isoforms polarized membrane-binding sites direct polarized membrane skeleton assembly." Mol Biol Cell **8**(10): 1933-1942.
Dubreuil, R. R., P. Wang, S. Dahl, J. Lee and L. S. Goldstein (2000). "Drosophila beta spectrin functions independently of alpha spectrin to polarize the Na,K ATPase in epithelial cells." J Cell Biol **149**(3): 647-656.
Duclos, F., U. Boschert, G. Sirugo, J. L. Mandel, R. Hen and M. Koenig (1993). "Gene in the region of the Friedreich ataxia locus encodes a putative transmembrane protein expressed in the nervous system." Proc Natl Acad Sci U S A **90**(1): 109-113.
Ducuing, A. and S. Vincent (2016). "The actin cable is dispensable in directing dorsal closure dynamics but neutralizes mechanical stress to prevent scarring in the Drosophila embryo." Nat Cell Biol **18**(11): 1149-1160.
Dunn, B. S., L. Rush, J. Y. Lu and T. Xu (2018). "Mutations in the Drosophila tricellular junction protein M6 synergize with Ras(V12) to induce apical cell delamination and invasion." Proc Natl Acad Sci U S A **115**(33): 8358-8363.
Einheber, S., G. Zanazzi, W. Ching, S. Scherer, T. A. Milner, E. Pelies and J. L. Salzer (1997). "The Axonal Membrane Protein Caspr, a Homologue of Neurexin IV, Is a Component of the Septate-like Paranodal Junctions That Assemble during Myelination." J Cell Biol **139**(6): 1495-1506.
Elegheert, J., V. Cvetkovska, A. J. Clayton, C. Heroven, K. M. Vennekens, S. N. Smukowski, M. C. Regan, W. Jia, A. C. Smith, H. Furukawa, J. N. Savas, J. de Wit, J. Begbie, A. M. Craig and A. R. Aricescu (2017).

"Structural Mechanism for Modulation of Synaptic Neuroligin-Neurexin Signaling by MDGA Proteins." Neuron **96**(1): 242-244.
Esmangart de Bournonville, T. and R. Le Borgne (2020). "Interplay between Anakonda, Gliotactin, and M6 for Tricellular Junction Assembly and Anchoring of Septate Junctions in Drosophila Epithelium." Curr Biol **30**(21): 4245-4253 e4244.
Evans, E. and D. Needham (2002). "Physical properties of surfactant bilayer membranes: thermal transitions, elasticity, rigidity, cohesion and colloidal interactions." The Journal of Physical Chemistry **91**(16): 4219-4228.
Faivre-Sarrailh, C. (2020). "Molecular organization and function of vertebrate septate-like junctions." Biochim Biophys Acta Biomembr **1862**(5): 183211.
Faivre-Sarrailh, C., S. Banerjee, J. Li, M. Hortsch, M. Laval and M. A. Bhat (2004). "Drosophila contactin, a homolog of vertebrate contactin, is required for septate junction organization and paracellular barrier function." Development **131**(20): 4931-4942.
Farhadifar, R., J. C. Roper, B. Aigouy, S. Eaton and F. Julicher (2007). "The influence of cell mechanics, cell-cell interactions, and proliferation on epithelial packing." Curr Biol **17**(24): 2095-2104.
Fehon, R. G., I. A. Dawson and S. Artavanis-Tsakonas (1994). "A Drosophila homologue of membrane-skeleton protein 4.1 is associated with septate junctions and is encoded by the coracle gene." Development **120**: 545-557.
Filshie, B. K. and N. E. Flower (1977). "Junctionnal structure in Hydra " J Cell Sci **23**: 151-172.
Finegan, T. M., N. Hervieux, A. Nestor-Bergmann, A. G. Fletcher, G. B. Blanchard and B. Sanson (2019). "The tricellular vertex-specific adhesion molecule Sidekick facilitates polarised cell intercalation during Drosophila axis extension." PLoS Biol **17**(12): e3000522.
Fletcher, G. C., E. P. Lucas, R. Brain, A. Tournier and B. J. Thompson (2012). "Positive feedback and mutual antagonism combine to polarize Crumbs in the Drosophila follicle cell epithelium." Curr Biol **22**(12): 1116-1122.
Flower, N. E. and B. K. Filshie (1975). "Junctional structures in the midgut cells of Lepidopteran Caterpillars." J Cell Sci **17**: 221-239.
Formoso, K., M. D. Garcia, A. C. Frasch and C. Scorticati (2015). "Filopodia formation driven by membrane glycoprotein M6a depends on the interaction of its transmembrane domains." J Neurochem **134**(3): 499-512.
Founounou, N., N. Loyer and R. Le Borgne (2013). "Septins regulate the contractility of the actomyosin ring to enable adherens junction remodeling during cytokinesis of epithelial cells." Dev Cell **24**(3): 242-255.
Fox, R. M. and D. J. Andrew (2015). "Changes in organelle position and epithelial architecture associated with loss of CrebA." Biol Open **4**(3): 317-330.
Fox, R. M., C. D. Hanlon and D. J. Andrew (2010). "The CrebA/Creb3-like transcription factors are major and direct regulators of secretory capacity." J Cell Biol **191**(3): 479-492.
Fristrom, D. K. (1982). "Septate junctions in imaginal disks of Drosophila a model for the redistribution of septa during cell rearrangement." J Cell Biol **94**: 77-87.
Fulford, A., N. Tapon and P. S. Ribeiro (2018). "Upstairs, downstairs: spatial regulation of Hippo signalling." Curr Opin Cell Biol **51**: 22-32.
Furuse, M. and Y. Izumi (2017). "Molecular dissection of smooth septate junctions: understanding their roles in arthropod physiology." Ann N Y Acad Sci **1397**(1): 17-24.
Furuse, M. and S. Tsukita (2006). "Claudins in occluding junctions of humans and flies." Trends Cell Biol **16**(4): 181-188.
Gamblin, C. L., E. J. Hardy, F. J. Chartier, N. Bisson and P. Laprise (2014). "A bidirectional antagonism between aPKC and Yurt regulates epithelial cell polarity." J Cell Biol **204**(4): 487-495.
Gamblin, C. L., F. Parent-Prevost, K. Jacquet, C. Biehler, A. Jette and P. Laprise (2018). "Oligomerization of the FERM-FA protein Yurt controls epithelial cell polarity." J Cell Biol **217**(11): 3853-3862.

Gangwar, S. P., X. Zhong, S. Seshadrinathan, H. Chen, M. Machius and G. Rudenko (2017). "Molecular Mechanism of MDGA1: Regulation of Neuroligin 2:Neurexin Trans-synaptic Bridges." Neuron **94**(6): 1132-1141 e1134.
Gaspar, P., M. V. Holder, B. L. Aerne, F. Janody and N. Tapon (2015). "Zyxin antagonizes the FERM protein expanded to couple F-actin and Yorkie-dependent organ growth." Curr Biol **25**(6): 679-689.
Genova, J. L. and R. G. Fehon (2003). "Neuroglian, Gliotactin, and the Na+/K+ ATPase are essential for septate junction function in Drosophila." J Cell Biol **161**(5): 979-989.
Gho, M., Y. Bellaiche and F. Schweisguth (1999). "Revisiting the Drosophila microchaete lineage: a novel intrinsically asymmetric cell division generates a glial cell." Development **126**(16): 3573-3584.
Gho, M., M. Lecourtois, G. Geraud, J. W. Posakony and F. Schweisguth (1996). "Subcellular localization of Suppressor of Hairless in Drosophila sense organ cells during Notch signalling." Development **122**(6): 1673-1682.
Gilbert, M., J. Smith, A. J. Roskams and V. J. Auld (2001). "Neuroligin 3 is a vertebrate gliotactin expressed in the olfactory ensheathing glia, a growth-promoting class of macroglia." Glia **34**(3): 151-164.
Goodwin, K., S. J. Ellis, E. Lostchuck, T. Zulueta-Coarasa, R. Fernandez-Gonzalez and G. Tanentzapf (2016). "Basal Cell-Extracellular Matrix Adhesion Regulates Force Transmission during Tissue Morphogenesis." Dev Cell **39**(5): 611-625.
Graf, F., C. Noirot-Timothee and C. Noirot (1982). "The specialization of septate junctions in regions of tricellular junctions I. Smooth septate junctions (=Continuous junctions)." J Ultrastruct Res **78**: 136-151.
Grawe, F., A. Wodarz, B. Lee, E. Knust and H. Skaer (1996). "The Drosophila genes crumbs and stardust are involved in the biogenesis of adherens junctions." Development **122**: 951-959.
Green, C. R. and P. R. Bergquist (1982). "Phylogenetic relationships within the invertebrata in relation to the structure of Septate Junctions and the development of 'Occluding' junctional types." J Cell Sci **53**: 279-305.
Green, C. R. and N. E. FLower (1980). "Two new septate junctions in the phylum coelentera." J Cell Sci **42**: 43-59.
Grenningloh, G., E. J. Rehm and C. S. Goodman (1991). "Genetic analysis of growth cone guidance in drosophila Fasciclin II functions as a neuronal recognition molecule." Cell **67**: 45-57.
Grevengoed, E. E., J. J. Loureiro, T. L. Jesse and M. Peifer (2001). "Abelson kinase regulates epithelial morphogenesis in Drosophila." J Cell Biol **155**(7): 1185-1198.
Guillot, C. and T. Lecuit (2013). "Adhesion disengagement uncouples intrinsic and extrinsic forces to drive cytokinesis in epithelial tissues." Dev Cell **24**(3): 227-241.
Guillot, C. and T. Lecuit (2013). "Mechanics of epithelial tissue homeostasis and morphogenesis." Science **340**(6137): 1185-1189.
Guo, Z. and B. Ohlstein (2015). "Stem cell regulation. Bidirectional Notch signaling regulates Drosophila intestinal stem cell multipotency." Science **350**(6263).
Haas, A. J., C. Zihni, A. Ruppel, C. Hartmann, K. Ebnet, M. Tada, M. S. Balda and K. Matter (2020). "Interplay between Extracellular Matrix Stiffness and JAM-A Regulates Mechanical Load on ZO-1 and Tight Junction Assembly." Cell Rep **32**(3): 107924.
Halberg, K. A., S. M. Rainey, I. R. Veland, H. Neuert, A. J. Dornan, C. Klambt, S. A. Davies and J. A. Dow (2016). "The cell adhesion molecule Fasciclin2 regulates brush border length and organization in Drosophila renal tubules." Nat Commun.
Hall, S., C. Bone, K. Oshima, L. Zhang, M. McGraw, B. Lucas, R. G. Fehon and R. E. t. Ward (2014). "Macroglobulin complement-related encodes a protein required for septate junction organization and paracellular barrier function in Drosophila." Development **141**(4): 889-898.
Hall, S. and R. E. t. Ward (2016). "Septate Junction Proteins Play Essential Roles in Morphogenesis Throughout Embryonic Development in Drosophila." G3 (Bethesda) **6**(8): 2375-2384.
Harris, K. P. and U. Tepass (2008). "Cdc42 and Par proteins stabilize dynamic adherens junctions in the Drosophila neuroectoderm through regulation of apical endocytosis." J Cell Biol **183**(6): 1129-1143.

Harris, T. J. and M. Peifer (2004). "Adherens junction-dependent and -independent steps in the establishment of epithelial cell polarity in Drosophila." J Cell Biol **167**(1): 135-147.
Harris, T. J. and M. Peifer (2005). "The positioning and segregation of apical cues during epithelial polarity establishment in Drosophila." J Cell Biol **170**(5): 813-823.
Harris, T. J. C., J. K. Sawyer and M. Peifer (2009). Chapter 3 How the Cytoskeleton Helps Build the Embryonic Body Plan**:** 55-85.
Hatte, G., C. Prigent and J. P. Tassan (2018). "Tight junctions negatively regulate mechanical forces applied to adherens junctions in vertebrate epithelial tissue." J Cell Sci **131**(3).
Heisenberg, C. P. and Y. Bellaiche (2013). "Forces in tissue morphogenesis and patterning." Cell **153**(5): 948-962.
Helmstadter, M., T. B. Huber and T. Hermle (2017). "Using the Drosophila Nephrocyte to Model Podocyte Function and Disease." Front Pediatr **5**: 262.
Hemphala, J., A. Uv, R. Cantera, S. Bray and C. Samakovlis (2003). "Grainy head controls apical membrane growth and tube elongation in response to Branchless/FGF signalling." Development **130**(2): 249-258.
Herszterg, S., A. Leibfried, F. Bosveld, C. Martin and Y. Bellaiche (2013). "Interplay between the dividing cell and its neighbors regulates adherens junction formation during cytokinesis in epithelial tissue." Dev Cell **24**(3): 256-270.
Higashi, T., T. R. Arnold, R. E. Stephenson, K. M. Dinshaw and A. L. Miller (2016). "Maintenance of the Epithelial Barrier and Remodeling of Cell-Cell Junctions during Cytokinesis." Curr Biol **26**(14): 1829-1842.
Higashi, T. and H. Chiba (2020). "Molecular organization, regulation and function of tricellular junctions." Biochim Biophys Acta Biomembr **1862**(2): 183143.
Higashi, T. and A. L. Miller (2017). "Tricellular junctions: how to build junctions at the TRICkiest points of epithelial cells." Mol Biol Cell **28**(15): 2023-2034.
Hijazi, A., M. Haenlin, L. Waltzer and F. Roch (2011). "The Ly6 protein coiled is required for septate junction and blood brain barrier organisation in Drosophila." PLoS One **6**(3): e17763.
Hijazi, A., W. Masson, B. Auge, L. Waltzer, M. Haenlin and F. Roch (2009). "boudin is required for septate junction organisation in Drosophila and codes for a diffusible protein of the Ly6 superfamily." Development **136**(13): 2199-2209.
Hildebrandt, A., R. Pflanz, M. Behr, T. Tarp, D. Riedel and R. Schuh (2015). "Bark beetle controls epithelial morphogenesis by septate junction maturation in Drosophila." Dev Biol **400**(2): 237-247.
Hoffman, B. D. and A. S. Yap (2015). "Towards a Dynamic Understanding of Cadherin-Based Mechanobiology." Trends Cell Biol **25**(12): 803-814.
Honda, A., Y. Ito, K. Takahashi-Niki, N. Matsushita, M. Nozumi, H. Tabata, K. Takeuchi and M. Igarashi (2017). "Extracellular Signals Induce Glycoprotein M6a Clustering of Lipid Rafts and Associated Signaling Molecules." J Neurosci **37**(15): 4046-4064.
Hong, Y., B. Stronach, N. Perrimon, L. Y. Jan and Y. N. Jan (2001). "Drosophila Stardust interacts with Crumbs to control polarity of epithelia but not neuroblasts." Nature **414**: 634-638.
Hopkins, A. M., S. V. Walsh, P. Verkade, P. Boquet and A. Nusrat (2003). "Constitutive activation of Rho proteins by CNF-1 influences tight junction structure and epithelial barrier function." J Cell Sci **116**(Pt 4): 725-742.
Hortsch, M., A. J. Bieber, N. H. Patel and C. S. Goodman (1990). "Differential splicing generates a nervous system Specific form of drosophila neuroglian." Neuron **4**: 697-709.
Huang, J., S. Wu, J. Barrera, K. Matthews and D. Pan (2005). "The Hippo signaling pathway coordinately regulates cell proliferation and apoptosis by inactivating Yorkie, the Drosophila Homolog of YAP." Cell **122**(3): 421-434.
Huang, J., W. Zhou, W. Dong, A. M. Watson and Y. Hong (2009). "Directed, efficient, and versatile modifications of the Drosophila genome by genomic engineering." Proceedings of the National Academy of Sciences of the United States of America **106**: 8284-8289.

Ile, K. E., R. Tripathy, V. Goldfinger and A. D. Renault (2012). "Wunen, a Drosophila lipid phosphate phosphatase, is required for septate junction-mediated barrier function." Development **139**(14): 2535-2546.
Isasti-Sanchez, J., F. Münz-Zeise, M. Lancino and S. Luschnig (2021). "Transient opening of tricellular vertices controls paracellular transport through the follicle epithelium during Drosophila oogenesis." Developmental Cell.
Itoh, M., S. Tsukita, Y. Yamazaki and H. Sugimoto (2012). "Rho GTP exchange factor ARHGEF11 regulates the integrity of epithelial junctions by connecting ZO-1 and RhoA-myosin II signaling." Proc Natl Acad Sci U S A **109**(25): 9905-9910.
Izumi, Y., K. Furuse and M. Furuse (2021). "The novel membrane protein Hoka regulates septate junction organization and stem cell homeostasis in the Drosophila gut." J Cell Sci **134**(6).
Izumi, Y. and M. Furuse (2014). "Molecular organization and function of invertebrate occluding junctions." Semin Cell Dev Biol **36**: 186-193.
Izumi, Y., M. Motoishi, K. Furuse and M. Furuse (2016). "A tetraspanin regulates septate junction formation in Drosophila midgut." J Cell Sci **129**(6): 1155-1164.
Izumi, Y., Y. Yanagihashi and M. Furuse (2012). "A novel protein complex, Mesh-Ssk, is required for septate junction formation in the Drosophila midgut." J Cell Sci **125**(Pt 20): 4923-4933.
Jacob, L., M. Opper, B. Metzroth, B. Phannavong and B. M. Mechler (1987). "Structure of the I(2)gl gene of Drosophila and delimitation of its tumor suppressor domain." Cell **50**: 215-225.
Jaspers, M. H., K. Nolde, M. Behr, S. H. Joo, U. Plessmann, M. Nikolov, H. Urlaub and R. Schuh (2012). "The claudin Megatrachea protein complex." J Biol Chem **287**(44): 36756-36765.
Jesaistis, L. A. and D. A. Goodenough (1994). "Molecular characterization and tissue distribution of ZO-2, a tight junction protein homologous to ZO-1 and the Drosophila discs-large tumor suppressor protein." J Cell Biol **124**(6): 949-961.
Jiang, H. and B. A. Edgar (2009). "EGFR signaling regulates the proliferation of Drosophila adult midgut progenitors." Development **136**(3): 483-493.
Jimenez, A. J., P. Maiuri, J. Lafaurie-Janvore, S. Divoux, M. Piel and F. Perez (2014). "ESCRT machinery is required for plasma membrane repair." Science **343**(6174): 1247136.
Jonusaite, S., A. Donini and S. P. Kelly (2016). "Occluding junctions of invertebrate epithelia." J Comp Physiol B **186**(1): 17-43.
Kale, G. R., X. Yang, J. M. Philippe, M. Mani, P. F. Lenne and T. Lecuit (2018). "Distinct contributions of tensile and shear stress on E-cadherin levels during morphogenesis." Nat Commun **9**(1): 5021.
Kallay, L. M., A. McNickle, P. J. Brennwald, A. L. Hubbard and L. T. Braiterman (2006). "Scribble associates with two polarity proteins, Lgl2 and Vangl2, via distinct molecular domains." J Cell Biochem **99**(2): 647-664.
Kaplan, J. H. (2002). "Biochemistry of Na,K-ATPase." Annu Rev Biochem **71**: 511-535.
Kemphues, K. J., J. R. Priess, D. G. Morton and N. Cheng (1988). "Identification of genes required for cytoplasmic localization in early C. elegans embryos." Cell **52**: 311-320.
Khadilkar, R. J. and G. Tanentzapf (2019). "Septate junction components control Drosophila hematopoiesis through the Hippo pathway." Development **146**(7).
Khadilkar, R. J., W. Vogl, K. Goodwin and G. Tanentzapf (2017). "Modulation of occluding junctions alters the hematopoietic niche to trigger immune activation." Elife **6**.
Khoury, M. J. and D. Bilder (2020). "Distinct activities of Scrib module proteins organize epithelial polarity." Proc Natl Acad Sci U S A **117**(21): 11531-11540.
Kiehart, D. P., J. M. Crawford, A. Aristotelous, S. Venakides and G. S. Edwards (2017). "Cell Sheet Morphogenesis: Dorsal Closure in Drosophila melanogaster as a Model System." Annu Rev Cell Dev Biol **33**: 169-202.
Kim, J. A., D. Kim, S. Y. Won, K. A. Han, D. Park, E. Cho, N. Yun, H. J. An, J. W. Um, E. Kim, J. O. Lee, J. Ko and H. M. Kim (2017). "Structural Insights into Modulation of Neurexin-Neuroligin Trans-synaptic Adhesion by MDGA1/Neuroligin-2 Complex." Neuron **94**(6): 1121-1131 e1126.

Kistner, U., B. M. Wenzel, R. W. Veh, C. Cases-Langhoff, A. M. Garner, U. Appeltauer, B. Voss, E. D. Gundelfinger and C. C. Garner (1993). "SAP90, a rat presynaptic protein related to the product of the Drosophila tumor suppressor gene dlg-A." Journal of Biological Chemistry **268**(7): 4580-4583.
Klambt, C. and O. Schmidt (1986). "Developmental expression and tissue distribution of the lethal (2) giant larvae protein of Drosophila melanogaster." EMBO J **5**(11): 2955-2961.
Klapholz, B. and N. H. Brown (2017). "Talin - the master of integrin adhesions." J Cell Sci **130**(15): 2435-2446.
Koch, U. and F. Radtke (2010). Notch Signaling in Solid Tumors. Notch Signaling**:** 411-455.
Konigsmann, T., I. Parfentev, H. Urlaub, D. Riedel and R. Schuh (2020). "The bicistronic gene wurmchen encodes two essential components for epithelial development in Drosophila." Dev Biol **463**(1): 53-62.
Koulouras, G., A. Panagopoulos, M. A. Rapsomaniki, N. N. Giakoumakis, S. Taraviras and Z. Lygerou (2018). "EasyFRAP-web: a web-based tool for the analysis of fluorescence recovery after photobleaching data." Nucleic Acids Res **46**(W1): W467-W472.
Kunda, P., A. E. Pelling, T. Liu and B. Baum (2008). "Moesin controls cortical rigidity, cell rounding, and spindle morphogenesis during mitosis." Curr Biol **18**(2): 91-101.
Lagenaur, C., V. Kunemund, G. Fischer, S. Fushiki and M. Schachner (1992). "Monoclonal M6 antibody interferes with neurite extension of cultured neurons." J Neurobiol **23**(1): 71-88.
Lamb, R. S., R. Ward, L. Schweizer and R. G. Fehon (1998). "Drosophila coracle, a Member of the Protein 4.1 Superfamily, Has Essential Structural Functions in the Septate Junctions and Developmental Functions in Embryonic and Adult Epithelial cells." Mol Biol Cell **9**(12): 3505-3519.
Laprise, P., S. Beronja, N. F. Silva-Gagliardi, M. Pellikka, A. M. Jensen, C. J. McGlade and U. Tepass (2006). "The FERM protein Yurt is a negative regulatory component of the Crumbs complex that controls epithelial polarity and apical membrane size." Dev Cell **11**(3): 363-374.
Laprise, P., K. M. Lau, K. P. Harris, N. F. Silva-Gagliardi, S. M. Paul, S. Beronja, G. J. Beitel, C. J. McGlade and U. Tepass (2009). "Yurt, Coracle, Neurexin IV and the Na(+),K(+)-ATPase form a novel group of epithelial polarity proteins." Nature **459**(7250): 1141-1145.
Laprise, P., S. M. Paul, J. Boulanger, R. M. Robbins, G. J. Beitel and U. Tepass (2010). "Epithelial polarity proteins regulate Drosophila tracheal tube size in parallel to the luminal matrix pathway." Curr Biol **20**(1): 55-61.
le Duc, Q., Q. Shi, I. Blonk, A. Sonnenberg, N. Wang, D. Leckband and J. de Rooij (2010). "Vinculin potentiates E-cadherin mechanosensing and is recruited to actin-anchored sites within adherens junctions in a myosin II-dependent manner." J Cell Biol **189**(7): 1107-1115.
Lebovitz, R. M., K. Takeyasu and D. M. Fambrough (1989). "Molecular characterization and expression of the (Na+ + K+)-ATPase alpha-subunit in Drosophila melanogaster." EMBO J **8**(1): 193-202.
Lecuit, T. and A. S. Yap (2015). "E-cadherin junctions as active mechanical integrators in tissue dynamics." Nat Cell Biol **17**(5): 533-539.
Lemaitre, B., E. Nicolas, L. Michaut, J. M. Reichhart and J. A. Hoffmann (1996). "The Dorsoventral Regulatory Gene Cassette spätzle Toll cactus Controls the Potent Antifungal Response in Drosophila Adults." Cell **86**: 973-983.
Letizia, A., D. He, S. Astigarraga, J. Colombelli, V. Hatini, M. Llimargas and J. E. Treisman (2019). "Sidekick Is a Key Component of Tricellular Adherens Junctions that Acts to Resolve Cell Rearrangements." Dev Cell **50**(3): 313-326 e315.
Letizia, A., S. Ricardo, B. Moussian, N. Martin and M. Llimargas (2013). "A functional role of the extracellular domain of Crumbs in cell architecture and apicobasal polarity." J Cell Sci **126**(Pt 10): 2157-2163.
Levayer, R., C. Dupont and E. Moreno (2016). "Tissue Crowding Induces Caspase-Dependent Competition for Space." Curr Biol **26**(5): 670-677.
Levayer, R., B. Hauert and E. Moreno (2015). "Cell mixing induced by myc is required for competitive tissue invasion and destruction." Nature **524**(7566): 476-480.
Levayer, R. and T. Lecuit (2012). "Biomechanical regulation of contractility: spatial control and dynamics." Trends Cell Biol **22**(2): 61-81.

Lewis, E. B. (1978). "A gene complex controlling segmentation in Drosophila." Nature **276**(7): 565-570.
Lim, H. Y., H. Bao, Y. Liu and W. Wang (2019). "Select Septate Junction Proteins Direct ROS-Mediated Paracrine Regulation of Drosophila Cardiac Function." Cell Rep **28**(6): 1455-1470 e1454.
Lim, H. Y., W. Wang, J. Chen, K. Ocorr and R. Bodmer (2014). "ROS regulate cardiac function via a distinct paracrine mechanism." Cell Rep **7**(1): 35-44.
Limmer, S., A. Weiler, A. Volkenhoff, F. Babatz and C. Klambt (2014). "The Drosophila blood-brain barrier: development and function of a glial endothelium." Front Neurosci **8**: 365.
Ling, C., Y. Zheng, F. Yin, J. Yu, J. Huang, Y. Hong, S. Wu and D. Pan (2010). "The apical transmembrane protein Crumbs functions as a tumor suppressor that regulates Hippo signaling by binding to Expanded." Proc Natl Acad Sci U S A **107**(23): 10532-10537.
Litwack, E. D., R. Babey, R. Buser, M. Gesemann and D. D. O'Leary (2004). "Identification and characterization of two novel brain-derived immunoglobulin superfamily members with a unique structural organization." Mol Cell Neurosci **25**(2): 263-274.
Llimargas, M., M. Strigini, M. Katidou, D. Karagogeos and J. Casanova (2004). "Lachesin is a component of a septate junction-based mechanism that controls tube size and epithelial integrity in the Drosophila tracheal system." Development **131**(1): 181-190.
Lopez-Gay, J. M., H. Nunley, M. Spencer, F. di Pietro, B. Guirao, F. Bosveld, O. Markova, I. Gaugue, S. Pelletier, D. K. Lubensky and Y. Bellaiche (2020). "Apical stress fibers enable a scaling between cell mechanical response and area in epithelial tissue." Science **370**(6514).
Lord, B. A. and D. R. DiBona (1976). "Role of the septate junction in the regulation of paracellular transepithelial flow." J Cell Biol **71**(3): 967-972.
Low, B. W., H. S. Preston, A. Sato, L. S. Rosen, J. E. Searl, A. D. Rudko and J. S. Richardson (1976). "Three dimensional structure of erabutoxin b neurotoxic protein Inhibitor of acetylcholine receptor." Proc Natl Acad Sci U S A **73**(9): 2991-2994.
Lu, H. and D. Bilder (2005). "Endocytic control of epithelial polarity and proliferation in Drosophila." Nat Cell Biol **7**(12): 1232-1239.
Lue, R. A., S. M. Marfatia, D. Branton and A. H. Chishti (1994). "Cloning and characterization of hdlg the human homologue of the Drosophila discs large tumor suppressor binds to protein 4.1." Proc Natl Acad Sci U S A **91**(21): 9818-9822.
Luschnig, S., T. Batz, K. Armbruster and M. A. Krasnow (2006). "serpentine and vermiform encode matrix proteins with chitin binding and deacetylation domains that limit tracheal tube length in Drosophila." Curr Biol **16**(2): 186-194.
Lye, C. M., H. W. Naylor and B. Sanson (2014). "Subcellular localisations of the CPTI collection of YFP-tagged proteins in Drosophila embryos." Development **141**(20): 4006-4017.
Mahowald, A. P. (1972). "Ultrastructural observations on oogenesis in Drosophila." J Morphol **137**: 29-48.
Mandai, K., H. Nakanishi, A. Satoh, H. Obaishi, M. Wada, H. Nishioka, M. Itoh, A. Mizoguchi, T. Aoki, T. Fujimoto, Y. Matsuda, S. Tsukita and Y. Takai (1997). "Afadin A Novel Actin Filament–binding Protein with One PDZ Domain Localized at Cadherin-based Cell-to-Cell Adherens Junction." J Cell Biol **139**(2): 517-528.
Manning, L. A., K. Z. Perez-Vale, K. N. Schaefer, M. T. Sewell and M. Peifer (2019). "The Drosophila Afadin and ZO-1 homologues Canoe and Polychaetoid act in parallel to maintain epithelial integrity when challenged by adherens junction remodeling." Mol Biol Cell **30**(16): 1938-1960.
Manning, S. A., B. Kroeger and K. F. Harvey (2020). "The regulation of Yorkie, YAP and TAZ: new insights into the Hippo pathway." Development **147**(8).
Marinari, E., A. Mehonic, S. Curran, J. Gale, T. Duke and B. Baum (2012). "Live-cell delamination counterbalances epithelial growth to limit tissue overcrowding." Nature **484**(7395): 542-545.
Martin, A. C., M. Kaschube and E. F. Wieschaus (2009). "Pulsed contractions of an actin-myosin network drive apical constriction." Nature **457**(7228): 495-499.
Martin, P. and J. Lewis (1992). "Actin cables and epidermal movement in embryonic wound healing." Nature **360**: 179-183.

Maruyama, R. and D. J. Andrew (2012). "Drosophila as a model for epithelial tube formation." Dev Dyn **241**(1): 119-135.
Matamoro-Vidal, A. and R. Levayer (2019). "Multiple Influences of Mechanical Forces on Cell Competition." Curr Biol **29**(15): R762-R774.
Mathew, D., L. S. Gramates, M. Packard, U. Thomas, D. Bilder, N. Perrimon, M. Gorczyca and V. Budnik (2002). "Recruitment of Scribble to the Synaptic Scaffolding Complex Requires GUK-holder, a Novel DLG Binding Protein." Curr Biol **12**: 531-539.
Matsui, T., M. Maeda, Y. Doi, S. Yonemura, M. Amano, K. Kaibuchi, S. Tsukita and S. Tsukita (1998). "Rho-Kinase Phosphorylates COOH-terminal Threonines of Ezrin Radixin Moesin (ERM) Proteins and Regulates Their Head-to-Tail Association." J Cell Biol **140**(3): 647-657.
Matsuo, T., K. Takahashi, E. Suzuki and D. Yamamoto (1999). "The Canoe protein is necessary in adherens junctions for development of ommatidial architecture in the Drosophila compound eye." Cell Tissue Res **298**(3): 397-404.
McGill, M. A., R. F. McKinley and T. J. Harris (2009). "Independent cadherin-catenin and Bazooka clusters interact to assemble adherens junctions." J Cell Biol **185**(5): 787-796.
Medina, E., J. Williams, E. Klipfell, D. Zarnescu, G. Thomas and A. Le Bivic (2002). "Crumbs interacts with moesin and beta(Heavy)-spectrin in the apical membrane skeleton of Drosophila." J Cell Biol **158**(5): 941-951.
Meng, W. and M. Takeichi (2009). "Adherens junction: molecular architecture and regulation." Cold Spring Harb Perspect Biol **1**(6): a002899.
Micchelli, C. A. and N. Perrimon (2006). "Evidence that stem cells reside in the adult Drosophila midgut epithelium." Nature **439**(7075): 475-479.
Miller, P. W., D. N. Clarke, W. I. Weis, C. J. Lowe and W. J. Nelson (2013). "The evolutionary origin of epithelial cell-cell adhesion mechanisms." Curr Top Membr **72**: 267-311.
Misra, J. R. and K. D. Irvine (2018). "The Hippo Signaling Network and Its Biological Functions." Annu Rev Genet **52**: 65-87.
Monier, B. and M. Suzanne (2015). "The Morphogenetic Role of Apoptosis." Curr Top Dev Biol **114**: 335-362.
Morais-de-Sa, E., V. Mirouse and D. St Johnston (2010). "aPKC phosphorylation of Bazooka defines the apical/lateral border in Drosophila epithelial cells." Cell **141**(3): 509-523.
Moyer, K. E. and J. R. Jacobs (2008). "Varicose: a MAGUK required for the maturation and function of Drosophila septate junctions." BMC Dev Biol **8**: 99.
Müller, B. M., U. Kistner, R. W. Veh, C. Cases-Langhoff, B. Becker, E. D. Gundelfinger and C. C. Garner (1995). "Molecular characterization and spatial distribution of SAP97, a novel presynaptic protein homologous to SAP90 and the Drosophila discs-large tumor suppressor protein." J Neurosci **15**(3): 2354-2366.
Munjal, A. and T. Lecuit (2014). "Actomyosin networks and tissue morphogenesis." Development **141**(9): 1789-1793.
Muschalik, N. and E. Knust (2011). "Increased levels of the cytoplasmic domain of Crumbs repolarise developing Drosophila photoreceptors." J Cell Sci **124**(Pt 21): 3715-3725.
Nagarkar-Jaiswal, S., P. T. Lee, M. E. Campbell, K. Chen, S. Anguiano-Zarate, M. C. Gutierrez, T. Busby, W. W. Lin, Y. He, K. L. Schulze, B. W. Booth, M. Evans-Holm, K. J. Venken, R. W. Levis, A. C. Spradling, R. A. Hoskins and H. J. Bellen (2015). "A library of MiMICs allows tagging of genes and reversible, spatial and temporal knockdown of proteins in Drosophila." Elife **4**.
Nam, S. C. and K. W. Choi (2003). "Interaction of Par-6 and Crumbs complexes is essential for photoreceptor morphogenesis in Drosophila." Development **130**(18): 4363-4372.
Nance, J. and J. A. Zallen (2011). "Elaborating polarity: PAR proteins and the cytoskeleton." Development **138**(5): 799-809.
Nelson, K. S., M. Furuse and G. J. Beitel (2010). "The Drosophila Claudin Kune-kune is required for septate junction organization and tracheal tube size control." Genetics **185**(3): 831-839.

Neuert, H., P. Deing, K. Krukkert, E. Naffin, G. Steffes, B. Risse, M. Silies and C. Klambt (2020). "The Drosophila NCAM homolog Fas2 signals independently of adhesion." Development **147**(2).
Nguyen, D. N. T., Y. Liu, M. L. Litsky and R. Reinke (1997). "The sidekick gene, a member of the immunoglobulin superfamily, is required for pattern formation in the Drosophila eye." Development **124**: 3303-3312.
Nieto, M. A., R. Y. Huang, R. A. Jackson and J. P. Thiery (2016). "Emt: 2016." Cell **166**(1): 21-45.
Niklas, K. J. (2014). "The evolutionary-developmental origins of multicellularity." Am J Bot **101**(1): 6-25.
Nilton, A., K. Oshima, F. Zare, S. Byri, U. Nannmark, K. G. Nyberg, R. G. Fehon and A. E. Uv (2010). "Crooked, coiled and crimpled are three Ly6-like proteins required for proper localization of septate junction components." Development **137**(14): 2427-2437.
Noirot-Timothee, C., F. Graf and C. Noirot (1982). "The specialization of septate junctions in regions of tricellular junctions II. Pleated septate junctions." J Ultrastruct Res **78**: 152-165.
Noirot-Timothée, C. and C. Noirot (1980). "Septate and Scalariform Junctions in Arthropods." **63**: 97-140.
Nunes de Almeida, F., R. F. Walther, M. T. Presse, E. Vlassaks and F. Pichaud (2019). "Cdc42 defines apical identity and regulates epithelial morphogenesis by promoting apical recruitment of Par6-aPKC and Crumbs." Development **146**(15).
Nüsslein-Volhard, C. and E. Wieschaus (1980). "Mutations affecting segment number and polarity in Drosophila." Nature **287**(30): 795-801.
Oda, Y., T. Sugawara, Y. Fukata, Y. Izumi, T. Otani, T. Higashi, M. Fukata and M. Furuse (2020). "The extracellular domain of angulin-1 and palmitoylation of its cytoplasmic region are required for angulin-1 assembly at tricellular contacts." J Biol Chem **295**(13): 4289-4302.
Odenwald, M. A., W. Choi, W. T. Kuo, G. Singh, A. Sailer, Y. Wang, L. Shen, A. S. Fanning and J. R. Turner (2018). "The scaffolding protein ZO-1 coordinates actomyosin and epithelial apical specializations in vitro and in vivo." J Biol Chem **293**(45): 17317-17335.
Ohata, S., R. Aoki, S. Kinoshita, M. Yamaguchi, S. Tsuruoka-Kinoshita, H. Tanaka, H. Wada, S. Watabe, T. Tsuboi, I. Masai and H. Okamoto (2011). "Dual roles of Notch in regulation of apically restricted mitosis and apicobasal polarity of neuroepithelial cells." Neuron **69**(2): 215-230.
Ohlstein, B. and A. Spradling (2006). "The adult Drosophila posterior midgut is maintained by pluripotent stem cells." Nature **439**(7075): 470-474.
Ohsawa, S., J. Vaughen and T. Igaki (2018). "Cell Extrusion: A Stress-Responsive Force for Good or Evil in Epithelial Homeostasis." Dev Cell **44**(3): 284-296.
Ooshio, T., R. Kobayashi, W. Ikeda, M. Miyata, Y. Fukumoto, N. Matsuzawa, H. Ogita and Y. Takai (2010). "Involvement of the interaction of afadin with ZO-1 in the formation of tight junctions in Madin-Darby canine kidney cells." J Biol Chem **285**(7): 5003-5012.
Oshima, K. and R. G. Fehon (2011). "Analysis of protein dynamics within the septate junction reveals a highly stable core protein complex that does not include the basolateral polarity protein Discs large." J Cell Sci **124**(Pt 16): 2861-2871.
Osswald, M. and E. Morais-de-Sa (2019). "Dealing with apical-basal polarity and intercellular junctions: a multidimensional challenge for epithelial cell division." Curr Opin Cell Biol **60**: 75-83.
Osterfield, M., C. A. Berg and S. Y. Shvartsman (2017). "Epithelial Patterning, Morphogenesis, and Evolution: Drosophila Eggshell as a Model." Dev Cell **41**(4): 337-348.
Otani, T. and M. Furuse (2020). "Tight Junction Structure and Function Revisited." Trends Cell Biol **30**(10): 805-817.
Otani, T., T. Ichii, S. Aono and M. Takeichi (2006). "Cdc42 GEF Tuba regulates the junctional configuration of simple epithelial cells." J Cell Biol **175**(1): 135-146.
Otani, T., T. P. Nguyen, S. Tokuda, K. Sugihara, T. Sugawara, K. Furuse, T. Miura, K. Ebnet and M. Furuse (2019). "Claudins and JAM-A coordinately regulate tight junction formation and epithelial polarity." J Cell Biol **218**(10): 3372-3396.

Otey, C. A. and O. Carpen (2004). "α-actinin revisited A fresh look at an old player." Cell Motil. Cytoskeleton **58**: 104-111.
Padash-Barmchi, M., K. Browne, K. Sturgeon, B. Jusiak and V. J. Auld (2010). "Control of Gliotactin localization and levels by tyrosine phosphorylation and endocytosis is necessary for survival of polarized epithelia." J Cell Sci **123**(Pt 23): 4052-4062.
Padash-Barmchi, M., K. Charish, J. Que and V. J. Auld (2013). "Gliotactin and Discs large are co-regulated to maintain epithelial integrity." J Cell Sci **126**(Pt 5): 1134-1143.
Pannen, H., T. Rapp and T. Klein (2020). "The ESCRT machinery regulates retromer-dependent transcytosis of septate junction components in Drosophila." Elife **9**.
Patel, N. H., P. M. Snow and C. S. Goodman (1987). "Characterization and Cloning of Fasciclin III A glycoprotein expressed on a subset of neurons and axon pathways in Drosophila." Cell **48**: 975-988.
Paul, S. M., M. J. Palladino and G. J. Beitel (2007). "A pump-independent function of the Na,K-ATPase is required for epithelial junction function and tracheal tube-size control." Development **134**(1): 147-155.
Paul, S. M., M. Ternet, P. M. Salvaterra and G. J. Beitel (2003). "The Na+/K+ ATPase is required for septate junction function and epithelial tube-size control in the Drosophila tracheal system." Development **130**(20): 4963-4974.
Pellikka, M., G. Tanentzapf, M. Pinto, C. Smith, C. J. McGlade, D. F. Ready and U. Tepass (2002). "Crumbs, the Drosophila homologue of human CRB1/RP12, is essential for photoreceptor morphogenesis." Nature **416**: 143-149.
Perkins, L. A., L. Holderbaum, R. Tao, Y. Hu, R. Sopko, K. McCall, D. Yang-Zhou, I. Flockhart, R. Binari, H. S. Shim, A. Miller, A. Housden, M. Foos, S. Randkelv, C. Kelley, P. Namgyal, C. Villalta, L. P. Liu, X. Jiang, Q. Huan-Huan, X. Wang, A. Fujiyama, A. Toyoda, K. Ayers, A. Blum, B. Czech, R. Neumuller, D. Yan, A. Cavallaro, K. Hibbard, D. Hall, L. Cooley, G. J. Hannon, R. Lehmann, A. Parks, S. E. Mohr, R. Ueda, S. Kondo, J. Q. Ni and N. Perrimon (2015). "The Transgenic RNAi Project at Harvard Medical School: Resources and Validation." Genetics **201**(3): 843-852.
Petri, J., M. H. Syed, S. Rey and C. Klambt (2019). "Non-Cell-Autonomous Function of the GPI-Anchored Protein Undicht during Septate Junction Assembly." Cell Rep **26**(6): 1641-1653 e1644.
Pinheiro, D., E. Hannezo, S. Herszterg, F. Bosveld, I. Gaugue, M. Balakireva, Z. Wang, I. Cristo, S. U. Rigaud, O. Markova and Y. Bellaiche (2017). "Transmission of cytokinesis forces via E-cadherin dilution and actomyosin flows." Nature **545**(7652): 103-107.
Pocha, S. M., T. Wassmer, C. Niehage, B. Hoflack and E. Knust (2011). "Retromer controls epithelial cell polarity by trafficking the apical determinant Crumbs." Curr Biol **21**(13): 1111-1117.
Pokutta, S., F. Drees, Y. Takai, W. J. Nelson and W. I. Weis (2002). "Biochemical and structural definition of the l-afadin- and actin-binding sites of alpha-catenin." J Biol Chem **277**(21): 18868-18874.
Pollard, T. D. (2016). "Actin and Actin-Binding Proteins." Cold Spring Harb Perspect Biol **8**(8).
Popkova, A., M. Rauzi and X. Wang (2021). "Cellular and Supracellular Planar Polarity: A Multiscale Cue to Elongate the Drosophila Egg Chamber." Front Cell Dev Biol **9**: 645235.
Poulson, D. F. (1937). "Chromosomal Deficiencies and the Embryonic Development of Drosophila Melanogaster." Proc Natl Acad Sci U S A **23**(3): 133-137.
Priya, R. and A. S. Yap (2015). "Active tension: the role of cadherin adhesion and signaling in generating junctional contractility." Curr Top Dev Biol **112**: 65-102.
Rauskolb, C., G. Pan, B. V. Reddy, H. Oh and K. D. Irvine (2011). "Zyxin Links Fat Signaling to the Hippo Pathway." PLoS Biol **9**(6).
Rauskolb, C., S. Sun, G. Sun, Y. Pan and K. D. Irvine (2014). "Cytoskeletal tension inhibits Hippo signaling through an Ajuba-Warts complex." Cell **158**(1): 143-156.
Razzell, W., M. E. Bustillo and J. A. Zallen (2018). "The force-sensitive protein Ajuba regulates cell adhesion during epithelial morphogenesis." J Cell Biol **217**(10): 3715-3730.
Razzell, W., W. Wood and P. Martin (2014). "Recapitulation of morphogenetic cell shape changes enables wound re-epithelialisation." Development **141**(9): 1814-1820.

Rera, M., R. I. Clark and D. W. Walker (2012). "Intestinal barrier dysfunction links metabolic and inflammatory markers of aging to death in Drosophila." Proc Natl Acad Sci U S A **109**(52): 21528-21533.
Resnik-Docampo, M., K. M. Cunningham, S. M. Ruvalcaba, C. Choi, V. Sauer and D. L. Jones (2021). "Neuroglian regulates Drosophila intestinal stem cell proliferation through enhanced signaling via the epidermal growth factor receptor." Stem Cell Reports.
Resnik-Docampo, M., C. L. Koehler, R. I. Clark, J. M. Schinaman, V. Sauer, D. M. Wong, S. Lewis, C. D'Alterio, D. W. Walker and D. L. Jones (2017). "Tricellular junctions regulate intestinal stem cell behaviour to maintain homeostasis." Nat Cell Biol **19**(1): 52-59.
Richard, M., F. Grawe and E. Knust (2006). "DPATJ plays a role in retinal morphogenesis and protects against light-dependent degeneration of photoreceptor cells in the Drosophila eye." Dev Dyn **235**(4): 895-907.
Richard, M., N. Muschalik, F. Grawe, S. Ozuyaman and E. Knust (2009). "A role for the extracellular domain of Crumbs in morphogenesis of Drosophila photoreceptor cells." Eur J Cell Biol **88**(12): 765-777.
Riento, K. and A. J. Ridley (2003). "Rocks: multifunctional kinases in cell behaviour." Nat Rev Mol Cell Biol **4**(6): 446-456.
Riga, A., V. G. Castiglioni and M. Boxem (2020). "New insights into apical-basal polarization in epithelia." Curr Opin Cell Biol **62**: 1-8.
Robbins, R. M., S. C. Gbur and G. J. Beitel (2014). "Non-canonical roles for Yorkie and Drosophila Inhibitor of Apoptosis 1 in epithelial tube size control." PLoS One **9**(7): e101609.
Roeth, J. F., J. K. Sawyer, D. A. Wilner and M. Peifer (2009). "Rab11 helps maintain apical crumbs and adherens junctions in the Drosophila embryonic ectoderm." PLoS One **4**(10): e7634.
Roh, M. H., O. Makarova, C. J. Liu, K. Shin, S. Lee, S. Laurinec, M. Goyal, R. Wiggins and B. Margolis (2002). "The Maguk protein, Pals1, functions as an adapter, linking mammalian homologues of Crumbs and Discs Lost." J Cell Biol **157**(1): 161-172.
Roper, K. (2012). "Anisotropy of Crumbs and aPKC drives myosin cable assembly during tube formation." Dev Cell **23**(5): 939-953.
Rugendorff, A., A. Younossi-Hartenstein and V. Hartenstein (1994). "Embryonic origin and differentiation of the Drosophila heart." Rouxs Arch Dev Biol **203**: 266-280.
Russo, J., S. Dupas, F. Frey, Y. Carton and M. Brehelin (1996). "Insect immunity: early events in the encapsulation process of parasitoid (Leptopilina boulardi) eggs in resistant and susceptible strains of Drosophila." Parasitology **112 (Pt 1)**: 135-142.
Sabino, D., N. H. Brown and R. Basto (2011). "Drosophila Ajuba is not an Aurora-A activator but is required to maintain Aurora-A at the centrosome." J Cell Sci **124**(Pt 7): 1156-1166.
Salazar, A. M., M. Resnik-Docampo, M. Ulgherait, R. I. Clark, M. Shirasu-Hiza, D. L. Jones and D. W. Walker (2018). "Intestinal Snakeskin Limits Microbial Dysbiosis during Aging and Promotes Longevity." iScience **9**: 229-243.
Samarasekera, G. and V. J. Auld (2018). "C-terminal Src kinase (Csk) regulates the tricellular junction protein Gliotactin independent of Src." Mol Biol Cell **29**(2): 123-136.
Sansonetti, P. J., J. Mounier, M. C. Prévost and R. M. Mège (1994). "Cadherin expression is required for the spread of Shigella flexneri between epithelial cells." Cell **76**: 829-839.
Sawyer, J. K., W. Choi, K. C. Jung, L. He, N. J. Harris and M. Peifer (2011). "A contractile actomyosin network linked to adherens junctions by Canoe afadin helps drive convergent extension." Mol Biol Cell **22**: 2491-2508.
Sawyer, J. K., N. J. Harris, K. C. Slep, U. Gaul and M. Peifer (2009). "The Drosophila afadin homologue Canoe regulates linkage of the actin cytoskeleton to adherens junctions during apical constriction." J Cell Biol **186**(1): 57-73.
Scheffer, L. L., S. C. Sreetama, N. Sharma, S. Medikayala, K. J. Brown, A. Defour and J. K. Jaiswal (2014). "Mechanism of Ca(2)(+)-triggered ESCRT assembly and regulation of cell membrane repair." Nat Commun **5**: 5646.

Schindelin, J., I. Arganda-Carreras, E. Frise, V. Kaynig, M. Longair, T. Pietzsch, S. Preibisch, C. Rueden, S. Saalfeld, B. Schmid, J. Y. Tinevez, D. J. White, V. Hartenstein, K. Eliceiri, P. Tomancak and A. Cardona (2012). "Fiji: an open-source platform for biological-image analysis." Nat Methods **9**(7): 676-682.
Schulte, J., K. Charish, J. Que, S. Ravn, C. MacKinnon and V. J. Auld (2006). "Gliotactin and Discs large form a protein complex at the tricellular junction of polarized epithelial cells in Drosophila." J Cell Sci **119**(Pt 21): 4391-4401.
Schulte, J., U. Tepass and V. J. Auld (2003). "Gliotactin, a novel marker of tricellular junctions, is necessary for septate junction development in Drosophila." J Cell Biol **161**(5): 991-1000.
Schwabe, T., X. Li and U. Gaul (2017). "Dynamic analysis of the mesenchymal-epithelial transition of blood-brain barrier forming glia in Drosophila." Biol Open **6**(2): 232-243.
Scorticati, C., K. Formoso and A. C. Frasch (2011). "Neuronal glycoprotein M6a induces filopodia formation via association with cholesterol-rich lipid rafts." J Neurochem **119**(3): 521-531.
Shapiro, L. and W. I. Weis (2009). "Structure and biochemistry of cadherins and catenins." Cold Spring Harb Perspect Biol **1**(3): a003053.
Sharifkhodaei, Z., M. Padash-Barmchi, M. M. Gilbert, G. Samarasekera, T. A. Fulga, D. Van Vactor and V. J. Auld (2016). "The Drosophila tricellular junction protein Gliotactin regulates its own mRNA levels through BMP-mediated induction of miR-184." J Cell Sci **129**(7): 1477-1489.
Sidor, C., T. J. Stevens, L. Jin, J. Boulanger and K. Roper (2020). "Rho-Kinase Planar Polarization at Tissue Boundaries Depends on Phospho-regulation of Membrane Residence Time." Dev Cell **52**(3): 364-378 e367.
Silver, J. T., F. Wirtz-Peitz, S. Simoes, M. Pellikka, D. Yan, R. Binari, T. Nishimura, Y. Li, T. J. C. Harris, N. Perrimon and U. Tepass (2019). "Apical polarity proteins recruit the RhoGEF Cysts to promote junctional myosin assembly." J Cell Biol **218**(10): 3397-3414.
Simoes Sde, M., J. T. Blankenship, O. Weitz, D. L. Farrell, M. Tamada, R. Fernandez-Gonzalez and J. A. Zallen (2010). "Rho-kinase directs Bazooka/Par-3 planar polarity during Drosophila axis elongation." Dev Cell **19**(3): 377-388.
Simoes Sde, M., A. Mainieri and J. A. Zallen (2014). "Rho GTPase and Shroom direct planar polarized actomyosin contractility during convergent extension." J Cell Biol **204**(4): 575-589.
Skau, C. T. and C. M. Waterman (2015). "Specification of Architecture and Function of Actin Structures by Actin Nucleation Factors." Annu Rev Biophys **44**: 285-310.
Skouloudaki, K., D. K. Papadopoulos, P. Tomancak and E. Knust (2019). "The apical protein Apnoia interacts with Crumbs to regulate tracheal growth and inflation." PLoS Genet **15**(1): e1007852.
Skowyra, M. L., P. H. Schlesinger, T. V. Naismith and P. I. Hanson (2018). "Triggered recruitment of ESCRT machinery promotes endolysosomal repair." Science **360**(6384).
Snow, P. M., A. J. Bieber and C. S. Goodman (1989). "Fasciclin III A novel homophilic adhesion molecule in Drosophila." Cell **59**: 313-323.
Sotillos, S., M. T. Diaz-Meco, E. Caminero, J. Moscat and S. Campuzano (2004). "DaPKC-dependent phosphorylation of Crumbs is required for epithelial cell polarity in Drosophila." J Cell Biol **166**(4): 549-557.
Stephenson, R. E., T. Higashi, I. S. Erofeev, T. R. Arnold, M. Leda, A. B. Goryachev and A. L. Miller (2019). "Rho Flares Repair Local Tight Junction Leaks." Dev Cell **48**(4): 445-459 e445.
Stewart, M., C. Murphy and J. W. Fristrom (1972). "The recovery and preliminary characterization of X chromosome mutants affecting imaginal discs of Drosophila melanogaster." Dev Biol **27**: 71-83.
Stork, T., S. Thomas, F. Rodrigues, M. Silies, E. Naffin, S. Wenderdel and C. Klambt (2009). "Drosophila Neurexin IV stabilizes neuron-glia interactions at the CNS midline by binding to Wrapper." Development **136**(8): 1251-1261.
Strand, D., I. Raska and B. M. Mechler (1994). "The Drosophila lethal(2)giant larvae tumor suppressor protein is a component of the cytoskeleton." J Cell Biol **127**(5): 1345-1360.
Strassburger, K., E. Kang and A. A. Teleman (2019). "Drosophila ZDHHC8 palmitoylates scribble and Ras64B and controls growth and viability." PLoS One **14**(2): e0198149.

Strigini, M., R. Cantera, X. Morin, M. J. Bastiani, M. Bate and D. Karagogeos (2006). "The IgLON protein Lachesin is required for the blood-brain barrier in Drosophila." Mol Cell Neurosci **32**(1-2): 91-101.
Stroschein-Stevenson, S. L., E. Foley, P. H. O'Farrell and A. D. Johnson (2006). "Identification of Drosophila gene products required for phagocytosis of Candida albicans." PLoS Biol **4**(1): e4.
Sun, B. and P. M. Salvaterra (1995). "Two Drosophila nervous system antigens, Nervana 1 and 2, are homologous to the beta subunit of Na+,K(+)-ATPase." Proc Natl Acad Sci U S A **92**: 5396-5400.
Svitkina, T. (2018). "The Actin Cytoskeleton and Actin-Based Motility." Cold Spring Harb Perspect Biol **10**(1).
Swanson, L. E., M. Yu, K. S. Nelson, P. Laprise, U. Tepass and G. J. Beitel (2009). "Drosophila convoluted/dALS is an essential gene required for tracheal tube morphogenesis and apical matrix organization." Genetics **181**(4): 1281-1290.
Syed, M. H., A. Krudewig, D. Engelen, T. Stork and C. Klambt (2011). "The CD59 family member Leaky/Coiled is required for the establishment of the blood-brain barrier in Drosophila." J Neurosci **31**(21): 7876-7885.
Takahashi, K., T. Matsuo, T. Katsube, R. Ueda and D. Yamamoto (1998). "Direct binding between two PDZ domain proteins Canoe and ZO-1 and their roles in regulation of the jun N-terminal kinase pathway in Drosophila morphogenesis." Mech Dev **78**: 97-111.
Takeichi, M. (2014). "Dynamic contacts: rearranging adherens junctions to drive epithelial remodelling." Nat Rev Mol Cell Biol **15**(6): 397-410.
Tanentzapf, G. and U. Tepass (2003). "Interactions between the crumbs, lethal giant larvae and bazooka pathways in epithelial polarization." Nat Cell Biol **5**(1): 46-52.
Tempesta, C., A. Hijazi, B. Moussian and F. Roch (2017). "Boudin trafficking reveals the dynamic internalisation of specific septate junction components in Drosophila." PLoS One **12**(10): e0185897.
Tepass, U. (1996). "Crumbs, a Component of the Apical Membrane, Is Required for Zonula Adherens Formation in Primary Epithelia of Drosophila." Dev Biol **177**: 217-225.
Tepass, U. (2012). "The apical polarity protein network in Drosophila epithelial cells: regulation of polarity, junctions, morphogenesis, cell growth, and survival." Annu Rev Cell Dev Biol **28**: 655-685.
Tepass, U. and V. Hartenstein (1994). "The Development of Cellular Junctions in the Drosophila Embryo." Developmental Biology **161**: 563-596.
Tepass, U. and E. Knust (1990). "Phenotypic and developmental analysis of mutations at the crumbs locus, a gene required for the development of epithelia in Drosophila melanogaster." Rouxs Arch Dev Biol **199**: 189-206.
Tepass, U., C. Theres and E. Knust (1990). "crumbs encodes an EGF-like protein expressed on apical membranes of Drosophila epithelial cells and required for organization of epithelia." Cell **61**: 787-799.
Thomas, U., E. Kim, S. Kuhlendahl, Y. Ho Koh, E. D. Gundelfinger, M. Sheng, C. C. Garner and V. Budnik (1997). "Synaptic Clustering of the Cell Adhesion Molecule Fasciclin II by Discs-Large and its Role in the Regulation of Presynaptic Structure." Neuron **19**: 787-799.
Thompson, B. J., F. Pichaud and K. Roper (2013). "Sticking together the Crumbs - an unexpected function for an old friend." Nat Rev Mol Cell Biol **14**(5): 307-314.
Tiklova, K., K. A. Senti, S. Wang, A. Graslund and C. Samakovlis (2010). "Epithelial septate junction assembly relies on melanotransferrin iron binding and endocytosis in Drosophila." Nat Cell Biol **12**(11): 1071-1077.
Trichas, G., A. M. Smith, N. White, V. Wilkins, T. Watanabe, A. Moore, B. Joyce, J. Sugnaseelan, T. A. Rodriguez, D. Kay, R. E. Baker, P. K. Maini and S. Srinivas (2012). "Multi-cellular rosettes in the mouse visceral endoderm facilitate the ordered migration of anterior visceral endoderm cells." PLoS Biol **10**(2): e1001256.
Uechi, H. and E. Kuranaga (2019). "The Tricellular Junction Protein Sidekick Regulates Vertex Dynamics to Promote Bicellular Junction Extension." Dev Cell **50**(3): 327-338 e325.
Valon, L. and R. Levayer (2019). "Dying under pressure: cellular characterisation and in vivo functions of cell death induced by compaction." Biol Cell **111**(3): 51-66.

van Deventer, S., A. B. Arp and A. B. van Spriel (2021). "Dynamic Plasma Membrane Organization: A Complex Symphony." Trends Cell Biol **31**(2): 119-129.
Van Itallie, C. M., A. J. Tietgens, E. Krystofiak, B. Kachar and J. M. Anderson (2015). "A complex of ZO-1 and the BAR-domain protein TOCA-1 regulates actin assembly at the tight junction." Mol Biol Cell **26**(15): 2769-2787.
VanHook, A. and A. Letsou (2008). "Head Involution in Drosophila Genetic andMorphogenetic Connections to Dorsal Closure." Dev Dyn **237**: 28-38.
Venema, D. R., T. Zeev-Ben-Mordehai and V. J. Auld (2004). "Transient apical polarization of Gliotactin and Coracle is required for parallel alignment of wing hairs in Drosophila." Dev Biol **275**(2): 301-314.
Vicente-Manzanares, M., X. Ma, R. S. Adelstein and A. R. Horwitz (2009). "Non-muscle myosin II takes centre stage in cell adhesion and migration." Nat Rev Mol Cell Biol **10**(11): 778-790.
Vincent, J. P., A. G. Fletcher and L. A. Baena-Lopez (2013). "Mechanisms and mechanics of cell competition in epithelia." Nat Rev Mol Cell Biol **14**(9): 581-591.
Vining, M. S., P. L. Bradley, C. A. Comeaux and D. J. Andrew (2005). "Organ positioning in Drosophila requires complex tissue-tissue interactions." Dev Biol **287**(1): 19-34.
von Hilchen, C. M., A. E. Bustos, A. Giangrande, G. M. Technau and B. Altenhein (2013). "Predetermined embryonic glial cells form the distinct glial sheaths of the Drosophila peripheral nervous system." Development **140**(17): 3657-3668.
Walther, R. F., M. Burki, N. Pinal, C. Rogerson and F. Pichaud (2018). "Rap1, Canoe and Mbt cooperate with Bazooka to promote zonula adherens assembly in the fly photoreceptor." J Cell Sci **131**(6).
Walther, R. F. and F. Pichaud (2010). "Crumbs/DaPKC-dependent apical exclusion of Bazooka promotes photoreceptor polarity remodeling." Curr Biol **20**(12): 1065-1074.
Wang, S., S. A. Jayaram, J. Hemphala, K. A. Senti, V. Tsarouhas, H. Jin and C. Samakovlis (2006). "Septate-junction-dependent luminal deposition of chitin deacetylases restricts tube elongation in the Drosophila trachea." Curr Biol **16**(2): 180-185.
Wang, Z., F. Bosveld and Y. Bellaiche (2018). "Tricellular junction proteins promote disentanglement of daughter and neighbour cells during epithelial cytokinesis." J Cell Sci **131**(11).
Wangler, M. F., S. Yamamoto and H. J. Bellen (2015). "Fruit flies in biomedical research." Genetics **199**(3): 639-653.
Ward IV, R. E., R. S. Lamb and R. G. Fehon (1998). "A Conserved Functional Domain of Drosophila Coracle is Required for Localization at the Septate Junction and has Membrane-organizing Activity." J Cell Biol **140**(6): 1463-1473.
Ward IV, R. E., L. Schweizer, R. S. Lamb and R. Fehon (2001). "The protein 4.1, ezrin, radixin, moesin (FERM) domain of Drosophila coracle, a cytoplasmic component of the septate junction, provides functions essential for embryonic development and imaginal cell proliferation." Genetics **159**: 219-228.
Ward, R. E., J. Evans and C. S. Thummel (2003). "Genetic modifier screens in Drosophila demonstrate a role for Rho1 signaling in ecdysone-triggered imaginal disc morphogenesis." Genetics **165**: 1397-1415.
Wei, S. Y., L. M. Escudero, F. Yu, L. H. Chang, L. Y. Chen, Y. H. Ho, C. M. Lin, C. S. Chou, W. Chia, J. Modolell and J. C. Hsu (2005). "Echinoid is a component of adherens junctions that cooperates with DE-Cadherin to mediate cell adhesion." Dev Cell **8**(4): 493-504.
Wells, R. E., J. D. Barry, S. J. Warrington, S. Cuhlmann, P. Evans, W. Huber, D. Strutt and M. P. Zeidler (2013). "Control of tissue morphology by Fasciclin III-mediated intercellular adhesion." Development **140**(18): 3858-3868.
Willott, E., M. S. Balda, A. S. Fanning, B. Jameson, C. Van Itallie and J. M. Anderson (1993). "The tight junction protein ZO-1 is homologous to the Drosophila discs-large tumor suppressor protein of septate junctions." Proc Natl Acad Sci U S A **90**(16): 7834-7838.
Wittek, A., M. Hollmann, R. Schleutker and S. Luschnig (2020). "The Transmembrane Proteins M6 and Anakonda Cooperate to Initiate Tricellular Junction Assembly in Epithelia of Drosophila." Curr Biol **30**(21): 4254-4262 e4255.

Wodarz, A., F. Grawe and E. Knust (1993). "CRUMBS is involved in the control of apical protein targeting during Drosophila epithelial development." Mech Dev **44**: 175-187.
Wodarz, A., U. Hinz, M. Engelbert and E. Knust (1995). "Expression of crumbs confers apical character on plasma membrane domains of ectodermal epithelia of drosophila." Cell **82**: 67-76.
Wood, R. L. (1959). "Intercellular Attachment in the Epithelium of Hydra." J Biophysic and Biochem Cytol **6**(3): 343-352.
Woods, D. F. and P. J. Bryant (1991). "The Discs-Large Tumor Suppressor Gene of Drosophila Encodes a Guanylate Kinase Homolog." Cell **66**: 451-464.
Woods, D. F., C. Hough, D. Peel, G. Callaini and P. J. Bryant (1996). "Dig Protein Is Required for Junction Structure, Cell Polarity, and Proliferation Control in Drosophila Epithelia." J Cell Biol **134**(6): 1469-1482.
Woods, D. F., J. W. Wu and P. J. Bryant (1997). "Localization of proteins to the apico-lateral junctions of Drosophila epithelia." Dev Genet **20**: 111-118.
Wu, Q., N. Kumar, V. Velagala and J. J. Zartman (2019). "Tools to reverse-engineer multicellular systems: case studies using the fruit fly." J Biol Eng **13**: 33.
Wu, S. K. and R. Priya (2019). "Spatio-Temporal Regulation of RhoGTPases Signaling by Myosin II." Front Cell Dev Biol **7**: 90.
Wu, V. M. and G. J. Beitel (2004). "A junctional problem of apical proportions: epithelial tube-size control by septate junctions in the Drosophila tracheal system." Curr Opin Cell Biol **16**(5): 493-499.
Wu, V. M., J. Schulte, A. Hirschi, U. Tepass and G. J. Beitel (2004). "Sinuous is a Drosophila claudin required for septate junction organization and epithelial tube size control." J Cell Biol **164**(2): 313-323.
Wu, V. M., M. H. Yu, R. Paik, S. Banerjee, Z. Liang, S. M. Paul, M. A. Bhat and G. J. Beitel (2007). "Drosophila Varicose, a member of a new subgroup of basolateral MAGUKs, is required for septate junctions and tracheal morphogenesis." Development **134**(5): 999-1009.
Xu, N., G. Bagumian, M. Galiano and M. M. Myat (2011). "Rho GTPase controls Drosophila salivary gland lumen size through regulation of the actin cytoskeleton and Moesin." Development **138**(24): 5415-5427.
Yamamoto, T., N. Harada, K. Kano, S. Taya, E. Canaani, Y. Matsuura, A. Mizoguchi, C. Ide and K. Kaibuchi (1997). "The Ras Target AF-6 Interacts with ZO-1 and Serves as a Peripheral Component of Tight Junctions in Epithelial Cells." J Cell Biol **139**(3): 785-795.
Yanagihashi, Y., T. Usui, Y. Izumi, S. Yonemura, M. Sumida, S. Tsukita, T. Uemura and M. Furuse (2012). "Snakeskin, a membrane protein associated with smooth septate junctions, is required for intestinal barrier function in Drosophila." J Cell Sci **125**(Pt 8): 1980-1990.
Yi, P., Z. Han, X. Li and E. N. Olson (2006). "The mevalonate pathway controls heart formation in Drosophila by isoprenylation of Ggamma1." Science **313**: 1301-1303.
Yi, P., A. N. Johnson, Z. Han, J. Wu and E. N. Olson (2008). "Heterotrimeric G proteins regulate a noncanonical function of septate junction proteins to maintain cardiac integrity in Drosophila." Dev Cell **15**(5): 704-713.
Yonemura, S., Y. Wada, T. Watanabe, A. Nagafuchi and M. Shibata (2010). "alpha-Catenin as a tension transducer that induces adherens junction development." Nat Cell Biol **12**(6): 533-542.
Yu, H. H. and J. A. Zallen (2020). "Abl and Canoe/Afadin mediate mechanotransduction at tricellular junctions." Science **370**(6520).
Zaffran, S. and M. Frasch (2002). "Early signals in cardiac development." Circ Res **91**(6): 457-469.
Zappia, M. P., M. A. Brocco, S. C. Billi, A. C. Frasch and M. F. Ceriani (2011). "M6 membrane protein plays an essential role in Drosophila oogenesis." PLoS One **6**(5): e19715.
Zeitler, J., C. P. Hsu, H. Dionne and D. Bilder (2004). "Domains controlling cell polarity and proliferation in the Drosophila tumor suppressor Scribble." J Cell Biol **167**(6): 1137-1146.
Zhang, B., L. Y. Chen, X. Liu, S. Maxeiner, S. J. Lee, O. Gokce and T. C. Sudhof (2015). "Neuroligins Sculpt Cerebellar Purkinje-Cell Circuits by Differential Control of Distinct Classes of Synapses." Neuron **87**(4): 781-796.
Zhang, C., J. M. Milunsky, S. Newton, J. Ko, G. Zhao, T. A. Maher, H. Tager-Flusberg, M. F. Bolliger, A. S. Carter, A. A. Boucard, C. M. Powell and T. C. Sudhof (2009). "A neuroligin-4 missense mutation

associated with autism impairs neuroligin-4 folding and endoplasmic reticulum export." J Neurosci **29**(35): 10843-10854.
Zhou, B., Y. Wu and X. Lin (2011). "Retromer regulates apical-basal polarity through recycling Crumbs." Dev Biol **360**(1): 87-95.
Zihni, C., C. Mills, K. Matter and M. S. Balda (2016). "Tight junctions: from simple barriers to multifunctional molecular gates." Nat Rev Mol Cell Biol **17**(9): 564-580.
Zito, K., R. D. Fetter, C. S. Goodman and E. Y. Isacoff (1997). "Synaptic Clustering of Fasciclin II and Shaker Essential Targeting Sequences and Role of Dlg." Neuron **19**: 1007-1016.

Résumé long

Le vivant existe sous de multiples formes, aussi bien en tant que Procaryotes ou Eucaryotes, que végétaux ou animaux. Parmi les animaux, on distingue les êtres unicellulaires, nommés Protozoaires, des êtres multicellulaires nommés Métazoaires. La complexité des Métazoaires a conduit à l'apparition et l'évolution de différents groupes de cellules organisées en tissus, formant des organes aux fonctions spécialisées. Un des organes étant apparu le plus tôt dans l'évolution est l'épithélium. Ce tissu est composé de différentes cellules qui ont pour point commun d'être jointes et polarisées selon un axe apico-basal grâce aux jonctions intercellulaires. Ce tissu confère une barrière mécanique, assurée par les jonctions adhérentes (AJ) et une barrière dite de perméabilité, assurée elle par les jonctions serrées (TJ) chez les vertébrés / jonctions septées (SJ) chez les invertébrés. En plus de s'assurer de l'homéostasie des organismes, les jonctions doivent permettre une plasticité et un remodelage des épithélia qui croissent et se renouvellent durant le développement, la morphogénèse ou encore la réparation tissulaire.

Au contact de deux cellules se trouve la jonction bicellulaire (BCJ), objet de nombreuses études depuis plusieurs décennies. Quand trois cellules se rencontrent, apparaît alors une jonction tricellulaire (TCJ). De récentes études démontrent que les TCJs sont impliquées dans l'orientation de la division cellulaire, le maintien de la barrière épithéliale ou la régulation des cellules souches intestinales par exemple. De même, elles ont été caractérisées comme étant le lieu de passage préférentiel de cellules immunitaires et cellules cancéreuses métastatiques. Ces TCJs sont aussi enrichies en régulateurs de voies de communication cellulaire impliquées dans le développement des tumeurs et l'invasion des cellules tumorales telle que la voie Hippo ou encore JNK. Curieusement, malgré ces fonctions essentielles, les TCJs demeurent largement méconnues.

De plus, le type de cancer le plus courant est le carcinome, représentant plus de 85% des cancers. Ce type de cancer a pour origine le tissu épithélial et apparaît la majorité du temps suite à une dérégulation des divisions cellulaires, de perte de la polarité cellulaire ou encore de défauts d'identité cellulaire. Ces cancers sont d'autant plus dangereux que s'opère la transition épithélio-mésenchymateuse, conduisant alors à la

dissémination des cellules tumorales dans l'organisme. Les thérapies développées depuis plusieurs décennies contre ces pathologies s'appuient sur la recherche fondamentale qui utilise comme outil de travail les organismes modèles. Un des plus connus à ce jour, maintes fois récompensé par le prix Nobel de médecine, est la *Drosophila melanogaster*. Environ 60% des gènes de la Drosophile ont un équivalent chez l'homme, notamment ceux impliqués dans la division cellulaire et la régulation des jonctions. De plus, c'est grâce à la Drosophile que les premiers gènes impliqués dans le cancer ont été découverts, comme le gène Notch dans les années 1930. De même, le processus de métastase est contrôlé par les gènes Snail et Twist qui furent aussi découverts chez la Drosophile.

Mon projet de thèse vise à comprendre, en utilisant la Drosophile comme système modèle, comment les cellules de l'épithélium se divisent correctement tout en maintenant l'intégrité du tissu. Plus précisément, j'étudie l'impact de la régulation des jonctions cellulaires sur ces processus. Pour que tout se déroule bien, il faut que les cellules épithéliales reforment leurs jonctions de manière robuste, sans quoi elles s'exposent à de nombreux problèmes.

Dans notre laboratoire, nous utilisons la partie dorsale du thorax de *Drosophila melanogaster*, appelé *notum*, un épithélium monocouche composé de cellules épithéliales, pour étudier les questions du remodelage des jonctions au cours de la division cellulaire ainsi que leur dynamique et intégrité. La Drosophile offre une vaste diversité d'outils génétiques (analyse clonale, nombreux mutants, collection de lignées GFP, RNA-i induit dans un tissu spécifique, …). L'équipe est également experte sur la technique du CRISPR/Cas9 et nous maîtrisons les approches d'imagerie non invasive en temps réel sur animal vivant et les approches biophysiques (nano chirurgie laser). Pour toute l'imagerie *in vivo*, les sondes fluorescentes ('tag au locus') sont fonctionnelles et exprimées à leur niveau physiologique (Fly TRAP, lignées CPTI, édition du génome).

Chez la Drosophile, quatre protéines transmembranaires sont reportées être exclusivement présentes aux TCJs : Sidekick (Sdk) qui se situe dans le plan des AJs et intervient dans le réarrangement des contacts cellulaires; Gliotactine (Gli) située

dans le plan des SJs, jouant un rôle dans la barrière de perméabilité et notamment l'établissement de la barrière hémato-encéphalique; Anakonda (Aka) située dans le plan des SJs, reportée comme la pièce maîtresse des TCJs et jouant un rôle également dans la barrière de perméabilité chez l'embryon de Drosophile; M6 la dernière protéine reportée enrichie à la TCJ dans le plan des SJs qui quant à elle, en son absence dans un contexte oncogénique mutant, entraîne l'invasion tumorale.

J'ai tout d'abord débuté ma thèse en étudiant les questions du remodelage des TCJ au cours de la division. Pour se faire, via des approches de microscopie confocale en temps réel, j'ai pu observer et décrire les processus sous-jacents. Ainsi, Sdk apparaît directement aux vertex au niveau des AJs tandis que Gli, Aka et M6 s'établissent dans le plan du dessous au niveau des SJs, au contact de l'anneau contractile d'acto-myosine encore nommé midbody. Ces trois protéines apparaissent après Sdk et une fois que l'AJ est formée. J'ai donc révélé que le remodelage et établissement des TCJs suivaient une logique temporelle et spatiale similaire à celles des BCJs, à savoir que la cellule forme d'abord l'AJ suivi par l'établissement des SJs.

Par la suite, je me suis intéressé à comprendre les relations qui existaient entre les protéines des TCJs via des approches de mutant. Pour se faire, j'ai induit des clones de cellules mutantes pour les protéines d'intérêt dans le *notum* au contact de cellules non mutantes que l'on appelle cellules wild-type (WT). Premièrement, j'ai pu confirmer que la protéine Aka était bien requise pour la présence de Gli à la TCJ dans le *notum,* de la même manière que cela avait été démontré dans l'embryon de Drosophile. Deuxièmement, j'ai également mis en évidence que M6 et Aka étaient toutes deux nécessaires l'une à l'autre pour leur présence à la TCJ ainsi que M6 pour Gli. De plus, Gli, bien que non requis pour la présence particulière d'Aka à la TCJ, permet une stabilisation du complexe protéique de la TCJ comme révélée par la technique de FRAP (Fluorescence Recovery After Photobleaching). De manière intéressante, j'ai observé l'apparition de déformations membranaires enrichies en protéines des SJs quand la TCJ était impactée suite à la perte d'un de ces composants. Associée avec ce phénotype, la perte des protéines de la TCJ conduit à l'absence des protéines des SJs spécifiquement au vertex, ce qui laisse penser que ce point particulier de la cellule permet un ancrage des SJs. Par la suite, j'ai testé l'opposé de la perte des composants de la TCJ, à savoir la perte des protéines de la BCJ. J'ai alors pu remarquer que les

protéines de la TCJ n'étaient plus restreintes aux vertex mais tendaient à s'étendre à la BCJ.

Durant ces deux premières années de thèse, j'ai donc caractérisé le remodelage en temps réel des TCJs et mis en évidence la fine relation qui s'opère entre les composants de la TCJ. Elles agissent également comme point d'ancrage pour les BCJ septées, garantissant l'intégrité de l'homéostasie du tissu. A l'inverse, l'intégrité de la BCJ septée est requise pour restreindre la localisation des composants de la TCJ. Tout ceci fait l'objet du premier article de ma thèse.

Cependant et de manière fortuite, j'ai observé que la perte d'Aka entraîne un enrichissement en E-cadhérine (E-cad), de la F-actine, d'une protéine partenaire de l'actine nommée Karst et la chaîne légère de la Myosine II non musculaire (MyoII) aux BCJs et TCJs. Similairement, j'ai observé que les cellules mutantes pour Aka montraient un signal de Sdk à la BCJ plus important que dans les cellules WT. Un enrichissement d'E-cad et NMY-II aux jonctions laissent présager d'un changement des forces mécaniques du tissu. Afin de comprendre si les tensions étaient changées dans ce contexte mutant, j'ai décidé de regarder des acteurs clés de la régulation de la tension. NMY-II exerce son action contractile grâce à son activation par la kinase Rok. Cette dernière est également enrichie aux TCJs et BCJs dans les cellules mutantes Aka, argumentant en faveur d'une augmentation de tension dans le tissu. Une autre manière de tester les forces de tension dans le tissu est par l'approche de nano chirurgie laser. En coupant l'AJ et en quantifiant la vitesse d'écartement des vertex adjacents à cette jonction, nous pouvons en déduire grâce à des modèles de physique, les propriétés mécaniques de ces cellules. C'est pourquoi j'ai comparé la vitesse d'écartement des cellules WT et mutantes pour Aka. Cependant, je n'ai pas pu observer de différences significatives entre les deux conditions. En revanche, utilisant d'autres marqueurs moléculaires témoins d'une augmentation de tension dans le tissu, tels que la Vinculine et Ajuba, j'ai observé leur enrichissement dans les conditions mutantes pour Aka, de manière similaire à Rok. De plus, les forces de tension jouent un rôle prépondérant lors de la division cellulaire en permettent à la nouvelle AJ qui s'établit de se construire avec une longueur suffisante. Tout défaut dans ce processus entraîne des anomalies de la longueur de la nouvelle AJ formée. Comparant à nouveau les cellules WT et mutantes pour Aka, j'ai observé des différences, avec des

longueurs d'AJ moindres dans le cas des cellules mutantes pour Aka, ajoutant du poids à l'hypothèse du défaut de tension en l'absence d'Aka.

Etant donné que des défauts au niveau des TCJs entraînent nécessairement des défauts à la SJ comme démontré lors du premier article, j'ai donc décidé de regarder si les effets observés sur les AJs dans les conditions mutantes pour Aka étaient reproduits dans les conditions mutantes pour les protéines des SJs. Comme supposé, j'ai observé à la fois les enrichissements de la E-Cad, NMY-II, F-actine ainsi qu'un enrichissement de Sdk à la BCJ. Ainsi, des défauts à la BCJ au niveau des SJs entraînent un remodelage de l'AJ comme dans le cas de cellules mutantes pour les protéines des TCJs.

Cependant, comment un défaut situé dans un plan différent des AJs peut entraîner de tels effets ? Plusieurs indices mentionnés dans les résultats précédents m'ont permis d'orienter mon travail de la manière suivante.

La kinase Rok et la protéine Karst sont deux composants connus pour interagir avec la protéine de polarité Crumbs (Crb). Crb est intéressante pour plusieurs raisons. Tout d'abord, il a été démontré dans le passé que chez l'embryon de Drosophile, des cellules de la trachée présentant des défauts de Crb voyaient leur quantité de membrane apicale augmentée, un phénotype qui pourrait ici être mis en perspective avec les extensions de membrane observées dans les mutants Aka. De plus, ces défauts de Crb étaient, dans cette étude, médiés par la perte d'une protéine appelée Shrub, un composant de la machinerie du trafic intracellulaire. De manière intéressante, la perte de Shrub induisait non seulement des défauts sur Crb et la membrane plasmique, mais aussi sur les SJs, ces dernières étant mal formées et leurs composants en partie délocalisés. De la même manière, des études préalables au sein de l'équipe avaient montré que la perte de Shrub dans le *notum*, induisait une disparition des composants de la SJ. Récemment, Shrub a à nouveau démontré son importance dans l'établissement des SJs. En effet, il est requis pour adresser correctement les protéines des SJs à la bonne localisation chez la Drosophile. Sa perte entraîne alors le blocage en position basale de nombreux composants des SJs. Enfin, une autre équipe a mis en évidence il y a quelques années, que si les SJs, formant la barrière hématoencéphalique chez la Drosophile, étaient perturbées, des excès membranaires et de protéines des SJs apparaissaient dans ces cellules.

Ainsi, l'hypothèse suivante émergeait. Des défauts de SJs dans les cellules du *notum* conduisent ces dernières à répondre comme observée dans la barrière hématoencéphalique, par une surproduction (ou des défauts de dégradation) des protéines des SJs en association avec un excès de membrane. Ceci serait plausible au vu des résultats obtenus dans le cadre de la perte d'Aka. Ensuite, j'ai donc regardé si Crb était perturbée dans les mutants Aka. Ceci est bien le cas comme démontré par un signal plus important au niveau apical médial, suggérant des défauts de trafic et/ou de recyclage/dégradation de la protéine. En parallèle, j'ai observé un phénotype similaire dans le cadre de mutants pour les SJs. Ensuite, j'ai découvert des agrégats de Shrub ainsi qu'une augmentation du nombre et de la taille de compartiments de recyclage appelés Multi Vesicular Bodies, révélés par la protéine HRS. Ces résultats sont accompagnés d'accumulation de protéines poly-ubiquitinées, marqueur de protéines adressées pour la dégradation. Tout ceci laisse à penser que des défauts de dégradation protéique ou bien d'une dégradation accrue sont ici à l'œuvre. Bien que moins tranchés, ces résultats ont aussi été observés dans les mutants Aka.

Par conséquent, le modèle suivant est proposé. Les cellules du *notum* mutantes pour Aka ou bien les protéines des SJs, détectent les défauts de la SJ. Elles tentent donc de compenser en exprimant et en adressant de nouvelles protéines des SJs. Parce que les SJs ne peuvent jamais être totalement réparées dû aux mutations, ce mécanisme se déroule en continue. Ceci conduit alors à entraver en partie l'action de Shrub, qui est requis pour adresser les protéines des SJs, mais aussi nécessaire à l'adressage de Crb en apical, ce qui se traduit par une accumulation de cette dernière en apicale. De ce fait, Crb qui interagit avec Rok et Karst va conduire au remodelage des AJs et aux augmentations de NMY-II, F-actine et E-Cad observées. En parallèle de tout ceci, parce que Shrub est entravée, des défauts de dégradation protéique apparaissent comme observés par les plus nombreuses vésicules HRS positives et les agrégats de protéines poly-ubiquitinées. Ces défauts pourraient tout aussi bien être dû à l'excès de dégradation des protéines des SJs. En effet, des lysosomes, compartiments de dégradation cellulaire, qui sont surchargés en agrégats protéiques peuvent être lésés et réparés par Shrub, ce qui serait une autre façon d'expliquer les agrégats de Shrub et de protéines poly-ubiquitinées. Tout ceci fait actuellement l'objet d'un second article en préparation.

Ainsi au cours de ma thèse, débutant par l'étude spécifique des composants des TCJs chez la Drosophile, j'ai été amené à étudier et caractériser les relations complexes et à multi-échelles des jonctions cellulaires. Tout d'abord, j'ai démontré le lien étroit qui unit les protéines des SJs et TCJs, les unes dépendant des autres pour pouvoir être ancrées ou bien restreintes au vertex. Ensuite, j'ai pu commencer à explorer comment des défauts jonctionnels induits à un niveau cellulaire particulier, pouvait se traduire par des défauts systémiques de la cellule.

Ces études, bien que fondamentales, révèlent la complexité du vivant et justifie d'autant plus l'utilisation d'organismes modèles tels que la Drosophile, plus simple d'utilisation, répondant aux critères des 3R sur la recherche animale, possédant une palette d'outils génétiques extraordinaire et permettant d'observer dans un contexte le plus proche du naturel possible, des mécanismes d'une variété inouïe. Ceci est d'autant plus justifié dans le cadre du remodelage des jonctions cellulaires que ces derniers sont impliqués, comme mentionné précédemment, dans les processus de métastase. Or en France, le cancer est actuellement la première cause de décès avec près de 157 000 morts en 2018. Bien que des progrès majeurs en termes de soins aient été accomplis cette dernière décennie, de nombreux problèmes restent sans solutions tels que les traitements ou la prévention des métastases. Ces métastases, responsables de près de 90% des décès, se forment suite à la transition épithélio-mésenchymateuse des cellules cancéreuses. Comprendre les mécanismes de cette transition reste donc impératif afin de prévenir ou de mettre en place des cibles thérapeutiques appropriées.

Acknowledgements

Je tiens à remercier tout particulièrement Pauline Spéder et Franck Pichaud d'avoir accepté d'évaluer mon travail en qualité de rapporteurs. Vos retours et conseils m'ont été précieux, je vous remercie sincèrement d'avoir pris de votre temps pour contribuer à la finalisation de cette thèse.

Je tiens aussi à remercier Bénédicte Sanson, Romain Levayer et Eric Chevet d'avoir accepté d'être membres de mon jury de thèse, d'évaluer mon travail et ma soutenance de thèse.

Je remercie à nouveau Bénédicte Sanson mais aussi Jean-Pierre Tassan, Antoine Guichet et Benoît Aigouy pour leurs précieux conseils en qualité de membres de mon comité de thèse tout au long de mon cursus.

Je remercie également la Fondation Recherche Médicale pour m'avoir accordé leur confiance à travers un financement de 4ème de thèse.

A présent, je tiens à te remercier Roland, du fond du cœur, pour tout ce que tu as fait pour moi au cours de ces 4 années. C'est grâce à toi que je suis devenu l'apprenti scientifique que je suis et c'est surtout grâce à toi, qui a su trouver les mots justes, toujours au bon moment, que je peux prendre à présent mon envol dans ce monde de la Recherche, Ô combien difficile mais captivant. Quelques mots ne peuvent suffire à témoigner de mon éternelle reconnaissance à ton égard, mais sache que tu peux être fier de ton enseignement que je tenterai au mieux d'honorer dans le futur. Wittgenstein disait, ce dont on ne peut parler, il faut le taire. Dans ta langue favorite, cela donne « Wovon man nicht sprechen kann, darüber muss man schweigen ». Je pense que ceci est à la fois la meilleure approximation que je pourrai donner de ma gratitude envers toi, mais aussi la manière la plus juste. Mille fois Merci.

C'est à ton tour Mathieu, toi qui fus mon premier maître de stage. C'est grâce à toi que la mouche a cessé d'être un organisme étranger à ma pensée. En effet, découper des Drosophiles avec un laser bi-photonique en imagerie confocale en temps réel, il y a de quoi éveiller des passions de scientifique. Je n'oublierai pas non plus nos duels de cow-boys à la Tony, ni ces pronostics sportifs pour le moins précis (tu tiens là ta reconversion). En revanche, tâche de manger plus de délicieux légumes du CHU pour garder cette forme olympique.

Merci beaucoup à toi Céline également, pour ton aide, ton écoute et ta bienveillance. Je m'excuse si parfois mes propos ou discussions n'étaient pas des plus optimistes mais au moins, le second degré à la fin embellissait tout ceci. Si j'avais quelques conseils pour le futur, je te dirais de garder ce calme dont tu as su faire preuve malgré la fièvre ou les grands froids du SP8. Courage, l'abnégation finit toujours par payer. Je te souhaite tout le meilleur pour le futur et à très bientôt je l'espère.

Marta c'est à ton tour. Je vais le faire en français comme ça tu pourras maintenir ce niveau C2 dûment obtenu (mais je ne ferai pas du Proust, je n'en ai pas le talent). Sache que tu as été une stagiaire très talentueuse, curieuse et qui a su me faire apprendre sur moi-même. Je suis heureux que tu puisses à présent t'épanouir au sein du labo avec ton propre projet. Ceci étant dit, tu vas me manquer également en tant qu'amie. Cela te forcera à venir me dire bonjour en Suisse. D'ailleurs, j'attends toujours d'entendre ce fameux Daniel Balavoine qui peine à venir. En tout cas, continue à garder cette joie de vivre qui te caractérise et vis à fond ces moments Bretons à venir. A très vite je l'espère. Ah oui, n'oublie pas de lire Nietzsche de temps à autre, un peu de baume au cœur est toujours le bienvenu durant les temps les plus sombres.

Merci à toi également Nathalie qui est arrivée au sein de l'équipe en cours de route de ma thèse. J'ai été ravi de faire ta connaissance et je te remercie pour toute l'aide indispensable que tu as amené en permanence à l'équipe.

Merci à toi Clara, qui a quitté l'institut une petite année avant moi. Je n'oublierai pas ces soirées Breizh session/été indien qui se terminent par une session bricolage et abattage de Pin de 30 mètres près de la côte le lendemain. Un grand merci également pour m'avoir initié à l'escalade, à cause de toi j'en suis maintenant rendu à vouloir grimper partout. Hâte de pouvoir te voir plus souvent près des montagnes alpines.

Merci à toi également Artem pour ton aide mais surtout pour ton amitié et ces bons moments passés au gré des soirées musicales, parfois plus festives que de raison.

Je tenais à remercier également tous mes anciens compagnons de foot de l'institut, de l'association LUCA et des instituts avoisinants pour avoir embellit mon quotidien durant cette thèse.

Un grand merci aussi aux anciens membres de l'équipe et aux nouveaux, in Droso et tout particulièrement à toi Karen, qui fut toujours là pour m'aider, me conseiller et m'épauler, sache que je te suis extrêmement reconnaissant.

Merci aussi aux membres de l'institut, à tous les niveaux, ainsi qu'aux membres de la plateforme de Microscopie.

Merci à mes compagnons marins, tout particulièrement à toi Denis, avec qui j'ai pu parcourir les mers de Quiberon, ramener ce magnifique trophée à Rennes mais surtout découvrir un merveilleux sport et de formidables chants.

Merci également à tous mes amis externes à mon milieu professionnel, vous allez me manquer.

Un grand merci à ma famille et ma belle-famille, votre soutien et réconfort m'ont été précieux.

Et pour terminer, je te remercierai toi Lili. Ta présence, tes innombrables soutiens, ta douceur et ton amour ont su apaiser tous les maux. Je n'ai pas besoin d'étaler ici tout ce que j'ai sur le cœur, alors un milliard de milliard de merci suffiront à esquisser la Gargantuesque gratitude que je te témoigne. J'ai hâte et suis fier de découvrir la Suisse et le futur à tes côtés. Espèce de Wapiti.

Title: Roles of bi and tricellular septate junctions in the homeostasis of the *Drosophila melanogaster notum*

Key words: Epithelium; Tricellular junction; Septate junction; Adherens junction; Intracellular trafficking

Abstract: Epithelia are tissues of organisms that provide a role of barrier against chemical and physical aggressions and undergo morphogenesis, repair or regenerate thanks to cell division. Epithelial cells are polarized and linked by bicellular junctions (BCJ) called adherens junction (AJ) at the apical level or septate junction (SJ) below and tricellular junctions (TCJ) where three cells met. Recently, TCJ have emerged as a key regulator of processes regulating cell division, stem cells but also tumourigenesis. Surprisingly, little is known concerning TCJ itself. During my PhD work, I used *Drosophila notum*, a monolayered epithelium, in combination with genetics, imaging and biophysics tools to decipher TCJ homeostasis. Four proteins have been described at TCJ: Sidekick (Sdk), enriched at the AJ level, and Gliotactin (Gli), Anakonda (Aka) and M6 at the SJ level. I first characterized TCJ components *de novo* recruitment at TCJ that assemble during epithelial cytokinesis. Second, I reported that Aka and M6 are the keystone of TCJ assembly. However, while Gli is not required for Aka recruitment at TCJ, Gli activity is needed to stabilize Aka there. I also uncovered that loss of TCJ components results in SJ morphology impairment leading to a major defect of the epithelium. Conversely, the specificity of localization of TCJ components relies on SJ integrity. In parallel, I observed that loss of TCJ integrity leads to E-cadherin as well as acto-myosin cytoskeleton enrichment at both TCJ and BCJ. These phenotypes also appear upon loss of pSJ proteins. Moreover, the AJ and acto-myosin cytoskeleton remodeling comes with ESCRT components HRS and Shrub defects along with Crumbs enrichment at the apical part of the cell. Moreover, I observed that the establishment of the new daughter/daughter cell interface is impaired upon TCJ loss of function. Hence, my PhD work sheds light on the links between TCJ, pSJs and AJs in the tissue and how defects at a specific junctional level, results in a global impairment of cell homeostasis.

Titre: Rôles des jonctions bi et tricellulaires septées dans l'homéostasie du *notum* de *Drosophila melanogaster*

Mots clés: Epithélium; Jonction tricellulaire; Jonction septée; Jonction adhérente; Traffic intracellulaire

Résumé: Les épithélia sont des tissus de l'organisme, jouant un rôle de barrière contre l'extérieur et impliqués dans le développement, la morphogénèse et la réparation tissulaire grâce à la division cellulaire. Ils sont composés de différentes cellules polarisées qui forment des jonctions bicellulaires (BCJ) dites adhérentes (AJ) ou septées (SJ) ainsi que des jonctions tricellulaires (TCJ) au contact de trois cellules. De récentes études démontrent que les TCJs sont impliquées dans de nombreux processus intervenant dans la division cellulaire, la régulation de cellules souches ou encore la tumorigénèse. Curieusement, les TCJs demeurent méconnues. J'utilise le *notum* de Drosophile, un épithélium monocouche, en combinaison avec des outils génétiques, d'imagerie et de biophysique pour étudier l'homéostasie des TCJs. Quatre protéines transmembranaires sont reportées enrichies aux TCJs : Sidekick (Sdk) dans le plan des AJs ; Gliotactine (Gli), Anakonda (Aka) et M6 dans le plan des SJs. J'ai caractérisé leur dynamique d'assemblage dans la division et démontré que M6 et Aka étaient les pièces maîtresses des TCJs en recrutant Gli. Cette dernière, bien que non nécessaire à la présence d'Aka à la TCJ, la stabilise. J'ai ensuite observé que la perte d'intégrité de la TCJ conduit à des déformations des SJs entraînant un défaut majeur de l'intégrité de l'épithélium. A l'inverse, la spécificité de localisation des protéines de la TCJ est régulée par l'intégrité des SJs. En parallèle, j'ai également remarqué que la perte d'intégrité de la TCJ entraîne un enrichissement d'E-Cadhérine et d'acto-myosine tout comme la perte de protéines des pSJs. De plus, j'ai pu observer que ces défauts étaient accompagnés d'agrégats des protéines ESCRT HRS et Shrub ainsi qu'un enrichissement de Crumbs au niveau apical de la cellule. De plus, enlever la protéine Aka conduit à un défaut d'établissement de la nouvelle jonction cellulaire lors de la division. Ce travail de thèse a donc permis de comprendre le lien qui existe entre la TCJ, les pSJs et AJs au sein du *notum* et comment des défauts dans un certain plan jonctionnel conduisent à des problèmes généralisés dans la cellule.

UNIVERSITÉ DE RENNES 1

Titre : Rôles des jonctions bi et tricellulaires septées dans l'homéostasie du *notum* de *Drosophila melanogaster*

Mots clés : Epithélium ; Jonction tricellulaire ; Jonction septée ; Jonction adhérente ; Traffic intracellulaire

Résumé : Les épithélia sont des tissus de l'organisme, jouant un rôle de barrière contre l'extérieur et impliqués dans le développement, la morphogénèse et la réparation tissulaire grâce à la division cellulaire. Ils sont composés de différentes cellules polarisées qui forment des jonctions bicellulaires (BCJ) dites adhérentes (AJ) ou septées (SJ) ainsi que des jonctions tricellulaires (TCJ) au contact de trois cellules. De récentes études démontrent que les TCJs sont impliquées dans de nombreux processus intervenant dans la division cellulaire, la régulation des cellules souches ou encore la tumorigénèse. Curieusement, les TCJs demeurent méconnues. J'utilise le *notum* de Drosophile, un épithélium monocouche, en combinaison avec des outils génétiques, d'imagerie et de biophysique afin d'étudier l'homéostasie des TCJs. Quatre protéines transmembranaires sont reportées enrichies aux TCJs : Sidekick (Sdk) dans le plan des AJs ; Gliotactine (Gli), Anakonda (Aka) et M6 dans le plan des SJs. J'ai caractérisé leur dynami-que d'assemblage dans la division et démontré que M6 et Aka étaient les pièces maîtresses des TCJs en recrutant Gli. Cette dernière, bien que non nécessaire à la présence d'Aka à la TCJ, la stabilise. J'ai ensuite observé que la perte d'intégrité de la TCJ conduit à des déformations des SJs entraînant un défaut majeur de l'intégrité de l'épithélium. A l'inverse, la spécificité de localisation des protéines de la TCJ est régulée par l'intégrité des SJs. En parallèle, j'ai également remarqué que la perte d'intégrité de la TCJ entraîne un enrichissement d'E-Cadhérine et d'acto-myosine tout comme la perte des pSJs. De plus, j'ai pu observer que ces défauts étaient accompagnés d'agrégats des protéines ESCRT HRS et Shrub ainsi qu'un enrichissement de Crumbs au niveau apical de la cellule. De plus, enlever la protéine Aka conduit à un défaut d'établissement de la nouvelle jonction cellulaire lors de la division. Ce travail de thèse a donc permis de comprendre le lien qui existe entre la TCJ, les pSJs et AJs au sein du notum et comment des défauts dans un certain plan jonctionnel conduisent à des problèmes généralisés dans la cellule.

Title : Roles of bi and tricellular septate junctions in the homeostasis of the *Drosophila melanogaster notum*

Keywords : Epithelium ; Tricellular junction ; Septate junction ; Adherens junction ; Intracellular trafficking

Abstract : Epithelia are tissues of organisms that provide a role of barrier against chemical and physical aggressions and undergo morphogenesis, repair or regenerate thanks to cell division. Epithelial cells are polarized and linked by bicellular junctions (BCJ) called adherens junction (AJ) at the apical level or septate junction (SJ) below and tricellular junctions (TCJ) where three cells met. Recently, TCJ have emerged as a key regulator of processes regulation cell division, stem cells but also tumourigenesis. Surprisingly, little is known concerning TCJ itself. During my PhD work, I used Drosophila notum, a monolayered epithelium, in combination with genetics, imaging and biophysics tools to decipher TCJ homeostasis. Four proteins have been described at TCJ : Sidekick (Sdk), enriched at the AJ level, and Gliotactin (Gli), Anakonda (Aka) and M6 at the SJ level. I first characterized TCJ components de novo recruitment at TCJ that assemble during epithelial cytokinesis. Second, I reported that Aka and M6 are the keystone of TCJ assembly. However, while Gli is not required for Aka recruitment at TCJ, Gli activity is needed to stabilize Aka there. I also uncovered that loss of TCJ components results in SJ morphology impairment leading to a major defect of the epithelium. Conversely, the specificity of localization of TCJ components relies on SJ integrity. In parallel, I observed that loss of TCJ integrity leads to to E-Cadherin as well as acto-myosin cytoskeleton enrichment at both TCJ and BCJ. These phenotypes also appear upon loss of pSJ proteins. Moreover, the AJ and acto-myosin cytoskeleton remodeling comes with ESCRT components HRS and Shrub defects along with Crumbs enrichment at the apical part of the cell. Moreover, I observed that the establishment of the new daugther/daughter cell interface is impaired upon TCJ loss of function. Hence, my PhD work sheds light on the links between TCJ, pSJs and AJs in the tissue and how defects at a specific junctional level, results in a global impairment of cell homeostasis.